Alma Mater Studiorum · Università di Bologna

Scuola di Scienze
Corso di Laurea Magistrale in Fisica del Sistema Terra

Thermal structure and dynamical modeling of a Mediterranean Tropical-like cyclone

Relatore:
Prof. Andrea Buzzi

Correlatore:
Dott. Piero Malguzzi

Presentata da:
Guido Cioni

Sessione II
Anno Accademico 2013/2014

Alma Mater Studiorum · Università di Bologna

Scuola di Scienze
Corso di Laurea Magistrale in Fisica del Sistema Terra

Thermal structure and dynamical modeling of a Mediterranean Tropical-like cyclone

Relatore:
Prof. Andrea Buzzi

Correlatore:
Dott. Piero Malguzzi

Presentata da:
Guido Cioni

Sessione II
Anno Accademico 2013/2014

Cieco chi non vede il sole, stolto chi nol conosce, ingrato chi non ringrazia; se tanto é il lume, tanto il bene, tanto il beneficio: per cui risplende, per cui eccelle, per cui giova; maestro de sensi, padre di sustanze, autor di vita.

Giordano Bruno - Spaccio de la bestia Trionfante

Sommario

I cicloni mediterranei simil-tropicali sono fenomeni alla mesoscala che condividono alcune caratteristiche tipiche dei cicloni tropicali come l'occhio privo di nubi e la forma spiraleggiante delle nuvole. Le osservazioni *in-situ* non sono ancora in grado di catturare la scala spaziale di questi sistemi, che oscilla tra 200 km e 30 km di raggio. Negli ultimi anni vari modelli numerici di previsione meteorologica sono stati utilizzati per simulare questi sistemi e predire la loro influenza sull'ambiente circostante. Nel presente lavoro di tesi è stata condotta un'analisi dettagliata di un tropical-like cyclone mediterraneo verificatosi nel gennaio del 2014. L'autore non è al corrente di altri studi riguardanti questo particolare evento al momento della pubblicazione. Al fine di delineare l'evoluzione del ciclone sono stati innanzitutto raccolti i dati dalle stazioni meteo, dai satelliti, dai radar e le testimonianze fotografiche. Successivamente, dopo aver identificato la traiettoria del ciclone e le sue caratteristiche generali, i modelli GLOBO, BOLAM e MOLOCH sviluppati presso l'istituto ISAC di Bologna sono stati utilizzati per simulare l'evento. Sono state trattate con particolare attenzione sia la fase mediterranea, sia quella atlantica, dato che il ciclone ha mostrato la presenza di un *precursore* fino a 3 giorni prima della sua formazione nel mare di Alboran. La fase mediterranea è stata studiata utilizzando diverse combinazioni dei modelli GLOBO, BOLAM e MOLOCH, in modo da valutare la migliore catena modellistica in grado di simulare questo tipo di fenomeno. I modelli BOLAM e MOLOCH hanno prodotto i risultati migliori, grazie all'aggiustamento della traiettoria erroneamente deviata dai modelli globali Global Forecast System (GFS) e European Centre for Medium-range Weather Forecasts (ECMWF). L'analisi della fase termica del ciclone ha mostrato la presenza di una struttura a nucleo caldo in molte fasi di vita del sistema, confermando l'ipotesi fatta sulla sua natura tropicale. I risultati hanno inoltre mostrato una grande sensibilità alle condizioni iniziali durante tutto il ciclo di vita del sistema, mentre la modifica della temperatura del mare ha condizionato piccoli cambiamenti solo nella fase Adriatica. La fase atlantica è stata studiata utilizzando i modelli GLOBO, BOLAM e con l'aiuto della stessa metodologia già sviluppata precedentemente. Dopo aver tracciato il precursore, sotto forma di minimo di pressione, dalle coste americane fino alla Spagna, è stata analizzata la sua fase termica. I parametri ottenuti hanno evidenziato la presenza di una struttura asimmetrica a nucleo freddo durante il transito sull'oceano atlantico, mentre il primo contatto con le acque del Mediterraneo ha causato una transizione molto rapida ad una struttura simmetrica con debole nucleo caldo. L'analisi della struttura tridimensionale ha rivelato la presenza di un PV-*streamer*, formatosi individualmente sulla Groenlandia e che ha successivamente interagito con il ciclone di fronte alle coste spagnole, favorendo una prima fase di intensificazione baroclina. Infine, è stato incoraggiato lo sviluppo di un sistema che tracci e studi la fase termica dei cicloni Mediterranei in modo automatico, utilizzando le ultime emissioni del modello operativo BOLAM, in modo da sfruttare le conoscenze acquisite nel seguente lavoro e permettere una previsione in tempo reale di eventuali transizioni tropicali.

Abstract

Mediterranean Tropical-like cyclones (TLCs) are meso-scale phenomena that exhibit many features typical of Tropical Cyclones like the free-cloud eye and the spirally distributed cloud bands. The *in-situ* observations are still unable to capture the small horizontal scales of these systems that spans from approximately 200 km to 30 km of radius. For this reason, in recent years, some Numerical Weather Prediction (NWP) models has been extensively used in order to simulate these systems and predict their influences on the environment. In the present work, a detailed analysis of a Mediterranean TLC occurred in January 2014 has been conducted. The author is not aware of other studies regarding this particular event at the publication of this thesis. In order to outline the cyclone evolution, observational data, including weather-stations data, satellite data, radar data and photographic evidence, were collected at first. After having identified the cyclone path and its general features, the GLOBO, BOLAM and MOLOCH NWP models, developed at ISAC-CNR (Bologna), were used to simulate the phenomenon. Particular attention was paid on the Mediterranean phase as well as on the Atlantic phase, since the cyclone showed a well defined precursor up to 3 days before the minimum formation in the Alboran Sea. The Mediterranean phase has been studied using different combinations of GLOBO, BOLAM and MOLOCH models, so as to evaluate the best model chain to simulate this kind of phenomena. The BOLAM and MOLOCH models showed the best performance, by adjusting the path erroneously deviated in the National Centre for Environmental Prediction (NCEP) and ECMWF operational models. The analysis of the cyclone thermal phase shown the presence of a deep-warm core structure in many cases, thus confirming the tropical-like nature of the system. Furthermore, the results showed high sensitivity to initial conditions in the whole lifetime of the cyclone, while the Sea Surface Temperature (SST) modification leads only to small changes in the Adriatic phase. The Atlantic phase has been studied using GLOBO and BOLAM model and with the aid of the same methodology already developed. After tracing the precursor, in the form of a low-pressure system, from the American East Coast to Spain, the thermal phase analysis was conducted. The parameters obtained showed evidence of a deep-cold core asymmetric structure during the whole Atlantic phase, while the first contact with the Mediterranean Sea caused a sudden transition to a shallow-warm core structure. The examination of Potential Vorticity (PV) 3-dimensional structure revealed the presence of a PV streamer that individually formed over Greenland and eventually interacted with the low-pressure system over the Spanish coast, favouring the first phase of the cyclone baroclinic intensification. Finally, the development of an automated system that tracks and studies the thermal phase of Mediterranean cyclones has been encouraged. This could lead to the forecast of potential tropical transition, against with a minimum computational investment.

Contents

Acronyms

ABL Atmospheric Boundary Layer. 24

AGCM Atmospheric General Circulation Model. 26

ASCAT Advance Scatterometer. 13

CAPE Convective Available Potential Energy. 45

CERSAT Centre ERS d'Archivage et de Traitement. 70

CISK Condition Instability of the Second Kind. 3

COMPARE Comparison of Mesoscale Prediction and Research Experiments. 20

DWD Deutsche WetterDienst. 100

ECMWF European Centre for Medium-range Weather Forecasts. v, vi, 12, 24, 49, 59, 66, 67

EM Electro-Magnetic. 4

GCM General circulation model. 29, 95

GFS Global Forecast System. v, 60, 66

GOES Geostationary Operational Environmental Satellite. 86

IR Infra-Red. 70, 104

ISAC Institute of Atmospheric Sciences and Climate. 20

ITCZ Inter-Tropical Convergence Zone. 2

Acronyms

LAM Limited Area Model. 20, 29, 35

MCC Mesoscale Convective System. 3

MEDEX MEDiterranean EXperiment on cyclones that produce high impact weather in the Mediterranean. 8

MODIS MODerate resolution Imaging Spectro-radiometer. 13, 104

MSLP Mean Sea Level Pressure. 8, 17, 30, 31, 45, 61, 94, 95, 97, 107, 110

MTLC Mediterranean Tropical-like Cyclone. xi, xii, 6, 29, 34, 43, 73, 91, 94, 95

NCEP National Centre for Environmental Prediction. vi, 9, 49

NCL NCAR Command Language. 28

NHC National Hurricane Center. 99, 104

NWP Numerical Weather Prediction. vi, xii, 6, 15, 20, 29, 35, 36, 49, 90, 92, 110

PV Potential Vorticity. vi, 61, 66, 67, 77–81, 90, 91, 94

PVU Potential Vorticity Units. 77, 79

RAM Random Access Memory. 23, 95

SEVIRI Spinning Enhanced Visible and InfraRed Imager. 84, 85

SST Sea Surface Temperature. vi, xi, xii, 7, 8, 24, 26, 36, 37, 41, 42, 52, 53, 68, 70–72, 94

SW Short-Wave. 70

TC Tropical Cyclone. 1–3, 6, 8, 104, 112

TKE Turbulent Kinetic Energy. 24

TLC Tropical-like cyclone. vi, 14, 17, 29, 31, 35, 40–42, 57, 73, 92, 111

UTC Coordinated Universal Time. 12, 13

WAF Weighted Average Flux. 23

WISHE Wind-Induced Surface Heat Exchange instability. 3

WMO World Meteorological Organization. 20

WV Water Vapour. xii, 84–86, 90, 94

Introduction

Reports of a number of small but exceptionally severe storms, feared by sailors for the harm produced to ships, date back to ancient times. In the *Dissertazione sopra il turbine atmosferico che la notte fra gli XI e i XII di Giugno 1749 devastò una gran parte di Roma*, P. Ruggiero Giuseppe Boscovich, writes:

Non è però, che ne' nostri mari ancora alcuna volta non si sieno vedute sorgere delle tempeste somigliantissime a' più spaventosi Uracani di America [...] e come i medesimi sogliono durar talora per un giorno intero, e un gran tratto di mare sconvolgono, e per molte leghe s'inoltrano dentro terra; così quello durò nel suo vigore un giorno intiero, e dall'Adriatico al Mediterraneo si distese attraversando tutta quanta l'Italia, e tutto, per quanto dall'alture di Napoli può scoprirli, il medesimo mare mise in scompiglio.

But it is not so uncommon that sometimes storms very similar to the feared hurricanes of America are observed to rise in our seas [...] and like those they use, at times, to last a whole day deranging a large part of the sea and advancing for many leagues into the land; thus it lasted a whole day in its vigour and spreaded from Adriatic to Mediterranean Sea crossing the whole Italy and, all the sea that we can see from the hills behind Naples, put in bustle.

It is well known that the Mediterranean Sea, apparently more calm in respect to the greater oceans, is sometimes affected by strong extra-tropical cyclones that cause torrential rains and high winds in large areas. This region is affected by numerous cyclogenesis events, in particular between Autumn and Winter when the latent and sensible heat fluxes reach their maximum values, thanks to very warm SST. However, a particular and rare type of cyclogenesis occurring in the Mediterranean, still poorly understood, is capable of creating systems with intensities comparable with those of Atlantic perturbations, but on a much smaller radius. Those systems, referred to as Mediterranean Tropical-like Cyclones (MTLCs), are genuine *Mediterranean storms* that may intensify and show features similar to hurricane systems like the warm core and the free-cloud eye. Currently, in-situ measures and satellite

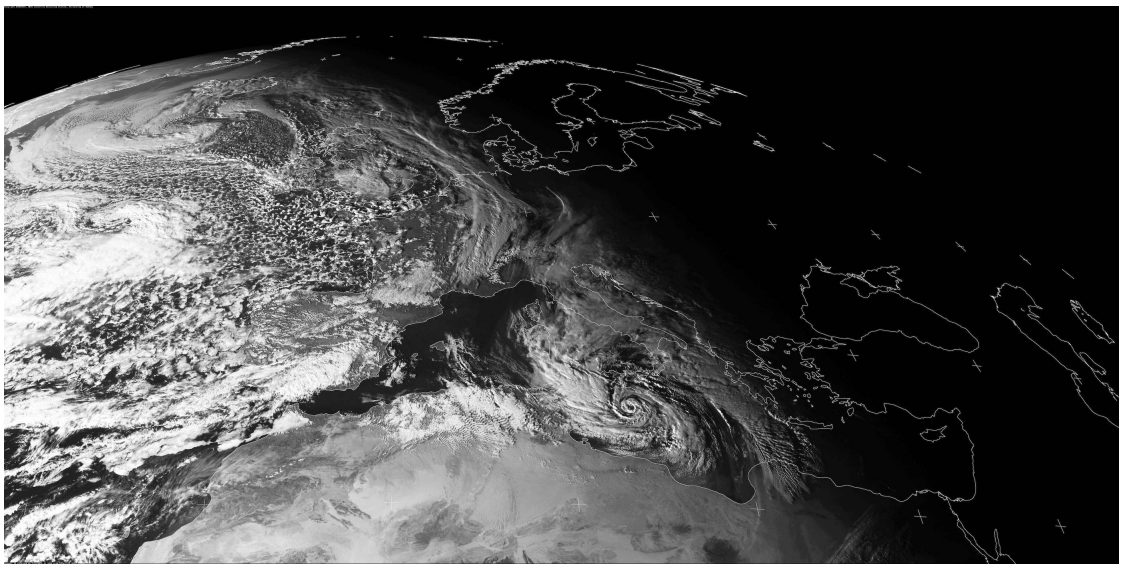

Figure 1.: A stunning view of the Euro-Asian continent on 7 November 2014 at 15 UTC, when a powerful Mediterranean Storm was interesting the Ionian Sea.

observations are the only means that permit to identify and track the evolution of MTLCs. Given the very small scales of these systems, predicting their evolution is a very difficult task, even with high-resolution meteorological models. For this reason, the studies regarding MTLCs often focus on the comparison of several models performance and on the execution of sensitivity tests. Initial conditions, SST definition, boundary conditions, model orography implementation, horizontal and vertical resolution, convection parametrization, heat flux parametrizations, all play a fundamental role in replicating the small-scale structure of medicanes. Since a formal complete theory has not yet been proposed, one of the ways to study the evolution of these systems consists in evaluating from case to case the dynamical relevant factors that concur to cyclone genesis and maintenance. Starting from this observation, NWP models are then used to perform simulation with different setup (no heat fluxes, no topography...) in order to compare the predicted cyclone path and strength. Later, the results are analysed and the *best* model setup is evaluated. The method just described will also be the one used in this work. In Chapter 1 a brief description of Tropical Cyclones and MTLCs is given, with a focus on Mediterranean basin cyclogenesis climatology. In Chapter 2 all observations, including in-situ measurements and satellite imagery, are collected, in order to outline the cyclone evolution over the Mediterranean Sea. In Chapter 3 a brief description of GLOBO, BOLAM and MOLOCH NWP models is presented, basing on the latest models update. In Chapter 4 the evolution of the Mediterranean cyclone is analysed in detail, by performing several model simulations and thermal phase analysis; the cyclone 3-dimensional structure is also studied in detail. In Chapter 5 the cyclone precursor is studied with the aid of satellite Water Vapour (WV) imagery and numerical simulations. Finally, Chapter 6 shows the conclusion of this work and the future perspectives for other similar works that are also suggested in Appendix C.

1

Tropical Cyclones and Mediterranean Hurricanes

Tropical Meteorology has been, and still is, an highly active field of study. The need to forecast the birth and evolution of intense phenomena such as *hurricanes* and *typhoons* arise from the necessity of protection in the regions most affected by the strong winds, storm surge and floods. The typical circulation of tropical latitudes, and the dynamic of the systems that develop in these regions, are well established since decades, although a fervent debate is still underway. Although the Mediterranean area is not within tropical latitudes, sometimes systems similar to those observed in the tropics are found also in the Mediterranean Sea. The technological progress made in satellite observations allowed to reach an imagery spatial resolution of few hundred meters, thus permitting to study the Mediterranean cyclones' climatology in a modern meteorological sense. Given the presence of distinct tropical features (such as the free-cloud *eye*), the first approach to the study of these systems consisted in adapting the well established theories concerning Tropical Cyclones (TCs).

1.1. Tropical Cyclones

1.1.1. Classification

The term *cyclone* describes an intense depression of tropical or extra-tropical nature. The extra-tropical cyclones are, generally, big cold-core vortices typical of temperate and sub-tropical zones. They are characterized by discrete thunderstorm convection located near fronts, but far from the cyclone center. Conversely, TC is the generic term for a non-frontal synoptic scale low-pressure system over tropical or sub-tropical waters with organized (intense) convection near the center and definite cyclonic surface wind circulation. TCs with maximum sustained surface winds of less than 17 m/s (61 km/h) are usually called *tropical depressions*. Once the TC reaches winds of at least 17 m/s they are typically called a *tropical storm* or in Australia a Category 1 cyclone and are assigned a name. If winds reach 33 m/s (118 km/h), then they are called:

- *hurricane* in the North Atlantic Ocean, the North-east Pacific Ocean east of the date-line, or in the South Pacific Ocean east of 160°E,

- *typhoon* in the Northwest Pacific Ocean west of the dateline,
- *severe tropical cyclone* or Category 3 cyclone and above in the South-west Pacific Ocean west of 160°E or in South-east Indian Ocean east of 90°E
- *very severe cyclonic storm* in the North Indian Ocean,
- *tropical cyclone* in the South-west Indian Ocean,

It should be noted that the terms *hurricane* and *typhoon* reflect only a difference in geographical location, but not of underlying physical principles. The Saffir-Simpson (see [103]) scale is often used to categorize these phenomena

Category	Max sustained winds (km/h)	Impact	Example
1	119-153	minimal	Hurricane Dolly (2008)
2	154-177	moderate	Hurricane Frances (2004)
3	178-208	extensive	Hurricane Ivan (2004)
4	209-251	extreme	Hurricane Charley (2004)
5	> 251	catastrophic	Hurricane Andrew (1992)

Table 1.1.: Saffir-Simpson scale.

1.1.2. Genesis and maintenance mechanisms

TCs form in the so called Inter-Tropical Convergence Zone (ITCZ), a narrow band ranging from ± 5 to ± 20 degrees of latitude, where the Coriolis force is able to supply the vorticity required for the development of these systems. Several favourable precursor environmental

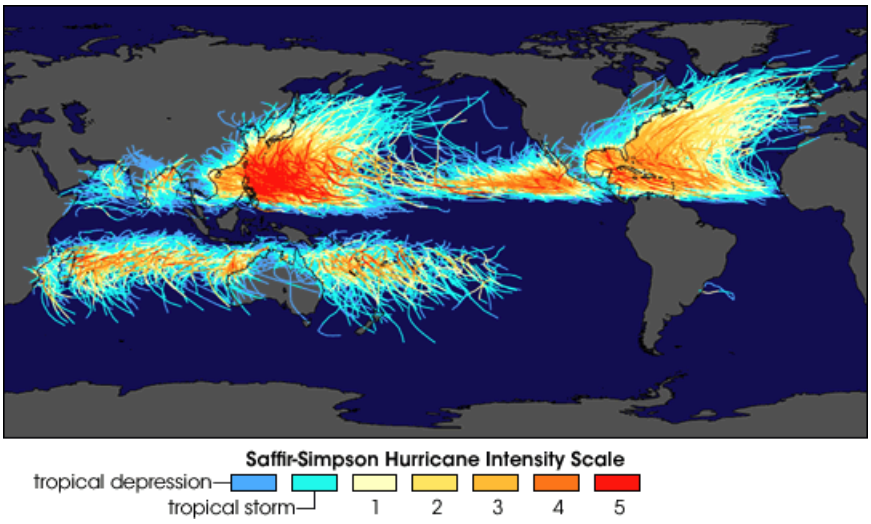

Figure 1.1.: Tropical Cyclones tracks through a 30 years period (1985-2005).

conditions must be in place to undergo tropical cyclogenesis, although these conditions are

necessary but non sufficient. For this reason, it is far more natural to assume that TCs' genesis is a series of events arising by chance from quantitative fluctuations of the normal disturbances, with the probability of further evolution gradually increasing as it proceeds (Ooyama [83]). The favourable conditions can be divided into:

- Warm ocean waters (of at least 26°) throughout a sufficient depth (Emanuel [34]),
- an atmosphere potentially unstable to moist convection,
- relatively moist layers near the mid-troposphere,
- a minimum distance of at least 500 km from the equator,
- a pre-existing near-surface disturbance with sufficient vorticity and convergence since tropical cyclones cannot be generated spontaneously,
- low values (less than about 10 m/s) of vertical wind shear between the surface and the upper troposphere.

The disturbance that lead to TC development include decaying extra-tropical systems (often Mesoscale Convective Systems (MCCs)) and easterly waves (Riehl [96], Dunn [32]), especially North African Easterly wave. Once the system enters the growth phase, thunderstorms release large amounts of latent heat which warms the mid- and upper-troposphere. As a result of this heating, air begins to diverge consequently lowering the surface pressure. The warm waters of the ocean enhance the conductive heating that balance the adiabatic cooling as the air cross the isobars: a warm core is thus maintained, perpetuating the storm. If vertical shear was present, the heat in the core of the hurricane would be transported away from the center, not allowing to further strengthening. The surface friction in the boundary layer balances the storms strength by limiting its intensity but maintaining its fuel supply by enhancing latent heat fluxes. The past years led to the formulation of several theories of intensification (Wind-Induced Surface Heat Exchange instability (WISHE), Condition Instability of the Second Kind (CISK) among the many) that depict the system growth by means of linear (Charney and Eliassen [25]) or nonlinear (Emanuel [34]) equations. Aside from the intensification phase, the steady state of the mature Hurricane[1] may be idealized as an axisymmetric vortex in hydrostatic and rotational balance (Emanuel [36]). The cyclonic flow reaches its maximum near the surface and decreases with height, becoming anticyclonic near the top of the storm. This flow configuration is related, by means of the thermal wind relationship, to a warm core structure near the center of the vortex[2]. The transverse circulation is thermally direct (except in the eye) and consist of a radial inflow within a boundary level (1-2 km deep), ascent mostly within a narrow, outward-sloping eye-wall, and in a radial outflow in a thin layer at the storm top. The typical structure of a mature Hurricane is shown in Figure 1.2. In the central zone, the so called *eye*, skies are relatively clear, winds subside to near calm and temperatures are often several degrees warmer than

[1]From now on, the Hurricane will be considered as the ideal model for the description of the steady state of a mature TC.

[2]This topic will be further discussed in Chapter 4.

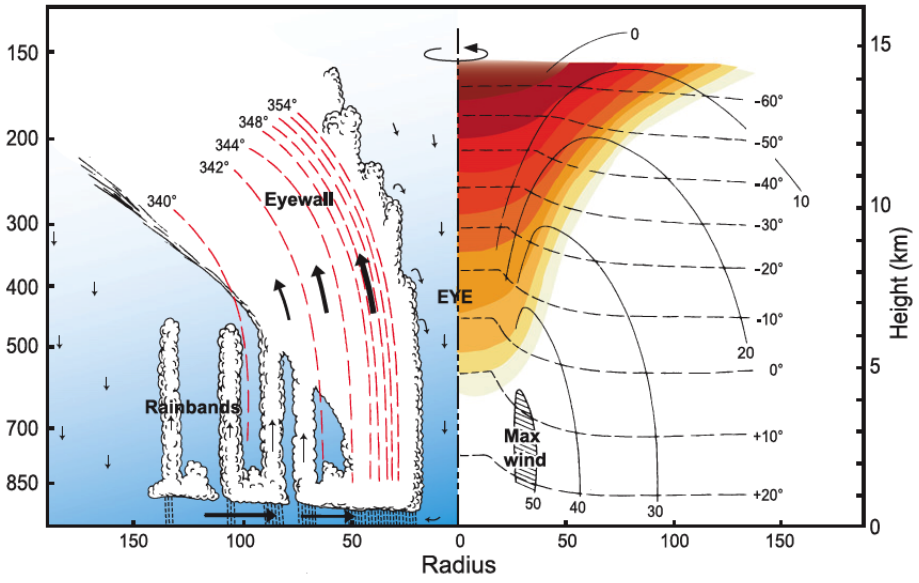

Figure 1.2.: Radial cross section through an idealized, axially symmetric hurricane. On the left, the radial and vertical mass fluxes are indicated by arrows and equivalent potential temperature (K) is indicated by dashed lines. On the right tangential velocity $[m/s]$ is indicated by solid lines and temperature [°C] is indicated by the dashed lines. [From Houze, [54]].

the surrounding eye wall. This is due to the subsidence motions from storms in the eye wall that result in an adiabatic warming which also creates a strong inversion that suppresses convection. The eye wall, which surrounds the eye, contains the most turbulent conditions and the most intense thunderstorms, since the greater updrafts develop in this area. The theory proposed by Emanuel [34] suggests to regard the steady tropical cyclone as a Carnot heat engine in which air flowing inward near the sea surface acquires moist entropy from the sea surface, ascends, and eventually releases heat by radiation in the lower-stratosphere or upper-troposhere. Figure 1.3 depicts the thermodynamic phase described hereinafter:

a-b : Isothermal Expansion: air from the lower atmospheric layers approaches the center of the cyclone decreasing the pressure and increasing its entropy because of a loss in kinetic energy and a simultaneous transfer of enthalpy from the sea surface (latent heat). The angular momentum decreases due to friction with the surface.

b-c : Adiabatic Expansion: air ascends within deep convective clouds in the eye-wall of the storm and then flows out, conserving angular momentum and entropy. The latent heat is converted into sensible heat as water vapour condenses, maintaining the total heat content constant.

c-d : Isothermal Compression: air descends in the lower stratosphere, maintaining a nearly constant temperature, while losing heat by thermal (Electro-Magnetic (EM)) radiation to space.

d-a : Adiabatic Compression: air descends more rapidly to the surface, conserving angular momentum and entropy.

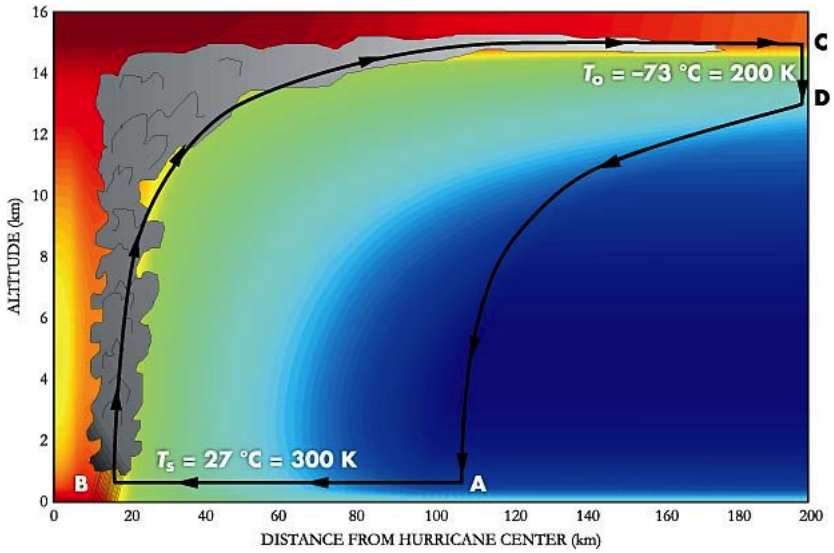

Figure 1.3.: The Hurricane Carnot cycle: the colors depict entropy distribution (blue-green indicates lower entropy; red-yellow indicates higher entropy).

However, this model does not account for many real-world effects like the heat loss due to condensation of rainwater and the dissipation of heat absorbed from the ocean in the distant environment. Furthermore, there is one interesting feature that differentiate the mature Hurricane from a Carnot steam engine. In this system, the mechanical energy produced by the engine is used to do something outside the engine itself, like power a locomotive or a car. The frictional dissipation, like the one produced by the contact between tires and asphalt, turns the kinetic energy into heat, which is lost to the environment. In a Hurricane, the mechanical energy produced by the Carnot-like heat engine shows up as the energy of the winds. Nevertheless, almost all of the frictional dissipation occurs in the inflow layer, where the power of the winds is converted back into heat, which then flows back into the system. Thus, some of what would have been wasted heat energy is recycled back into the front end of the heat engine. This makes hurricanes somewhat more powerful than they would be otherwise.

1.2. Mediterranean Tropical-like cyclones

The climate of the Mediterranean basin is characterized by a large seasonal variability made up by hot dry summer and warm wet winters. The geographical placement of this area, between the subtropical anticyclone belt and the mid-latitude westerlies, partially contributes to the seasonal characterization, that is largely affected also by orographic configuration. Very high mountain ranges (Atlas, Alps..), relatively warm sea, all bear important consequences on the atmospheric regional circulations. While warm water can acts as a reservoir of heat and moisture, enhancing the land-sea contrast, the complex orography may interact with a baroclinic wave approaching the region, giving rise to a wide variety of cyclogenesis events (Speranza et al. [106]). Due to the high impact of Mediterranean cyclones in

coastal regions, several studies tried to build a climatology of these systems (e.g. Campins et al. [18]). The study of the spatial distribution led to the recognition of several preferred

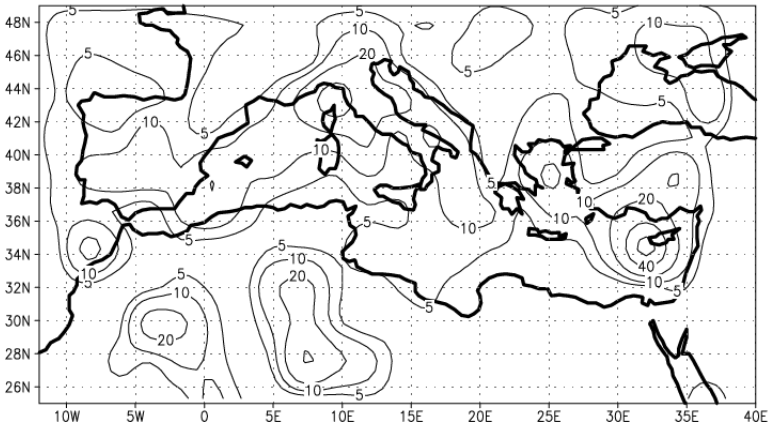

Figure 1.4.: Mean number of cyclone centers in a 2.25°×2.25° grid, obtained with ERA-40 analysis dataset. Contour intervals: 5,10,20,40 and 60 centres/year. [from Campins [18]].

regions for cyclogenesis, with two main maxima over Cyprus and in the gulf of Genoa (see Figure 1.4). Other regions with an appreciable number of cyclone centers are the Sahara, the Adriatic and the Aegean Seas, the gulf of Cadis and the Algerian Sea. Aside from the horizontal distribution, often shaped by the orography, the vertical structure of these systems has been investigated in detail. Some recent studies (e.g. Trigo et al. [112]) have revealed that Mediterranean cyclones are smaller in scale that their Atlantic counterparts. While meteorological phenomena exhibit a large variety of spatial and temporal scales, the resolution of a NWP model determines the scales that are detectable. Therefore, in order to precisely describe small-scale cyclones, it is necessary to use a high-resolution original field, in both horizontal and vertical space discretization (Campins et al. [19]). The Mediterranean low pressure systems are often categorized as *extra-tropical* cyclones, since the energy required to grow is gained from the horizontal temperature gradients. Conversely, the *tropical* cyclones, described in the first section of this chapter, obtain their energy from the release of energy due to cloud/rain formation from the warm moist air of the tropics. Sometimes, a TC will transform into an extra-tropical cyclone as it recurves poleward and to the east. Occasionally, an extra-tropical cyclone will lose its frontal features, develops convection near the center of the storm and transforms into a full-fledged tropical cyclone. For this reason this classification implies the existence of hybrid cyclones, where the tropical or extra-tropical features both survive for a limited period of time. Mediterranean cyclones have nearly always a baroclinic nature, although it is occasionally possible to identify very intense cyclonic system, quite similar to TCs. These systems were called *Medicanes* firstly by (Emanuel, [33]), merging the two words *Medi*terranean Hurri*cane*[3], to emphasize the resemblance with TCs. This type of cyclones was first observed in the early 80's and initially interpreted as similar to the *Polar Low* phenomenon, low pressure systems that develops in polar latitudes (see Rasmussen [91], Montgomery et al. [78], Harrold and Browning [47] and Rasmussen

[3]In this work, the terms *Medicane* and MTLC are used to denote the same physical phenomenon.

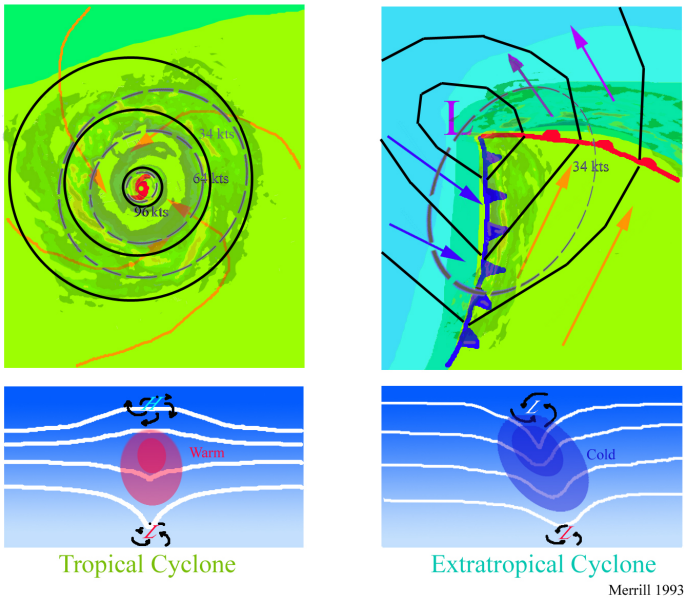

Figure 1.5.: The top schematics show horizontal maps of the surface temperature, pressure, and wind fields associated with a tropical cyclone (left) and an extratropical cyclone (right). Colors indicate temperature (blue 15°C, blue green 20°C, green 25°C). Dashed lines indicate surface windspeeds, solid lines are isobars. The bottom schematics show vertical maps of the pressure surfaces, temperature anomalies, and circulation at the surface and tropopause. [from `http://www.aoml.noaa.gov/hrd/tcfaq/A7.html`]

[90]). The Polar Lows are formed due to the instability created by the thermal gradient between the cold air, coming from the ice shelf, and the relatively warm sea. Several case studies have investigated the main features of medicanes, including observational evidence (Ernst and Matson [38] ; Rasmussen and Zick [92]; Lagouvardos et al. [62] ; Pytharoulis et al. [88]; Reale and Atlas [93]; Moscatello et al. [80]) as well as modeling aspects (Fita et al. [41]; Homar et al. [52]; Moscatello et al. [81]; Davolio et al. [31]; Miglietta et al. [75]; Tous et al. [110]). The picture emerging from the aforementioned studies is that of low pressure systems that, even its originally baroclinic nature (extra-tropical cyclones), can undergo a new stage of development driven by convection and air-sea interaction, whenever they meet specific environmental conditions such as water much warmer than the seasonal average. In this stage the cyclone assumes features similar to those of tropical vortices, such as an almost perfect vertical symmetry, a spirally shaped cloud cover with an eye in the middle, and a warm core visible in the temperature field. The case of January 1995 has been extensively studied (Lagouvardos et al. [62]; Pytharoulis et al. [88]): while in the first study a warm core near the surface were detected by a ship measurement, in the second study the importance of sensible and latent heat fluxes for the genesis of these systems has been demonstrated. In order to further understand the importance of air-sea interaction, Tous and Romero [109] recently discovered that a SST of 15°C is a significance threshold needed for the genesis of a Medicane. However, since Polar Lows form on very cold waters (typically 5 to 8 ° C), it is clear that the relevant factor is constituted by the air-sea temperature gradient, and not by the SST value only. The dependence on the SST and heat fluxes has been investigated

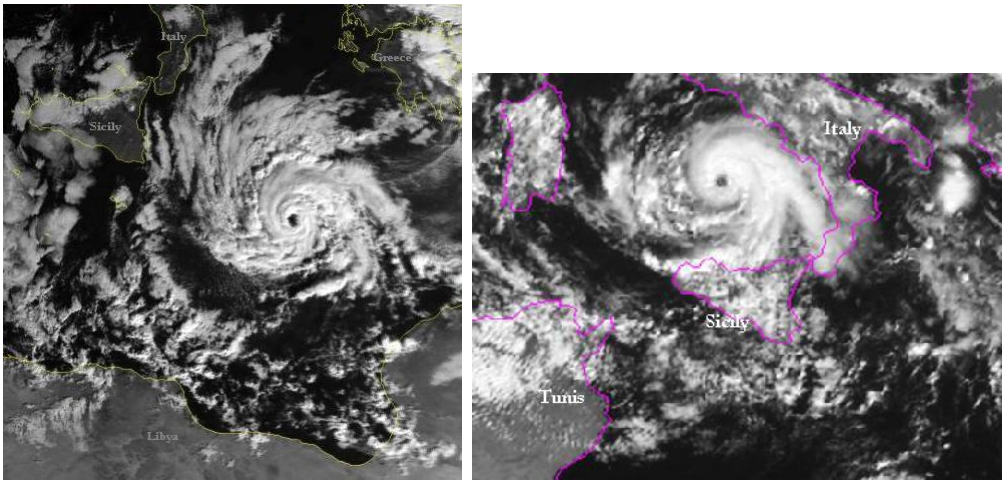

(a) The Mediterranean Hurricane *Celeno* of 14-18 January 1995. The maximum wind reported by a ship was 135 km/h (see Phytaroulis et al., [88]).

(b) The Mediterranean Hurricane Cornelia of 6-11 October 1996.

Figure 1.6.: Satellite imagery for two medicane case studies.

by many authors (Homar et al. [52]; Miglietta et al. [72]; Davolio et al. [31]) showing that genesis and maintenance of medicanes is strictly related to SST and sea surface heat fluxes. In particular, Davolio et al. [31] showed that the predicted Mean Sea Level Pressure (MSLP) can vary up to 40 hPa depending on whether latent heat and sensible heat fluxes are turned on or off. Furthermore, Emanuel [33] demonstrated, using a theoretical environment, that a cold upper low over the Mediterranean area can produce strong cyclogenesis even in area of small baroclinicity, by exploiting the large air-sea thermodynamic disequilibrium.

1.2.1. A brief climatology

The attempts to build a robust climatology of Medicanes made in recent years have revealed various issues. In particular:

- Medicanes seem rare phenomena. Some lists of possible medicanes events are maintained updated on the website `http://www.uib.cat/depart/dfs/meteorologia/METEOROLOGIA/MEDICANES/` and `http://www.medicanes.altervista.org/`. The total number of events amounts to a few tens over a 40-year period (1976-2014).

- Objective detection in reanalysis dataset is not applicable since the spatial scale of medicanes is often lower than 100 km. The detection algorithms that have been developed for TCs, and extra-tropical cyclones (e.g. MEDiterranean EXperiment on cyclones that produce high impact weather in the Mediterranean (MEDEX) database), are unable to capture the small-scale dynamics of these systems.

- Satellite-based research permits to identify the cloud patterns typical of tropical depression but are not able to construct an objective detection of the systems. Tous and

Romero [109] showed that over four hundred possible medicanes cases, only six cases were identified by the algorithm developed.

It is therefore clear that the identification of a clear-cut demarcation line between medicanes and *ordinary* Mediterranean cyclones is not an easy task, especially with automated algorithms. Cavicchia et al. [20] applied a downscaling methodology to six decades of NCEP reanalysis, thus permitting to reach the high-resolution needed for medicanes detection and study. The objective criteria used for medicanes detection in this work were[4]:

- presence of warm-core symmetrical environment (for more than 10% of the cyclone track, alternatively 6 hours), using the parameters suggested by Hart [48] and described in Chapter 4;
- wind speeds (averaged on a circle around the pressure minimum) higher than 18 m/s for more than 10% of the cyclone track (alternatively 6 hours);
- wind speed (averaged on a circle around the pressure minimum) at 850 hPa higher than wind speed at 300 hPa.
- maximum wind speed (in a circle around the pressure minimum) higher than 29 m/s for a time longer than 4 hours.

The geographical patterns of genesis and trajectories of the medicanes detected by using this algorithm are shown in Figure 1.7. The regions where genesis occurs more frequently are the Western Mediterranean, with an outstanding maximum near the Balearic islands, and the Ionian Sea. It is worth noting that the geographical distribution depicted in Figure 1.7 does not coincide with the one of *ordinary* Mediterranean cyclones (Figure 1.4). The seasonal distribution showed in Figure 1.8 is characterized by no events in Summer, an high activity in Autumn and a peak in January.

[4]For a detailed description of the algorithm please refer to Cavicchia et al., [20]

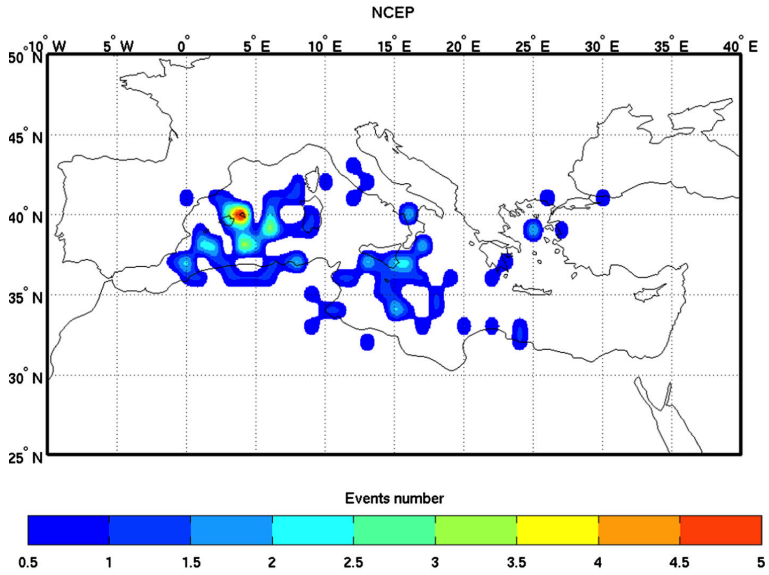

(a) Genesis density (first location in the track) per $1° \times 1°$ box.

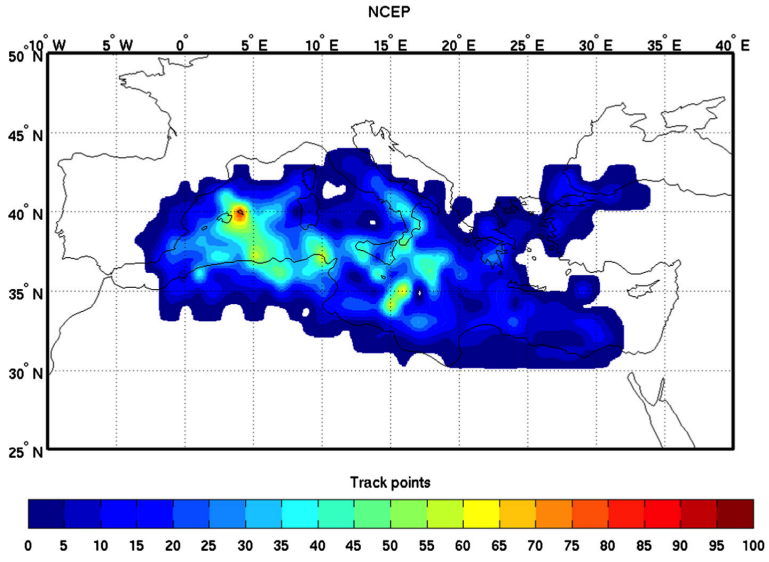

(b) Track density per $1° \times 1°$ box.

Figure 1.7.: Location of all medicanes detected by Cavicchia et al. [20].

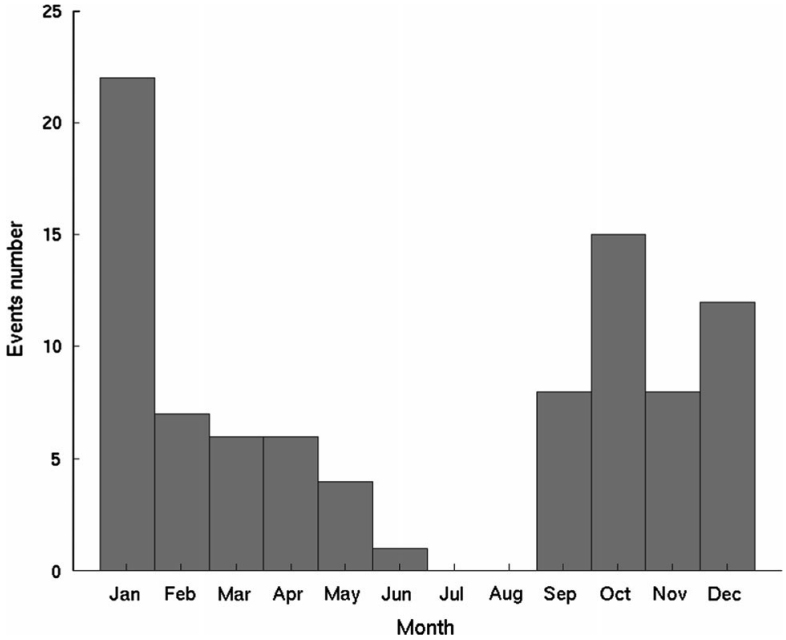

Figure 1.8.: Number of medicanes per month (total number in the period 1948-2011) [from Cavicchia et al. [20]].

2 Observational Analysis

2.1. Formation and development

The cyclone focus of this study formed in the morning of 19 January 2014 on the eastern Spanish coast, between Malaga and Gibraltar. Strong winds were associated with an upper air low prior to the formation of the Mediterranean cyclone. The official weather station of Gibraltar's airport reported sustained winds with a maximum[1] of 103.7 km/h (W) at 6:50 Coordinated Universal Time (UTC). The synoptic situation prior to the formation and the development of the cyclone is displayed in Figure 2.1. The ECMWF analysis at 00 UTC (01 local time) shows a baroclynic wave from the Atlantic extending towards the Iberian Peninsula. At this time several pressure minima were embedded in this upper-air trough, while two high pressure systems were located respectively in the North-Atlantic ocean at low latitudes and on Egypt. A close examination of Meteosat Visible imagery showed that the

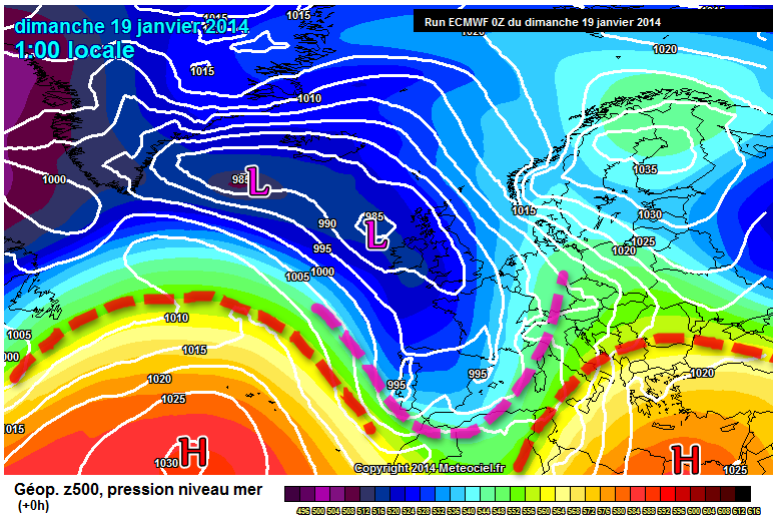

Figure 2.1.: ECMWF model analysis at 00:00 UTC, 19 January 2014, interpolated by Meteociel. White contour: Mean sea-level pressure. Filled Contour: Geopotential Height at 500 hPa.

[1]The measure is official and certified by WMO standard - 10 meters surface winds.

formation time of the Mediterranean cyclone was at about 09 UTC on 19 January 2014 (not shown), over the Alboran Sea. The system initially formed as an extra-tropical cyclone, and quickly turned into a sub-tropical storm[2] in the subsequent hours. The MODerate resolution Imaging Spectro-radiometer (MODIS) sensor from AQUA Satellite captured (Figure 2.2) the cyclone about 2 hours after the initial formation (11 UTC), showing high convective clouds with a minimum brightness temperature of 220 K (about $-53°$ C). Figure 2.3 shows that

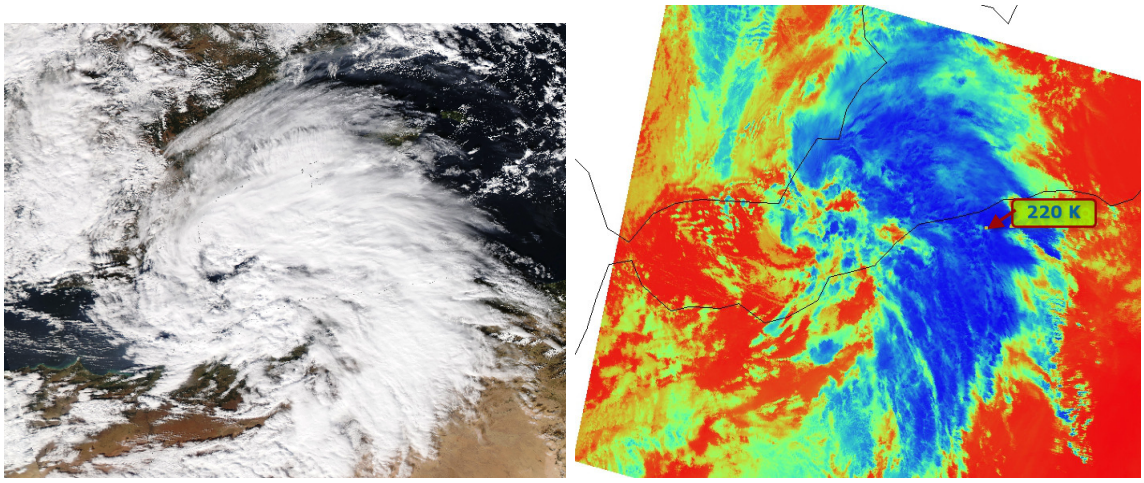

(a) Composite RGB Image (b) Brightness Temperature

Figure 2.2.: MODIS Aqua Imagery of 19 January 2014 - 11 UTC

several weather stations on the coast of Malaga experienced a drop of pressure and an increase of wind gust at the time when the cyclone was forming. The data from Alhaurin, Estepona and El Palo indicate that the minimum pressure reached was about 989 hPa in the first hours of 19 January. At about 12 UTC, the wind direction retrieved from satellite data Advance Scatterometer (ASCAT) showed a defined vortex with maximum speed of about 50 knots (92 km/h). According to Figure 2.4 the center of the system was located near Cartagena (Spain) at this time. After the formation, and throughout the first day of the life cycle (19 January), the cyclone moved to the East, following the coastline of Northern Africa. Intense rainfall and winds gust up to 80 km/h hit Algeri during the night (not shown). During this period the pressure in the center of the cyclone was rising to a steady value of 997 hPa, as shown in the MeteoCentre hourly analysis (not shown) and in the MetOffice daily analysis at 00 UTC on 20 January 2014 (Figure 2.5). During the night of 19 January and the early morning of 20 January the vortex signature in the cloud pattern vanished, as the cyclone was interacting with the orography of Sardinia Island. In the late morning of 20 January 2014, the cyclonic cloud pattern became evident again when the low pressure system got through Sardinia Island, as shown in Figure 2.6. At 12 UTC the image acquired from polar satellite

[2]A sub-tropical cyclone is a low-pressure system existing in the tropical or subtropical latitudes (anywhere from the equator to about 50°N) that has characteristics of both tropical cyclones and extra-tropical cyclones. Therefore, many of these cyclones exist in a weak to moderate horizontal temperature gradient region, but also receive much of their energy from convective clouds. If the maximum sustained winds are greater than or equal to 18 m/s they are called subtropical storms.

(a) Maps of station used

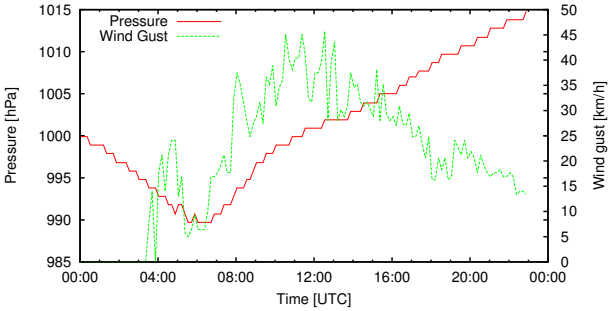

(b) Alhaurin

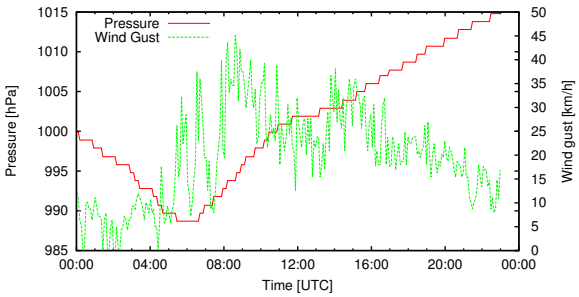

(c) Estepona

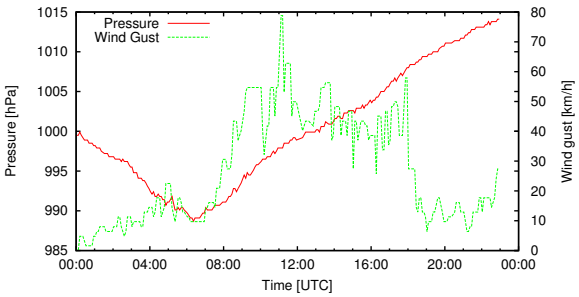

(d) El Palo

Figure 2.3.: Pressure and wind data from weather stations showed in the map.

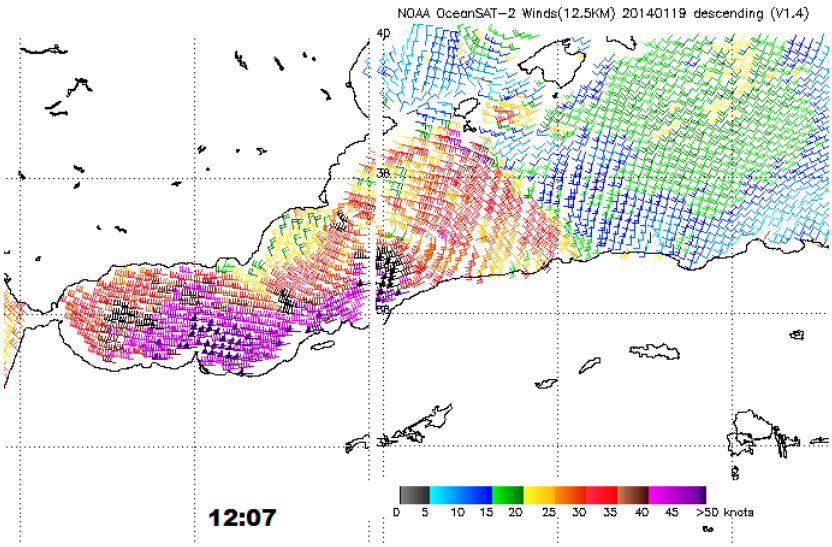

Figure 2.4.: Wind retrieved from OSCAT satellite data.

AQUA (Figure 2.7) showed a quite interesting cloud pattern with a visible eye and multiple cumulonimbus clouds with top temperature of about 227 K (not shown). In this stage of development, the cyclone acquired several features of TLCs, as showed later. Between 12 UTC and 16 UTC the cyclone moved to the East in the Tyrrhenian sea, making landfall on

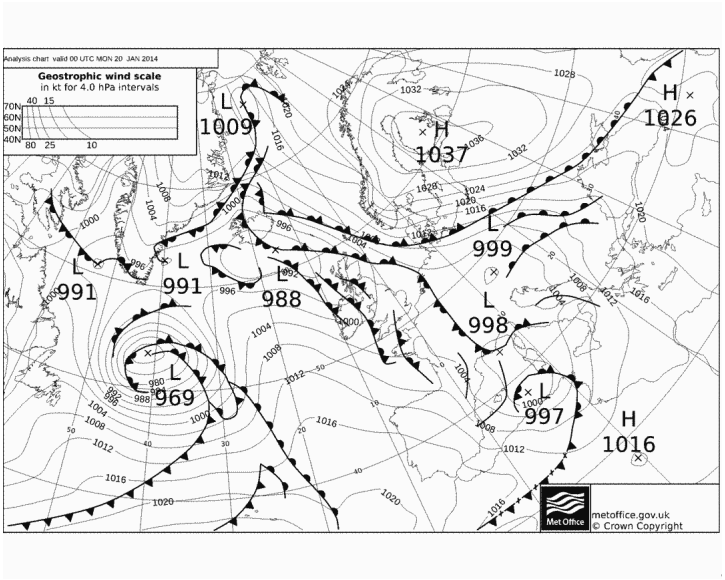

Figure 2.5.: MetOffice daily analysis with pressure contour and fronts drawed on the map. 20 January 2014 - 00 UTC

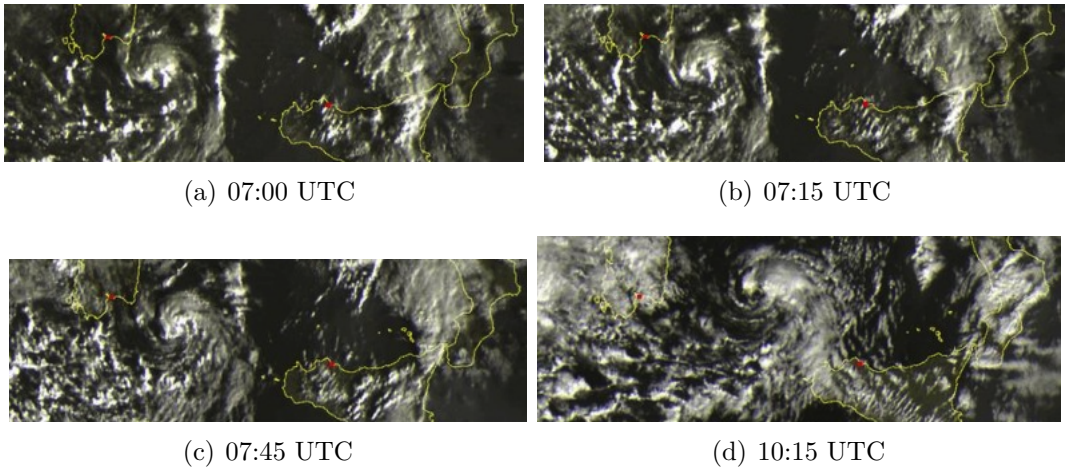

(a) 07:00 UTC

(b) 07:15 UTC

(c) 07:45 UTC

(d) 10:15 UTC

Figure 2.6.: Satellite imagery sequence (20 January 2014 from 07 UTC to 10 UTC)showing the new born of the cyclone.

the coast of Campania, between Naples and Salerno.

2.1.1. Analysis of landfall over Italy

It has been shown (Moscatello et al. [80] ; Davolio et al. [31]) that the small scale of this vortexes (few tens of km) cannot be resolved by coarse resolution NWP models but only with observational analysis. Therefore, landfall and land cross of this system can provide insight into the study of the mesoscale structure. Figure 2.8 shows the satellite imagery related to the instants immediately preceding the landfall. In all pictures, the

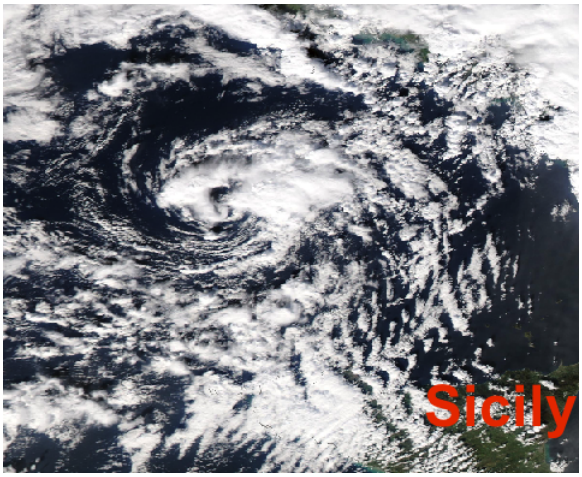

[!htb]

Figure 2.7.: MODIS Aqua Image acquired on 20 January 2014 12 UTC .

spirally distributed cloud bands are evident, while an overshooting top is quite noticeable in the first two instants. Using the images presented in Figure 2.8 and data from the weather

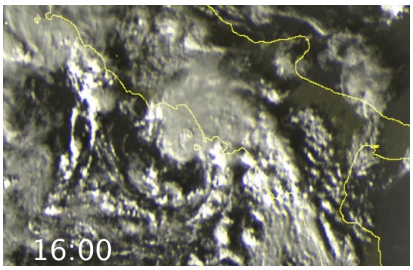

(a) 15:00 UTC

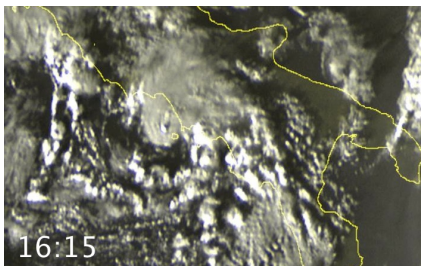

(b) 15:15 UTC

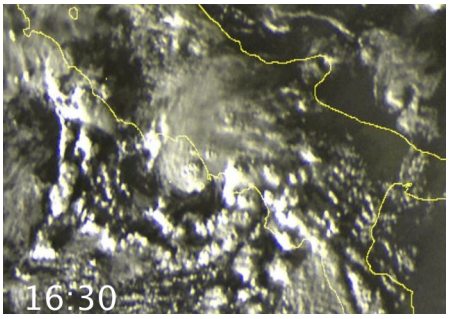

(c) 15:30 UTC

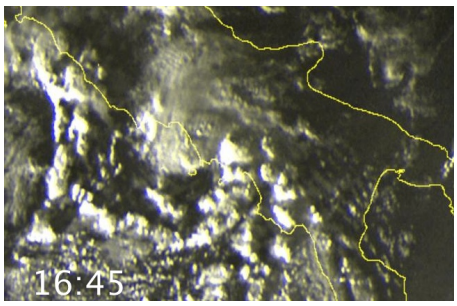

(d) 15:45 UTC

Figure 2.8.: Satellite imagery sequence (20 January 2014 from 16 UTC to 16:45 UTC) showing the landfall of the cyclone on Naples' coast.

stations, it can be inferred that the low pressure minimum made landfall at about 15:45 UTC near Naples. Unfortunately, the data from the Campania regional weather stations network are unavailable, so unofficial weather data were used instead. The weather station of Procida island reported a maximum wind gust of 98 km/h at 15:45 UTC and a minimum

pressure of 994 hPa a few minutes earlier (not shown). Several weather stations near Naples reported a sudden drop of pressure, as showed in Figure 2.9. An interpolation of pressure

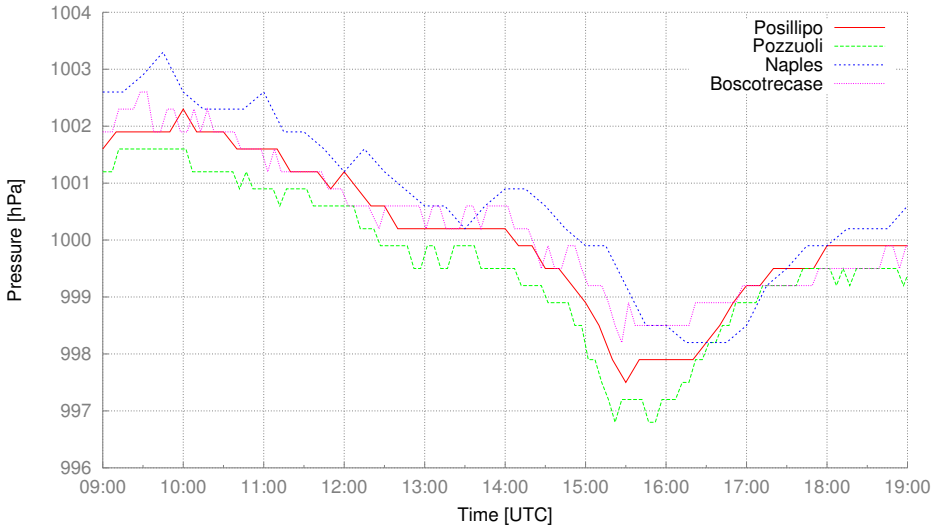

Figure 2.9.: Pressure from several weather stations along the Naples coastline as a function of time (UTC).

data from weather station network could be helpful in discriminating the minimum transit over land and has been tried. However, the presence of orography and the lack of data result in a contamination of the MSLP maps that make this investigation useless. The lightning detection network Blitzortung showed a moderate activity over the Thyrrenian Sea with over 400 strikes between 12 UTC and 18 UTC (not shown). Later on, the cyclone interaction with Italian orography became more significant and no vortex signature was detected in satellite imagery, until the low pressure system made contact with Adriatic Sea in the late evening of 20 January.

2.1.2. The final phase over the Adriatic Sea

Afterwards, the cyclone firstly moved eastward towards Croatia, but then started to follow a circular trajectory that gave it a South-Westward direction. At about 11 UTC of 21 January the cyclone had gained strength again and the spirally distributed cloud bands were visibile in the satellite imagery (not shown). During the following hours the cyclone continued to move southward, following the Italian coastline of Adriatic and producing moderate precipitations, as shown in infra-red satellite and radar imagery reported in Figur 2.10. Several weather stations located on the Adriatic Sea, between Ancona and San Benedetto del Tronto, reported accumulated precipitations up to 40 mm. In this phase, the cyclone acquired again the characteristic features of a TLC. As the cyclone moved farther to the South, the cloud structure related to the low pressure system began to shrink until the air mass made contact with the Gargano Peninsula (Southern Italy). The interaction with orography led to the formation of a minimum on the eastern side of the peninsula in the late morning of 22 January. At 10 UTC the image acquired by TERRA satellite (Figure 2.11) showed again spirally distributed cloud bands, although convection appeared much weakened

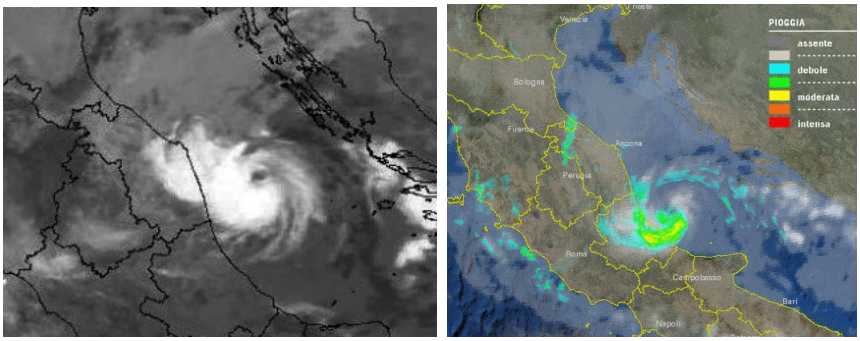

(a) NOAA POES Satellite Infrared Image acquired on 21 January 2014 at 16:13 UTC

(b) Precipitation Intensity retrieved from radar measurement on 21 January 2014 at 16:45 UTC; data from Italian national radar mosaic

Figure 2.10.: Satellite and Radar imagery of 21 January 2014 afternoon.

in comparison to the previous day. Seven hours later the cyclone was making landfall over

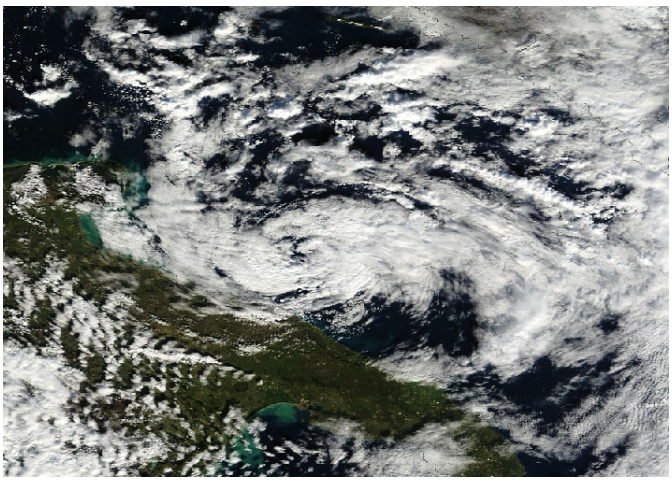

Figure 2.11.: MODIS Terra Image acquired on 22 January 2014 10 UTC .

the coast of Albany where it vanished.
Satellite imagery and MSLP analysis made possible an accurate inspection of the cyclone trajectory during the entire lifecycle, from 19 January 2014 to 22 January 2014. Figure 2.12 shows the trajectory obtained with the analysis of all data presented before.

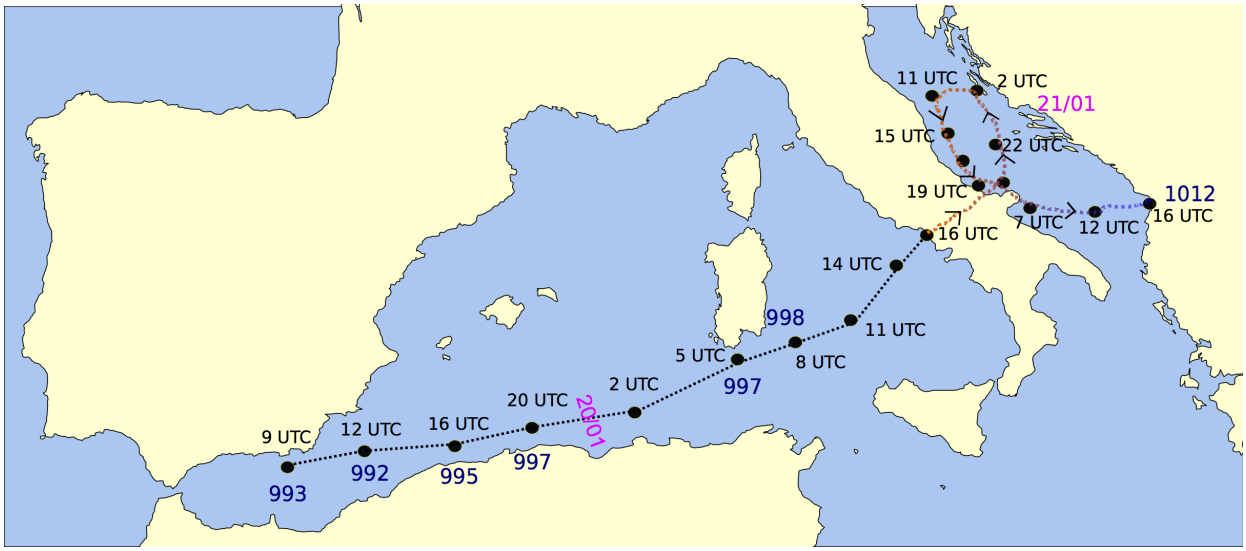

Figure 2.12.: Cyclone trajectory with time (black) and pressure minimum (blue) superimposed.

3

The GLOBO, BOLAM and MOLOCH meteorological models

In this chapter a short description of the BOLAM (BOlogna Limited Area Model), GLOBO (Global version of BOLAM), and MOLOCH (LOCal MOdel) NWP models developed at CNR-Institute of Atmospheric Sciences and Climate (ISAC) (Bologna) is presented.

3.1. The BOLAM model

The BOLAM model was first created in 1992, and continuously developed over the following years (Buzzi et al. [15]; Malguzzi and Tartaglione [68]; Buzzi and Foschini [16]; Malguzzi et al. [67]). The model was tested and compared with many other mesoscale Limited Area Models (LAMs), over the Comparison of Mesoscale Prediction and Research Experiments (COMPARE) multi-annual project organized by the World Meteorological Organization (WMO). A model inter-comparison was conducted on a case of mid-latitude explosive cyclogenesis (Gyakum et al. [46]), on a well documented case of flow over orography in the presence of lee waves and wakes (Georgelin et al. [44]), and on a case of explosive development of a tropical cyclone over the Pacific (Nagata et al. [82]). BOLAM turned out to be the second best model in the first case and the best one in the other cases. Further tests confirmed its satisfactory performance. The BOLAM model is being used operationally by various Italian national agencies and regional meteorological services, by the National Observatory of Athens in Greece, by the National Center for Hydrological and Meteorological Forecasting (NCHMF) of Vietnam. Recently, a chemical and aerosol transport model BOLCHEM has been developed at ISAC, starting from the BOLAM dynamical core.

3.1.1. BOLAM main features

BOLAM is a hydrostatic LAM based on the time integration of the *primitive equations*. The prognostic variables are the wind components u and v, the virtual temperature T_v, the surface pressure p_s, the specific humidity q and the turbulent kinetic energy TKE. The

primitive equations are summarized in the following equalities.

$$
\begin{aligned}
\frac{\partial u}{\partial t} &= uv\frac{\tan\varphi}{a} + fv - \frac{u}{a\cos\varphi}\frac{\partial u}{\partial\lambda} - \frac{v}{a}\frac{\partial u}{\partial\varphi} - \dot{\sigma}\frac{\partial u}{\partial\sigma} - \frac{R_d T_v \sigma^\alpha}{a\cos\varphi p}\frac{\partial p_s}{\partial\lambda} - \frac{1}{a\cos\varphi}\frac{\partial\Phi}{\partial\lambda} + K_u \\
\frac{\partial v}{\partial t} &= -u^2\frac{\tan\varphi}{a} - fu - \frac{u}{a\cos\varphi}\frac{\partial v}{\partial\lambda} - \frac{v}{a}\frac{\partial v}{\partial\varphi} - \dot{\sigma}\frac{\partial v}{\partial\sigma} - \frac{R_d T_v \sigma^\alpha}{a\cos\varphi p}\frac{\partial p_s}{\partial\varphi} - \frac{1}{a\cos\varphi}\frac{\partial\Phi}{\partial\varphi} + K_v \\
0 &= \frac{\partial}{\partial t}\left(\frac{\partial p}{\partial\sigma}\right) + \frac{\partial}{\partial x}\left(u\frac{\partial p}{\partial\sigma}\right) + \frac{\partial}{\partial y}\left(v\frac{\partial p}{\partial\sigma}\right) + \frac{\partial}{\partial\sigma}\left(\dot{\sigma}\frac{\partial p}{\partial\sigma}\right) \\
\frac{\partial T_v}{\partial t} &= -\frac{u}{a\cos\varphi}\frac{\partial T_v}{\partial\lambda} - \frac{v}{a}\frac{\partial T_v}{\partial\varphi} - \dot{\sigma}\frac{\partial T_v}{\partial\sigma} - \frac{R_d T_v \omega}{c_p p} + K_T + F_T \\
\frac{\partial q}{\partial t} &= -\frac{u}{a\cos\varphi}\frac{\partial q}{\partial\lambda} - \frac{v}{a}\frac{\partial q}{\partial\varphi} - \dot{\sigma}\frac{\partial q}{\partial\sigma} + K_q + F_q \\
\frac{\partial\Phi}{\partial\sigma} &= -R_d T_v \frac{p_0 - \alpha(p_0 - p_s)\sigma^{\alpha-1}}{p} \\
p &= \rho R_d T_v
\end{aligned}
$$

whit obvious notation (see [55] and Appendix D). This group of equations forms the core of the model, also called *dynamic*. The F terms represent the contribution to the temporal trends due to non-adiabatic processes (also called *physics*), i.e. the physical processes that cause heating or cooling and phase changes of water. The K terms represents the contribution arising from the parameterization of turbulent processes (vertical diffusion).
The water cycle for stratiform precipitation is described by means of five additional prognostic variables: cloud ice, cloud water, rain, snow and graupel. The purpose of the model is to predict the future state of the atmosphere once fields at the initial time (analysis) and the boundary conditions on the frame of the integration domain are known. The model prognostic variables (wind speed, pressure, temperature, specific humidity, snow cover, specific concentration of liquid and ice clouds and hydrometeors and quantities that define the state of the soil) are distributed in the vertical on a non-regular Lorenz grid (see Lorenz [65]), with higher resolution in the atmospheric boundary layer near the surface. The vertical discretization is based on a hybrid vertical coordinate system, in which the terrain-following sigma coordinate $\sigma = p/p_s$ gradually tends to a pure pressure coordinate with increasing height above the ground. The relaxing factor from σ to p is prescribed as a function of the orography height in the domain and is defined as:

$$\alpha \leq \frac{p_0}{p_0 - \min p_s} \tag{3.1}$$

The pressure value at a fixed value of σ is computed as

$$p = p_0\sigma - (p_0 - p_s)\sigma^\alpha \tag{3.2}$$

where p_s designates surface pressure and p_0 is a reference pressure. Figure 3.1 shows an example of this coordinate on a bell-shaped mountain. The horizontal discretization is based on a staggered Arakawa C-grid (Arakawa and Lamb [4]) in (optionally) rotated geographical coordinates (latitude-longitude). In the rotated system the equator is located at the cen-

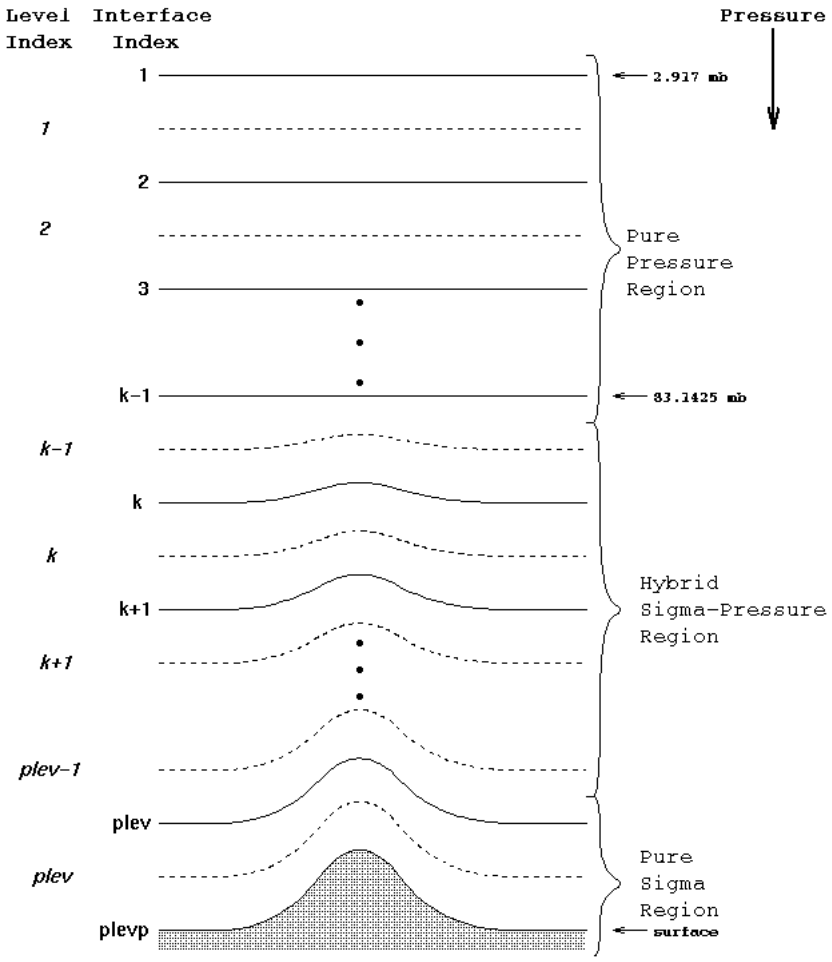

Figure 3.1.: Vertical discretization obtained by using the hybrid coordinate system described in the text.

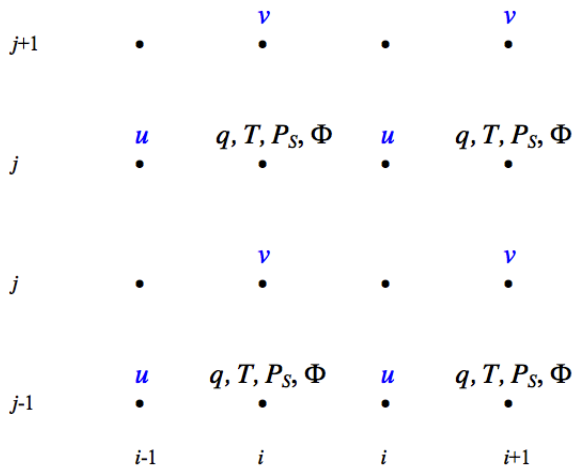

Figure 3.2.: Horizontal discretization of BOLAM data fields on the Arakawa C type grid.

ter of the integration domain, which has rectangular shape; this stratagem minimizes grid anisotropy caused by the convergence of meridians toward the pole. The advection scheme implemented is the Weighted Average Flux (WAF) scheme (Billet and Toro [8]). The temporal integration scheme employed is an explicit time-split, except for sound waves which are vertically propagated via an implicit scheme; a forward-backward one is used for gravity modes. The time-split scheme allows to treat motions of different time scales separately, as well as requiring the storage of only one level of temporal prognostic variables, minimizing the Random Access Memory (RAM) utilized for the simulation.

3.1.2. BOLAM parametrizations

The physic parametrizations are essential in order to account for the small-scale phenomena that happen at a spatial scale smaller than the model grid spacing. Every model makes use of a different set of parametrizations that are continuously updated as the micro-physical processes study goes further. The BOLAM physics includes atmospheric water cycle, turbulence and orographic drag, surface and soil processes, and radiation.

Water cycle

The atmospheric water cycle scheme is based on the explicit assumptions of spectral distributions of clouds (droplets and ice crystals) and of liquid and solid hydrometeors. The spectral properties of hydrometeors are simulated assuming a generalized gamma function distribution. The main processes described by the micro-physical scheme are:

- nucleation of cloud water (cw) and of cloud ice (ci);
- condensation and evaporation of cw;
- freezing of cw;
- nucleation sublimation and melting of ci;
- auto-conversion of cw and ci;
- sublimation of snow and graupel in both directions;
- collection-accretion-riming : 13 different hydrometeor interaction processes involving rain (freezing or not), snow and graupel (dry or melting), cw and ci;
- melting and evaporation of hydrometeors;
- terminal fall speeds computation and fall process, using a conservative-diffusive backward-upstream integration scheme;
- thermodynamic feedback based on enthalpy conservation.

The effects of deep moist convection development are parameterized using the Kain-Fritsch convective scheme (Kain and Fritsch [57]), updated to its latest revision (Kain and Fritsch [56]). Parameterization of shallow moist convection is also implemented as comprised in that scheme, with some modifications.

Turbulence and orographic drag

The surface layer and the planetary boundary layer are modelled accordingly to the similarity theory (Monin and Obukhov [77]). The mixing-length based turbulence closure model, widely used to compute the Atmospheric Boundary Layer (ABL) fluxes for atmospheric modelling, is applied to parameterize the turbulent vertical diffusion of momentum, heat and moisture. The turbulence closure is of order 1.5 (E-l scheme, Zampieri et al. [117]), in which the Turbulent Kinetic Energy (TKE) is predicted. In order to account for buoyancy effects in a stratified ABL, the Blackadar mixing length (Blackadar [10]) is used together with stability functions depending on the Richardson number. For the unstable ABL case, a modified version of the non-local mixing length of Bougeault and Lacarrere (Bougeault and Lacarrere [11]) is applied. The roughness length is computed as a function of vegetation and of sub-grid orography variance. Over the sea, a Charnock roughness parameter (Charnock [26]) is employed, accounting for the wave height as a function of the surface wind speed. The SST is computed, depending on the latent and sensible heat fluxes and radiative fluxes, using a simple slab ocean model. A parameterization of the orographic wave drag, associated with the deceleration of the mean flow passing over orography, is applied.

Surface, soil and vegetation processes

A soil model using 4 to 6 layers is also employed. The layer thickness increases with depth, from a few cm to more than 1 m. The model evaluates surface energy, momentum, water and snow balances, heat and water vertical transfer, vegetation effects at the surface (evapotranspiration, precipitation interception, wilting effects etc.) and within the soil (extraction of water by roots). The geographical distribution of different soil types and physical features is also accounted for, as well as water freezing and melting effects.

Radiation

The atmospheric radiation is computed with a combined application of the RG scheme (Ritter and Geleyn [97]) and the ECMWF scheme (Morcrette [79]; Mlawer et al. [76]). Since the ECMWF scheme is much more computationally expensive than the RG scheme, it cannot be applied at each time step and each grid column; therefore, the RG scheme is preferentially employed, being applied extensively at all grid points and in rapid update mode, whereas the ECMWF scheme is applied at alternate points and at long intervals to compute corrections to the RG scheme. The ECMWF radiation library includes definitions of the *climatology* (seasonal and geographical distribution) of different types of aerosol and of atmospheric composition. The model has been recently upgraded so that all the inputs (astronomical functions, aerosol, ozone, greenhouse gases, albedo, emissivity and clouds) are now fully consistent between the two (GR and ECMWF) schemes.

3.1.3. BOLAM software features

The entire BOLAM code is written in Fortran 90 language. The model is fully parallelized through the domain splitting technique. The horizontal domain of the model is discretized

into a set of GNLON points in the longitudinal direction and GNLAT points in the latitudinal direction. Parallelism is achieved by dividing the physical domain in NPROCSX for NPROCSY parts and assigning a different process to each subdomain, to be run on processors (*core*) or on virtual process of the same processor(*hyper-threading*). The dimensions of the subdomains matrices are contained in the integer parameters NLON and NLAT. Since the relationships between these parameters to the global ones are[1]

$$\begin{cases} \text{NLON} = \frac{\text{GNLON}-2}{\text{NPROCSX}} \\ \text{NLAT} = \frac{\text{GNLAT}-2}{\text{NPROCSY}} \end{cases} \tag{3.3}$$

the choice of global dimension GNLON and GNLAT must correspond to integer values of NLON and NLAT computed using equation 3.3. BOLAM highest suitable resolution is limited by the hydrostatic approximation and the parameterization of convection, being typically 6 to 8 km. In this work a resolution of 0.075 × 0.075 (8.3 km) is used. For accurately simulating smaller space scales, one-way nested simulations may be performed, typically by nesting the MOLOCH model into BOLAM. However, operational use of MOLOCH models require great computational power, thus MOLOCH nesting is usually performed using GFS forecasts. BOLAM acts as a means to conveniently proceed from larger to smaller scales, thereby reducing integration time and enhancing accuracy.

3.1.4. BOLAM domain

The BOLAM domains used in this work have different size in dependence of the type of investigation conducted. In Figure 3.3 the domain used in chapter 4 is shown. In chapter 5

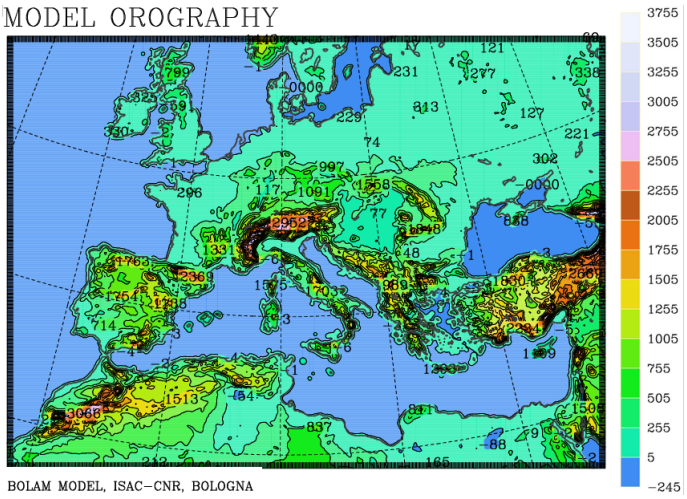

Figure 3.3.: BOLAM domain and orography used in chapter 4 .

an extended domain is used, as shown in Figure 3.4.

[1]The supercomputer used in this work use NPROCSX=NPROCSY=8.

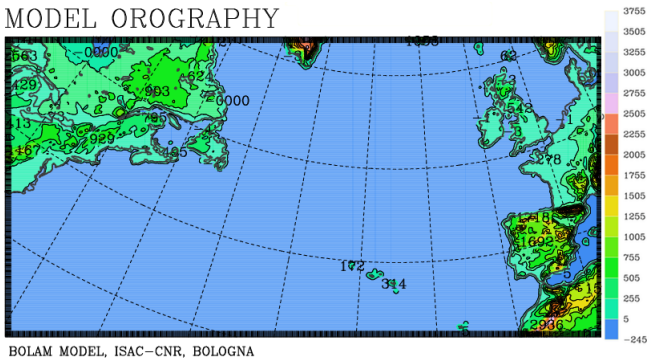

Figure 3.4.: BOLAM domain and orography used in chapter 5 .

3.2. The GLOBO model

The GLOBO model is a grid-point based Atmospheric General Circulation Model (AGCM) that integrates the atmospheric equations on a regular latitude/longitude grid. The GLOBO model shares with the BOLAM model most of dynamical and physical aspects, although the grid geometry differs considerably near the Poles, where special filtering techniques (digital and Fourier) are applied to cope with the singularity in regular latitude-longitude coordinates. The SST evolution is modelled with a mixed layer ocean. A full description of the dynamics and physical parameterizations of the model is given in Malguzzi et al [66]. GLOBO is currently used at ISAC-CNR to produce 6-day global forecasts, at the resolution of 0.29 $\times$ 0.40 degrees and 60 levels, using NOAA-GFS analysis fields as initial conditions. In this work GLOBO has been used with GFS Analysis fields to run 72 h simulations that have been used as initial and boundary condition for BOLAM (or MOLOCH) model forecast.

3.3. The MOLOCH model

MOLOCH is a non-hydrostatic, fully compressible, convection resolving model initially created at ISAC-CNR in 2002. It has been developed in order to perform forecasts with higher spatial detail, allowing an explicit representation of convective phenomena. The MOLOCH model is currently being employed in real-time forecasting by several Italian agencies (for instance, Regione Liguria uses it for public weather forecasting). Furthermore, it is being used for real-time weather forecasting at the CNR-ISAC institute in Bologna on behalf of the National Civil Protection Department.

3.3.1. MOLOCH main features

MOLOCH integrates the non-hydrostatic, fully compressible equations for the atmosphere, with a resolution of 0.027 $\times$ 0.027 degrees, equivalent to 2.98 km, and 50 vertical levels. Although the horizontal resolution in the operational model was brought to 0.014 $\times$ 0.014 degrees (1.55 km) since 20 February 2014, in this work a coarser resolution was used. The set of prognostic variables (pressure p, absolute temperature T, specific humidity q, hori-

zontal (u, v) and vertical w components of wind velocity, turbulent kinetic energy TKE and five water species) are represented on the latitude-longitude, optionally rotated, Arakawa C-grid. MOLOCH shares several features with BOLAM, although a fundamental difference concerns the vertical coordinate. A hybrid terrain-following coordinate ζ, smoothly relaxing to horizontal surfaces with increasing height, as implicitly defined by equation 3.4, is employed.

$$\zeta = H\left(1 - \mathrm{e}^{-\frac{z-h(1-\zeta/H)}{H}}\right) \tag{3.4}$$

Here, h is the height of the orography $(h(x.y) \leq z \leq \infty)$, $H = \frac{R_d T_0}{g}$ is the troposphere scale height and T_0 a reference temperature. Model dynamics are integrated in time with an implicit scheme for sound waves vertical propagation, while explicit, time-split schemes are implemented for the remaining terms of the equations of motion. Three-dimensional advection is computed using the Eulerian Weighted Average Flux scheme, just like in BOLAM. Horizontal second-order diffusion and a small divergence damping are included to prevent energy accumulation to small spatial scales.

3.3.2. MOLOCH parametrizations

The physical scheme consists of atmospheric radiation, sub-grid turbulence, water cycle microphysics, and a soil model with vegetation. These features are similar to those of the BOLAM model scheme. However, specific differences are introduced in the MOLOCH scheme in order to treat the processes characterizing convective systems. In particular, the MOLOCH scheme has the capability of describing the so-called two-moment microphysics, by integrating in time the spatial distribution of the number density of *cw* and *ci* , describing the cloud spectra evolution.

3.3.3. MOLOCH domain

The MOLOCH model is used only in Chapter 4, so the domain employed roughly coincides with the BOLAM one.

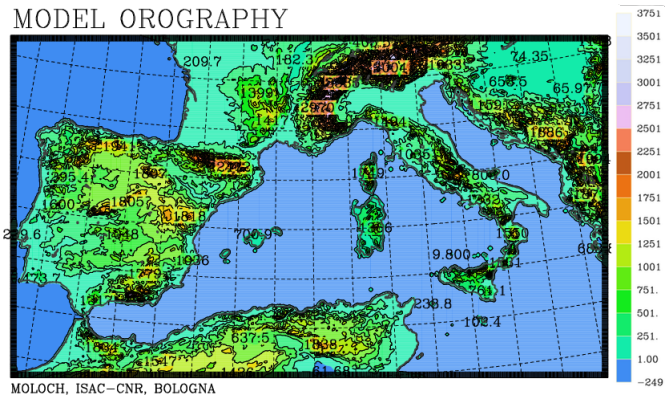

Figure 3.5.: MOLOCH domain and orography used in chapter 4 .

3.4. Models execution process

The BOLAM and MOLOCH models need the initial and boundary conditions in order to integrate the equations of motion within a selected domain. The GLOBO forecast or ECMWF analysis are employed as such fields for both models. The GLOBO model require itself an initial condition, which is obtained by processing the GFS analysis and eventually generating an `inicom.mhf` file[2]. The GLOBO 72h forecasts, contained in the file `globolam.mhf`, are then used to initialize the BOLAM or MOLOCH simulation by a one-way nesting. In this stage, the so called *pre-processing* stage, several interpolations of data fields take place, in order to obtain data compatible with the resolution domain indicated in the *configuration file*(`.inp`). Several output file (`input_i.mhf` where `i` varies between 1 and the last time step) are eventually generated, which will be subsequently used as initial and boundary conditions during the actual simulation. The BOLAM output file (`bolam.mhf`) can be used in the same manner described before, to nest a MOLOCH simulation. The model output file is finally post-processed and a `.ppf` file (ASCII format), containing all output fields in readable format, is generated. This is compatible with graphics software such as NCAR Command Language (NCL) Graphics, which can plot the requested meteorological fields using the model levels. The post-processing executable is modified in Chapter 4, allowing the possibility to write a binary file (`data1.bin`) containing all data required for cyclone tracking (MSLP value, lat-lon coordinates) and thermal analysis (Geopotential Height values on all pressure levels).
All the simulations are performed on the Debian Gnu Linux computer cluster *Vivaldi*, composed of 4 nodes dual Intel Xeon X5550 (2×4 core multi thread) and a I7-2700K master.

[2] `mhf` stands for Model History File.

4

The Mediterranean phase: Thermal and Dynamical analysis

4.1. Introduction

Mediterranean TLCs often form and dissipate over open sea, thus making an objective analysis really difficult due to the lack of data (no weather stations, only a few buoys). While this is true also for Hurricanes, the much bigger dimension of the latter systems makes an indirect analysis more reliable. In fact, only after the advent of satellite data imagery, the evidence of these Mediterranean *Hurricanes* started to emerge. Satellite data provide the only reliable way to discern the peculiar characteristics of *Medicanes* like the free-cloud eye and the spirally distributed cloud bands. Given the very small scales of these systems (few tens of km) compared to Hurricanes or Typhoons, operational analysis and NWP models with coarse spatial resolution often fail to detect and predict their strength and trajectory. Over the last few years there have been numerous attempts to simulate these systems using LAMs nested in General circulation models (GCMs): Miglietta et al.[72], Moscatello et al. [81], Homar et al. [52], Fita et al. [41], Phytharoulis et al. [88], Davolio et al. [31], Reed et al. [94], Lagouvardos et al. [62]. In most of these cases the model predicted fairly well the observed behaviour of the system, even though the cyclone minimum and trajectory do not always correspond to those deduced from satellite imagery. However, as pointed out before, the simulation data can be compared with observations only if the cyclone cross land at least once. In particular, the cyclone of 26 September 2006 crossed an area of Southern Italy characterized by an high density of observational data (2 radar and a meso-network of weather stations). The results presented in Moscatello et al. [80] provides unrivaled experimental evidence of the mesoscale structure of a MTLC. Given the low resolution of operational analysis, a study of Mediterranean *Hurricanes* is suitable only using LAM data output with finer resolution, or using downscaling techniques (Cavicchia et Von Storch [20]).

4.2. Cyclone detection and tracking

Several methodologies for the detection and tracking of cyclones in general have been proposed by many authors (Picornell et al. [87]; Hart [48]; Cavicchia et al. [20]). In particular, Picornell [87] suggested the following criteria in order to detect the position of a cyclone center at a given instant:

- relative minimum in the MSLP field;
- mean pressure gradient greater than (or equal to) 0.5 hPa per 100 km at least in six of the eight principal directions around the minimum (for the detection of Medicanes a more restrictive threshold of 3.2 hPa per 100 km is used).

In the aforementioned paper, the cyclone domain is limited by the zero-vorticity line surrounding the minimum pressure position, and the 700 hPa level is considered as the *steering level* for the cyclone displacement. However, the proposed criteria are too complicated to be implemented and not all necessary in the present analysis. Since there is no need to develop an algorithm suitable for a long-term climatology, but only for one case study, the code developed for this work has been tuned in order to obtain good agreement with the observational data presented in Chapter 2. In particular, the FORTRAN language was used to create an algorithm that detects and tracks the pressure minimum over the GLOBO, BOLAM and MOLOCH domains. In order to achieve this goal, MSLP field, geopotential height at pressure levels and other metadata (land-sea mask, lat-lon coordinates of the model grid, hour of forecast) were saved into a binary file. Afterwards, the file was read by the FORTRAN algorithm that detects and tracks the MSLP minimum by following the steps described below:

1. At the first time instant the algorithm carries out a MSLP minimum search over a fraction of the model domain considering only grid points over the sea [1];
2. At the second time instant the algorithm carries out the same MSLP minimum search, following the rules defined in the previous point;
3. From the third time instant onwards, the algorithm performs a MSLP minimum search in a box centred on a grid point which is located on the straight line passing through the coordinates of the last two known positions (see Figure 4.1). In this way, a first guess of the pressure minimum position (black point in Figure 4.1) is found, assuming that the cyclone center moved from the last known positions with a constant speed.

The box size is suitably chosen in order to find always a single minimum. A constraint of this type is needed in order not to compromise the cyclone tracking when multiple pressure minima are located near the cyclone center. In this way, the coordinates of the MSLP minimum and its value, are saved every hour. This technique proved to correctly detects and follows the minimum over the entire domain, even when the system crossed Italy and interacted with orography. Figure 4.2 shows the cyclone path, obtained with this algorithm and plotted on the Mediterranean area topography.

[1] This is achieved using the `fmask` (land-sea mask) available in the BOLAM, MOLOCH and GLOBO models.

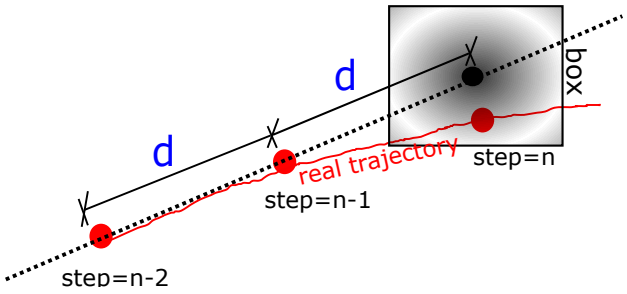

Figure 4.1.: Graphical explanation of the tracking algorithm.

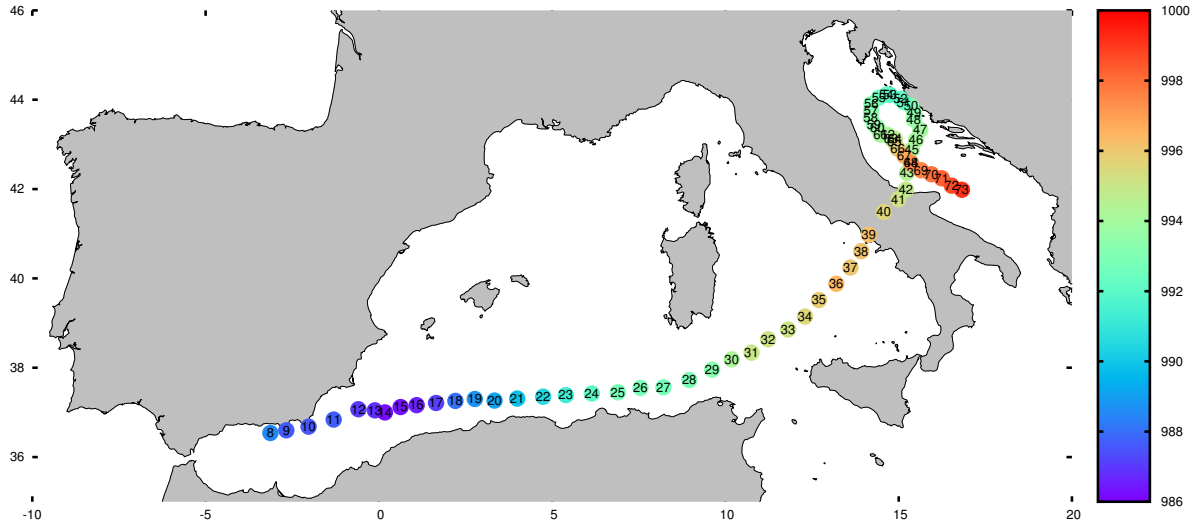

Figure 4.2.: Example of cyclone track obtained with the algorithm explained in the text. The color palette represents minimum pressure value, while the number superimposed on the colored points identify the hour of the simulation.

4.3. Cyclone Phase Space description

The formation, development and decay of TLCs can be investigated using a classification of the three-dimensional nature of the cyclone structure, referred to here as *cyclone phase*. Using the temporal variation of the *cyclone phases* it is possible to construct a phase space which represents the history of the cyclone. A productive phase space would require parameters that simultaneously describe the strength of the warm/cold core structure together with the stage of extra-tropical development (formation, intensification, occlusion and decay). Hart [48] proposed a cyclone phase space based on three parameters: the lower-tropospheric thermal asymmetry B, the lower-tropospheric thermal wind V_t^{L} and the upper-troposheric thermal wind V_t^{U}. While a complete description of the cyclone structure requires the synthesis of the model diagnostics data (e.g. potential vorticity, cyclone tilt..) and direct observations (satellite data, surface data), the three chosen parameters successfully summarize the cyclone phase in a graphical and intuitive way.

4.3.1. Cyclone thermal asymmetry

The large-scale horizontal temperature gradient concur to some fraction of extra-tropical cyclones development, giving an asymmetric or frontal nature to the system. Conversely, the development of tropical cyclones is not affected by large-scale horizontal temperature gradients. Furthermore, the strength of the temperature gradients in the former groups (tropical/extra-tropical) varies with time, depending on the stage of cyclone development. Therefore, the frontal nature of the cyclone (or lack thereof) and its sign are fundamental indicators of the type of the cyclone and of its stage of evolution. Hart suggests to describe this feature by means of the *storm-motion-relative low troposhere thickness asymmetry* parameter B defined as:

$$B = h(\overline{\Phi_{600\ \mathrm{hPa}} - \Phi_{900\ \mathrm{hPa}}}|_{\mathrm{R}} - \overline{\Phi_{600\ \mathrm{hPa}} - \Phi_{900\ \mathrm{hPa}}}|_{\mathrm{L}}) \tag{4.1}$$

where Φ is the geopotential isobaric height, R (L) indicates right (left) of current storm motion, and the overbar indicates the areal mean over a semicircle of radius R_{ex}, called *exploration radius*. The integer h takes a value of $+1$ for the Northern Hemisphere and -1 for the Southern Hemisphere, so it will be omitted from here onwards. Figure 4.3 shows the graphical representation of this parameter. Using the hydrostatic relationship and the ideal gases law the derivation of the hypsometric relation 4.2 is straightforward:

$$\Phi_2 - \Phi_1 = R_d \int_{p_2}^{p_1} T \, \mathrm{d}(\ln p) \tag{4.2}$$

where $1, 2$ are two isobaric levels, T is the temperature and p is the pressure. By comparing equations 4.1 and 4.2 it can be inferred that the parameter proposed by Hart measures a gradient of mean-layer (900-600 hPa) temperature perpendicular to the motion of the storm, and not simply the range of temperature across the cyclone circulation. As suggested by

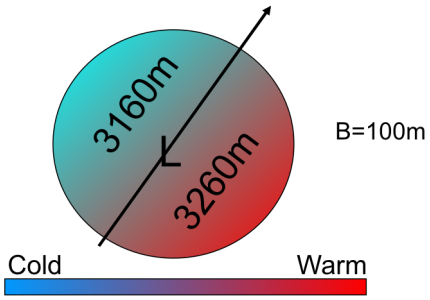

Figure 4.3.: Graphic representation of the mathematical expression in equation 4.1. The arrow indicates storm relative direction, while R_{ex} is the radius of the circle.

Picornell et al. [87], Chaboureau et al. [23], Miglietta et al. [75] the exploration radius of 500 km, proposed by Hart, can smooth out the warm-core structure typical of *Medicanes* and it's suitable only for studies related to large scale systems like Hurricanes. In the present work, after several attempts to use a time dependent radius, a constant radius of approximately 70 km is used instead[2]. As proposed by Picornell et al. [87] several pairs

[2]In Appendix B a formal motivation is given.

of lower-troposphere levels (700-900 hPa, 750-950 hPa) were tried instead, but the results showed no great dependence on these parameters, so the default 600-900 hPa were used. On the basis of the value assumed by B it's possible to distinguish various type and phases:

$B \gg 0$ developing extratropical cyclone; thermally asymmetric or frontal nature.

$B \simeq 0$ mature tropical cyclone; thermally symmetric or non-frontal nature.

The threshold proposed by Hart for distinguishing a tropical thermal gradient from a non-tropical thermal gradient is $B = 10\text{m}$.

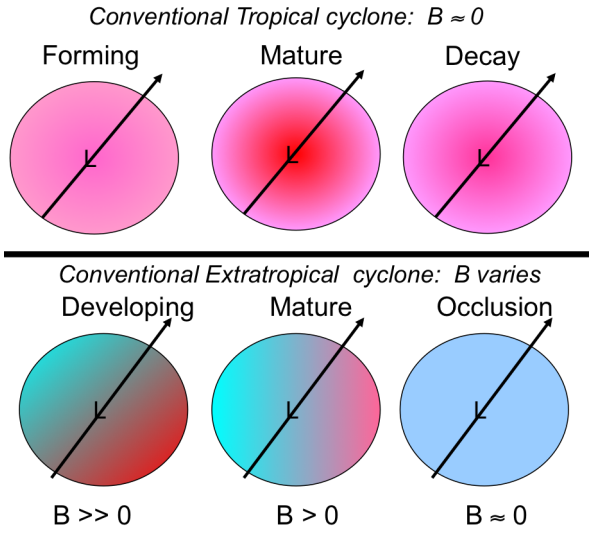

Figure 4.4.: Graphic variation of parameter B.

4.3.2. Cyclone cold and warm core

The thermal wind relationship

$$\mathbf{V}_g(z_2) - \mathbf{V}_g(z_1) = \frac{R}{f} \ln\left(\frac{p_1}{p_2}\right) \mathbf{k} \times \nabla\overline{T} = \frac{1}{f}\mathbf{k} \times \nabla(\Phi_2 - \Phi_1) = \mathbf{V}_t \tag{4.3}$$

symbolizes the link between the geostrophic wind variation with height and the horizontal mean temperature gradient, or the geopotential height perturbation $\Phi_2 - \Phi_1$. Thus, the change of geostrophic wind with height, above the surface cyclone center, detects the warm core (decrease) or cold core (increase) nature of the cyclone. Even though all cyclones possess both cold and warm core, depending on the atmospheric layer examined, in this work only the tropospheric phase is considered. The distinction between the aforementioned types of cores is made upon the examination of two tropospheric layers: 900-600 hPa, consistent with the definition of B, and 600-300 hPa. If the absolute value of the equation 4.3 is considered and the space derivative is discretized, the following equation is obtained

$$|\Delta\mathbf{V}_g| = |\mathbf{V}_t| = \frac{R}{f} \ln\left(\frac{p_1}{p_2}\right) \frac{\Delta\overline{T}}{d} = \frac{1}{f}\frac{\Delta\Phi}{d} \tag{4.4}$$

where the cyclone geopotential height perturbation $\Delta\Phi = \Phi_{\max} - \Phi_{\min}$ is evaluated within a radius of R_{ex} and d is the distance between the two extrema. Thus, the value of $\Delta\Phi$ computed from the model output data, is proportional to the magnitude of the thermal wind. Moreover, if the constants are neglected and a scaled thermal wind is considered, the vertical structure of the cyclone is defined as the vertical derivative of $\Delta\Phi$ on the pressure levels:

$$\frac{\partial \Delta\Phi}{\partial \ln p} = -|\mathbf{V}_t| \tag{4.5}$$

By performing a linear regression fit to the vertical profile of $\Delta\Phi$ into the two layers aforementioned two parameters are obtained, namely V_t^{L}, in the 900-600 hPa layer, and V_t^{U} in the 600-300 hPa layer. Positive values of $-|V_t|$ indicate a warm-core cyclone within the layer, while negative values indicate a cold-core cyclone.

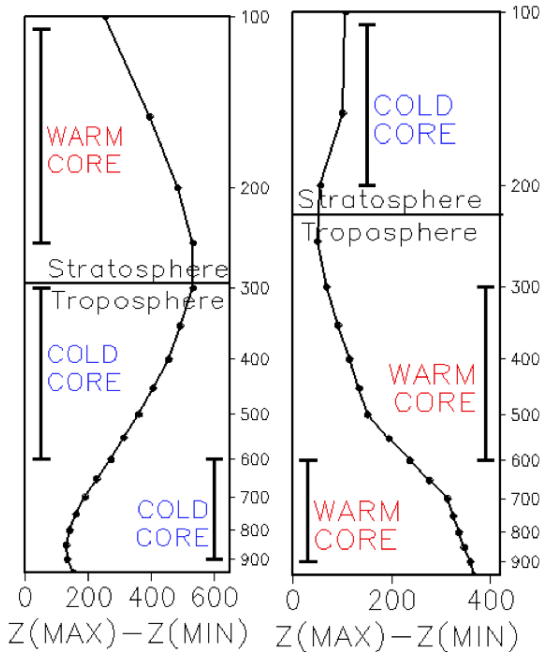

Figure 4.5.: Vertical profiles of $\Delta\Phi$ for two cases of the past proposed by Hart: Hurricane Floyd and Cleveland Superbomb. See [48]. Here $\Delta\Phi = \Delta Z$

However, some limitations of this method should be pointed out. In MTLCs, Ro $\gtrsim 1$ since $U \sim 25$m/s and $L \sim 200$km. Thus, the geostrophic approximation may not be valid, especially when the diameter of the cyclone drops below 100 km so that the centrifugal force is no longer negligible. The hydrostatic approximation affects the final results too, albeit to a lesser extent. In fact the strong updrafts found in the eye-wall are characterized by considerable vertical acceleration that makes the hydrostatic equilibrium a questionable approximation. While this is not a real problem in hurricanes, where horizontal scales are orders of 1000 km, the Hart parameters obtained in a case of small-scale TLC may be controversial.

4.3.3. The Hart diagram

The three parameters $B, V_t^{\mathrm{L}}, V_t^{\mathrm{U}}$ define the three-dimensional cyclone phase space which is presented using two cross sections through the idealised cube: $-V_t^{\mathrm{L}}$ versus B and $-V_t^{\mathrm{L}}$ versus $-V_t^{\mathrm{U}}$. The full life cycle of a cyclone can be described using the trajectory through the phase

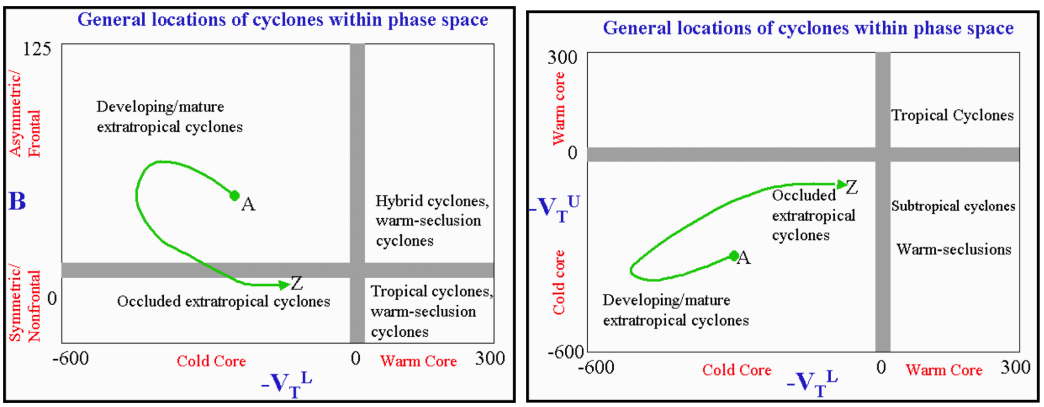

(a) $-V_t^{\mathrm{L}}$ versus B (b) $-V_t^{\mathrm{L}}$ versus $-V_t^{\mathrm{U}}$

Figure 4.6.: Examples of cyclone phase space projections, also known has Hart Diagram.

diagram, with time instants superimposed on the points colored according to the value of the minimum pressure. The latest advance in the assimilation and processing of NWP data made possible to create an algorithm that produces real-time phase space diagram for all the cyclones in the world, using GFS, ECMWF or other models. In particular, image similar to Figure 4.7, could help to identify and forecast a transition between the extra-tropical and tropical phases of the cyclone. It should be remembered that these graphs are obtained using forecast model data, and not analysis, so the nature of the cyclone may differ from the real one. Since only LAM and reanalysis have been used in literature to perform the Hart analysis, an attempt to use MOLOCH model data has been made, with encouraging results. The algorithms described has been extensively tested in two episodes of tropical cyclone and extra-tropical cyclone in Appendix A .

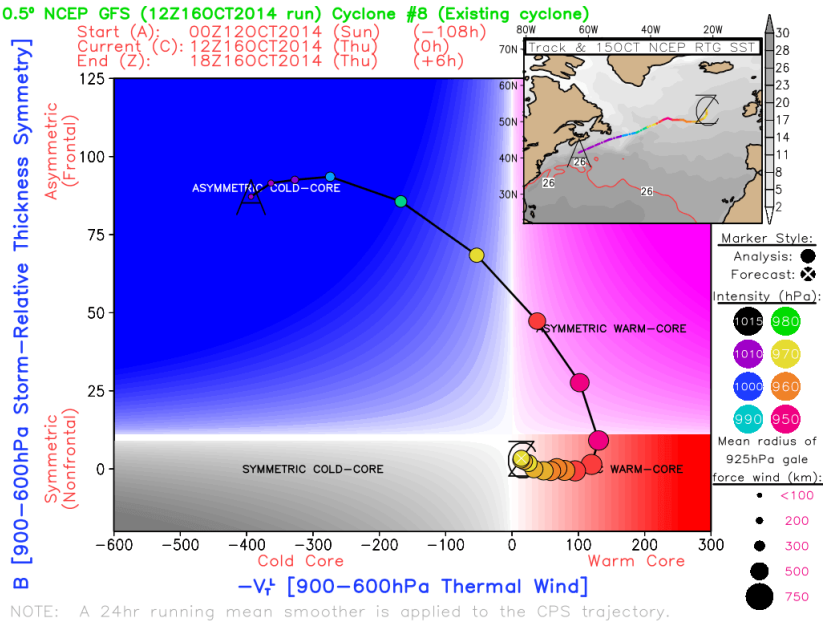

Figure 4.7.: Example of cyclone phase space projections available on the website `http://moe.met.fsu.edu/cyclonephase/`

4.4. Case studies and results

The event described in Chapter 2 has been analysed using several models combinations among the GLOBO, BOLAM and MOLOCH NWP models presented in Chapter 3. First

Identifier	Initial Condition	Initialization Time	GLOBO	BOLAM	MOLOCH	SST data
G1	NCEP	19/01/14 00 UTC	√			Model
B1	NCEP	19/01/14 00 UTC	√	√		Model
M1	NCEP	19/01/14 00 UTC	√	√	√	Model
M2	NCEP	19/01/14 00 UTC	√		√	Model
B2	ECMWF	19/01/14 00 UTC		√		Model
B3	NCEP	19/01/14 00 UTC	√	√		MyOcean
M3	NCEP	19/01/14 00 UTC	√	√	√	MyOcean
B1-20	NCEP	20/01/14 00 UTC	√	√		Model
B3-20	NCEP	20/01/14 00 UTC	√	√		MyOcean
B2-20	ECMWF	20/01/14 00 UTC	√	√		Model
M1-20E	ECMWF	20/01/14 00 UTC	√	√	√	Model

Table 4.1.: Overview of the different model combination used, identified by a unique case study identifier.

of all, GLOBO, BOLAM and MOLOCH models have been used in the *default* scenario: the initial condition was obtained from the NCEP-GFS model on 19 January 2014 at 00 UTC and SST was derived from the model analysis. All the models covered a 72 hours time integration. This setup is common to the G1, B1 and M1 cases.
In order to evaluate the sensitivity to SST, two simulations were performed with SST obtained from MyOcean (`http://www.myocean.eu/`) project, namely B3 and M3 cases.
The initial conditions were changed in several simulations, since early results shown great

dependence on these features. In B1-20, B3-20, B2-20 and M1-20E cases the simulations were initialized one day after, on 20 January 2014, so as to evaluate the cyclone behaviour in the last phase of development. For this reason, these simulations covered only a 48 hours time integration. In these last cases also the SST definition and the initial condition origin (ECMWF or GFS) were changed, in B3-20 and B2-20 cases, respectively. For each one of the cases presented in Table 4.1 an analysis of the trajectory and of the cyclone phase space has been conducted, and the results are shown below.

4.4.1. Case G1

Identifier	Initial Condition	Initialization Time	GLOBO	BOLAM	MOLOCH	SST data
G1	NCEP	19/01/14 00 UTC	√			Model

The GLOBO model has been used with initial conditions provided by the GFS-NCEP analysis. Figure 4.8 shows that the obtained cyclone track is slightly different from the real one (see Figure 2.12). The low pressure center deviates to the North as soon as it

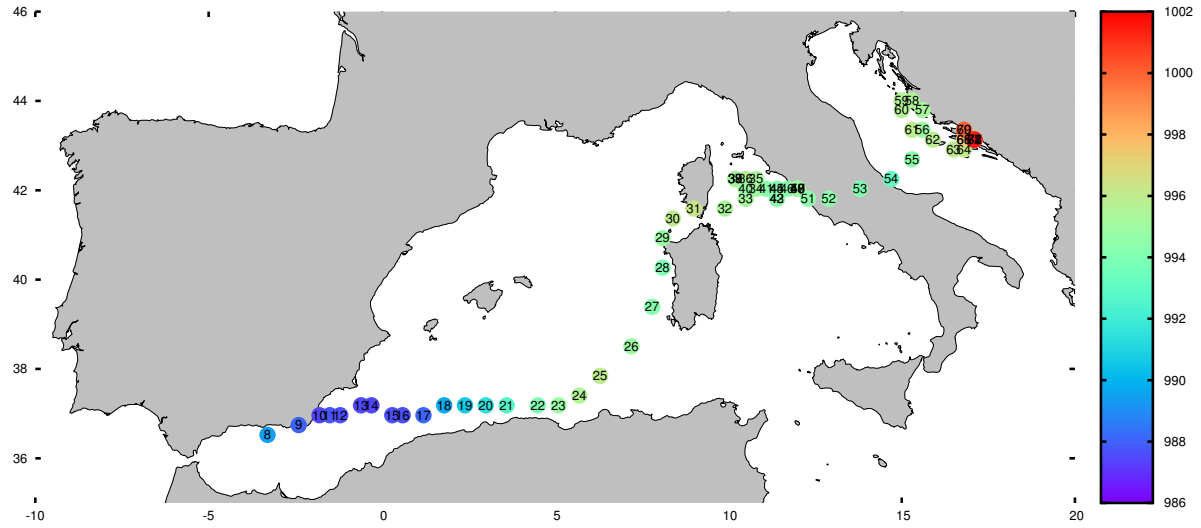

Figure 4.8.: Cyclone path obtained with GLOBO Model.

interacts with the orography of Sardinia and with another minimum placed over Corsica. This northward deviation, that may be due also to the inability to properly resolve the Mediterranean area orography, is highlighted in the MSLP field of the two forecast reported in Figure 4.9. It shows that the spatial resolution of GLOBO model (approximately 24 km at mid latitudes) is not enough to capture the small scale features of the cyclone. It is worth noting that the GFS forecast initialized at the same time (19 January 2014) yielded to the same incorrect path, as shown in Figure 4.10. Given the results of this simulation, no thermal phase/symmetry analysis has been conducted.

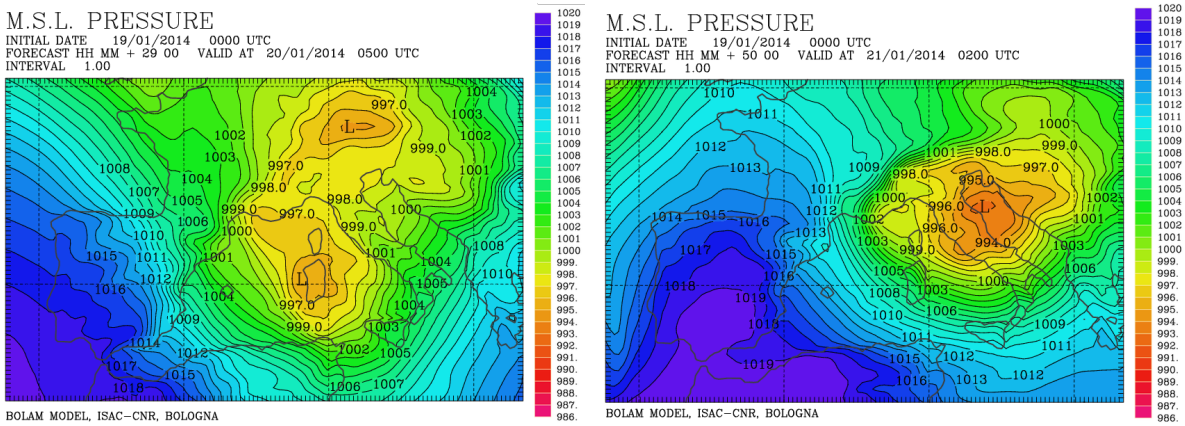

(a) 20 January 2014 - 05 UTC (b) 21 January 2014 - 02 UTC

Figure 4.9.: MSLP (Mean Sea Level Pressure) forecasted by GLOBO Model. Note the northwards deviation with respect to the observed trajectory 2.12.

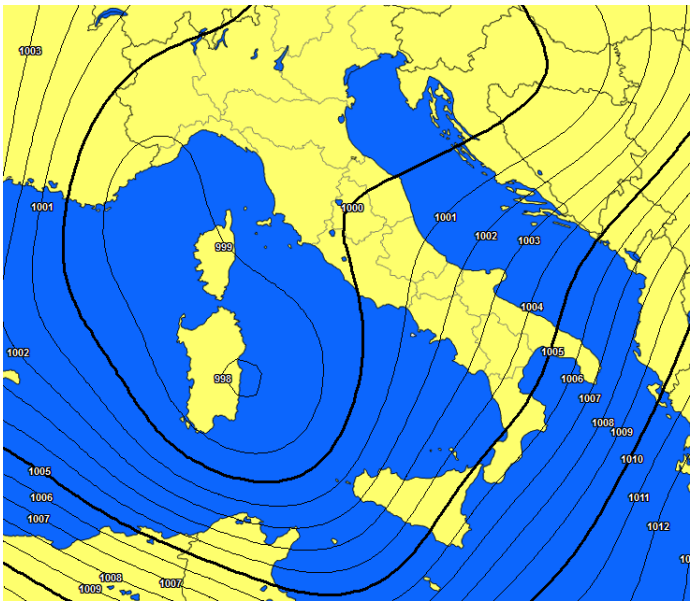

Figure 4.10.: MSLP GFS model forecast for 20 January 2014 at 07 UTC

4.4.2. Case B1

Identifier	Initial Condition	Initialization Time	GLOBO	BOLAM	MOLOCH	SST data
B1	NCEP	19/01/14 00 UTC	√	√		Model

In this case, the BOLAM model[3] has been nested into the GLOBO forecast, with boundary conditions given every one hour. Figure 4.11 shows that BOLAM forecast dramatically improves the cyclone path prediction, correctly placing the landfall on the coast near Naples.

[3]As specified in Chapter 3 the adopted horizontal resolution for BOLAM model is 0.075×0.075 degrees.

The temporal integration carried out by the LAM model is able to successfully reproduce

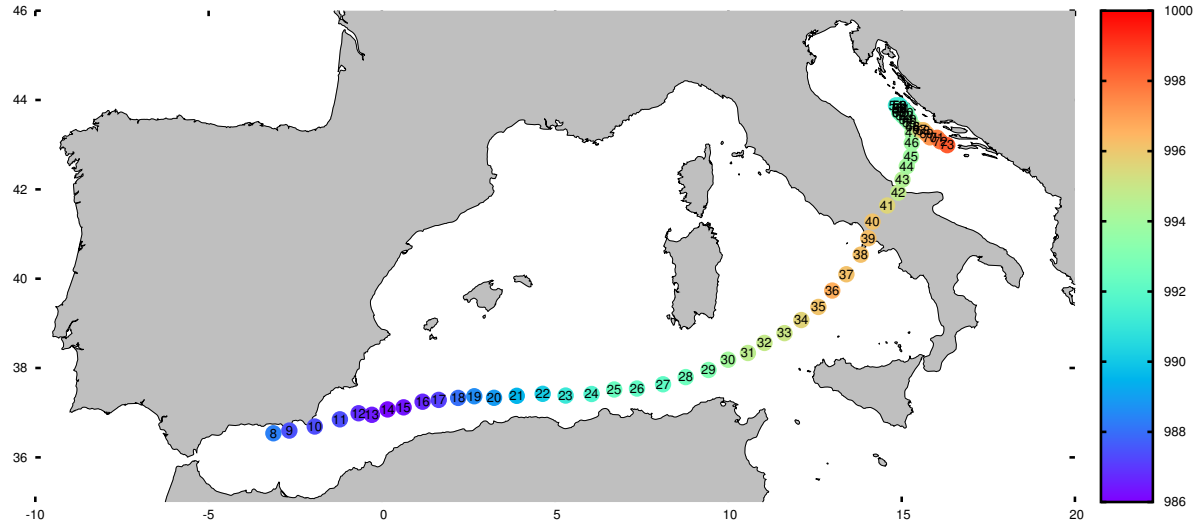

Figure 4.11.: Cyclone path obtained with BOLAM Model in the B1 case.

the dynamic and thermodynamic environment where the cyclone is developing, producing a better approximation of its track over the domain. The analysis of the pressure minimum and maximum wind speed computed by the BOLAM model makes it possible to distinguish the various phases of the cyclone lifecycle. A careful analysis of Figure 4.12 reveals:

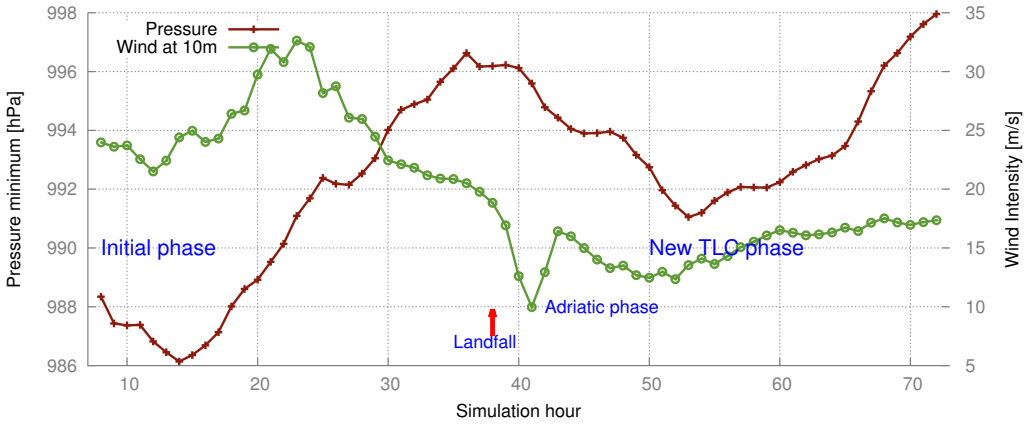

Figure 4.12.: Pressure minimum and maximum wind speed computed by the BOLAM model. The maximum of wind is searched over a circle of radius R_{ex}.

- the initial rapid deepening of the low pressure system which coincides with the maximum winds computed (and observed),
- the subsequent rise in pressure,
- the decrease of wind speed due to the increase friction of the ground during the landfall phase,

- the new low pressure deepening in the Adriatic phase, where features typical of TLCs were found, as described in Section 2.1.2.

However, given the maxima over 30 m/s, the models overestimates the surface wind, while it underestimates the value of the pressure minimum (986 hPa versus 991 hPa). The parameter B assumes very low values, below the threshold of $B = 10$m proposed by Hart [48], indicating symmetry of the simulated cyclone. While the distinction between symmetric and asymmetric cyclones is based upon the threshold aforementioned, the sign of the parameter B allows one to distinguish between thermally direct circulation (warm advection downstream of the cyclone: $B > 0$) and thermally indirect circulation (cold advection downstream of the cyclone: $B < 0$)[4]. Figure 4.13 (a) shows that the value of parameter B fluctuates

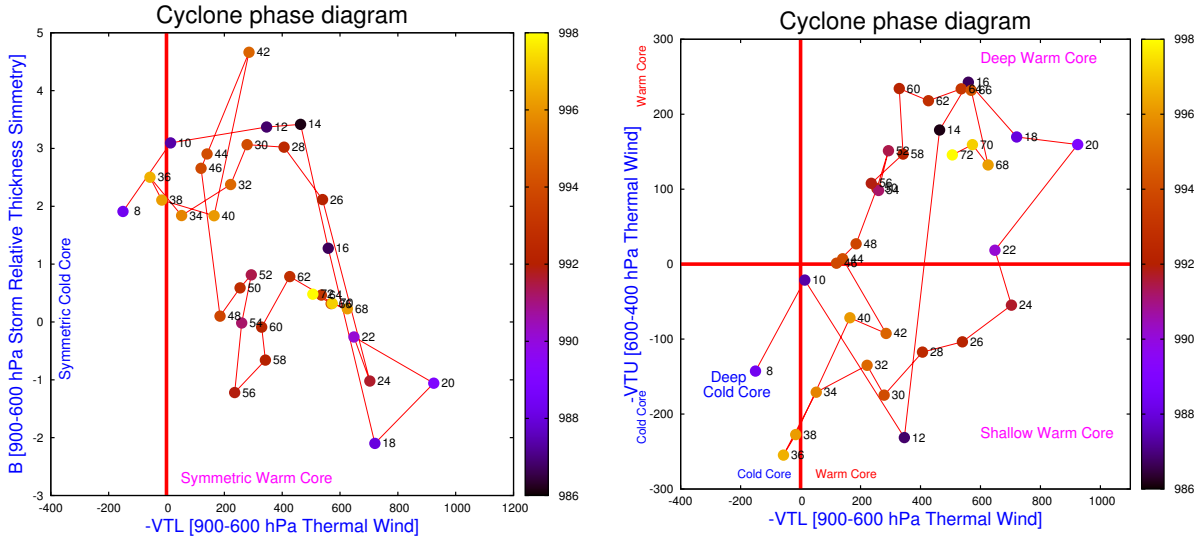

(a) $-V_t^{\mathrm{L}}$ versus B (b) $-V_t^{\mathrm{U}}$ versus $-V_t^{\mathrm{L}}$

Figure 4.13.: Cyclone phase space diagrams for the case B1.

between 5 and -2 meters, indicating a symmetric system with a prevalence of thermally direct circulation. Nevertheless, the second phase space diagram presented in Figure 4.13 (b) allows to make a detailed study of the phase predicted by the model. In particular:

- In the first 20 hours the system undergoes a transition between three different phases, from a deep-cold core to a relatively weak warm core, ending with a deep warm core at the 14$^{\mathrm{th}}$ hour of the simulation. By looking back at Figures 4.12 and 4.11 one can argue that this time corresponds to the absolute minimum value of MSLP pressure, when the system is located between Spain and the North-African coast.

- Until the contact with the Adriatic Sea, the system possesses a shallow warm core.

[4]See also Hart [48], Sutcliffe [107], Petterseen [86], Trenberth [111].

- From the 44th time step onwards, the low pressure system remains in a deep-warm-core phase

4.4.3. Case M1

Identifier	Initial Condition	Initialization Time	GLOBO	BOLAM	MOLOCH	SST data
M1	NCEP	19/01/14 00 UTC	√	√	√	Model

In this case of study the MOLOCH model has been nested into the BOLAM model output, with boundary conditions given every one hour. Later on it will be shown that this constraint is needed for an optimal simulation of the cyclone evolution. The trajectory obtained with this simulation, shown in Figure 4.14, is quite different from the observed one, since the cyclone deviates northwards after Sardinia. As a result of this deviation, the evolution of the system is not well predicted, and the cyclone covers a track completely different in the Adriatic Sea. The fail of this simulation in modelling the cyclone evolution is almost certainly

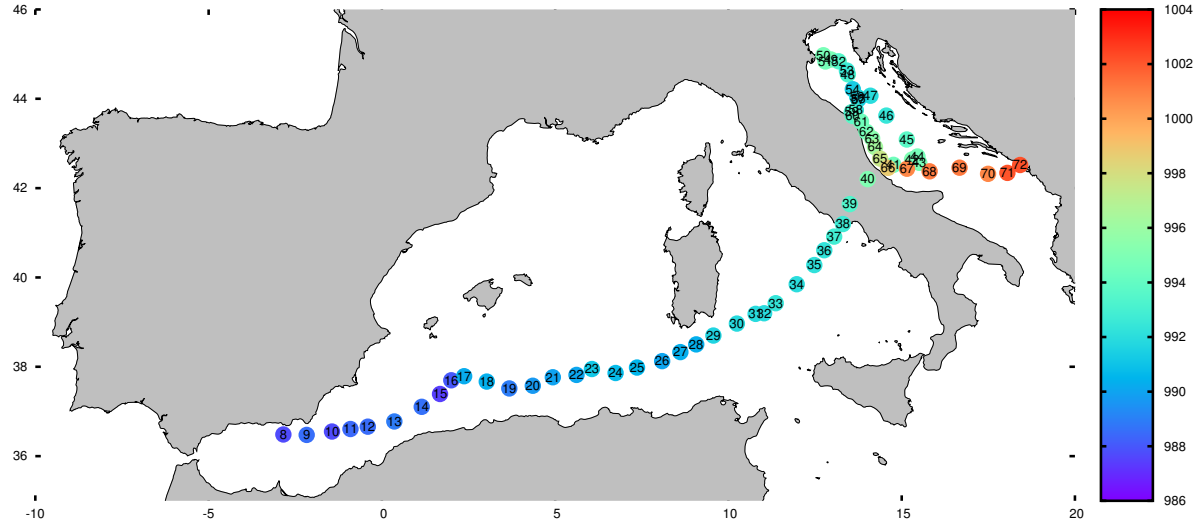

Figure 4.14.: Cyclone path obtained with MOLOCH Model in the M1 case.

due to the lack of reliable temperature data over the Adriatic Sea, where the cyclone showed a new stage of deepening. A new approach to this problem is considered in the B3 case. Given the poor results obtained in this case, the thermal analysis has not been carried out.

4.4.4. Case B3

Identifier	Initial Condition	Initialization Time	GLOBO	BOLAM	MOLOCH	SST data
B3	NCEP	19/01/14 00 UTC	√	√		MyOcean

Miglietta et al. [75] have shown that a well defined SST grid is necessary to correctly forecast Mediterranean TLCs. In fact, the SST plays an important role in the formation

and development of these intense cyclones: Tous and Romero [109] identified the 15°C as the lowest threshold for Medicanes formation, while Emanuel [34] identified the 26°C threshold for Hurricane formation. The MyOcean SST Analysis presented in Figure 4.15 shows temperatures around 14-15°C in the zone of formation of the event. Moreover, the

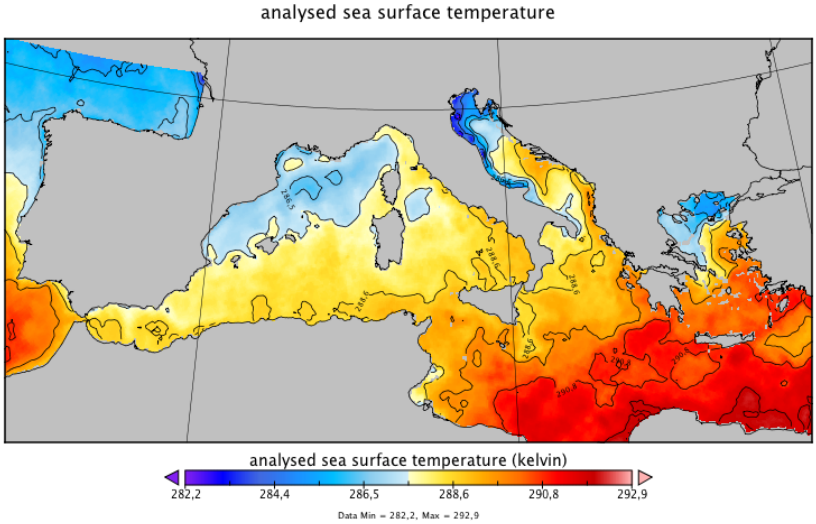

Figure 4.15.: SST analysis for 19 January 2014 00 UTC - MyOcean.

SST anomalies shown in Figure 4.16, locate warm waters in the Adriatic Sea, suggesting a connection with the observed cyclone intensification in this area. Emanuel [33] showed

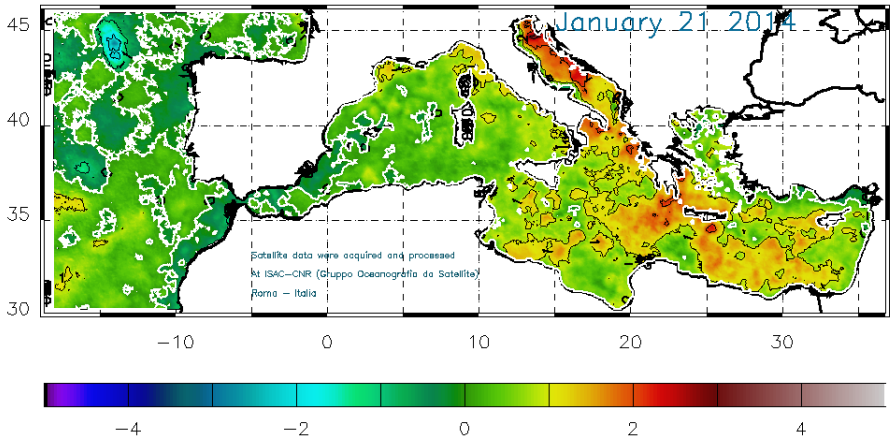

Figure 4.16.: SST anomalies for 21 January 2014 - ISAC-CNR GOS.

that the genesis and maintenance of Mediterranean Hurricanes is related to the difference between SST and air temperature. Since the air temperature strictly depends on the synoptic configuration, a change of ± 1 or 2 degrees in the SST may affect the genesis and evolution of TLC events over the Mediterranean. All these remarks suggest the use of an SST obtained from an external analysis. MyOcean provides daily analyses of Mediterranean SST retrieved

from satellite data at a resolution of 0.0625°×0.0625°. This data is used in the BOLAM nesting (`prebolam` process) to define the two water level temperatures. Figure 4.17 shows that the path obtained shares many similarities with the observed one, although no circular trajectory is obtained in the Adriatic phase. Since the pressure-wind trend obtained is very

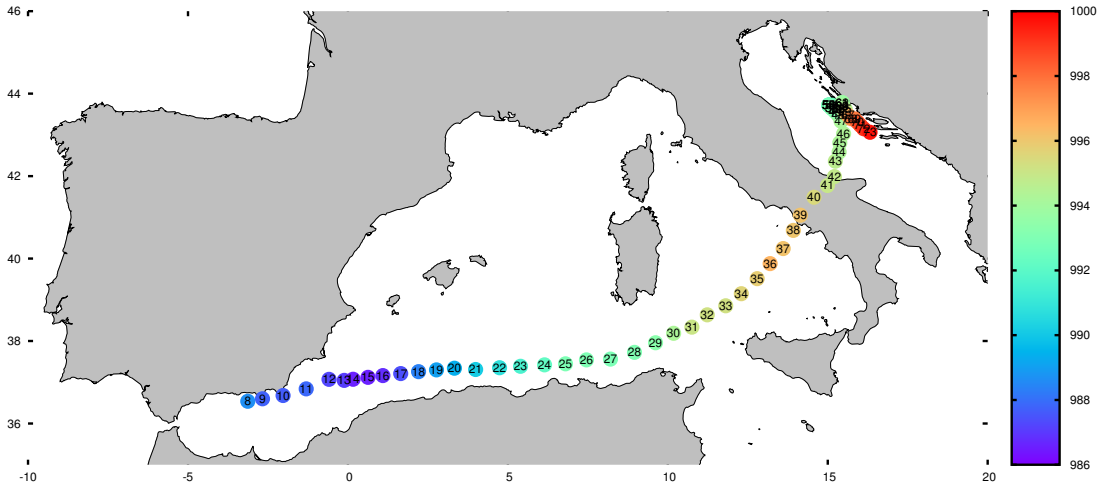

Figure 4.17.: Cyclone path obtained with BOLAM Model in the B3 case.

similar to the one showed in Figure 4.12, the corresponding chart is not shown. Conversely, the thermal structure computed in this case shows major differences. According to the results presented in Figure 4.18 the cyclone possesses a deep-cold-core structure before and after making landfall on the Naples' coast. The deep-warm-core structure typical of MTLCs is forecasted only in the initial phase (between Spain and Sardinia) and in the final phase when the cyclone is weakening. It is worth noting that the comparison of thermally direct/indirect circulation, achieved by looking at Figure 4.18 (a) and Figure 4.13 (a), shows a distinction in both cases between two group of individual phases (time step 8-16 and 26-46 versus 18-24 and 48-73).

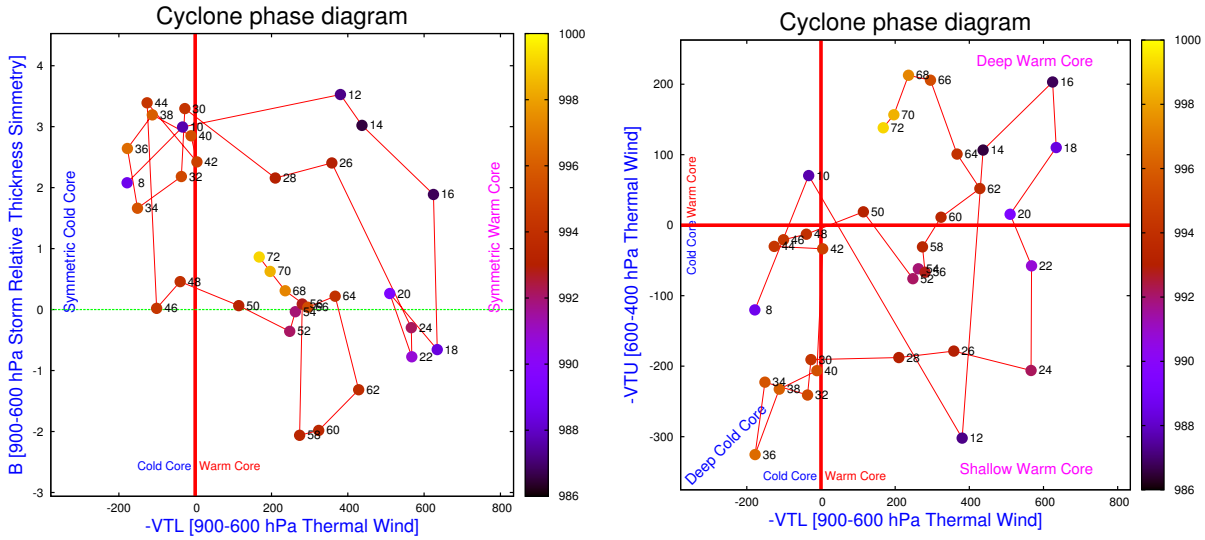

(a) $-V_t^{\mathrm{L}}$ versus B (b) $-V_t^{\mathrm{U}}$ versus $-V_t^{\mathrm{L}}$

Figure 4.18.: Cyclone phase space diagrams for the case B3.

4.4.5. Case M3

Identifier	Initial Condition	Initialization Time	GLOBO	BOLAM	MOLOCH	SST data
M3	NCEP	19/01/14 00 UTC	√	√	√	MyOcean

Given the good results obtained with the simulation performed in the B3 case, the BOLAM model output was used as an input for the simulation of MOLOCH model carried out on the same domain and in the same range of time. Figure 4.19 reveals that the cyclone path obtained slightly differs from that presented in Figure 4.17, showing a more northward deviation after the interaction with Sardinia island. The difference is more easily noticeable

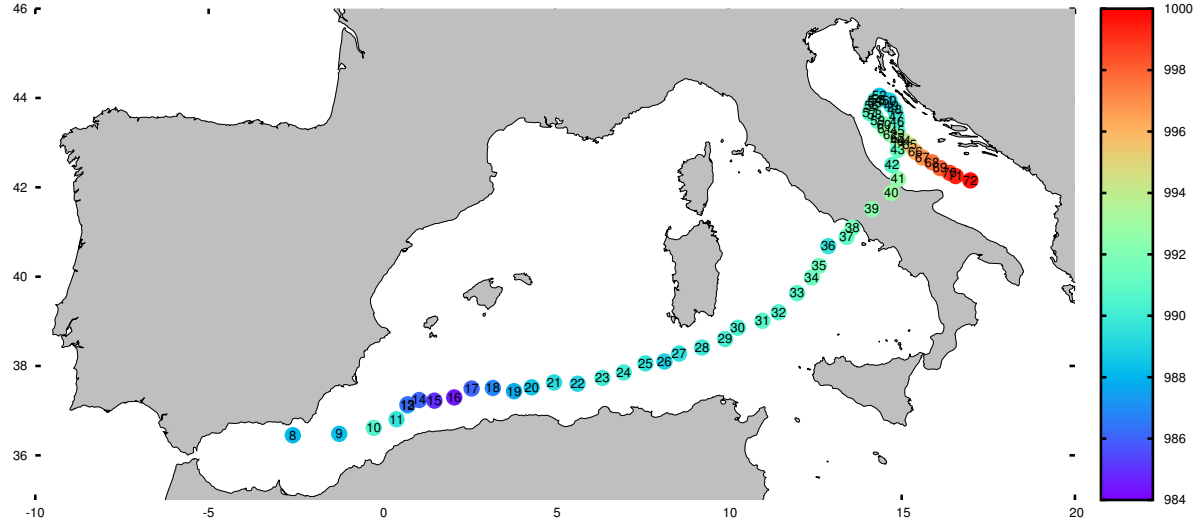

Figure 4.19.: Cyclone path obtained with MOLOCH Model in the M3 case.

in the Adriatic phase showed in Figure 4.20, when the cyclone trajectory shows a circle with a very small radius. The spatial resolution of about 2 km of MOLOCH model is able to reproduce the organized convection driving the cyclone intensification, in particular during the Adriatic phase when the system exhibits a very small radius of about 60 km. These differences are even more evident if the MOLOCH model output individual fields are analyzed in detail. During the entire Western-Mediterranean and Thyrrenian phase (up to the 38th hour) the surface latent heat fluxes identify a localized maximum (ranging from 500 to 200 W/m^{-2}) in the vicinity of the cyclone. Even though a localized maximum up to 300 W/m^{-2} is visible also in the sensible heat fluxes near the cyclone center at some hours, the correlation between the cyclone path is weaker. This confirms the difference between polar lows and medicanes, since in the first case sensible heat fluxes should prevail over the latent heat fluxes. Both heat fluxes show a maximum around the 22nd simulation hour, when the cyclone was located east of Algeri. The MSLP field shows at least two closed isobars (with 1-hPa interval) for the entire simulation time, even when the cyclone reaches the last phase of the life cycle (from the 60th hour onwards), with very small radius. The wind speed at 10 meters shows vectors rotating counter-clockwise around the pressure minimum although this structure is well evident only in the first 15 hours and in the Adriatic phase. Convective

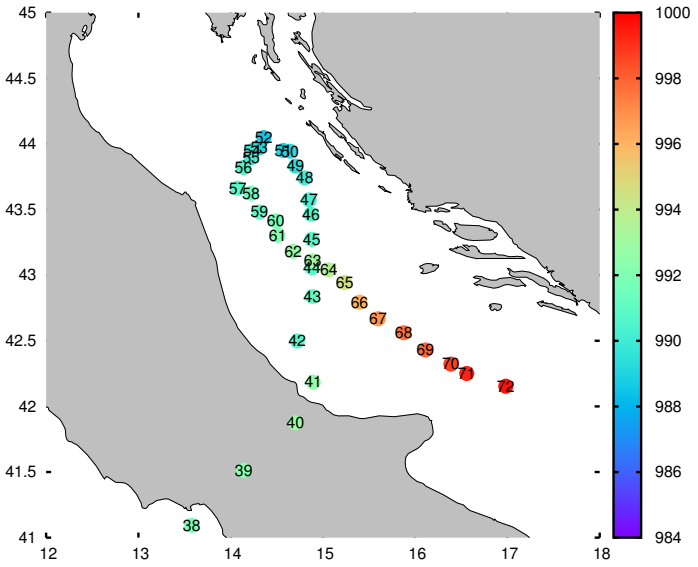

Figure 4.20.: Cyclone path obtained with MOLOCH Model in the M3 case - detail of Figure 4.19 in the Adriatic sea.

Available Potential Energy (CAPE) values show an isolated maximum of 1000 J/kg following the cyclone trajectory during the whole Adriatic phase. The MOLOCH model is thus able to resolve the convection that was taking place at that moment.
The pressure and wind trend over time is slightly different from that shown in Figure 4.12. Aside from the too low value obtained for the pressure minimum, the data contained in

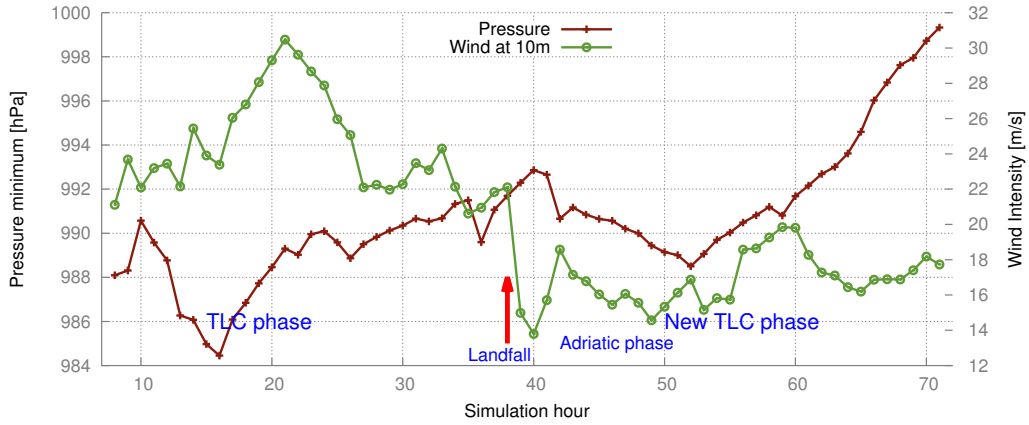

Figure 4.21.: Pressure minimum and maximum wind speed computed with MOLOCH model. The maximum of the wind is searched over a circle of radius R_{ex}.

Figure 4.21 show some interesting features of the cyclone life cycle:

1. The initial deepening of the low pressure system is predicted before the approach near Sardinia,

2. The maximum wind intensity is predicted long after the initial formation, about the

20^{th} hour of simulation, showing poor agreement with observational data[5],

3. The rise of pressure and reduction of wind intensity are correctly predicted at the moment when the system makes landfall on the Italian coast,

4. In the Adriatic phase the new deepening of the low pressure system is correctly forecasted.

A careful comparison of Figure 4.21 and Figure 4.12 reveals that the two predicted trends show similar features. As one might expect, the MOLOCH model output contains fields highly affected by *numerical noise*: an example of this effect can be seen in Figure 4.22 ,where multiple L (low) and H (high) pressure are founds over the domain. These fluctuations may

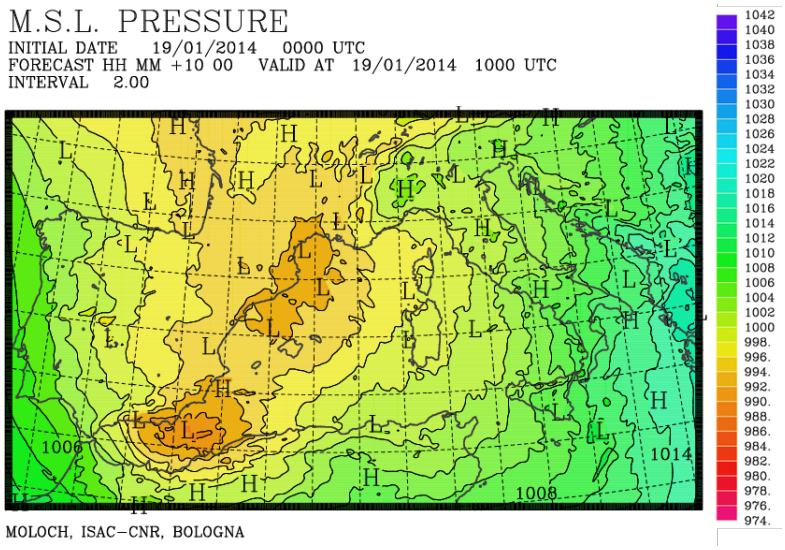

Figure 4.22.: MSLP value at 20 UTC on 20 January 2014, obtained in the MOLOCH simulation of the case M3.

cause problems during the computation of the parameters needed for thermal phase study. The computed values of B, $-V_t^{\text{L}}$, $-V_t^{\text{U}}$ shown indeed an high degree of variability, which was reduced using a 9-points smoothing filter on the geopotential height. The values showed in Figure 4.23 (a) match with the results found in case B3, since the system always possesses a symmetrical structure. However, the parameter B takes values much larger than those obtained before, although the $B = 10$m threshold is never reached. The phase diagram contained in Figure 4.23 (b) does not identify the presence of a deep-cold core throughout the whole life cycle of the cyclone. The warm core structure is highlighted by the very high values of $-V_t^{\text{L}}$ and $-V_t^{\text{U}}$ during the first phase of intensification (hours 14-20 of 19 January) and the final Adriatic phase (hours 40-72). The difference of the values assumed by the aforementioned parameters during these two periods allows to clearly distinguish different cyclone intensities. It should be note that also the parameter $-V_t^{\text{L}}$ reaches very high values, showing an intense deep-warm core.

[5]Recall from chapter 2 that the strongest winds were observed when the cyclone was forming.

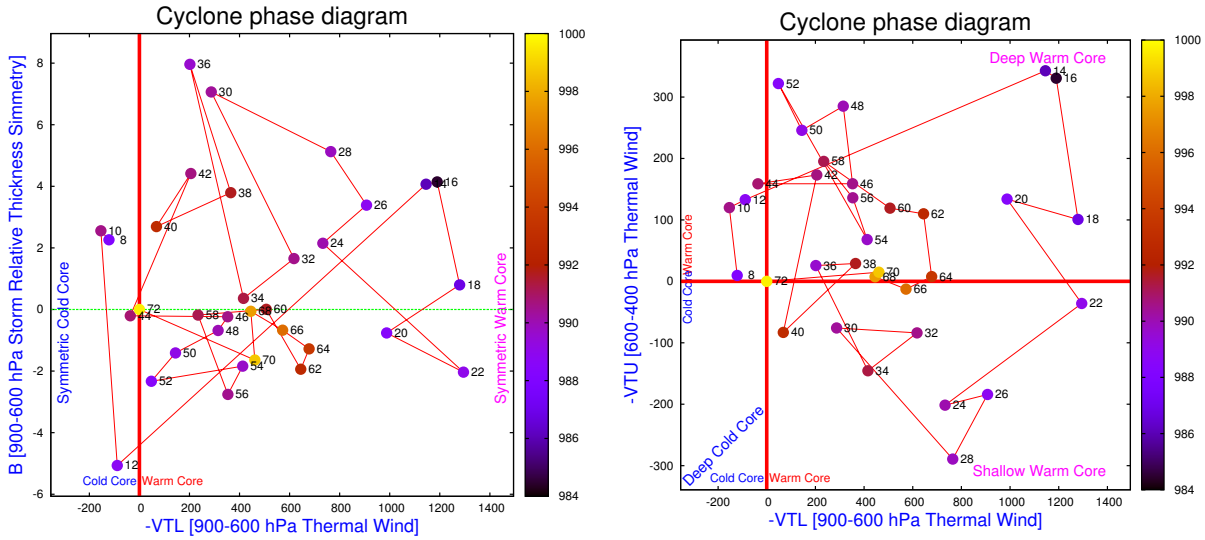

(a) V_t^{L} versus B

(b) $-V_t^{\mathrm{L}}$ versus $-V_t^{\mathrm{U}}$

Figure 4.23.: Cyclone phase space diagrams for the case M3.

4.4.6. Case B2

Identifier	Initial Condition	Initialization Time	GLOBO	BOLAM	MOLOCH	SST data
B2	ECMWF	19/01/14 00 UTC		√		Model

The NCEP and the ECMWF relative NWP models are often compared based on *forecast skill*, namely the difference between an observed and forecasted variable, e.g. 500 hPa geopotential height. In this case, ECMWF model has been used as initial condition and for setting the boundary conditions every 6 hours. The aim of this simulation is to evaluate the improvement of cyclone track forecast through the use of analysis data instead of model data. The simulations performed in the B1, M1, B3 and M3 cases make use of boundary conditions obtained from the forecast of the outer model. In this case, the simulation performed with BOLAM is forced with boundary conditions obtained from analyses and not forecast. Interestingly enough, the trajectory obtained from this simulation significantly differs both from the observed one and from the one obtained in the B1 and B3 cases, as shown in Figure 4.24. As already observed in case G1, but also in operational models like GFS, the cyclone path

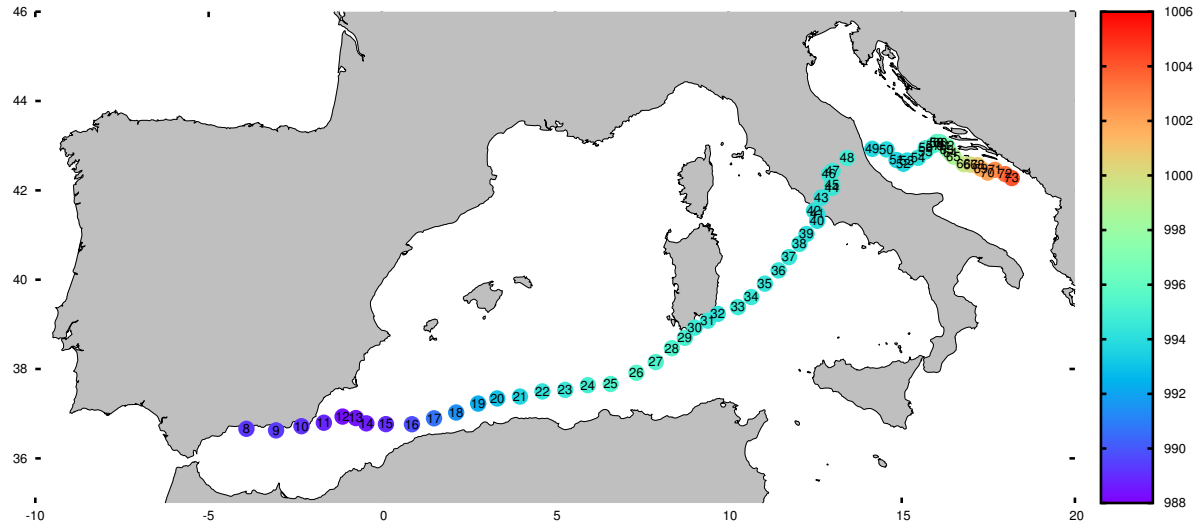

Figure 4.24.: Cyclone path obtained with BOLAM Model in the B2 case, with nesting inside the ECMWF Model.

predicted on 19 January 2014 deviates to the north as soon as it starts interacting with the orography of Sardinia. This deflection is clearly visible in the MSLP field computed for the morning of 20 January 2014, showed in Figure 4.25. While the original low pressure system is still located on the western side of Sardinia Island, the interaction with orography have created another minimum on the Eastern side, that is moving eastward. In this simulation the pressure-wind data, as well as the thermal structure parameters, are meaningless, since the original cyclone is not well simulated. This is confirmed by a rapid analysis of the cyclone phase diagram of this case (not shown) that clearly shows thermal winds near to zero for the whole simulation.

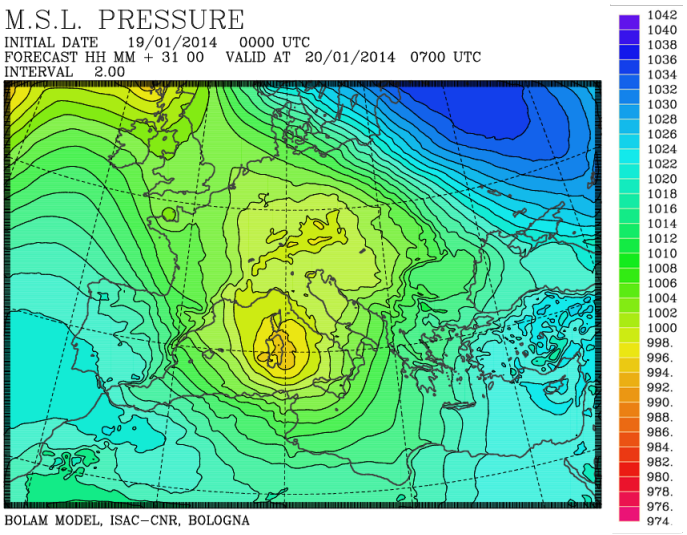

Figure 4.25.: MSLP value at 07 UTC on 20 January 2014, obtained in the BOLAM simulation of the case B2.

4.4.7. Case M2

Identifier	Initial Condition	Initialization Time	GLOBO	BOLAM	MOLOCH	SST data
M2	NCEP	19/01/14 00 UTC	√		√	Model

In this case the MOLOCH model simulation has been nested directly into the GLOBO model output. The results presented in the B cases have shown that the BOLAM model plays a vital role in correcting the cyclone trajectory. Therefore, the removal of this from the model chain may compromise the final result, as one can argue from Figure 4.26. The

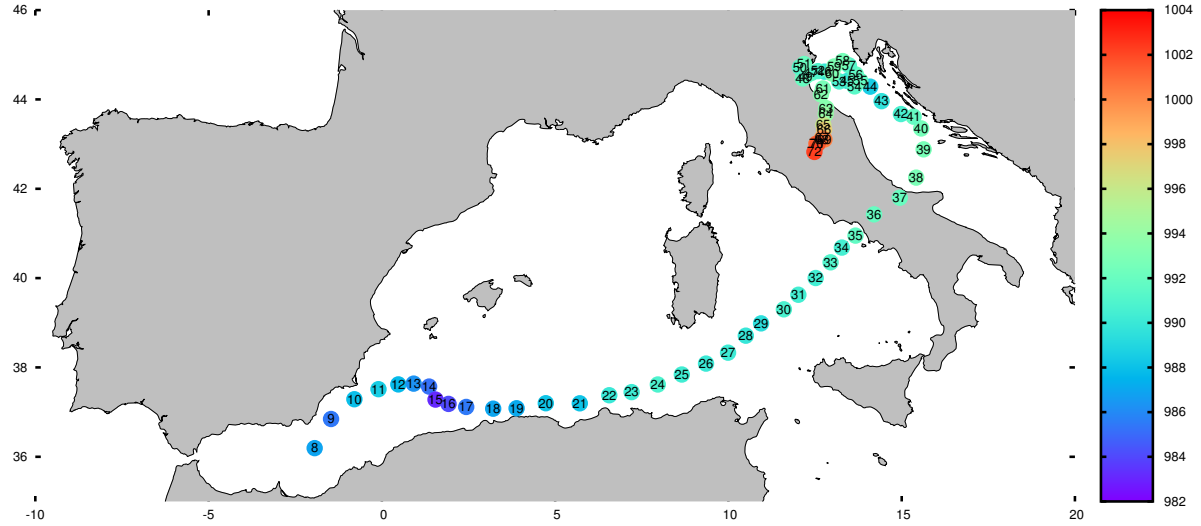

Figure 4.26.: Cyclone path obtained with MOLOCH Model in the M2 case.

cyclone exhibit first a southward drift, towards North Africa coast, while the landfall takes

place too far north. As a result of those forecast errors, the cyclone is diverted permanently northwards in the Adriatic Sea. This behaviour may also be due to the gap between the spatial resolution of GLOBO and MOLOCH models. Often, the ratio between the spatial resolution of the father model and the nested one is kept under 5, so as to comply with an empirical rule.

4.4.8. Cases B1-20, B2-20, B3-20 and M1-20E

Identifier	Initial Condition	Initialization Time	GLOBO	BOLAM	MOLOCH	SST data
B1-20	NCEP	20/01/14 00 UTC	√	√		Model
B3-20	NCEP	20/01/14 00 UTC	√	√		MyOcean
B2-20	ECMWF	20/01/14 00 UTC	√	√		Model
M1-20E	ECMWF	20/01/14 00 UTC	√	√	√	Model

The results presented in cases B3 and M3 show a moderate sensitivity to boundary conditions. In particular, difference in the SST distribution can change latent heat and sensible heat fluxes, the major mechanisms of intensification related to Tropical Cyclones (see Emanuel [34], Rotunno et al. [101] and Emanuel [33]). Conversely, case B2 shows an high sensitivity to initial conditions, since the results obtained with ECMWF analysis are quite different from those obtained with GFS. Changing the initial condition, and comparing the cyclone paths, may help investigating this sensitivity. In the B1-20 case the BOLAM model has been initialized with the GFS analysis of 20 January 2014 at 00 UTC, as shown in Table 4.1. The results presented in Figure 4.27 show that the original cyclone trajectory is missed even at the beginning. The low pressure system is positioned too much northward by the

Figure 4.27.: Cyclone path obtained with BOLAM Model in the B1-20 case, with changed initial condition.

analysis, even though it deviates southwards further on, making landfall farther south of Naples' coast. As a result of this, the cyclone makes contact with Adriatic Sea after the Salentine peninsula, negating any possibility to move northwards and to follow the observed

circular trajectory. The cause of such erroneous prediction could be identified in an underestimation of the intensity associated to the pressure minimum. While the value of the pressure minimum of 996 hPa does not differ substantially from the observed 994 hPa (see Chapter 2), in Figure 4.28 (a) only one isobar shows a closed circular shape. This may indicate a weaker cyclone, since the pressure gradient is smaller. The ECMWF analysis at

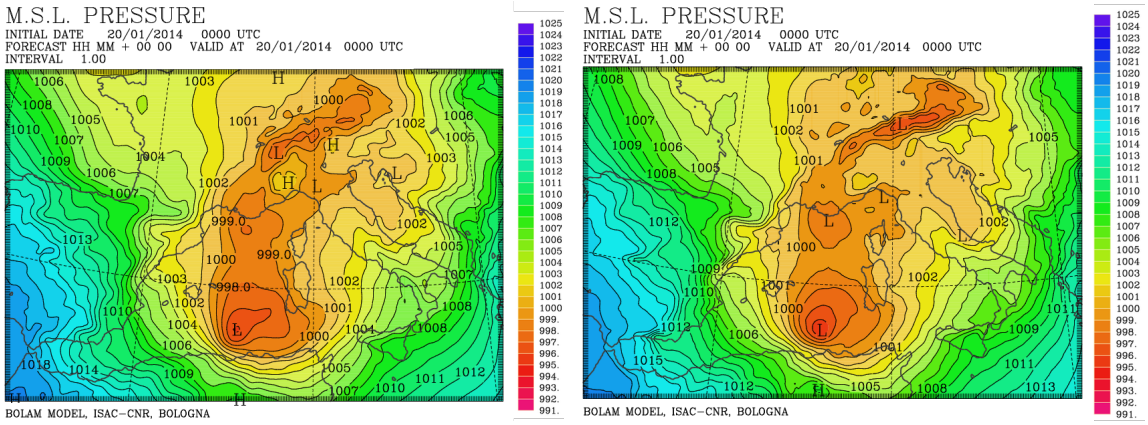

(a) GFS analysis (b) ECMWF analysis

Figure 4.28.: MSLP Analysis of the GFS and ECMWF model for 20 January 2014 - 00 UTC, plotted using the BOLAM model postprocessing.

the same time (Figure 4.28 (b)) shows a slightly different cyclone configuration, with a well defined circular shape but with the same minimum value (996 hPa). The use of the MyOcean SST does not help to improve the cyclone trajectory, since the cyclone deviates to the North and does not form a well defined minimum, as showed in Figure 4.29 This

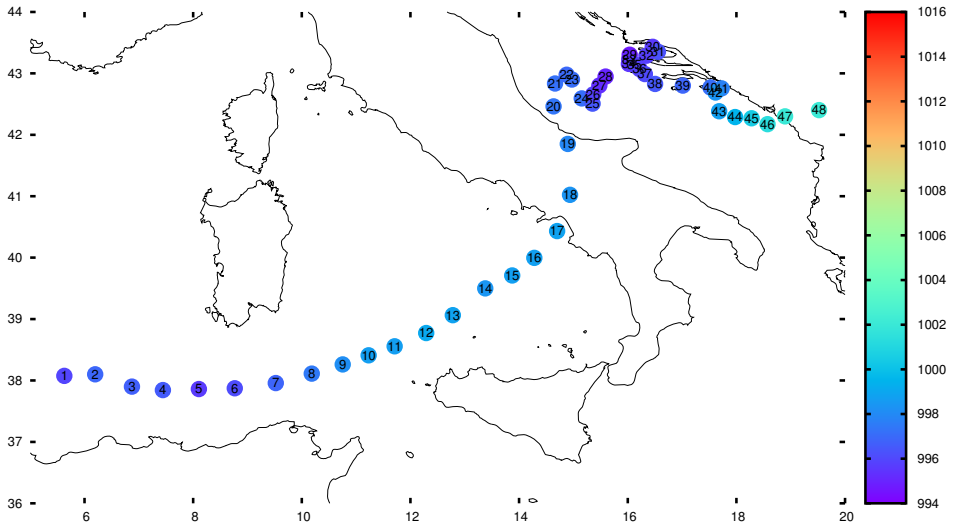

Figure 4.29.: Cyclone path obtained with BOLAM Model in the B3-20 case.

behaviour is evident also by looking only at the cyclone phase diagram reported in Figure

4.30, that shows mostly negative values of the thermal wind, indicating a cold-core structure alternated with not well defined thermal phases. Given the good quality of the ECMWF

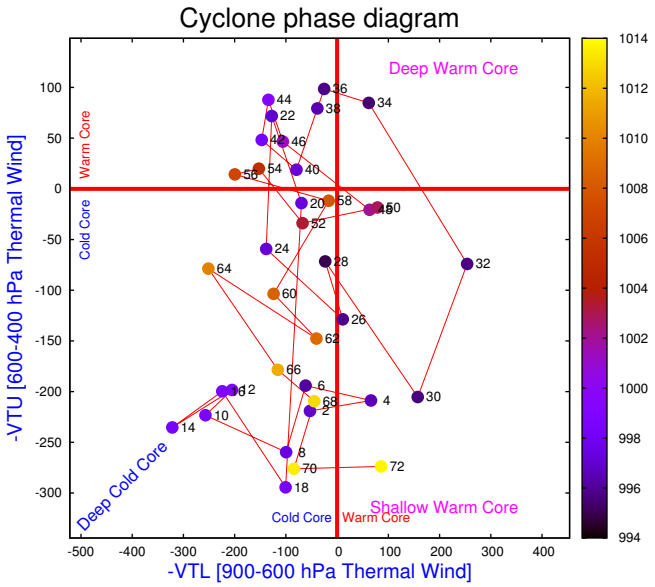

Figure 4.30.: Cyclone phase diagram obtained with BOLAM Model in the B3-20 case.

analysis showed in Figure 4.28 (a), another simulation has been carried out, using 6-hours ECMWF boundary conditions as in case B2, but starting from 20 January. The trajectory obtained is very different from the one of the aforementioned case. Figure 4.31 shows that both the Thyrrenian phase and the landfall position are forecasted with good agreement regarding to the observed cyclone trajectory. Despite the lack of a circular trajectory in the Adriatic phase, which can be attributed to the non-use of MyOcean SST, the phase of the cyclone shows some interesting features that are worth discussing. The pressure minimum value shows a nearly constant trend in the first hours, reaching 995 hPa during landfall, in agreement with the observations made on Procida Island. Later on, during the Adriatic phase, the pressure reaches a 992 hPa minimum on 21 January at 06 UTC. The wind intensity is underestimated in the initial phase, since weather stations reported wind gust of about 27 m/s, but it must be considered that the computed wind speed is a mean value. The values of parameter B reported in Figure 4.33 (a) again shows that the structure was in a symmetric state for the whole simulation time. Moreover, Figure 4.33 (b) highlights the transition occurred between the shallow warm core structure and the deep warm core structure, from the 22$^{\text{nd}}$ hour onwards. Using Figure 4.31 it may be concluded that the arrival over the Adriatic Sea greatly enhances the tropical-like features of the system.
In order to further evaluate the role of initial conditions, a MOLOCH simulation has been nested into the B1-20E case, with SST obtained from the model. In this situation, since the trajectory obtained in the BOLAM simulation is approximately correct, the MOLOCH model plays a vital role in creating the small-scale structure of the system. By comparing

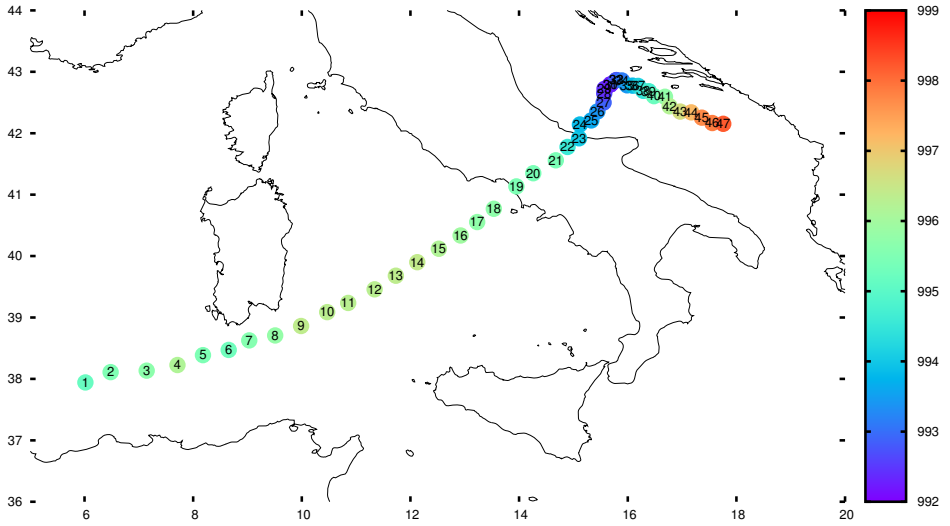

Figure 4.31.: Cyclone path obtained with BOLAM Model in the B1-20E case.

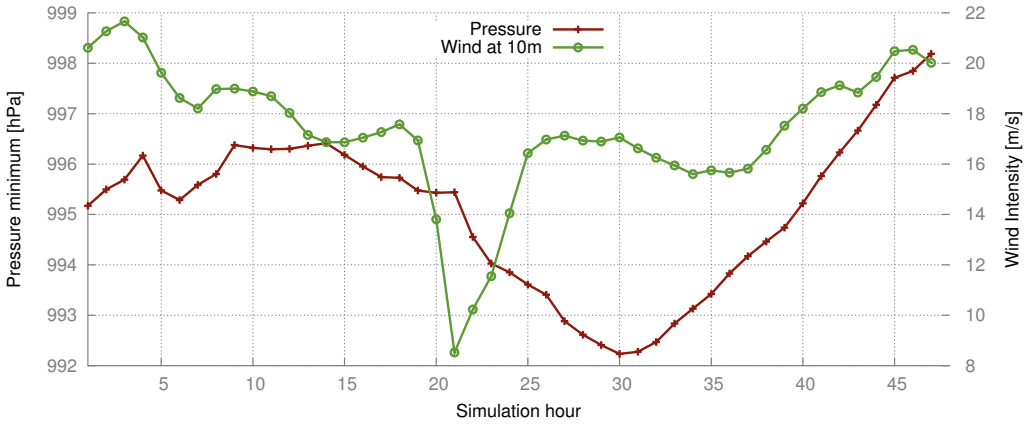

Figure 4.32.: Pressure minimum and maximum wind speed computed with BOLAM model. The maximum of the wind is searched over a circle of radius R_{ex}.

Figure 4.34 and Figure 4.31 it can be seen that the two cyclone trajectories slightly differ only in the Adriatic phase. In particular, the MOLOCH model is able to reproduce the circular trajectory as seen in observations and in M3 case. The forecasted pressure variation agrees with the one obtained in the B1-20E case, although the minimum is reached shortly before the 30^{th} hour (not shown). The wind intensity partially differs only in the final phase on the Adriatic Sea. According to the data presented in Figure 4.35 the cyclone possesses a warm-core symmetric structure for most of the life cycle. The system fluctuates between the shallow warm-core state and the deep-warm core phase, although the values of the thermal wind obtained are smaller than those obtained in other MOLOCH simulations.

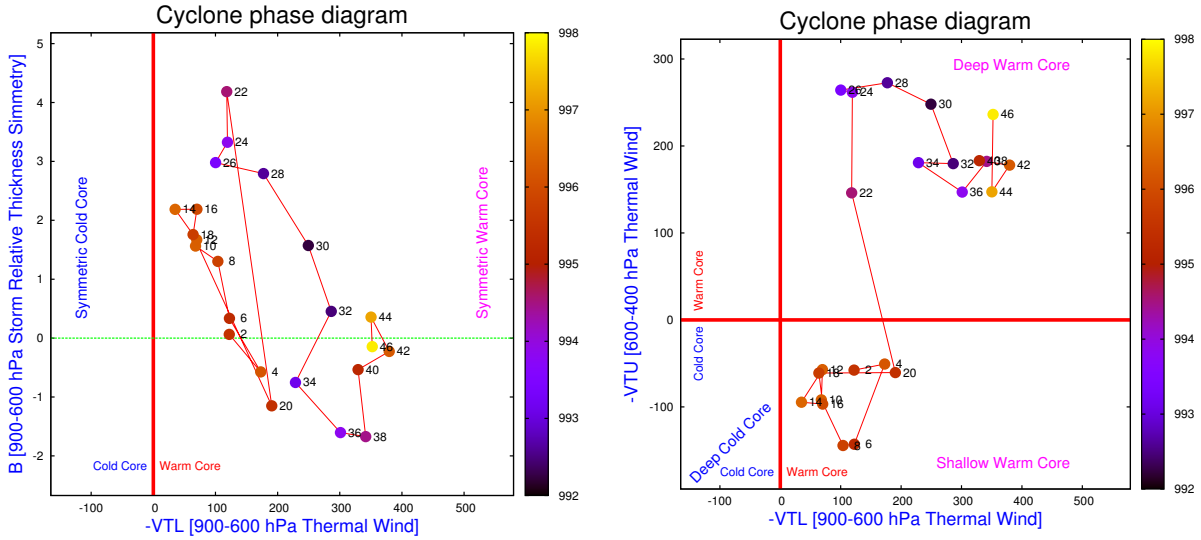

(a) $-V_t^{\mathrm{L}}$ versus B (b) $-V_t^{\mathrm{L}}$ versus $-V_t^{\mathrm{U}}$

Figure 4.33.: Cyclone phase space diagrams for the case B1-20E.

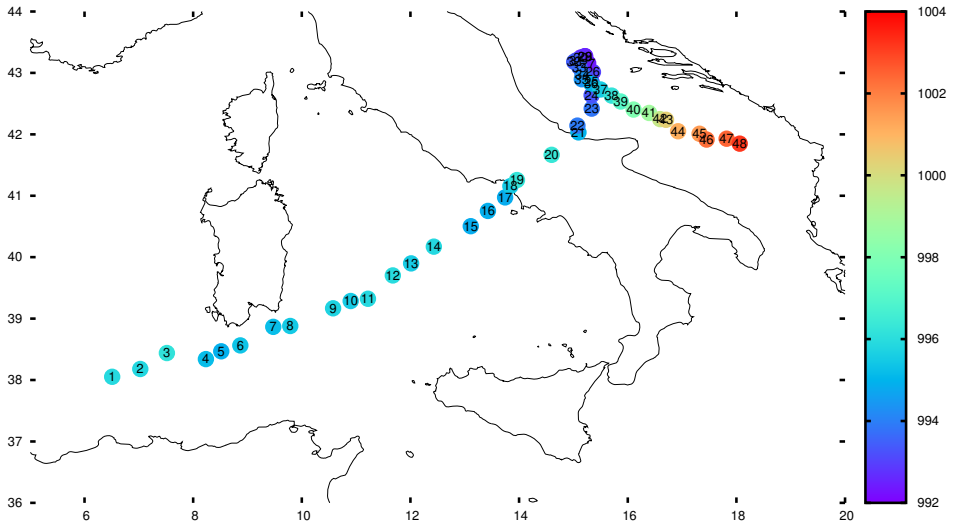

Figure 4.34.: Cyclone path obtained with MOLOCH Model in the M1-20E case.

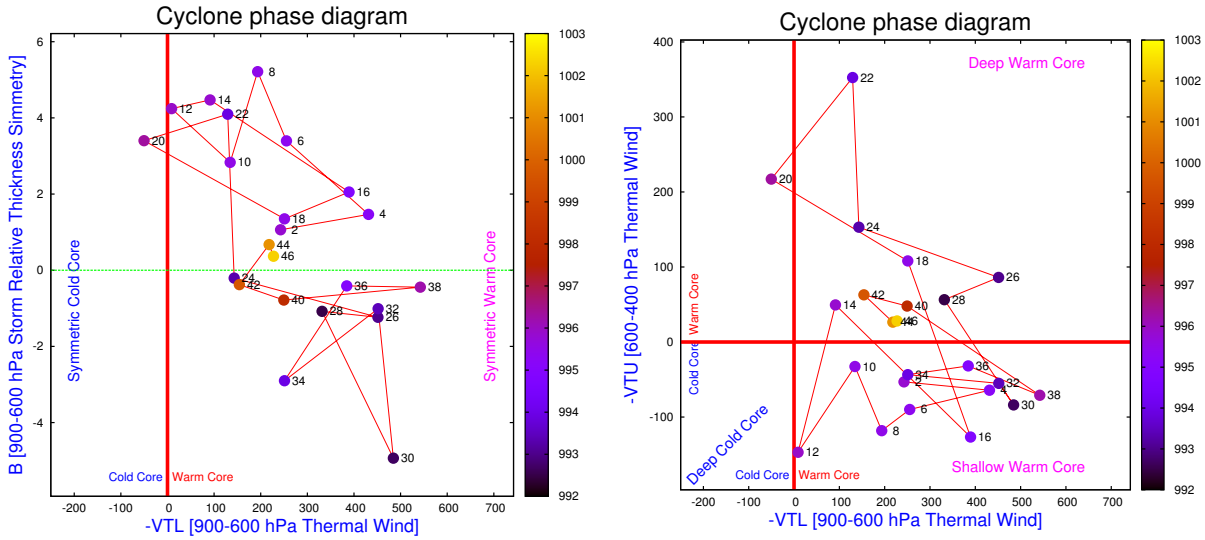

(a) $-V_t^{\mathrm{L}}$ versus B (b) $-V_t^{\mathrm{L}}$ versus $-V_t^{\mathrm{U}}$

Figure 4.35.: Cyclone phase space diagrams for the case M1-20E.

4.5. Overview of case studies

A comprehensive analysis of the results proposed in the previous section allows to identify the cases where the predicted evolution of the cyclone is in good agreement with the observed one. The forecasts made with alternative initial conditions (e.g. ECMWF instead of GFS, 20-01-2014 instead of 19-01-2014) have produced very different results, while the modified SST has led to small changes only in the Adriatic phase. Thus, the definition of the initial condition is fundamental and its reliability strongly affects the final results. This could be explained simply considering the small scale of the system analysed, which has a mean radius of a few tens of km. Such a small structure cannot be completely described with operational analyses, but can be predicted by the BOLAM and MOLOCH model, that have a finer spatial resolution. This difference can be seen by considering that the cyclone paths obtained with the simulations initialized on 19 January are more accurate than those obtained with the simulations initialized the day after. In other words, when the cyclone is already present (but misrepresented) in the initial condition, the model takes some time to develop the consistent dynamical structure of the cyclone itself, compromising its future evolution to some extent. As a consequence of this, the *older* forecasts are often more accurate than new ones, at least for these phenomena.
It's very useful to compare the various trajectory drawn on the same map, Figure 4.36, with the trajectory derived from observations, Figure 2.12. This graphical representation allows to distinguish the best simulations on the basis of three basic features:

- the presence of the first intense phase on the Alboran Sea,
- the cyclone path southward of the Sardinia Island,
- the landfall near Naples' coast,
- the subsequent intensification and the distinct TLC phase on the Adriatic Sea.

A careful consideration of all the trajectories, especially in their *Adriatic phase* (Figure 4.37), leads one to conclude that the cases that best simulate the observed behaviour are B1, B3 and M3, especially by considering the features explained before.
Using the results presented in the previous section it's possible to create another type of graphic tool that allows to identify the cyclone thermal phase together with the system position over the geographical domain. It has been shown that the following criteria are valid to distinguish the various thermal phases of the cyclone:

- $-V_t^{\mathrm{L}} < 0, \quad -V_t^{\mathrm{U}} < 0$: deep cold core
- $-V_t^{\mathrm{L}} > 0, \quad -V_t^{\mathrm{U}} < 0$: shallow warm core
- $-V_t^{\mathrm{L}} > 0, \quad -V_t^{\mathrm{U}} > 0$: deep warm core

It's useful to plot the cyclone path again, assigning a specific color to each thermal phase. By using the following approach, a direct comparison between simulation data and observations it's possible, since the phases of predicted intensification are reported directly on the map.

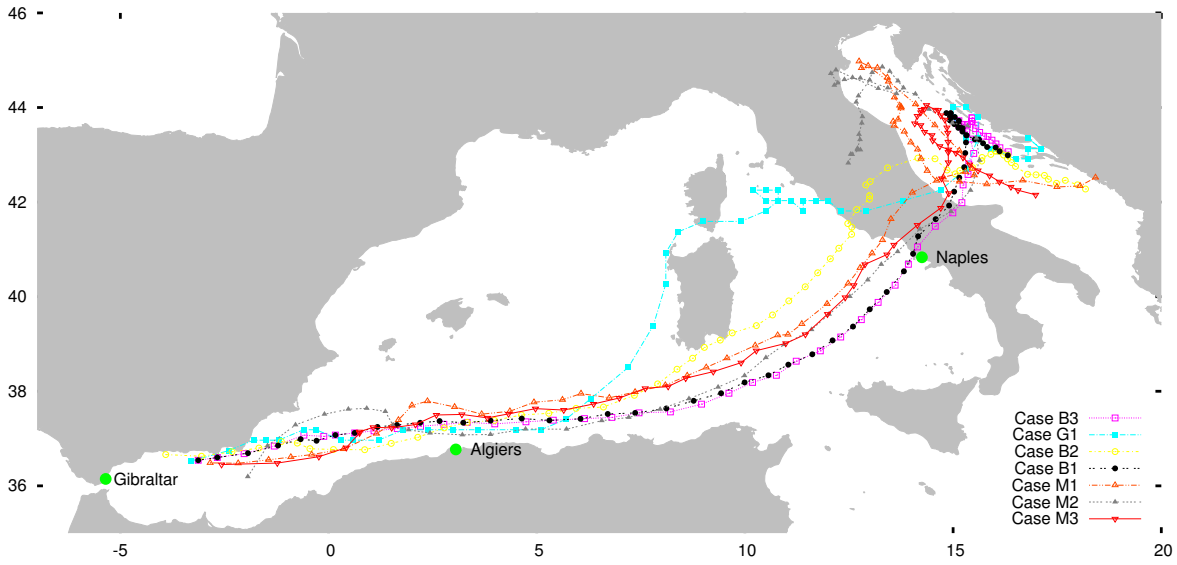

Figure 4.36.: Comparison of cyclone trajectory obtained in cases G1, B1, M1, M2 , B2, B3, M3. In order to compare the location of cyclone landfall, the position of Naples has been marked with a green point.

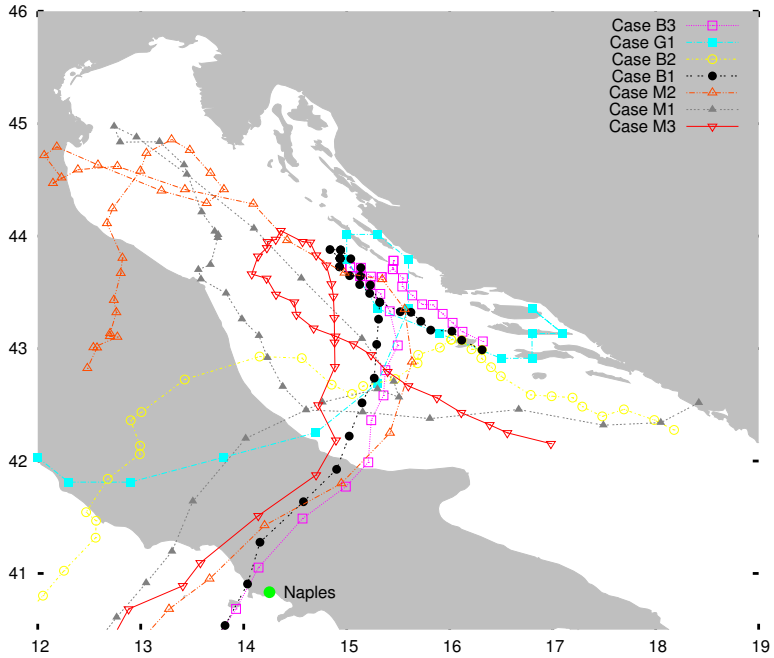

Figure 4.37.: Comparison of cyclone trajectory obtained in cases G1, B1, M1, M2, B2, B3, M3 - detail on the Adriatic Sea.

In Figure 4.38 the two mature phases of the cyclone, respectively over the Northern Africa coast and in the Adriatic Sea, are evident. Curiously enough, the Thyrrenian phase shows no evidence of a warm core structure.
The differences caused by using a different SST can be appreciated comparing Figure 4.38

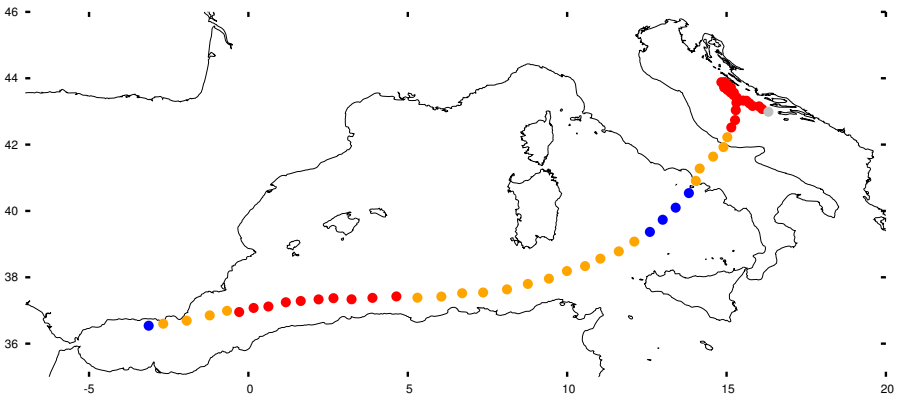

Figure 4.38.: Cyclone path forecasted in the B1 case. The color of each point matches a specific thermal phase: grey=undetermined, blue=deep cold core, orange=shallow warm core, red=deep warm core .

and Figure 4.39. In the Western Mediterranean both cases shows nearly identical cyclone phases. Conversely, the B3 case with modified SST shows evidence of a deep cold core structure during the whole Thyrrenian phase, while the cold core identified in the B1 case is limited to the 4 hours prior to landfall. Other differences can be highlighted in the Adriatic phase, where the cyclone, according to the B1 case, has always a deep warm core structure. Despite the lack of the circular trajectory, the B3 case correctly predicts the deep warm core structure only in the final phase of the simulation, from the 60^{th} hour onwards. The

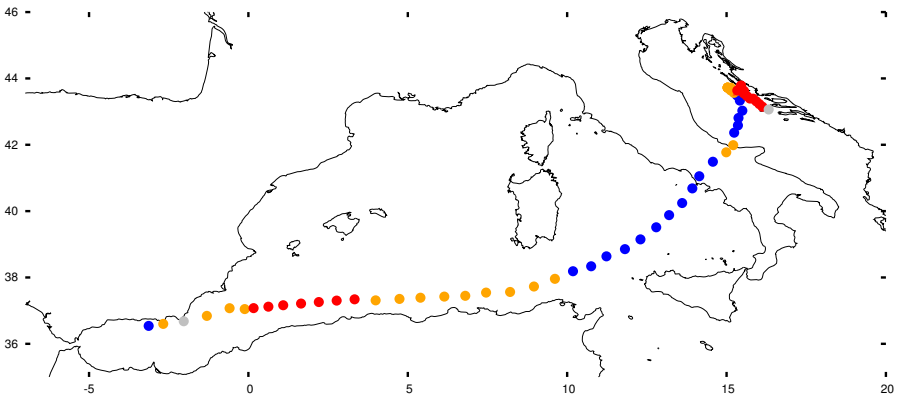

Figure 4.39.: Cyclone path forecasted in the B3 case. The color of each point matches a specific thermal phase: grey=undetermined, blue=deep cold core, orange=shallow warm core, red=deep warm core .

simulation carried out by the MOLOCH model in the M3 case shows no evidence of a deep cold core structure in the Thyrrenian phase, even though the two warm core phases identified are similar to those observed in the B1 and B3 cases. Figure 4.40 also shows that, during landfall, the cyclone was characterized by a deep-warm core structure. A similar comparison was conducted using the simulations initialized on 20 January, but for the sake of clarity the data were reported on a different map, shown in Figure 4.41. On the basis of the classification presented earlier, only the cases initialized with the ECMWF analysis

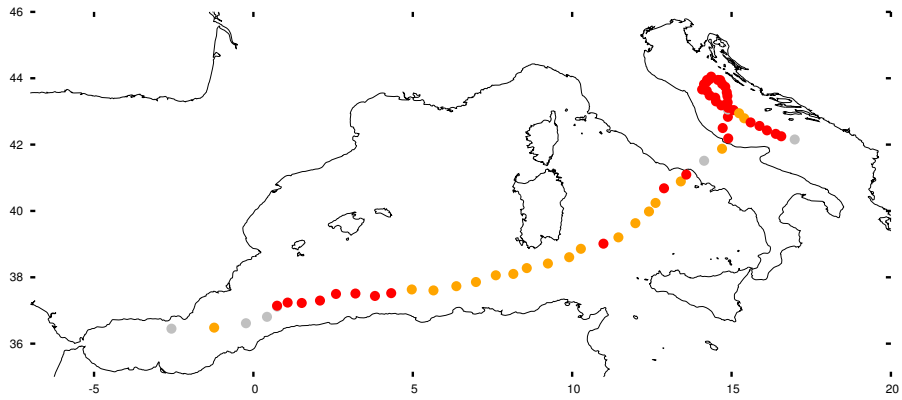

Figure 4.40.: Cyclone path forecasted in the M3 case. The color of each point matches a specific thermal phase: grey=undetermined, blue=deep cold core, orange=shallow warm core, red=deep warm core .

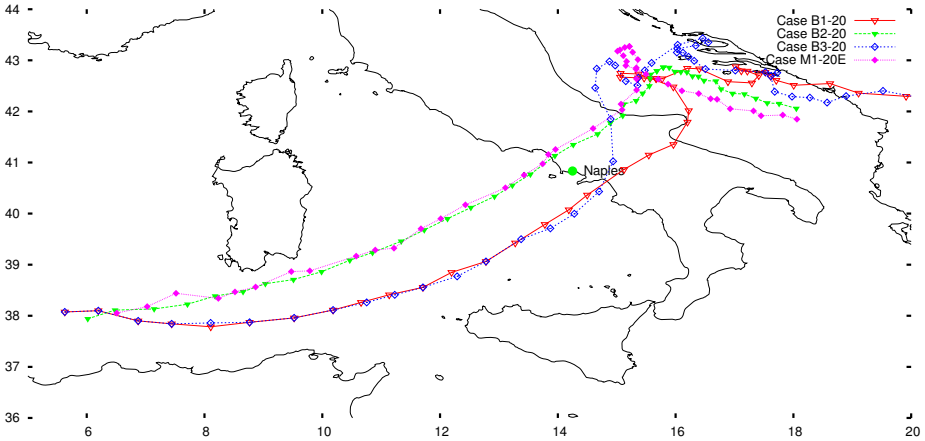

Figure 4.41.: Comparison of cyclone trajectory obtained in cases B1-20, B2-20, B3-20 and M1-20E. In order to compare the location of cyclone landfall, the position of Naples has been marked with a green point.

seem to meet the required features (landfall north of Naples, circular trajectory on the Adriatic Sea). The simulations performed with GFS analysis deviate to the south earlier and thus identify a wrong trajectory. Among these four cases, the M1-20E seems to better simulate the cyclone structure, especially in the Adriatic phase. The combination of cyclone phase and trajectory shown in Figure 4.42 seems to distinguish several interesting stages of development, including:

- a deep warm-core phase prior to the landfall, which may agree with the intensification observed upon arrival near Naples coast,
- a subsequent shallow warm-core phase during the first contact with the Adriatic warm waters,
- a final deep warm-core phase off the Salento peninsula.

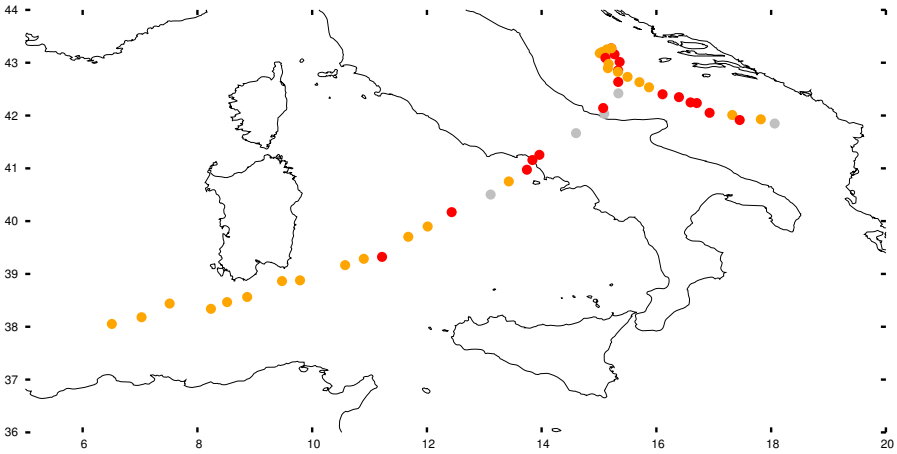

Figure 4.42.: Cyclone path forecasted in the M1-20E case. The color of each point matches a specific thermal phase: grey=undetermined, blue=deep cold core, orange=shallow warm core, red=deep warm core .

4.6. Cyclone three-dimensional structure

In the previous sections, the cyclone phase space analysis allowed to outline the three-dimensional structure of the cyclone by mean of three simple parameters. However, this type of analysis may fail to identify the features of some systems that exhibit a strange behaviour. In these cases a direct inspection of the three-dimensional structure of the cyclone is required. This goal can be achieved using several cross sections of the cyclone at various stages of the life cycle.
From the observation of Figure 4.21, and by comparing also the graphs obtained in the other cases, the cyclone seems to reach its maximum intensity at about the 15^{th} hour of simulation. The MSLP forecasted field in the B3 case, contained in Figure 4.43, shows a deep low, with several closed isobars, confirming that this instant corresponds to one of the most intense phases of the cyclone life-cycle. The zonal cross-section of the cyclone at this time shows the evidence of a low-tropospheric cyclonic circulation, with maximum wind intensity up to 20 m/s. Furthermore, Figure 4.44 (a) shows that the system is not completely symmetrical with respect to the z-axis, since the winds on the western side are more intense than those on the eastern side. The tilt of the wind speed isolines near the MSLP minimum indicates a strong intensification of surface winds, that can be assimilated to the eye-wall feature. A relative maximum is also present in the θ field. The humidity distribution shown in Figure 4.44 (b) locates a small area of relatively drier air above the MSLP minimum. However, the presence of an eye may be hidden by the medium- to high- cloud cover highlighted by the surrounding moist air . A significant maximum of PV partially overlaps on the area described before.
From the observations reported in chapter 2, it appears that convection plays a significant role during the first phase of cyclone intensification. Since the convection in BOLAM model is fully parametrized, with a certain degree of approximation, the model may not resolve properly the convection associated with the minimum deepening. The comparison of the

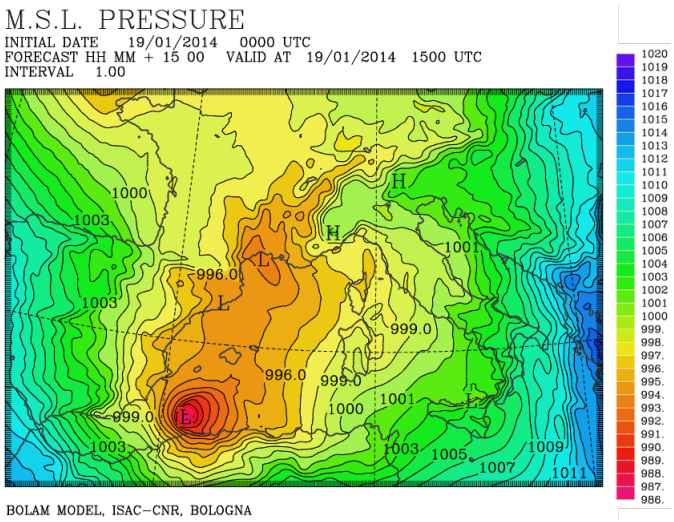

Figure 4.43.: MSLP field forecasted in the B3 case on 19 January at 15 UTC

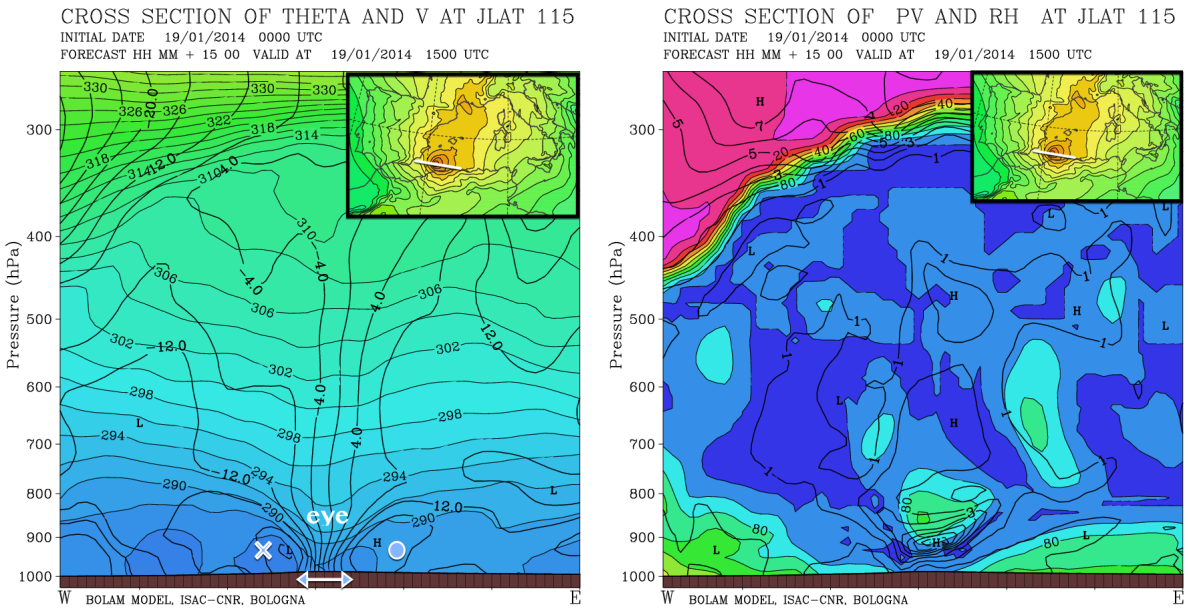

(a) θ, v (b) PV, RH

Figure 4.44.: Cross sections in the B3 case on 19 January at 15 UTC. The white line in the upper right panel indicates the path used for the cross section.

cross sections obtained with both BOLAM and MOLOCH models, shown in Figure 4.45, allows to distinguish many differences between the two models. The convection associated with the northern side of the cyclone is more prominent in the BOLAM cross section, but only because the MOLOCH model develops this upward motion on a tilted axis. While the low-level return flow, described in chapter 1, on the southern side of the cyclone is disturbed by the North-Africa orography in both models, MOLOCH seems to identify a cell with a different circulation to that would be expected. In order to avoid the contamination due to

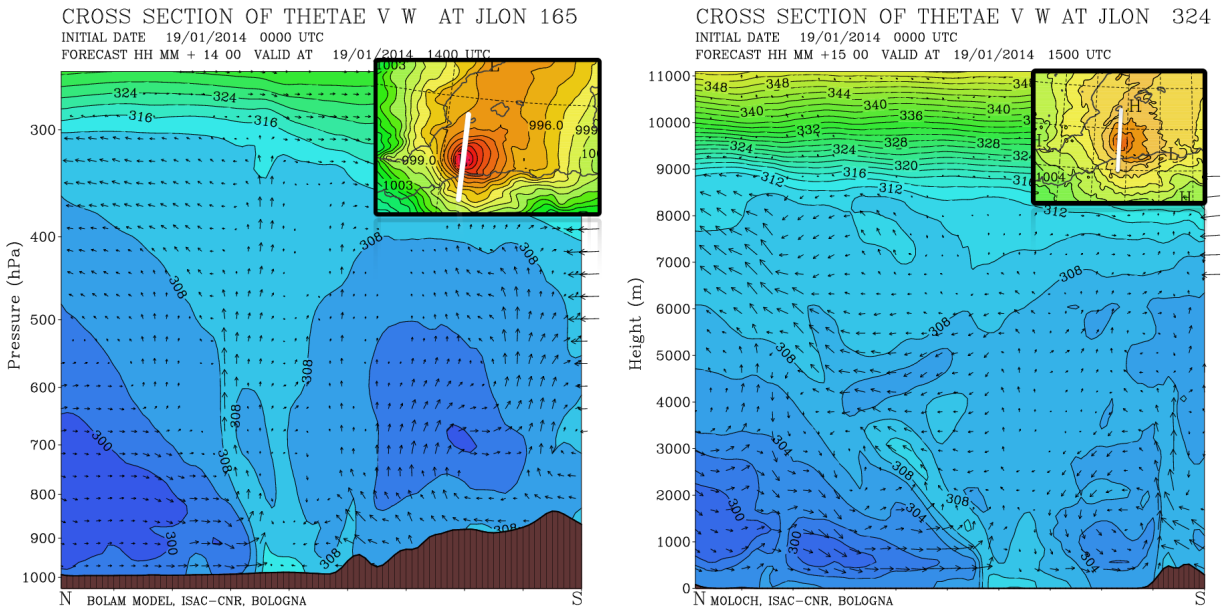

(a) θ_e, v, w in the B3 case

(b) θ_e, v, w in the M3 case

Figure 4.45.: Cross sections in the B3, M3 cases on 19 January at 15 UTC. The white line in the upper right/left panel indicates the path used for the cross section.

the effect of orography, zonal cross-sections of both models were considered but no significant upward motion was found in neither of them.
As the size of the cyclone tends to further decrease in the subsequent hours, the BOLAM model is not able to represent the entire structure of the system, so that its signature is less and less visible. In the Adriatic phase, when the cyclone has reached dimensions of approximately 40-50 km, only the MOLOCH model is still able to capture both the rotating winds and the remaining convection, as shown in Figure 4.46 (a) and (b) respectively. The good performance of the MOLOCH model in simulating the structure of the small-scale system can be evaluated also by looking at the model ouput in the M3 case. The simulated cloud cover shown in Figures 4.47 and 4.48 highlights the free-cloud eye and the spirally distributed cloud bands. The wind distribution shown in Figure 4.49 highlights the small-scale structure of the cyclone, with rapidly rotating winds over a small portion of the model domain in the Adriatic Sea.

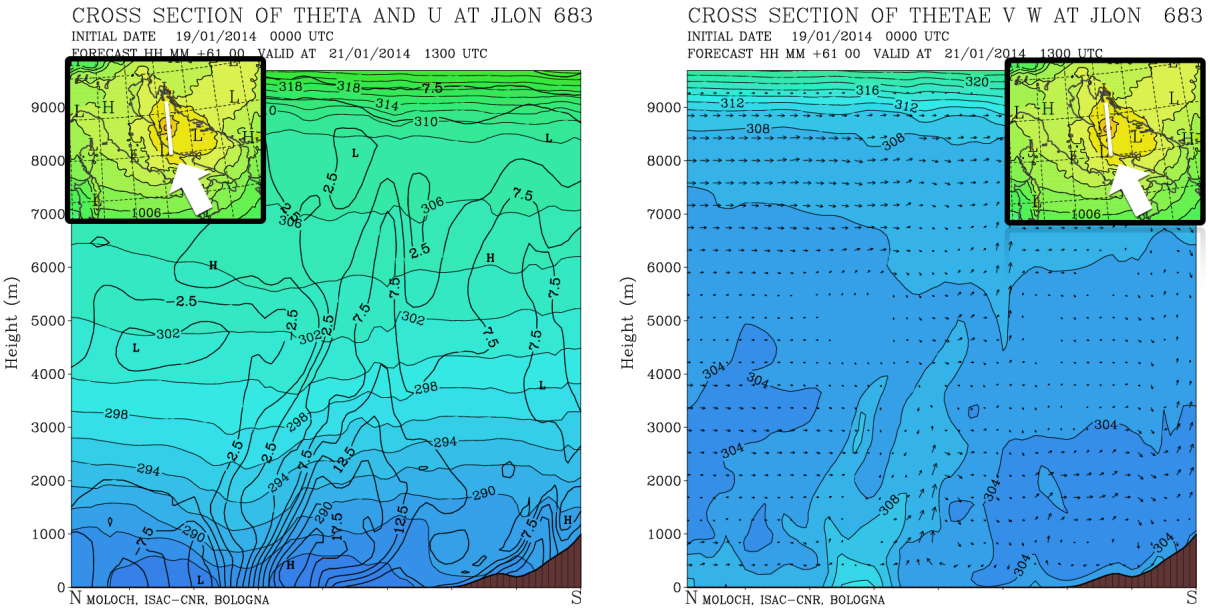

(a) θ, u (b) θ_e, v, w

Figure 4.46.: Cross sections in the M3 case on 21 January at 13 UTC. The white line in the upper left/right panel indicates the path used for the cross section.

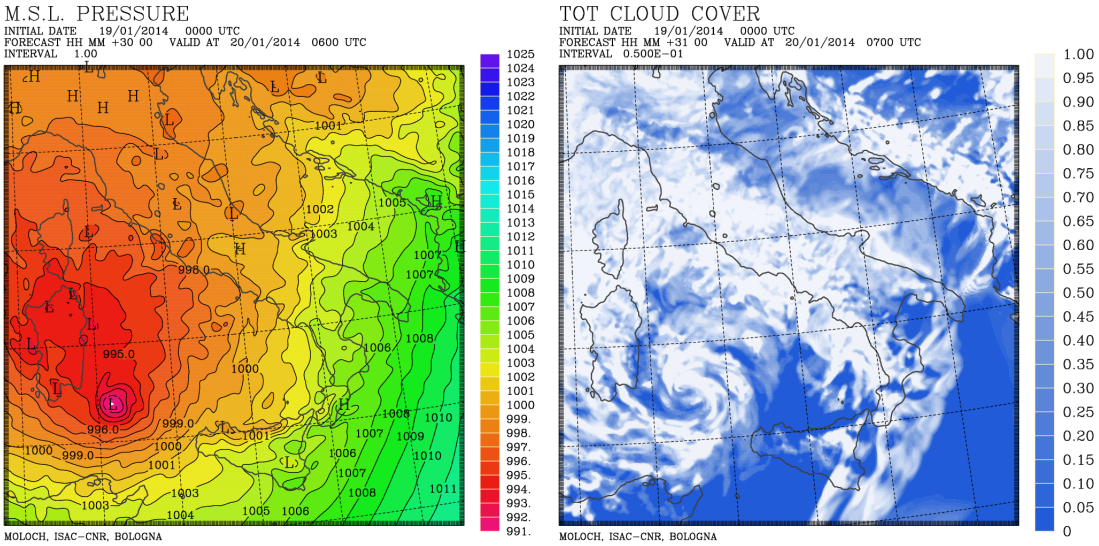

(a) MSLP (b) Total Cloud Cover

Figure 4.47.: Comparison between MSLP and Total Cloud Cover forecasted in the M3 case on 20 January 2014 at 06 UTC

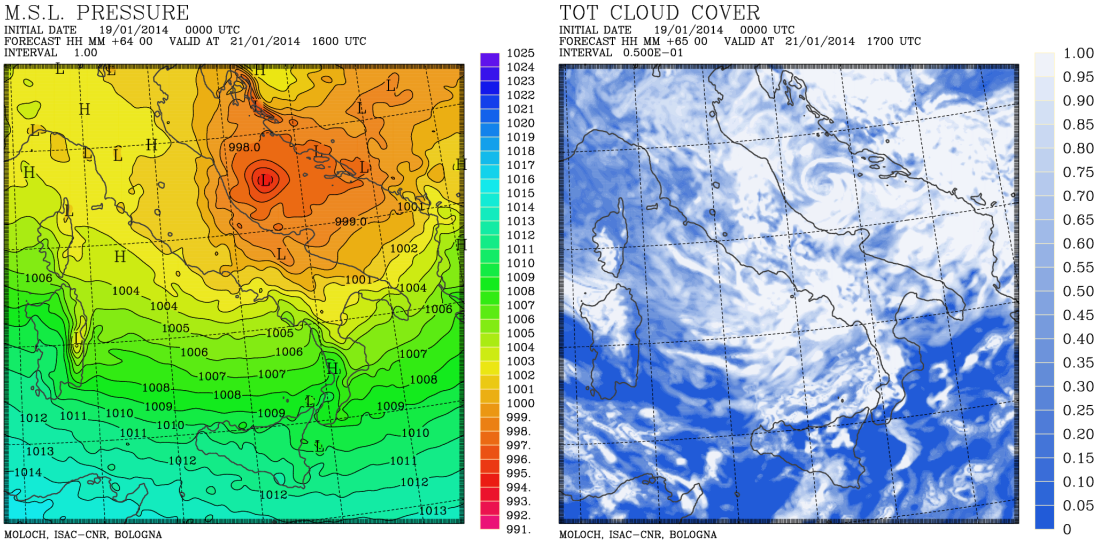

(a) MSLP (b) Total Cloud Cover

Figure 4.48.: Comparison between MSLP and Total Cloud Cover forecasted in the M3 case on 21 January 2014 at 16 UTC

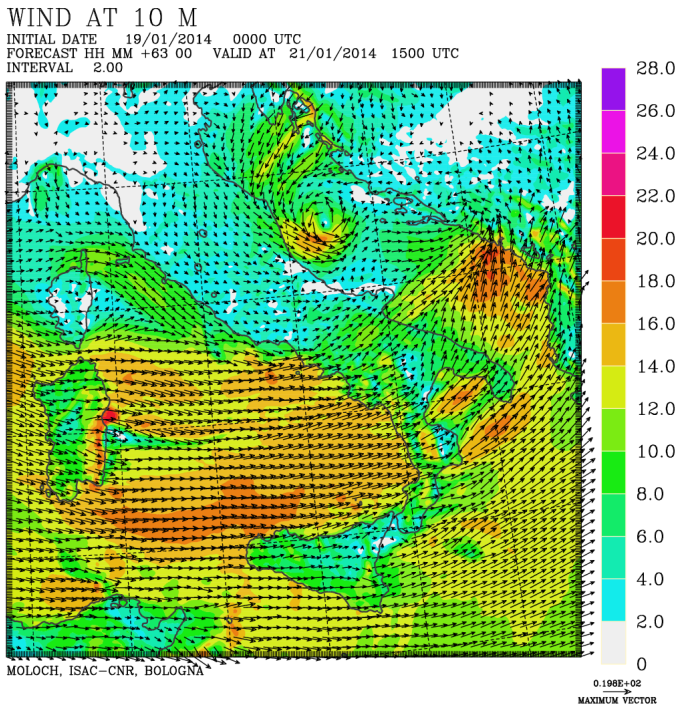

Figure 4.49.: 10 meters wind forecasted by the MOLOCH model on 21 January 2014 at 15 UTC.

4.6.1. Remarks on model initialization and boundary conditions

In section 4.4.8 the improvement of cyclone trajectory with ECMWF analysis, as compared toGFS, was shown for the simulation initialized on January 20. As discussed in section 4.5, the cyclone evolution depends to a large extent on the boundary and initial condition used. This is especially true for the case of a simulation initialized when the cyclone has already formed. While the simulation performed in the other cases may create the small-scale system during the time integration over 72 hours, a simulation initialized one day after must have an accurate analysis, in order to predict the cyclone evolution. However, such a prerogative is not always satisfied in neither ECMWF or GFS analysis, since the small spatial scale of Medicanes is hardly represented by coarse resolution analysis. The results presented in section 4.4.8, together with Figure 4.28 (a) and (b), already showed that minor differences between GFS and ECMWF analysis led to very different results. Thus, it's interesting to evaluate the differences in the vertical structure of the two initial conditions. Aside from the clearly different resolution adopted in the two analysis, the ECMWF structure shows a slightly stronger vortex, with wind maxima closer to each other. Moreover, the temperature perturbation shown in Figure 4.50 is more evident in the ECMWF analysis, where the disturbance reaches almost the 250 hPa level. It should be also noted that the dynamic tropopause is placed at higher altitudes in the ECMWF analysis. The cross sections

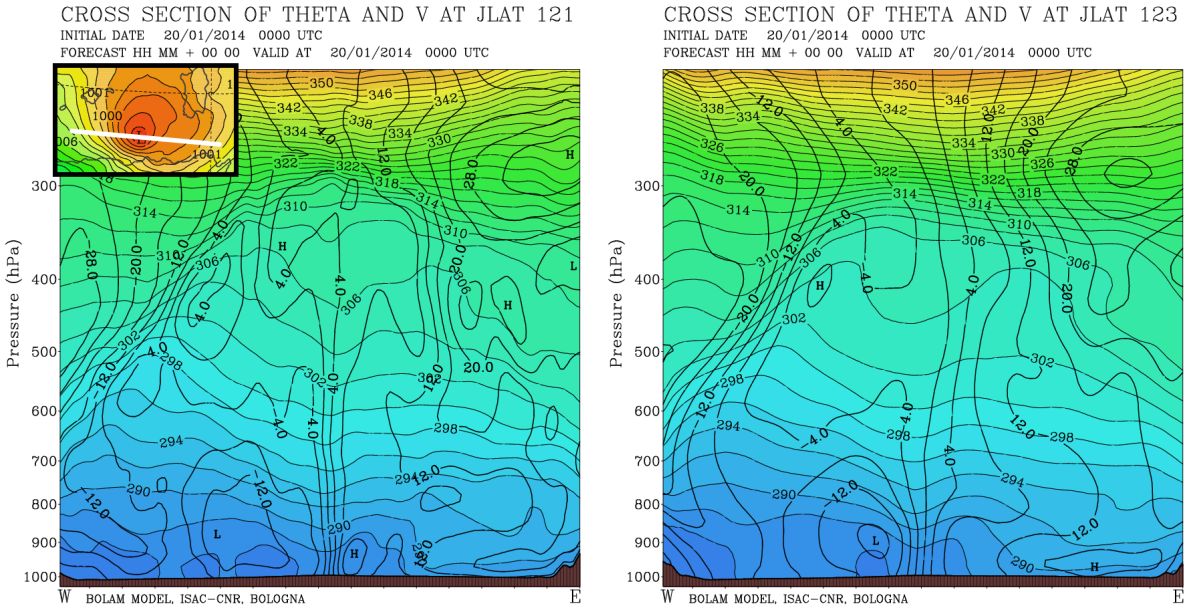

(a) θ, v in the ECMWF analysis

(b) θ, v in the GFS analysis

Figure 4.50.: Cross sections in the B1-20 and B1-20E cases on 20 January at 00 UTC (initial condition). The white line in the upper left panel of part (a) indicates the path used for the cross section.

presented in Figure 4.51 show an elongated PV maximum, with larger values in the ECMWF analysis, up to 3 PVU. Considering the low altitude where this maximum is located (about 800 hPa), it may be inferred that it played a key role in the *spin-up* and maintenance of the

cyclone. Another maximum of PV is evident in both cross-sections near the 300 hPa level, although the one described by ECMWF is more localized and intense.

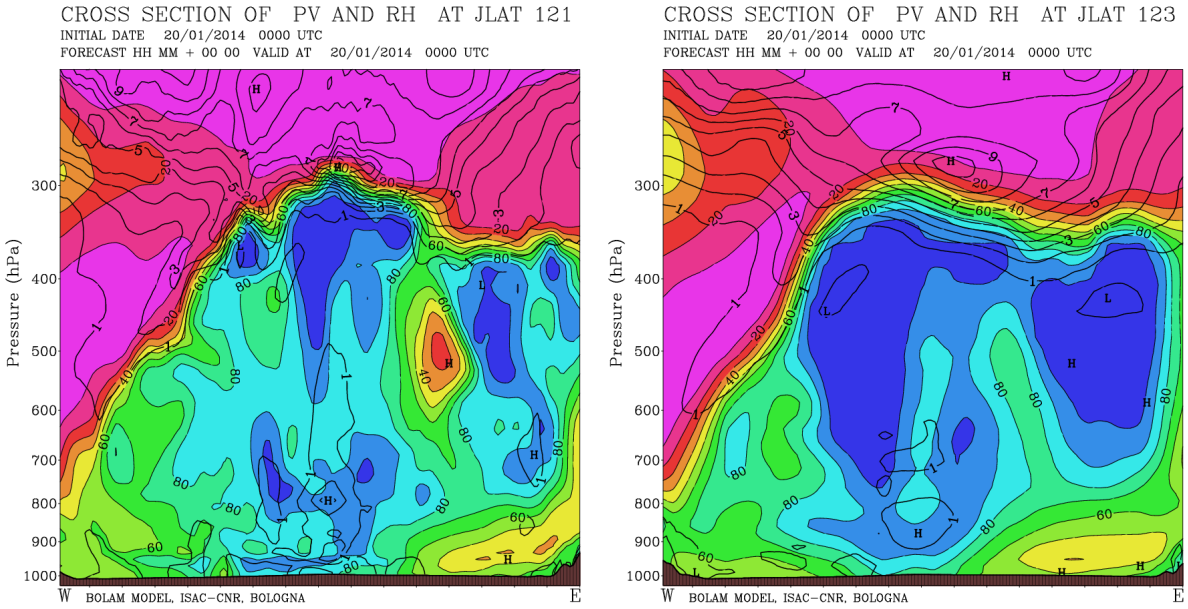

(a) PV, RH in the ECMWF analysis

(b) PV,RH in the GFS analysis

Figure 4.51.: Cross sections in the B1-20 and B1-20E cases on 20 January at 00 UTC (initial condition). The path used for the cross section is the same of Figure 4.50.

4.7. The role of SST

The warm waters of the Mediterranean sea play a key role in rejuvenating the cyclonic system over its entire life cycle. As explained in chapter 1, the driving force of tropical cyclones is mainly latent heat release through convection (Kuo [60]) and the mechanism of air-sea interaction (Emanuel [34]) is a crucial requirement for their intensification. Latent and sensible heat fluxes can be related to the air-sea temperature gradient with the usual *bulk formulas*:

$$\phi_{\mathrm{SH}} = \rho C_d c_p |\mathbf{V}| (T_{\mathrm{sea}} - T_a) \tag{4.6}$$

$$\phi_{\mathrm{LH}} = \rho C_d L_v |\mathbf{V}| (q_s - q_a) \tag{4.7}$$

where ρ is the air density, C_d is the drag coefficient, c_p is the specific heat at constant pressure, L_v the latent heat of vaporization, $|\mathbf{V}|$ is the surface wind speed, T_a is the air temperature, q_s, q_a are the specific humidity of saturated air and actual air, respectively. Emanuel [33] showed that the maximum wind intensity that a hurricane could reach in a steady state is given by

$$|\mathbf{V}_{\mathrm{max}}| = \frac{C_k}{C_d} \frac{T_{\mathrm{sea}} - T_a}{T_a} (h_s^* - h^*) \tag{4.8}$$

where C_k is the enthalpy exchange coefficient and h_s^* is the saturation moist static energy of air at the sea level at the sea surface temperature. In the Mediterranean Sea $|\mathbf{V}_{\max}|$ is usually too small to support tropical cyclones, but the advection of a cold upper low could greatly increase the air-sea thermal disequilibrium. Tous and Romero [109] have shown that *Medicane* genesis and intensification requires a SST of at least 15°C. In this case study the SST under the simulated cyclone is always lower than this threshold, except for the Thyrrhenian phase. The data shown in Figure 4.52 allow to identify a link between the

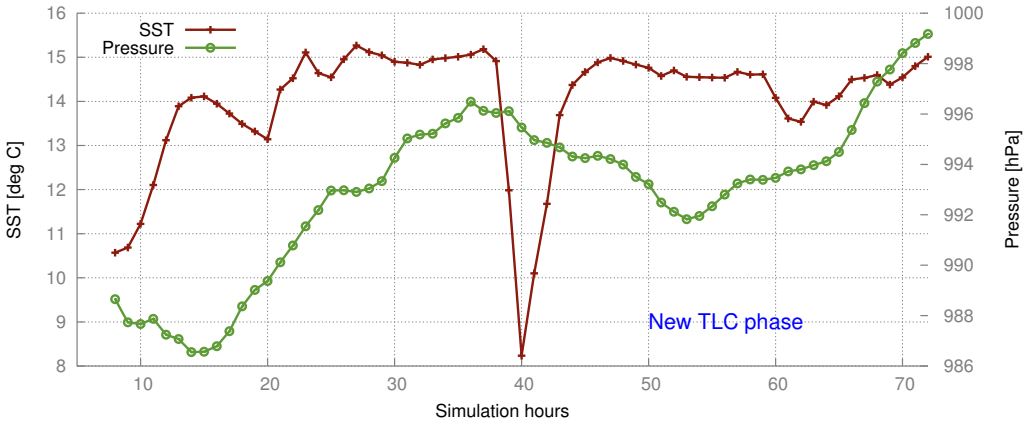

Figure 4.52.: Mean SST over a circle of radius R_{ex} and pressure as functions of time in the B3 simulation. The temperature drop between the 39$^{\text{th}}$ and the 45$^{\text{th}}$ hour is caused by the landfall: SST is not defined over land.

deepening of the low pressure system and the underlying SST rise, in particular between the 10-20 hours period and in the Adriatic phase.
Many authors (Cione and Uhlhorn [27] and references therein) have studied changes induced on the SST by the presence of hurricanes. The results showed that the heat fluxes associated with strong winds may cause storm-induced cold wake of up to 3-5°C of temperature deficit. In order to evaluate this effect, the SST data, both from model output and analysis, were considered. The SST analysis is provided every 24 hour, while the SST obtained from the model output can be evaluated every hour. In order to obtain fields as comparable as possible, the analysed SSTs have been smoothed using a 9-point spatial filter and time-averaged using a 3-day running mean. Figure 4.53 shows the SST difference between 21 January and 19 January, the first two days of the cyclone life-cycle[6]. From the analysis of Figure 4.53 a small correlation between cyclone trajectory and SST cold wake arises, especially in the Western Mediterranean (-0.3°C) and in the Thyrrenian sea ($-0.5 \div -0.6$°C). The same SST difference, computed using the model output, is shown in Figure 4.54. In this case, no filter was applied to the data, since the model does not have noise associated with the analysis. In Figure 4.54 the correlation between cold wake and cyclone trajectory is visible along the North-African coast and in the Thyrrenian Sea. The minima located on the Lion's Gulf and in the Balearic seas are caused by the Mistral wind that insisted for days: this correlation is highlighted in Figure 4.55, where the observed wind is reported. A direct comparison of

[6]Recall the cyclone trajectory presented in Figure 2.12.

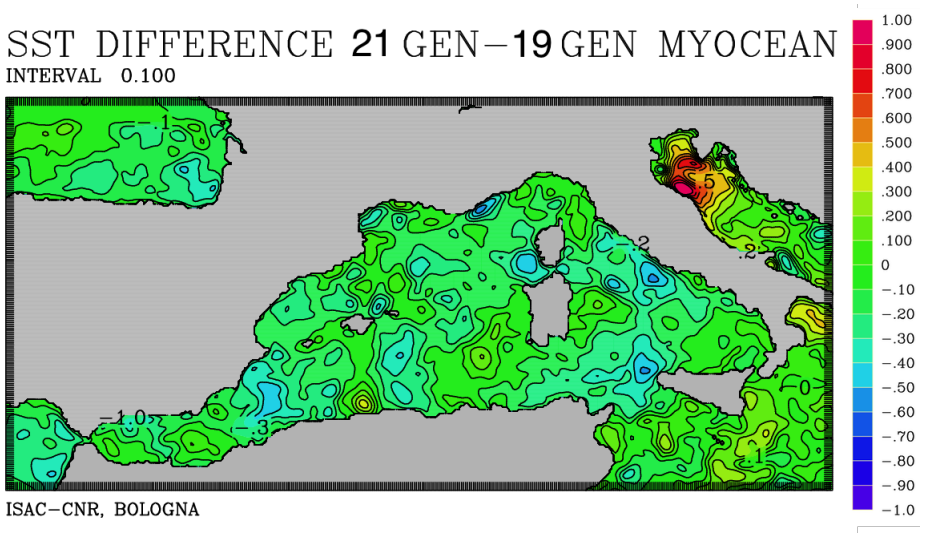

Figure 4.53.: Sea-Surface Temperature difference between 21 January 2014 and 19 January 2014. The data are provided by MyOcean and were filtered and averaged using a 3-days running mean.

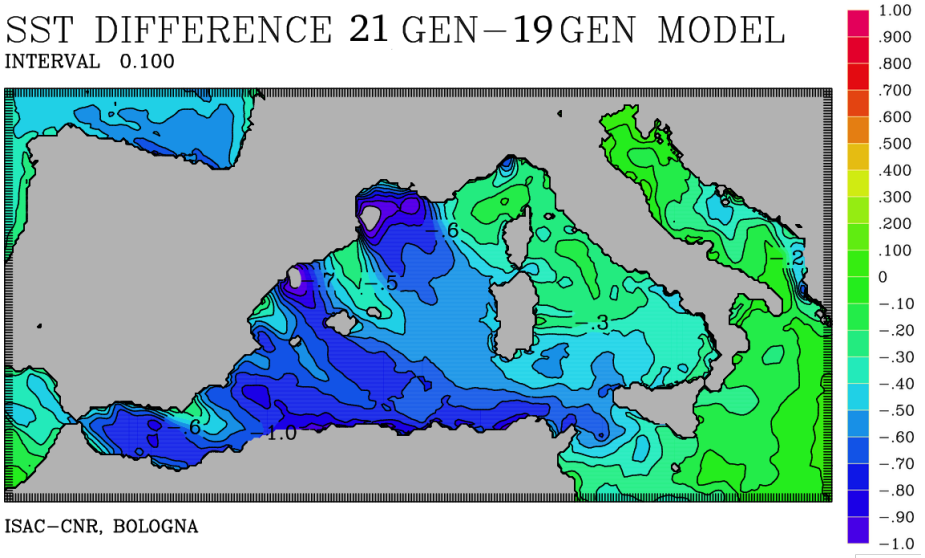

Figure 4.54.: Sea-Surface Temperature difference between 21 January 2014 and 19 January 2014. The data are taken directly from BOLAM model output in the B3 case.

Figure 4.54 and Figure 4.53 shows that the sea water cooling by wind induced sensible heat fluxes is overestimated in the aforementioned areas. This can be explained by considering the governing equation from the sea water temperature used in BOLAM, which considers a simple slab-ocean model with uniform depth. The temperature variation with time consists of a forcing term which depends on the heat fluxes at the surface and of a relaxing term that prevents high deviation from the initial state:

$$\frac{\partial}{\partial t} T_{\text{sea}}(t) = -C \underbrace{\left(\phi^{\uparrow}_{\text{SH}} + \phi^{\uparrow}_{\text{LH}} + \phi^{\uparrow}_{\text{IR}} + \phi^{\uparrow}_{\text{SW}}\right)}_{\text{forcing}} - \underbrace{\frac{1}{\tau}\left(T_{\text{sea}}(t) - T_{\text{sea}}(0)\right)}_{\text{relaxing}} \tag{4.9}$$

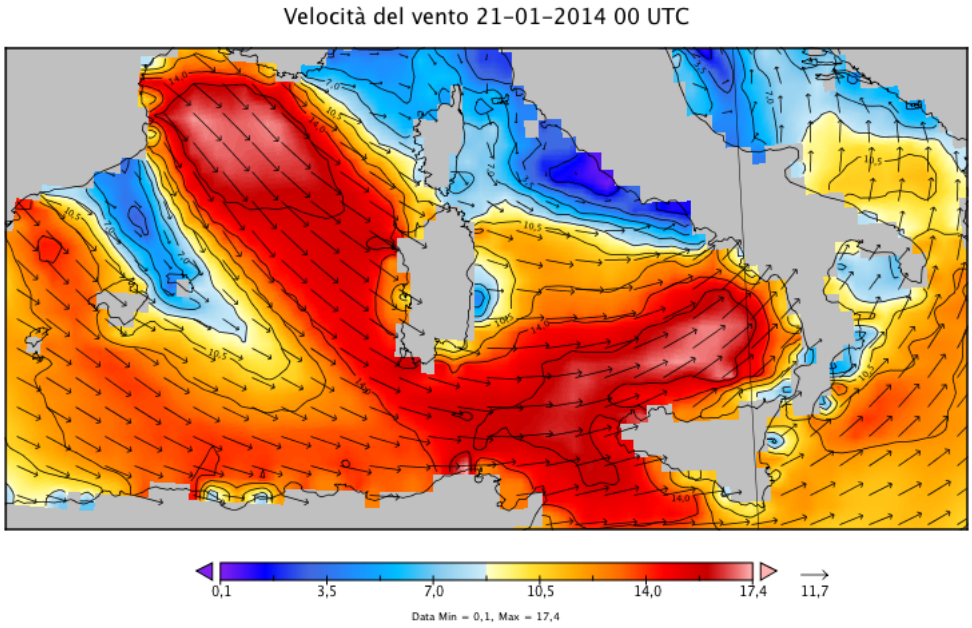

Figure 4.55.: Surface winds derived from satellite observations by the Centre ERS d'Archivage et de Traitement (CERSAT) institute, provided by MyOcean website and interpolated by the author using Panoply software. Vectors shows the direction of the wind, while colour filled contour indicate the intensity. The values are referred to 21 January 2014 at 00 UTC.

where $\phi_{\mathrm{IR}}, \phi_{\mathrm{SW}}$ are the Infra-Red (IR) and Short-Wave (SW) heat fluxes respectively, C is the heat capacity and τ is a relaxing time (of the order of 1.5 days). The heat capacity can be expressed by mean of the specific heat (c_p) and density of water, and of the mixed layer depth Δh:

$$\frac{1}{C} = c_p \cdot \rho \cdot \Delta h \tag{4.10}$$

In the BOLAM code this value is assumed equal to $0.33 \cdot 10^{-7}$, so that the height of the mixed layer is approximately equal to 7 meters. In order to correct the overestimation of the SST cooling, the heat capacity C should be reduced, for instance by increasing the height of the mixed layer Δh. A modified version of the BOLAM code, with a heat capacity of $C/2$, was used to perform a new simulation of the B3 case, with testing purpose. The minimum of SST difference between 21 January and 19 January decreased from -0.9 to -0.5, although the correlation with the observed difference was still low (not shown). While the predicted thermal phases of the cyclone were almost the same of the B3 case, the cyclone path forecast greatly improved in the Adriatic phase showed in Figure 4.56 where a circular trajectory appeared.
In order to further improve this forecast, the MOLOCH model has been nested into this BOLAM simulation with two different cases: in the first one the heat capacity C in the MOLOCH code has not been changed, while in the second one $C/2$ was used instead. These two cases showed high sensitivity to sea surface heat fluxes, since the trajectories obtained were completely different in the Adriatic phase. The cyclone trajectory obtained in the

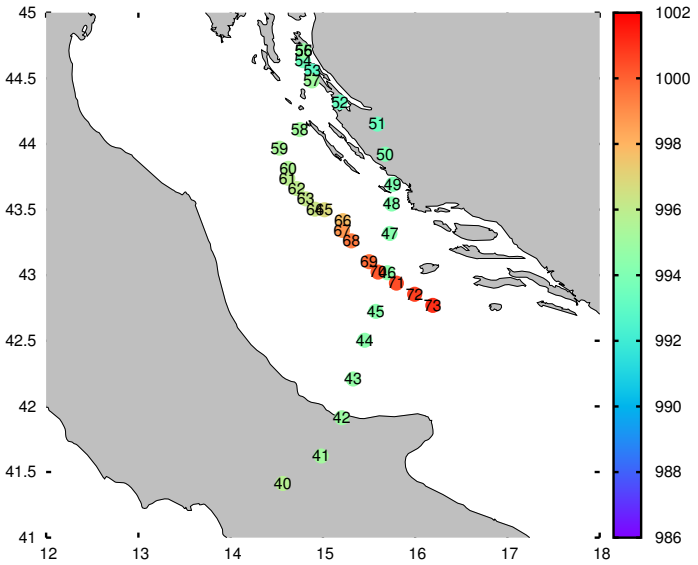

Figure 4.56.: Cyclone trajectory forecasted in the B3 case, using a modified heat capacity (see text for details).

MOLOCH simulation with heat capacity C, shown in Figure 4.57, is in very good agreement with the observed one. Conversely, the cyclone path forecasted with modified MOLOCH

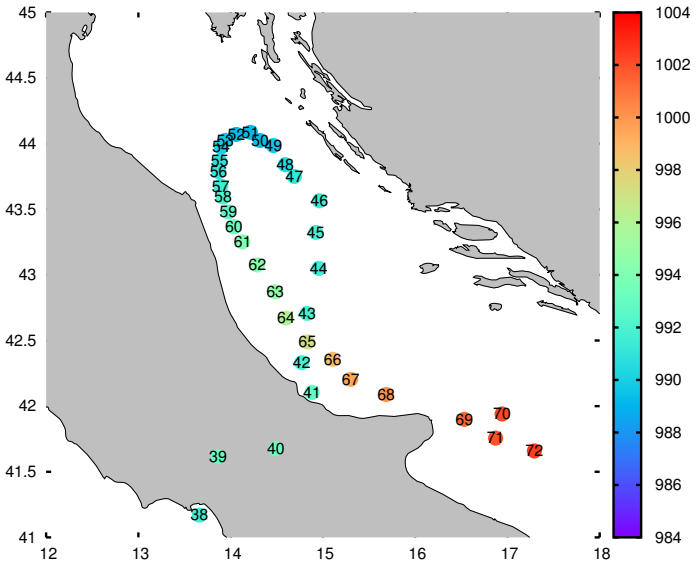

Figure 4.57.: Cyclone trajectory forecasted in the M3 case, modified by nesting into the B3 case with modified heat capacity.

heat capacity $C/2$ shows a very different pattern, with no circle trajectory on the Adriatic Sea (not shown). These results confirm what has already been noted in section 4.5:

- The BOLAM model is able to successfully simulate all the cyclone phases if the SST is accurately prescribed;

- There is strong sensitivity to SST distribution, especially in the Adriatic Sea. The positive anomaly of SST shown in case B3 discussion may concur to this behaviour.
- The simulation performed with the MOLOCH model does not show significant differences in the Mediterranean-Thyrrenian phase, while it corrects the cyclone trajectory in the Adriatic phase. This could be related to the very small structure possessed by the cyclone in this phase.

In order to better simulate events like the one studied, given the results shown before, the equation of the slab-ocean model should be revised by introducing a new heat capacity as a function of the different area, to discern between the different mixed layer features and of the surface wind speed. For this reason, the use of a coupled atmosphere-ocean would be desirable.

5

The Atlantic phase: Upper Air precursor Analysis

5.1. Introduction

The risk assessment related to the formation of TLCs over the Mediterranean Sea is crucial in order to limit the damage caused by strong winds, storm surge and floods. For this reason, several studies (Emanuel [33]; Tous and Romero [109]; Fita et al. [41]; Miglietta et al. [75]) have tried to characterized the meteorological environments associated with medicanes genesis and development. As stated in Chapter 1, a deep cut-off cold core low is usually observed at mid-upper tropospheric levels in association with the development of these systems. However, many special conditions may substantially influence the genesis and the further development. Tous and Romero [109] found that high values of mid-tropospheric relative humidity, significant diabatic contribution to the near surface level equivalent potential temperature and low values of troposheric wind shear[1] are important parameters involved in medicane genesis. Furthermore, Emanuel and Nolan [37], have shown that it's possible to obtain an index which expresses the probability of formation of medicanes, relying on the potential intensity defined by Emanuel (PI, see [35]). Using this index, Tous and Romero [109] have conducted a statistical study that indicated the possibility of fewer medicanes but a high number of strong MTLCs systems until the end of the century.
Nevertheless, no study has focused on the analysis of possible troposhere-stratosphere precursors in the days preceding the formation of a medicane. On the other hand, such research was conducted on hurricanes precursors, showing that the so-called *Easterly Wave* (Riehl [96]; Dunn [32]) contributes to the formation of nearly 85% of the major hurricanes (Landsea [63]) and to nearly all the tropical cyclones that occur in the Eastern Pacific Ocean (Avila and Pasch [7]). As for the Mediterranean area, many authors (Massacand et al. [71]; Fierli et al. [40]; Martius and Schwierz [69]; Argence et al. [6]) have studied the link between *potential vorticity streamers*[2] and heavy precipitation events in the Mediterranean. In this

[1] The similarity with the theory developed for hurricanes and exposed in chapter 1 should be noted

[2] A PV-streamer is an elongated band of potential vorticity located at the top of the troposphere. It is mesoscale in width and synoptic scale in length. PV-streamers are being investigated as contributing causes to severe local storms and flash floods through organized convection such as in mesoscale convective systems.

work, an analysis of a possible upper-air precursor is conducted, based on model simulations performed respectively 3 (17 gen) and 4 (16 gen) days before the cyclone formed over the Mediterranean Sea. In this chapter the GLOBO and BOLAM meteorological models are used, with the second one nested into the first one. Aside from the different domain, all the model features are the same described in Chapters 3 and 4.

5.2. Upper-air precursor identification and tracking

The disturbance which likely caused the medicane formation can be traced back upstream out of the Mediterranen area. Starting from the position of the pressure minimum in the morning of 19 January 2014, and going backward in time, it's possible to follow the disturbance, always in the form of a pressure minimum, over the North-Atlantic. At 00 UTC of 17 January 2014 the pressure minimum was located off the coast of Massachussets, North America, as shown in Figure 5.1. In the subsequent days, the pressure minimum moved to the

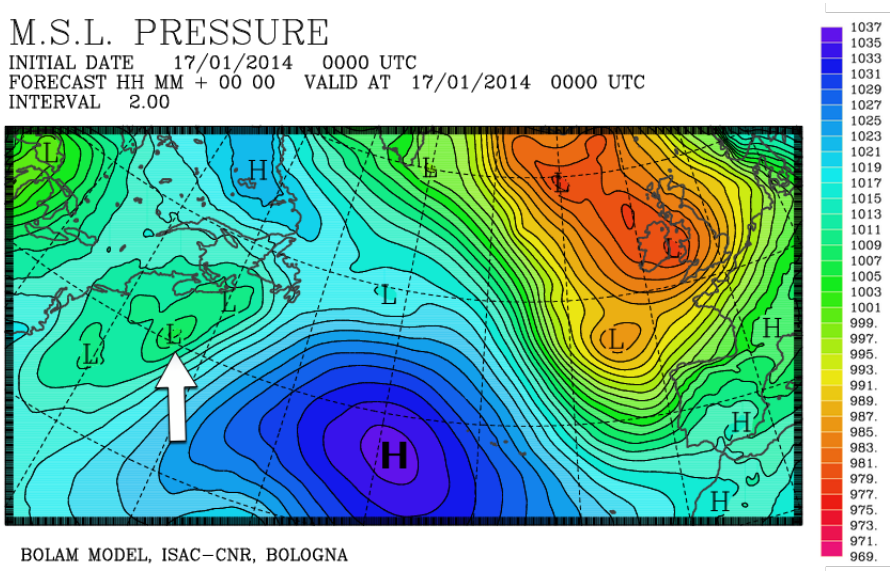

Figure 5.1.: Mean Sea Level pressure analysis at 00 UTC of 17 January 2014 .

East, following a curved path over the northern side of the Azores anticyclone, and eventually arrived on the western side of the low pressure system locate over the British Isles. Although the low pressure system was absorbed by this larger scale depression, a small-scale trough was clearly visible during the whole simulation time (see Figure 5.2). During the subsequent approach towards the Spanish coast, the minimum deepened from approximately 1000 hPa to 987 hPa; a possible reason for this behavior is proposed later on. The tracking of this system can be carried out using the same algorithm developed and explained in Section 4.2. However, two substantial modifications have been made in the code:

- The first search of the pressure minimum is carried out within a small box where the original precursor is observed. This is necessary to exclude the numerous and deeper relative minima that are present over the entire model domain.

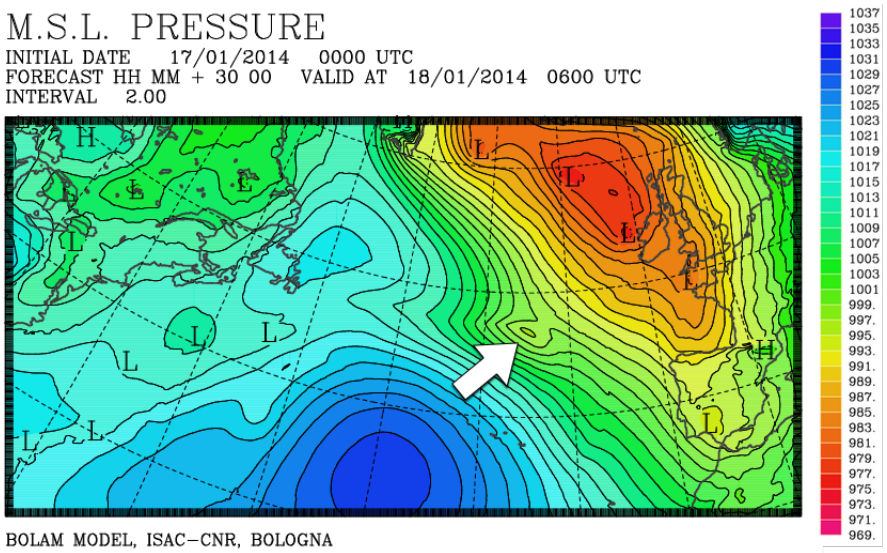

Figure 5.2.: The MSLP forecast for 18 January 2014 06 UTC shows the precursor embedded in the higher scale low pressure system located north of England .

- The radius $R_{ex} = R_{ex}(t)$ is now considered as a function of time, in order to account for the large variation of the system size. A wide range of different radii are assigned to three different phases (hours from 00 to 21, 22 to 30 and 31 to the end) .

With only these changes, the algorithm successfully finds and tracks the pressure minimum: the resulting trajectory is shown in Figure 5.3.

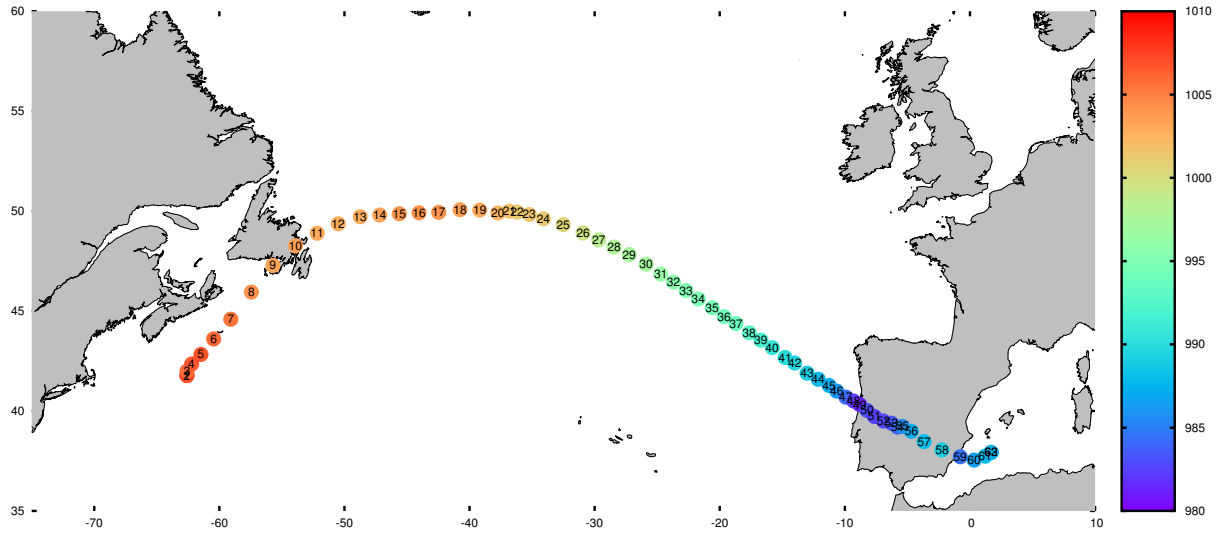

Figure 5.3.: Precursor trajectory. The pressure value is indicated by mean of the color bar. The last 10 time steps of the simulation are not shown, since the system is studied only outside the Mediterranean area.

The cyclone phase could be studied using the same method proposed by Hart [48] and employed in Chapter 4. Since the evidence of a warm-core structure is an indicator of the

hurricane-like phase, one can argue that the precursor phase may be characterized by a shallow-warm or deep-cold core structure. The right panel of Figure 5.4 confirms the argu-

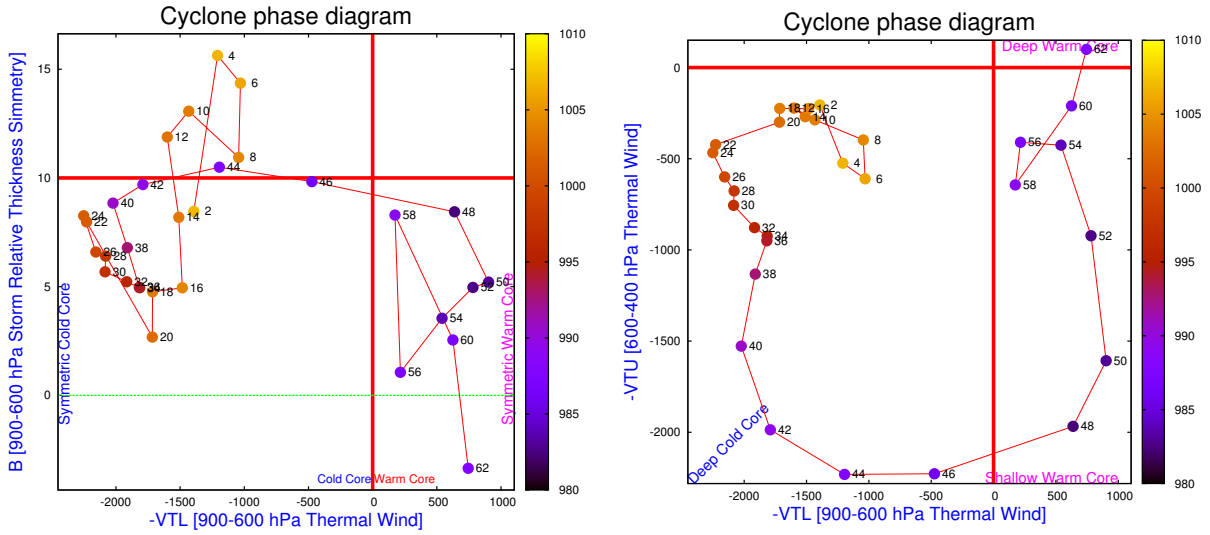

(a) $-V_t^{\mathrm{L}}$ versus B (b) $-V_t^{\mathrm{L}}$ versus $-V_t^{\mathrm{U}}$

Figure 5.4.: Cyclone phase space diagrams for the precursor phase.

ment explained above. In the first 2 days of the simulation (48 hours) the system possesses a deep-cold-core structure, typical of mature extra-tropical cyclones (Hart, [48]). During the following hours, the system undergoes a transition to a shallow-warm-core structure, exactly when the pressure minimum is deepening near the Spanish coast. The last time step shown in Figure 5.4 highlights the first evidence of a deep-warm core structure, given that the system is now on the Mediterranean Sea, eventually acquiring the first features typical of the Tropical-like phase (recall the path shown in Figure 5.3). The left panel of Figure 5.4 shows that the system has an asymmetrical structure only in the first 12 hours. It's worth noting that the $B = 10$ m threshold was never reached among the cases analyzed in Chapter 4. A careful analysis of Figure 5.5 allows to determine when the pressure undergoes a sharp decline, i.e. from the 20^{th} hour onwards. Furthermore, after the 37^{th} hour, a rapid deepening is observed from 994 hPa to 981 hPa, until the system makes landfall on the Spanish coast.

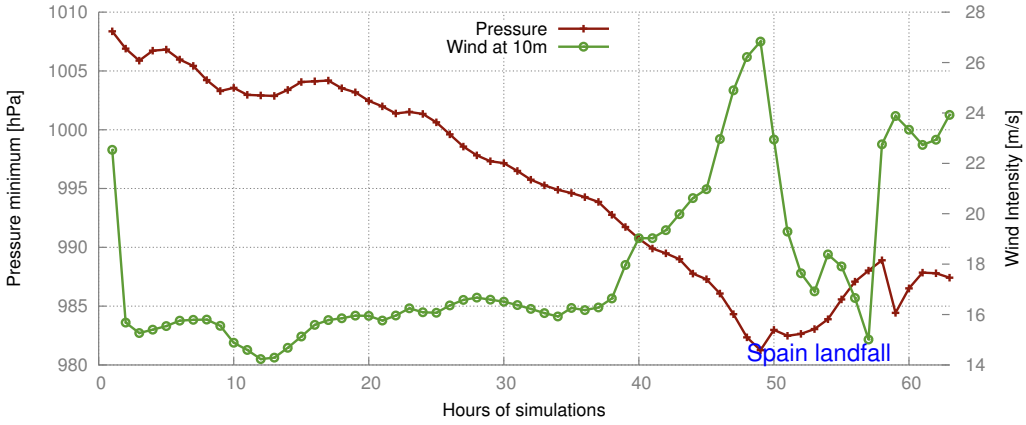

Figure 5.5.: Pressure minimum and maximum wind (computed on a radius R_{ex} around the pressure minimum) as a function of time (hours of model simulation).

5.3. Potential vorticity streamer

PV is a quantity that, following a parcel of air or water, can only be changed by diabatic or frictional processes. The idea of PV as a material invariant central to stratified, rotating fluid dynamics was first introduced and explored by Carl Gustaf Rossby in the 1930s. The first approximate formula by Rossby was then formalized by Ertel, using the Stokes' theorem. Equation 5.1 shows the common formulation used, where ζ_a is the absolute vorticity vector ($2\Omega + f$ in the Earth rotational system) and ρ is the mass density.

$$\text{PV} = \frac{\zeta_a \cdot \nabla\theta}{\rho} \tag{5.1}$$

The Potential Vorticity Units (PVU), defined by 5.2, are often used.

$$1\text{PVU} \equiv \frac{10^{-6} \cdot \text{K} \cdot \text{m}^2}{\text{kg} \cdot \text{s}} \tag{5.2}$$

Hoskins et al. [53] pointed out the correlation between potential vorticity exchange mechanisms and synoptic-scale features like the structure, origin and persistence of cutoff cyclones and blocking anticyclones, the physical mechanisms of Rossby wave propagation, baroclinic instability, and barotropic instability. According to Figure 5.6, the mean zonal potential vorticity ranges approximately from 0.3 to 0.5 PVU in the low and middle troposhere and reaches 1 PVU in the upper troposphere. Then, it increases sharply with height, becoming larger than 3 PVU in the lower stratosphere. This quasi-discontinuity allows to define the 1.5-PVU (or 2 PVU) surface as the *dynamical tropopause*, which divides the troposphere from the stratosphere. This climatological PV distribution is often perturbed by positive (negative) *anomalies*, i.e. regions with an isolated PV maximum (minimum), that modifies the temperature field and induces a cyclonic circulation that weakens towards the ground (Hoskins et al. [53]). Hoskins et al. also showed that, if the static stability is sufficiently low, the circulation induced by a PV anomaly may reach the ground. Figure 5.7 sketches the cyclogenesis mechanism by using the PV concept. When a tropopause dynamical positive

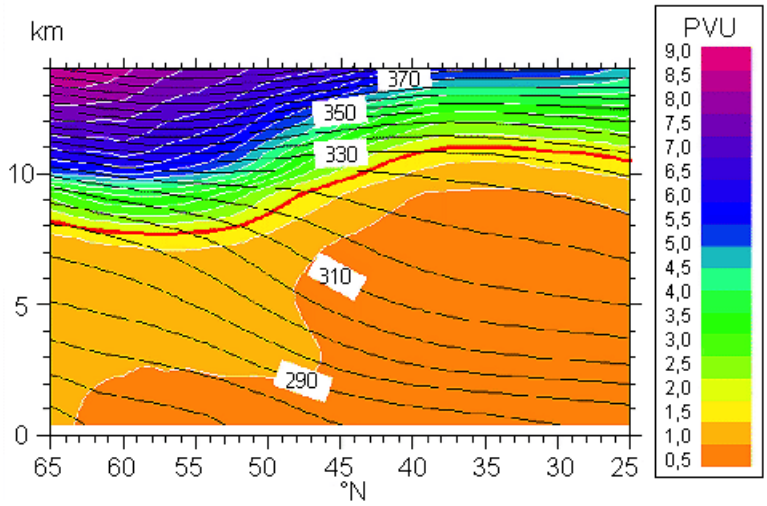

Figure 5.6.: Climatological zonal distribution of the potential vorticity (color areas) and of potential temperature (black lines in K intervals of 5 K). The 1.5-PVU surface (the so called dynamical tropopause) is given in red. Data from 1986-1995 ECMWF analyses [from Santurette and Georgiev, [102]].

PV anomaly approaches a baroclinic zone, the circulation associated with the low-level induced vorticity causes thermal advection (black arrow), leading to a low-level warm anomaly slightly east of the upper-level vorticity anomaly. This in turn may induce a cyclonic circulation (white arrow) that acts to reinforce the circulation pattern induced by the upper level anomaly, leading to further cyclogenesis. The properties of potential vorticity allows its use

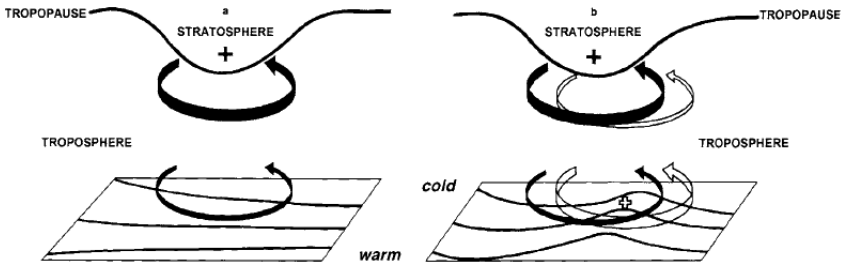

Figure 5.7.: A schematic picture of cyclogenesis associated with the arrival of an upper-level positive PV anomaly (referred to here as a tropopause dynamic anomaly, indicated by a solid '+' sign) over a low-level baroclinic region. The circulation induced by the anomaly is indicated by the solid arrow, and potential temperature contours are shown at the lower boundary by thin lines. A low-level PV anomaly (the open '+' sign in (b)), can also induce a cyclonic circulation, indicated by the open arrow in (b), that acts to reinforce the circulation pattern induced by the upper-level PV anomaly. [from Hoskins et al. [53]]

as a tracer of upper-level dynamics, which is crucial in mid-latitude synoptic developments. Upper-level cyclonic disturbances can be considered as upper-level positive PV anomalies penetrating into the upper troposhere.
It is worth investigating if the rapid intensification of the pressure minimum described in

the previous section is somehow linked with the aforementioned mechanism of cyclogenesis intensification. In order to study this possible correlation, an analysis of the upper air (between 350 hPa and 200 hPa) potential vorticity has been carried out. The use of this very variable is suggested by the works of several authors (Massacand et al. [71]; Fierli et al. [40]; Martius and Schwierz [69]; Argence et al. [6]). It is worth nothing that this method is slightly different from that proposed by Hoskins, where isentropic potential vorticity maps (i.e. at fixed θ) are used instead. However, if an anomaly is visible on an isobaric surface, there will be a corresponding anomaly also onto an appropriate isentropic surface. Figure 5.8 shows a PV anomaly with a maximum of 6.9 PVU extending from Greenlands towards the North Atlantic in the evening of 17 January. It should be noted that, at this time (the

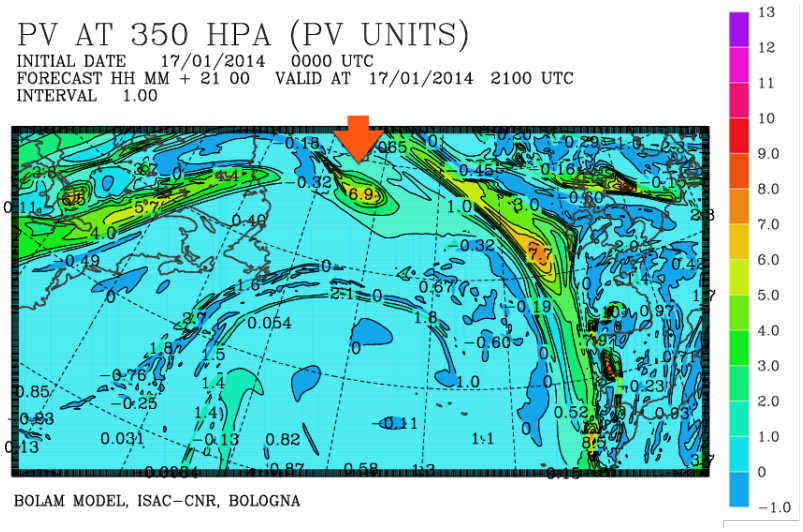

Figure 5.8.: Potential vorticity (PV units) forecasted by the BOLAM model for 17 January 2014 at 21 UTC. The red arrow indicates the anomaly described in the text.

21st hour), the low pressure minimum precursor was located far to the south, as shown in Figure 5.3. The vertical structure of this anomaly, described by the cross-sections of Figure 5.9, shows a PV maximum of 7 PVU extending up to 350 hPa. The θ,v cross-section shows a typical dipole-structure with coaxial wind maximum/minimum and an opposite sign perturbation in the potential temperature field. However, the cyclonic circulation induced by the PV anomaly is still located in the upper troposphere. During the following hours, the vorticity anomaly is advected to the East by the zonal flow, while the maximum of PV at 350 hPa increases, until it reaches 7.8 PVU on the morning of the next day. At the same time, the PV anomaly merges with another one located to the West, giving rise to an elongated band of potential vorticity anomaly. The PV forecast for 18 January 2014 shown in Figure 5.10 highlights the PV streamer structure. The vertical structure shown in Figure 5.11 (b) clearly highlights a descent of stratospheric air, towards the upper troposphere. A strong discontinuity is also marked by the variation of the air relative humidity, that undergoes a strong gradient between the very dry stratospheric air and the wet troposheric air. The PV anomaly is further advected to the South-East, following the same trajectory of the pressure minimum (Figure 5.3). These two different *anomalies* eventually meet in front of the Northern Spanish coast, right where the low pressure system undergoes a sudden deepening

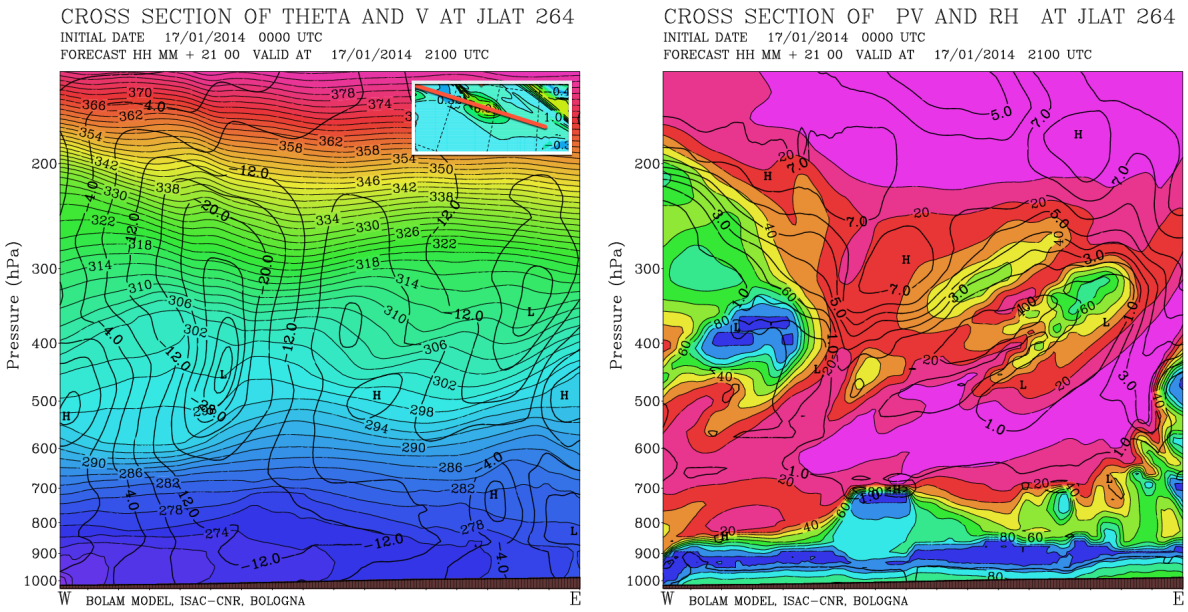

(a) θ, v (b) PV, RH

Figure 5.9.: Cross section of the upper-level PV streamer, obtained using the red line in the upper-right panel for 17 January 2014 at 21 UTC.

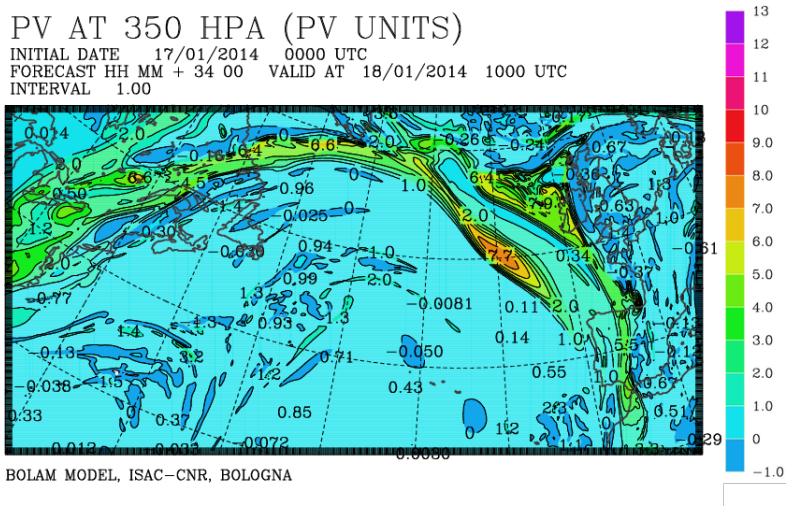

Figure 5.10.: Potential vorticity (PV units) forecasted by the BOLAM model for 18 January 2014 at 10 UTC.

(Figure 5.12). During the final hours of the simulation the PV anomaly follows the cyclone motion by remaining on the western side of the pressure minimum. The interaction with orography of the Iberian peninsula could be one of the reason underlying the subsequent stretching of the PV streamer, which is evident in Figure 5.13. The same tracking algorithm developed in section 4.2 has been applied to follow the maximum of PV over the model domain. The MSLP and 350 hPa-PV-maximum trajectories presented in Figure 5.14 are

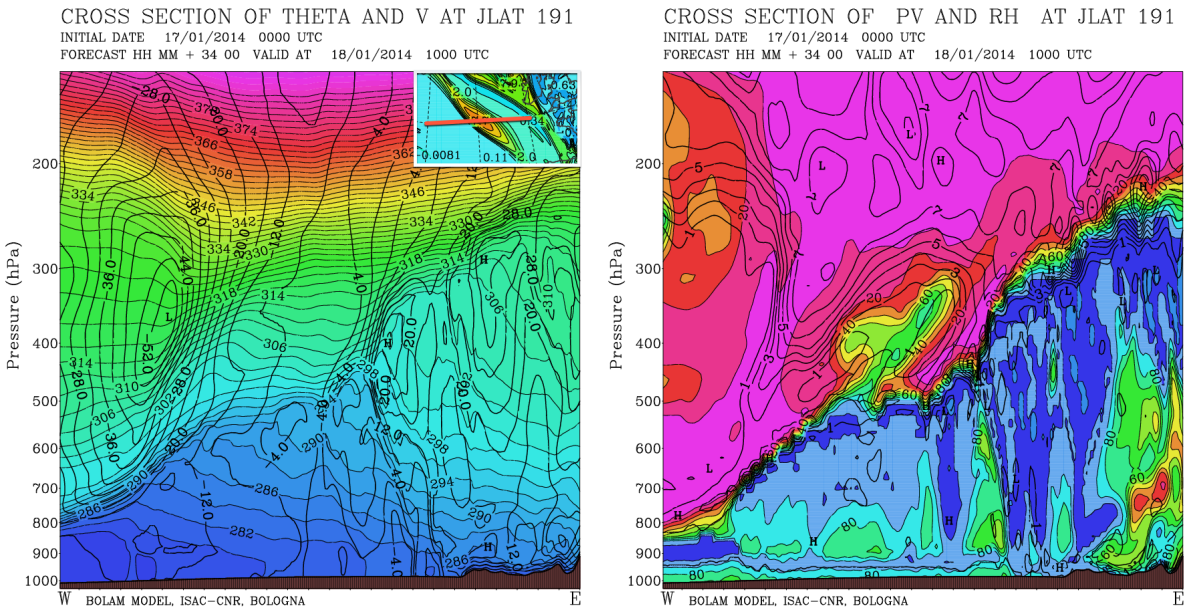

(a) θ, v (b) PV, RH

Figure 5.11.: Cross section of the upper-level PV streamer, obtained using the red line in the upper-right panel for 18 January 2014 at 10 UTC.

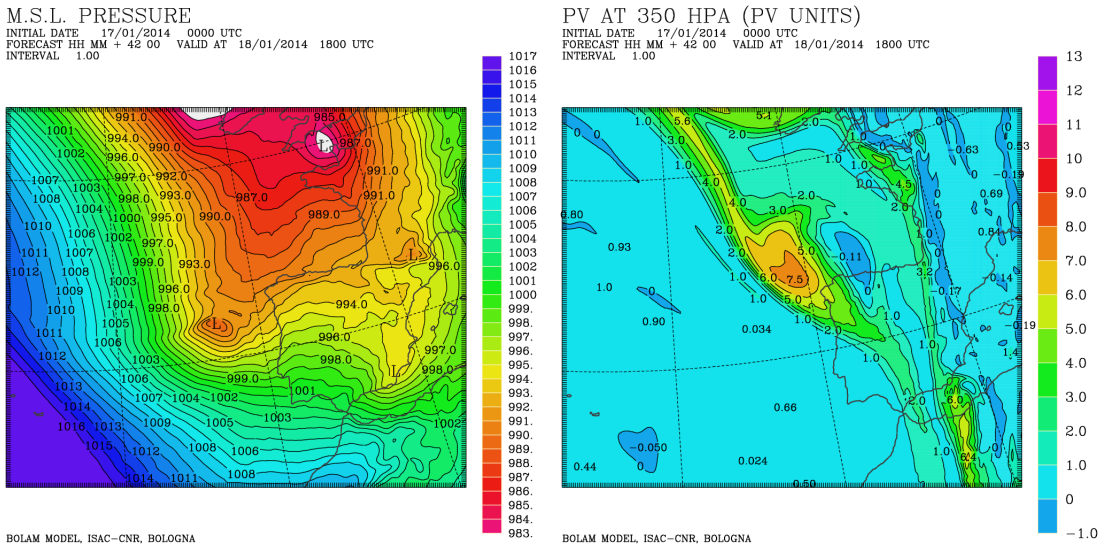

(a) MSLP (b) PV at 350 hPa

Figure 5.12.: Potential Vorticity and Mean Sea Level Pressure forecats for 18 January 2014 at 18 UTC.

initially far away from each other (21st hour of simulation) but gradually get closer, until the pressure and PV structure are almost superimposed.

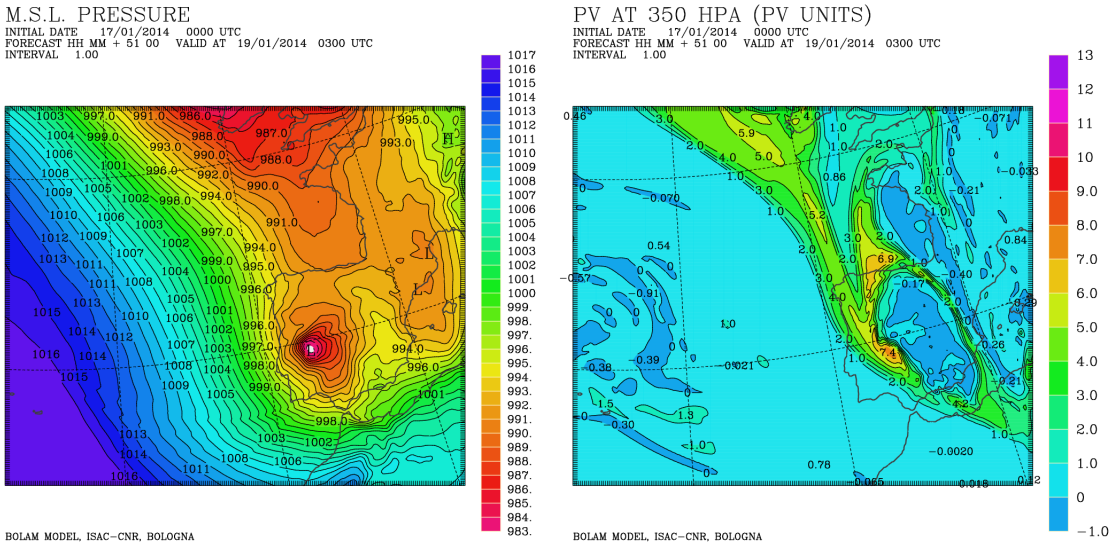

(a) MSLP (b) PV at 350 hPa

Figure 5.13.: Potential Vorticity and Mean Sea Level Pressure forecats for 19 January 2014 at 03 UTC.

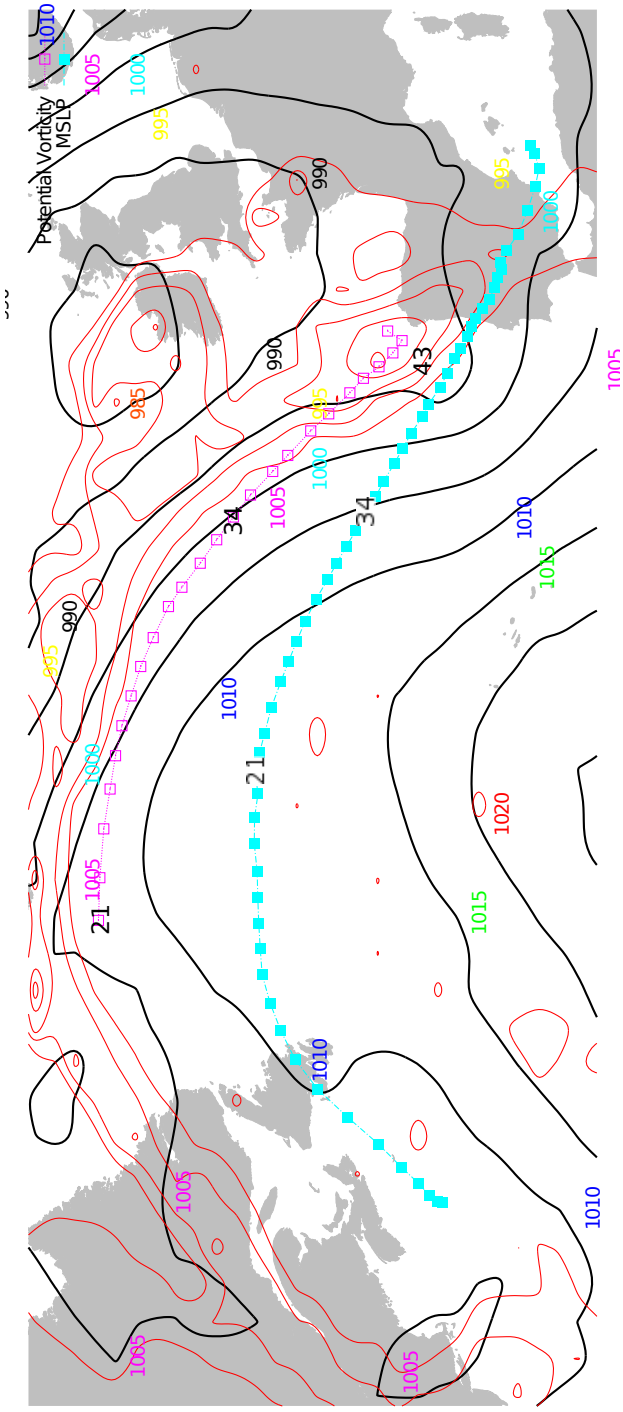

Figure 5.14.: MSLP minimum (light blue filled squares) and 350 hPa-PV maximum (purple empty squares) trajectories. The black and red contour shows respectively the MSLP and 350 hPa-PV field forecasted for 18 January at 18 UTC (43rd hour of the simulation). The numbers superimposed on both trajectories (21, 34, 43) are the simulation hours.

5.4. Water vapour imagery analysis

The instruments aboard meteorological satellite measure infrared and visible radiation in several wavelength ranges, over which radiation is significantly absorbed and reradiated by the atmospheric components in their gaseous, liquid or crystal form. Within the WV channels, infrared (thermal) radiation is emitted by solid objects such as cloud elements, precipitation and the surface of the Earth. For this reason, the channels in the WV absorption bands are sensitive to the profiles of both the temperature and the humidity. The Spinning Enhanced Visible and InfraRed Imager (SEVIRI) radiometer is equipped with two WV channels centered at 6.2 and 7.3 µm wavelengths within the water vapour absorption bands of 5.35-7.15 µm and 6.85-7.85 µm respectively. These absorption bands are related, by means of the radiative transfer theory, to the mean weighting functions shown in Figure 5.15. The data contained in Figure 5.15 show that the net radiation intensity reaching the

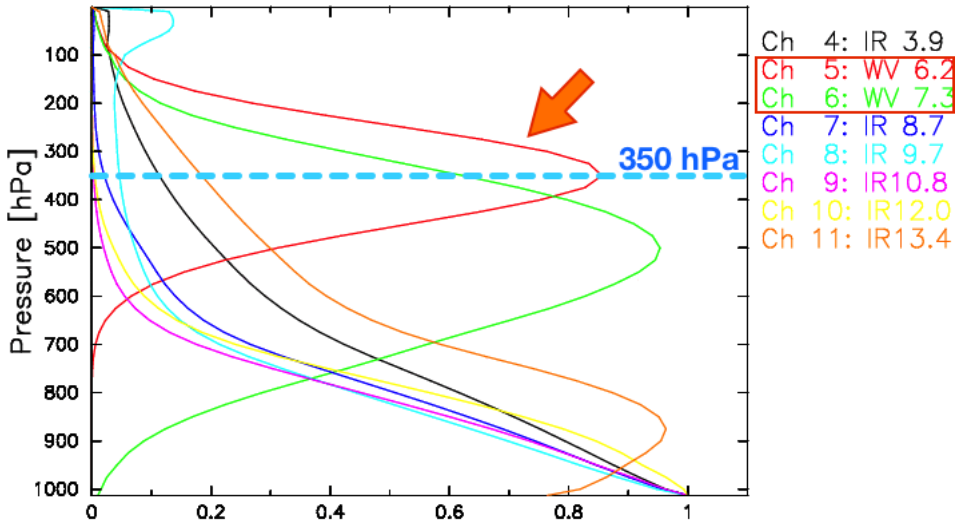

Figure 5.15.: Normalized weighting functions of the IR channels of the SEVIRI radiometer, calculated for summer period and mid-latitudes. The orange arrow indicates the weighting function relative to the channel used in this study, while the dashed line highlights the 350 hPa isobaric height, used in the previous section in order to study the PV-streamer structure.

satellite in the 6.2-µm band is very sensitive to differences in humidity within middle and high moist layers, the sensitivity range being maximum near 350 hPa.
The radiation intensity measured at the satellite is usually converted to an equivalent *brightness temperature*, which is plotted on a map using a gray scale: lighter shades indicate colder temperature, whereas darker grey shades indicate radiation arriving from a warmer area. If the temperature decreases monotonically with height (in most of the cases) the result of an increase in humidity is a decrease in the measured radiance. Furthermore, if there are no clouds above about 800 hPa, the WV images can be used qualitatively to identify areas of high and low humidity.
The WV gray shade interpretation is usually is associated with the acceptance of some kind of conceptual model. Weldon and Holmes [116] showed that, under simplified conditions, a water vapor image may be considered to represent a *moisture terrain* in which the light

shades are areas where low-level moisture extends upward to high altitudes, and the dark shades are areas where the high-tropospheric dry air extends downward to the lowest levels. Santurette and Georgiev [102] furthermore showed that WV imagery represents the upper troposphere dynamics from middle troposphere up to the tropopause. The areas of low tropopause dynamic height, which are associated with descending air and restrict the depth of tropospheric moisture, tend to produce dark gray shades on the image, whereas areas of ascending air or high tropopause height appear lighter. The evolution of the interactions between light and dark features in a sequence of satellite images indicates the development of important dynamical processes. In particular, while the formation of a white pattern in the WV imagery may be a precursor of surface cyclogenesis, dark-gray shade patterns may be associated with various mid- to upper-level dynamical features such as:

- descending motions,
- regions of high vorticity (or potential vorticity),
- tropopause dynamic anomalies that are upper-level precursor of cyclogenesis,

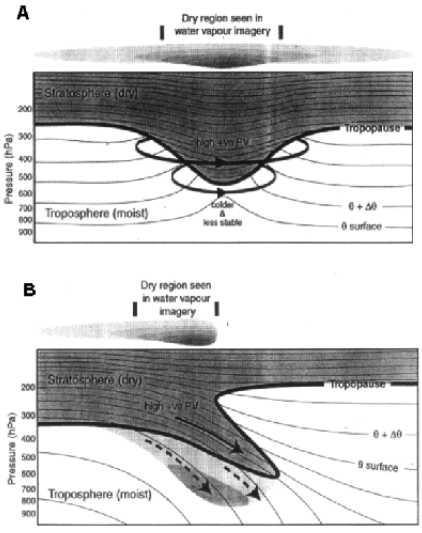

Figure 5.16.: Relation between potential vorticity anomalies and Water Vapour imagery.

In this regard, the analysis of WV imagery related to the studied event may help in the identification of the stratospheric air descent highlighted in the previous section. For the above reasons, a descent of dry stratospheric (or upper troposphere) air would appear as a dark band in WV satellite imagery. Figure 5.17 shows a narrow dark band extending from the North-Atlantic towards the Spanish Coast. At this time (18 January, 21 UTC) both the pressure minimum and the upper-level PV anomaly were located on the Spanish Coast. This is the first instant in which the dark band becomes clearly visible. Unfortunately, WV imagery are only available through geostationary satellites that have a very good time resolution but fail to represent data near to the poles. Moreover, the area from which the PV streamer may have arrived, lies between the dead zone on the border between SEVIRI

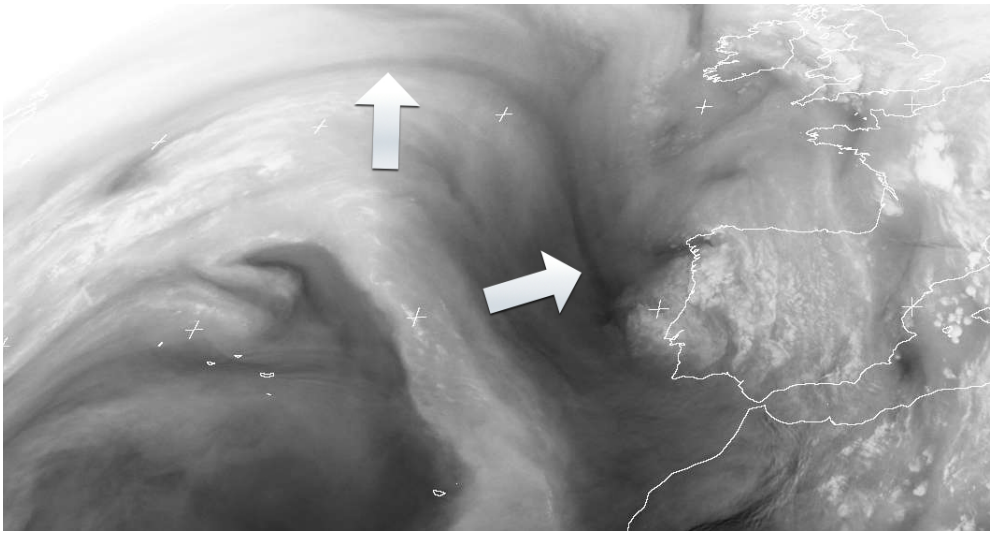

Figure 5.17.: Water Vapour Satellite Image obtained by Meteosat SEVIRI satellite in the 5.75-7.15 µm band, on 18 January 2014 at 21 UTC. The white arrows indicate the position of the narrow dark band.

and Geostationary Operational Environmental Satellite (GOES)-East satellite domains. Any attempt to follow back upstream the dark band in WV imagery failed. In the following hours (morning of 19 January 2014) the *tail* of the dark band in WV imagery moves eastward, following a spiral distribution around the low pressure minimum. It should be noted that the areas where the band originally formed still maintain the grey shade in satellite imagery. That is because once an area aloft has become dry, it tends to remain so until it is replaced by moist air. If no moistening occurs, the residual dry air will move depending on the associated wind fields. The WV imagery acquired in the morning of 19 January (day of the cyclone formation) were compared with the PV at 350 hPa obtained in the B3 case, since the simulation shown before (initialized on 17 January) placed the cyclone too far north. The comparison reported in Figure 5.18 shows a good agreement between the PV anomalies structure identified by the simulation and the dark band contained in the WV imagery. In particular, also the secondary maximum identified by the model near to the Northern Spanish coast is spotted in the WV imagery. In the following hours the structure outlined by the 350hPa-PV field differs substantially from the one observed in the WV imagery, as shown in Figure 5.19. This may be due to the vertical motion of the PV anomaly, a feature that cannot be identified in a horizontal slice of the PV, like that presented by choosing the 350 hPa isobaric level. The ring-like distribution of the PV anomaly on the 350 hPa isobaric height may be related to a bilobed 3-dimensional structure of the PV streamer.

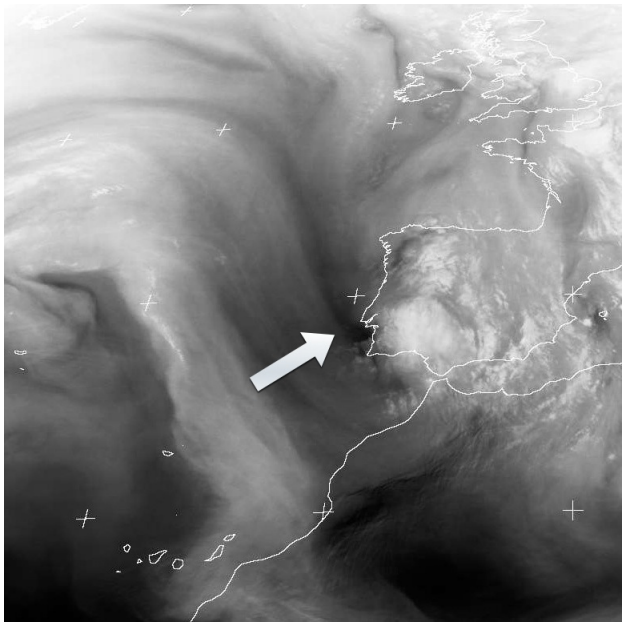

(a) 19 January 2014 - 00 UTC

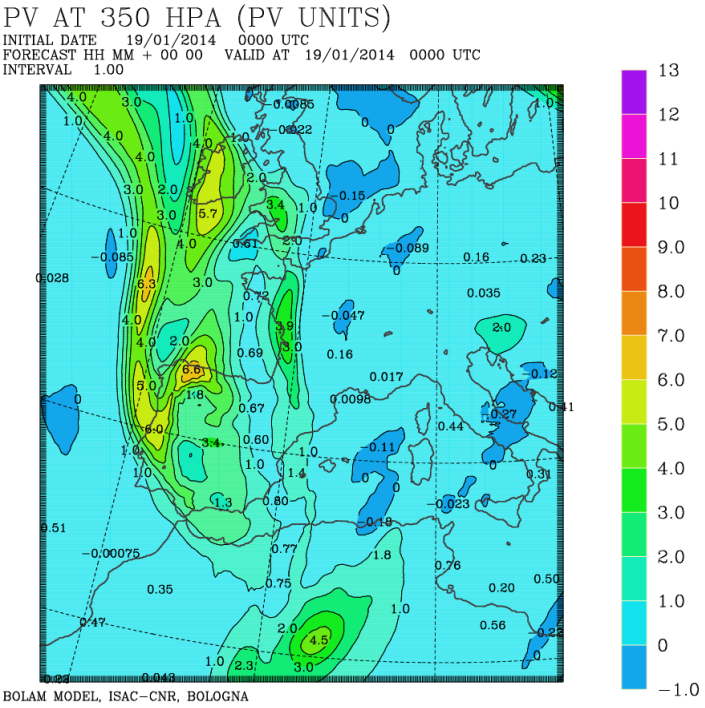

(b) 19 January 2014 - 00 UTC

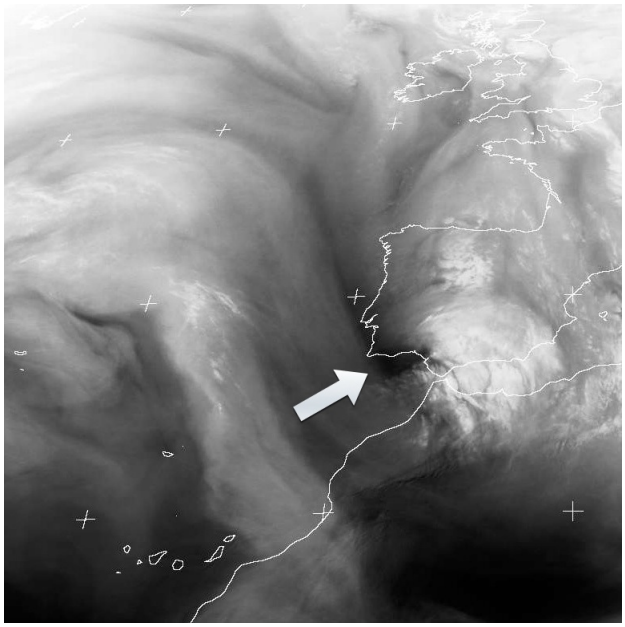

(c) 19 January 2014 - 03 UTC

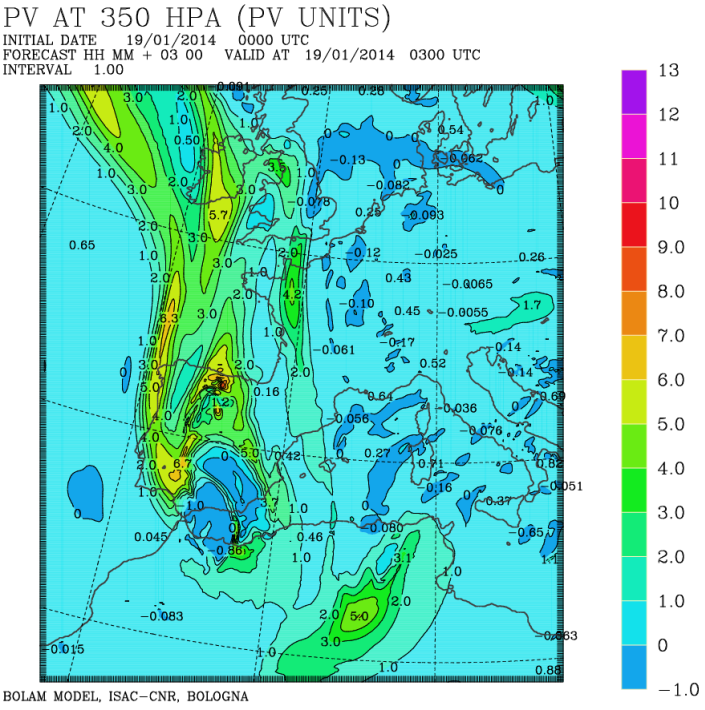

(d) 19 January 2014 - 03 UTC

Figure 5.18.: Comparison between WV Satellite Imagery obtained by Meteosat SEVIRI satellite in the 5.75-7.15 µm band and 350 hPa-PV structure in the B3 simulation.

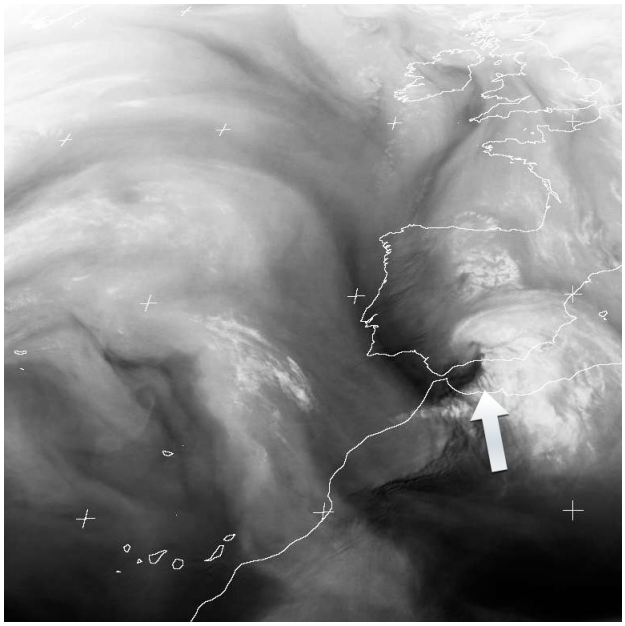

(a) 19 January 2014 - 06 UTC

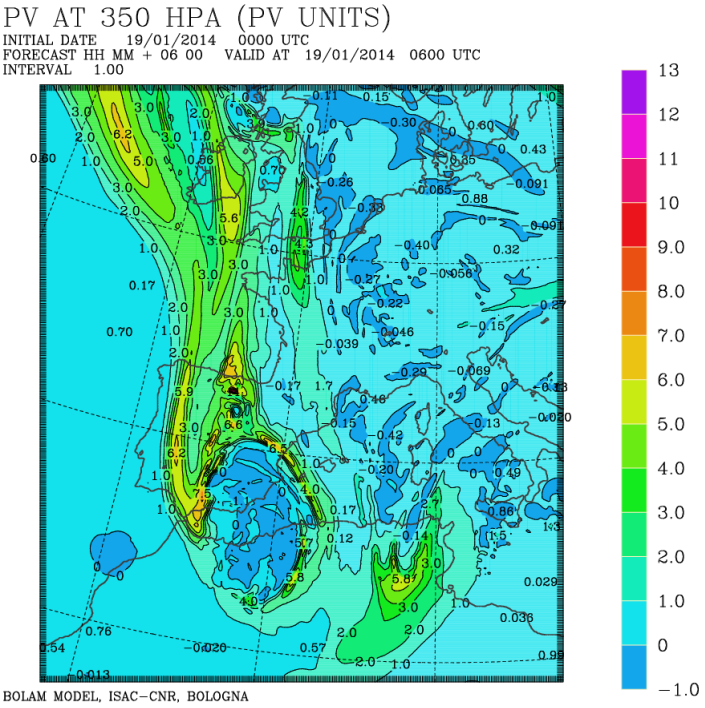

(b) 19 January 2014 - 06 UTC

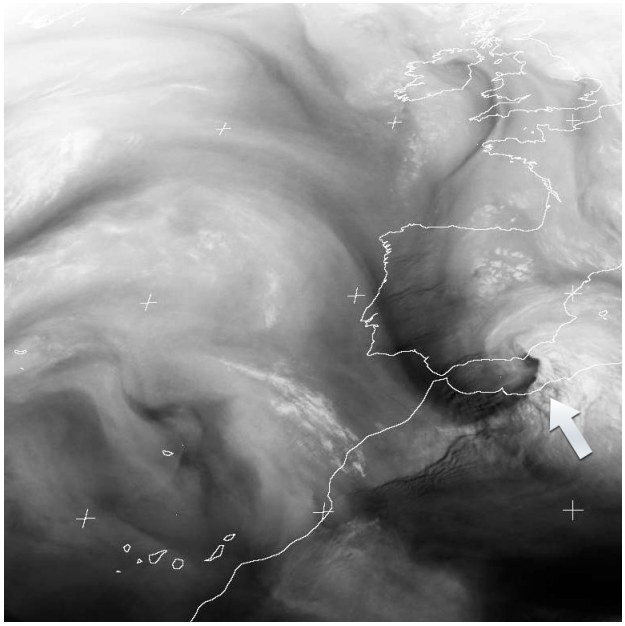

(c) 19 January 2014 - 09 UTC

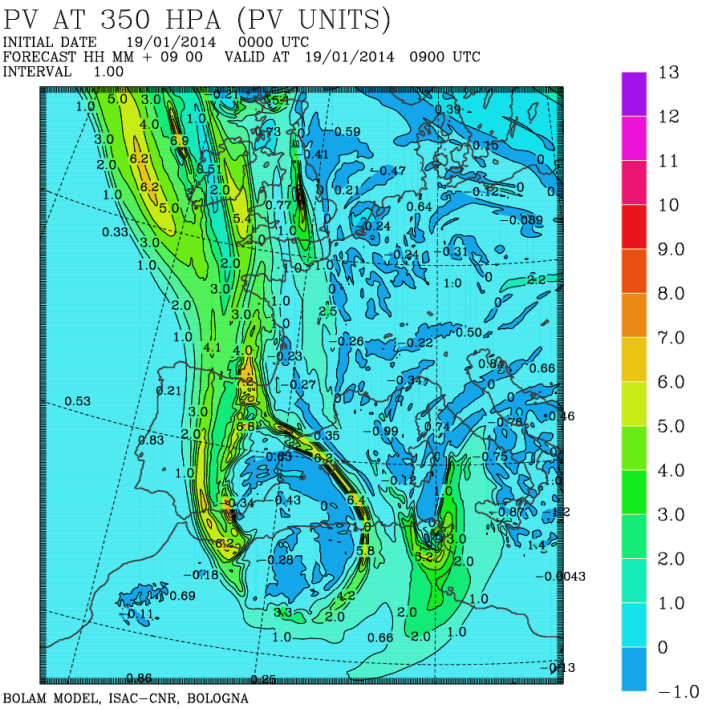

(d) 19 January 2014 - 09 UTC

Figure 5.19.: Comparison between WV Satellite Imagery obtained by Meteosat SEVIRI satellite in the 5.75-7.15 µm band and 350 hPa-PV structure in the B3 simulation.

5.5. PV precursor three-dimensional structure

The data contained in WV imagery should be interpreted not as a proxy of horizontal-cross section of PV at fixed level, but as a 2D representation of a vertical moving tropopause height. The PV data obtained by the model at fixed isobaric height is not able to correctly track the stratospheric air intrusion. In order to better understand the three-dimensional structure two ideal methods can be used:

- Compute the height of the dynamical tropopause (often 1.5 PVU isosurface) and draw a 2D map of this value,
- Produce a 3D representation of model output.

Vis5D is a free OpenGL-based volumetric visualization program for meteorological gridded datasets in 3+ dimensions that is able to represent variables in several ways. The BOLAM model output has been post-processed choosing a cropped domain that encloses Spain and the eastern Atlantic ocean. The results show the presence of a low-level PV anomaly above the cyclone, which gradually extends upward and eventually reaches the PV streamer highlighted in the previous section around the 50^{th} hour of simulation. Figure 5.20 shows the topography of the 1.8 PVU-surface, together with the geopotential height at 1000 hPa. The PV streamer

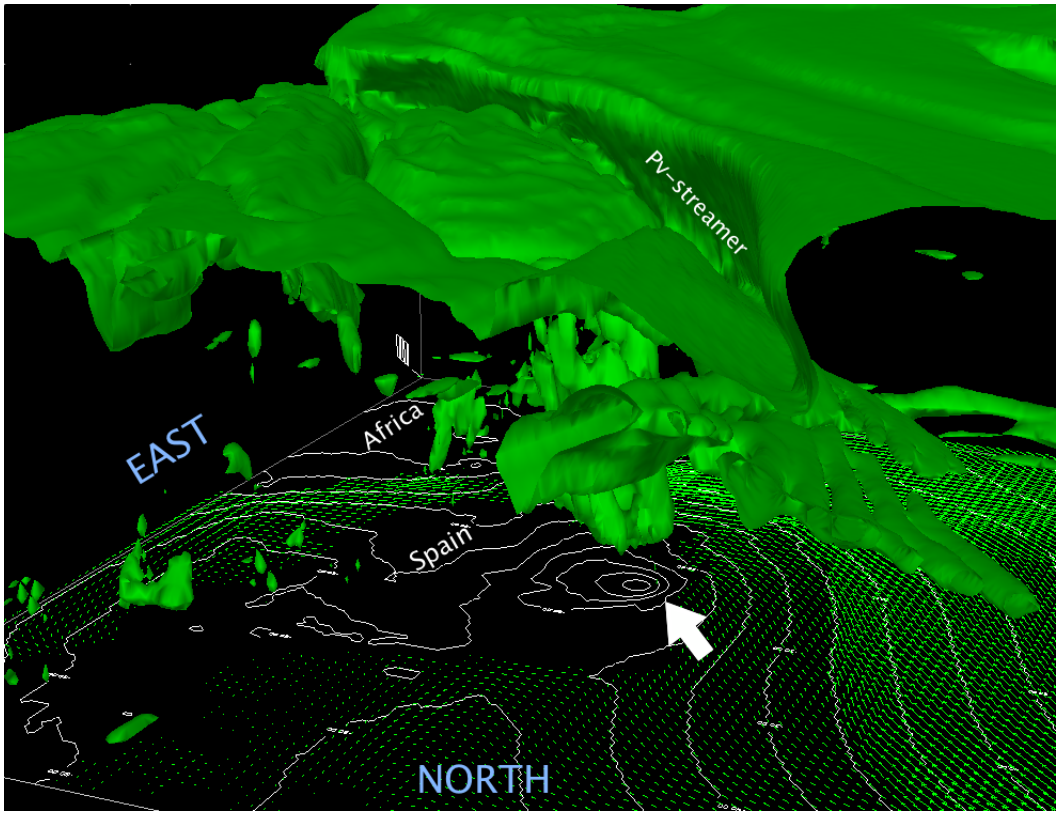

Figure 5.20.: 3D representation of the BOLAM model output on 19 January at 03 UTC. The green iso-surface represent the height of the 1.8-PVU surface. The geopotential height at 1000 hPa is shown by mean of the white contours, while 10m wind is indicated with green arrows.

is highlighted by the folding of the PV isosurface towards the ground, while the PV structure, related to the low-level anomaly, is located above the geopotential height minimum, indicated by the white arrow. The top view of the 1.8 PVU-isosurface above the cyclone reveals an interesting feature: during the cyclone deepening on the Alboran Sea the PV-isosurface tends to wrap around a center coincident with the low-level minimum. The similarity between the

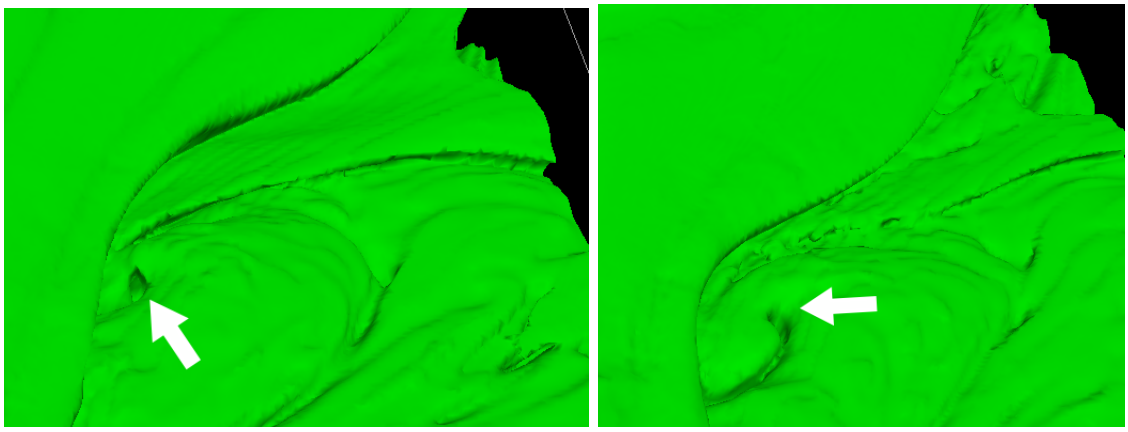

(a) 19 January 2014 - 04 UTC (b) 19 January 2014 - 09 UTC

Figure 5.21.: PV wrapping due to the surface cyclogenesis reinforcing the upper-level PV anomaly. Top view of the 1.8PVU-Isosurface.

structure contained in Figure 5.21 and the WV imagery should be noted.

5.6. Further remarks on the significance of PV-thinking

The relationship between satellite WV imagery and PV could be exploited in order to asses NWP model behaviour. Georgiev [45] showed that a significant correlation between WV imagery and 500-hPa potential vorticity anomalies is obtained in cases regarding Mediterranean cyclogenesis. Since the PV field in NWP models is obtained by the derivative of the velocity field, the numerical noise may be largely amplified in the final results. The structure obtained in the forecasted PV field thus becomes less defined as the spatial resolution of the model is increased. In extreme circumstances, i.e. when the noise in the spatial scale is comparable with the horizontal scale of the PV anomaly, this behaviour could mask the spatial structure of the precursor, resulting in erroneous results.
Homar [52] showed the significance of the upper-level PV anomaly in the initial phase of the cyclone formation. Using a potential-vorticity inversion technique, the author reduced the amplitude of the upper-level trough in the model initial condition. This technique makes use of the relationship contained in Equation 5.3 between PV, the *Montgomery* streamfunction $M = c_pT + gz$ and other thermodynamic parameters and constants (see Appendix D for a complete list of symbols).

$$\mathrm{PV} = -g\frac{f + \frac{1}{f}\nabla^2 M}{\frac{p_0}{R}\left(\frac{\partial M}{\partial \theta}\right)^{c_p/R-1}\frac{\partial^2 M}{\partial \theta^2}} \tag{5.3}$$

If PV>0 everywhere, this represents a (nonlinear) elliptic equation[3], to be solved for M with suitable boundary conditions: the knowledge of M allows to derive T, θ, $\mathbf{V}$ and all the other motion variables. Thus, a PV modification lead to a perturbation in all the analysis fields like geopotential height and temperature. The results obtained by Homar [52] suggest that the upper-level PV anomaly intensified the synoptic low and therefore enhanced the surface winds thus contributing to a notable increase in the latent-heat flux from the sea. It is worth nothing that the cyclone focus of the present study shares many features with the one described by Homar. Firstly, the PV anomaly described in the previous sections enhanced the south-westerly surface winds, as shown in Figure 5.22. The complex orography of North-

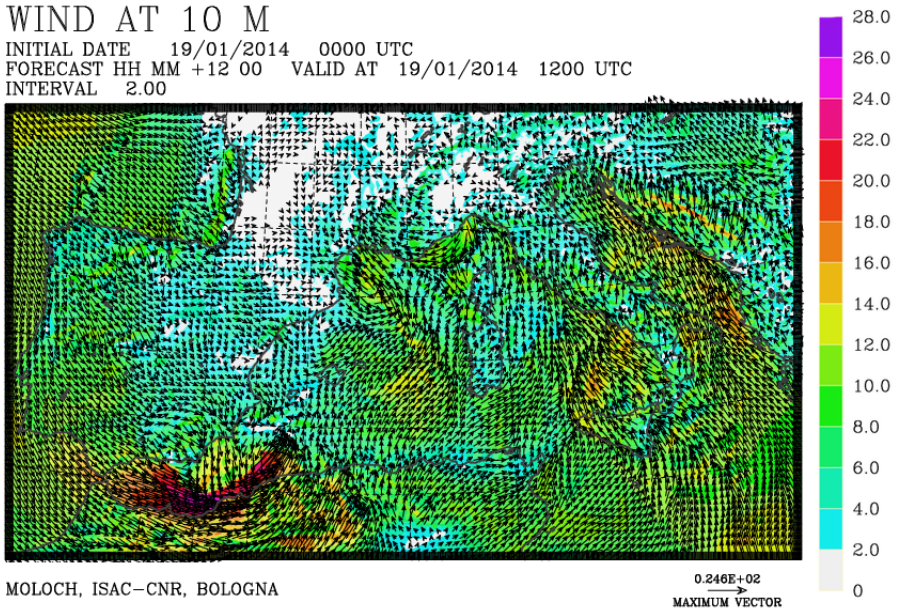

Figure 5.22.: 10 meters winds obtained in the M3 simulation. 19 January - 12 UTC.

Africa and Southern-Spain likely contributed to the observed and forecasted wind speed growth in the first hours through wind channelling, together with the PV-anomaly effect. This, in turn, enhanced the latent heat fluxes, as shown in Figure 5.23. Thus, the mesoscale features of the low-level flow due to the upper-level PV anomaly not only favoured the triggering of convection by creating convergent areas offshore Gibraltar, but also contributed to the convective destabilization of the lower troposphere through increased latent-heat flux from the sea. The presence of deep convection in the first phase of the cyclone life cycle is reflected also in the vertical structure, shown in Figure 5.24, where strong upward motions are evident, albeit on vertical scales different from those of typical eye-wall convection.
Since the influence of the PV precursor attains a crucial role in cyclone developing, a better knowledge of its distribution may help in forecasting small-scale cyclones like the one studied in this work. However, the field obtained from analysis often cannot adequately represents

[3]It should be noted that relationship 5.3 is valid only in the quasi-geostrophic approximation, and thus is not applicable in mesoscale phenomena like MTLCs. In this case, the equation was reported just as an example of a possible link between PV and motion variables.

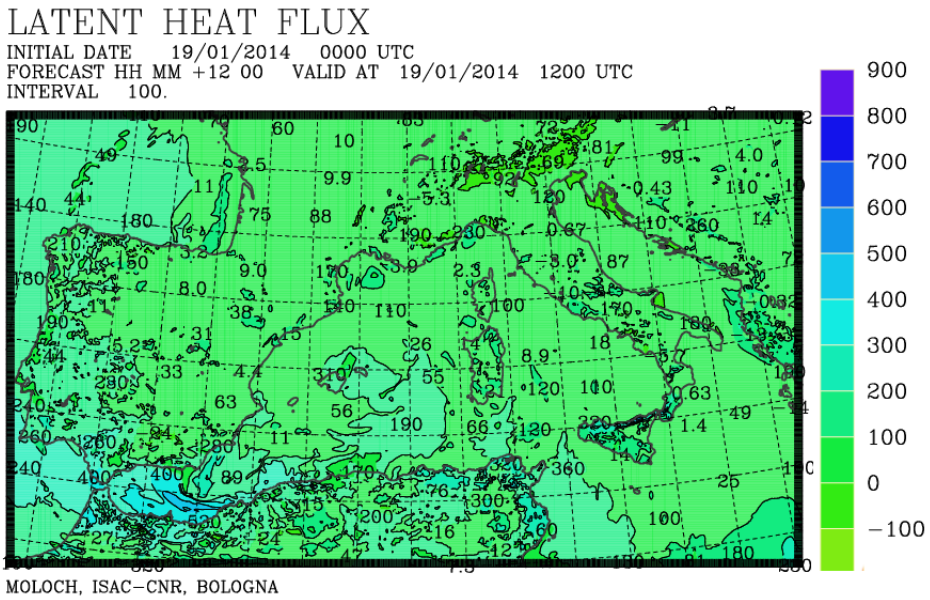

Figure 5.23.: Latent heat fluxes obtained in the M3 simulation. 19 January 2014 - 12 UTC.

Mediterranean TLCs typical circulations in NWP models. In order to overcome the sparse data coverage over the sea, a *bogusing* scheme is thus employed to force a tropical cyclone vortex into the numerical analysis (see Wang [115]; Hendricks and Peng [85] and references therein). In this particular case, the analytical vortex used for the model forcing could be inferred by the potential vorticity distribution derived from the water vapour imagery, as done by Argence et al. [5].

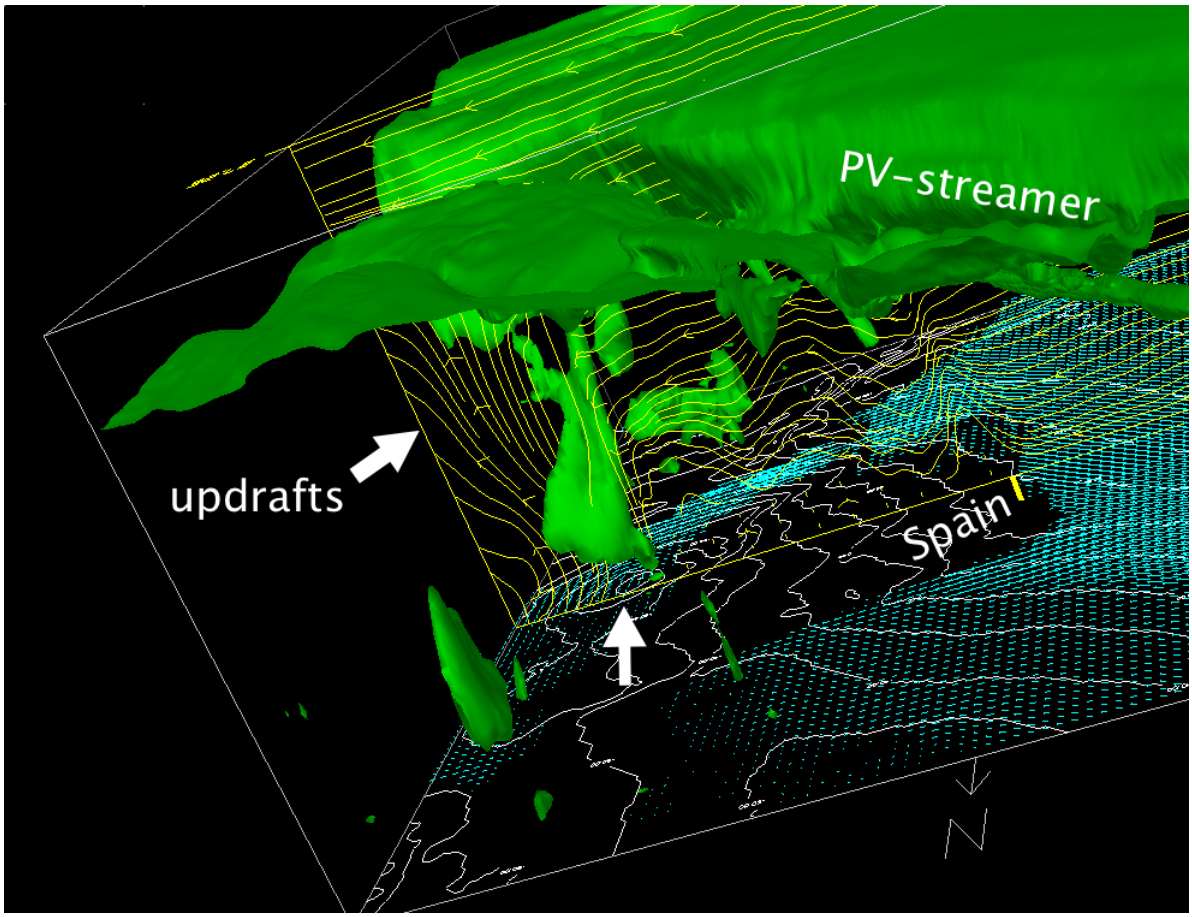

Figure 5.24.: 3D representation of the BOLAM model output on 19 January at 14 UTC. The green isosurface represent the height of the 1.8-PVU surface. The geopotential height at 1000 hPa is shown by mean of the white contours, while 10m wind is indicated with light-blue arrows. The streamfunction of the wind is displayed with the vertical slice coloured in yellow.

6 Conclusions and future perspectives

In the present work, a case of a MTLC has been analysed in detail. Starting from 3 days before the cyclone formation, a new type of dynamical investigation was performed using the GLOBO and BOLAM models developed at CNR-ISAC Institute in Bologna. The genesis of the cyclone was likely caused by a concurrence of two dynamical *precursors* that interacted on the Northern Spain coast: a PV upper-level anomaly coming from Greenland and a MSLP minimum advected from the American East Coast. Using the GLOBO and BOLAM models, the trajectories of these two elements were obtained and compared.
The results showed a convergence of the two trajectories over Northern Spain, together with a sudden deepening of the MSLP minimum and a transition from a deep-cold core structure to a shallow-warm core system. The WV imagery confirmed the descent of dry tropospheric air towards Spain several hours before the cyclone formation in the Alboran Sea. Thus, the interaction between the upper-level PV anomaly and the low-level flow induced by the MSLP minimum, played a key role in the intensification of the cyclogenesis, at least in the first hours of the cyclone life. In particular the MSLP low intensification, caused by the interaction between the PV anomaly and the baroclinic environment act to reinforce the surface wind speed that, in turn, increased the latent (and sensible) heat fluxes at air-sea surface, thus favouring the maintenance of convection.
Although the cyclone formed as an extra-tropical depression, most of the simulations performed showed a transition to a deep-warm core structure in the first 12 hours. Both BOLAM and MOLOCH models exhibited a good performance in simulating the cyclone trajectory over the Mediterranean Sea, while MOLOCH achieved better results in the Adriatic Sea. However, both models correctly predicted a deep-warm core structure in this late phase of the cyclone life.
The overall results were strongly affected by the choice of initial conditions and boundary conditions. In particular, the simulations obtained with 6-hourly-analysis forced boundary conditions did not show agreement with observations and performed worse than the one obtained only with a global initial condition.
The SST dependence has been examined in detail by performing several simulations with nested SST obtained from the MyOcean project. The results showed that BOLAM model overestimated the water cooling due to the surface winds. In order to correct this issue, the

slab-ocean model equation has been revised and a modified heat capacity has been proposed. The simulations performed with the modified BOLAM version produced better forecasts, especially in the Adriatic phase.
This work allowed to identify the best model setup required for a correct simulation of MTLCs. The operational versions of BOLAM and MOLOCH models published every day are directly nested into GFS forecast. In this case of study the GLOBO-BOLAM-MOLOCH model chain has proved to be more accurate that the operational forecasts aforementioned. The author thus hopes that the forecasts published at the CNR-ISAC will be performed with successive nesting in the near future, in order to better predict intense rainfall and severe weather events. Since this goal would result almost surely in an investment, given the costs required for the renewal of the computing resources used at CNR-ISAC, there are a few other objectives within easy reach. Since all the three diagnostics proposed by Hart [48] can be evaluated using solely the three-dimensional height field (and the MSLP field to track the cyclone), they have broad potential use in operational forecast communities. The results presented in Chapter 4, together with Appendix A and C, clearly show that the methodology proposed by Hart [48] works very well applied to BOLAM and MOLOCH meteorological models. For all the reasons cited above, the implementation of a live-detection and tracking algorithm, similar to the one found on `http://moe.met.fsu.edu/cyclonephase/`, for the Mediterranean (area) cyclones would be an interesting research perspective but also a very useful forecasting tool. The operational model data used by Hart are unable to resolve the small-scale cyclones of the Mediterranean area, since are based upon GCM model output. Conversely, an implementation of the aforementioned algorithm would provide a crucial support in forecasting potential extra-tropical/tropical transition and thus severe weather events in the Mediterranean area.
The author was able to compare the phase space diagrams published on the website, with the same obtained in Appendix A, for the same events. In these cases the results obtained with BOLAM model data were more in agreement with observational data, with respect to those published on the Hart website. Since the algorithm has been already developed and tested by the author, the only features to be implemented would be:

- a discerning method between multiple cyclones tracks, using several constraints like a minimum life time of 8-12 hours and a minimum pressure gradient,
- a graphical tool able to represent (and publish on the web) the Hart parameters in a convenient and intuitive way, similar to that presented in this work.

Figure 6.1 shows a possible graphical interface that allows to choose the cyclone for which the results of thermal phase analysis should be shown to the user. The ideal BOLAM-based algorithm implementation suggested before would produce an image similar to Figure 6.1 but for the whole operational model domain (Mediterranean area, together with some part of North-Atlantic). The author was able to verify that the thermal-phase-analysis algorithm, which also includes the tracking algorithm, requires a very limited execution time (ranging approximately between 1 and 5 seconds, based on the total time run of the model and of the domain resolution and size). The only phase of the algorithm that requires time is the initial one, when data are read from the binary file and saved into the RAM, but it is a

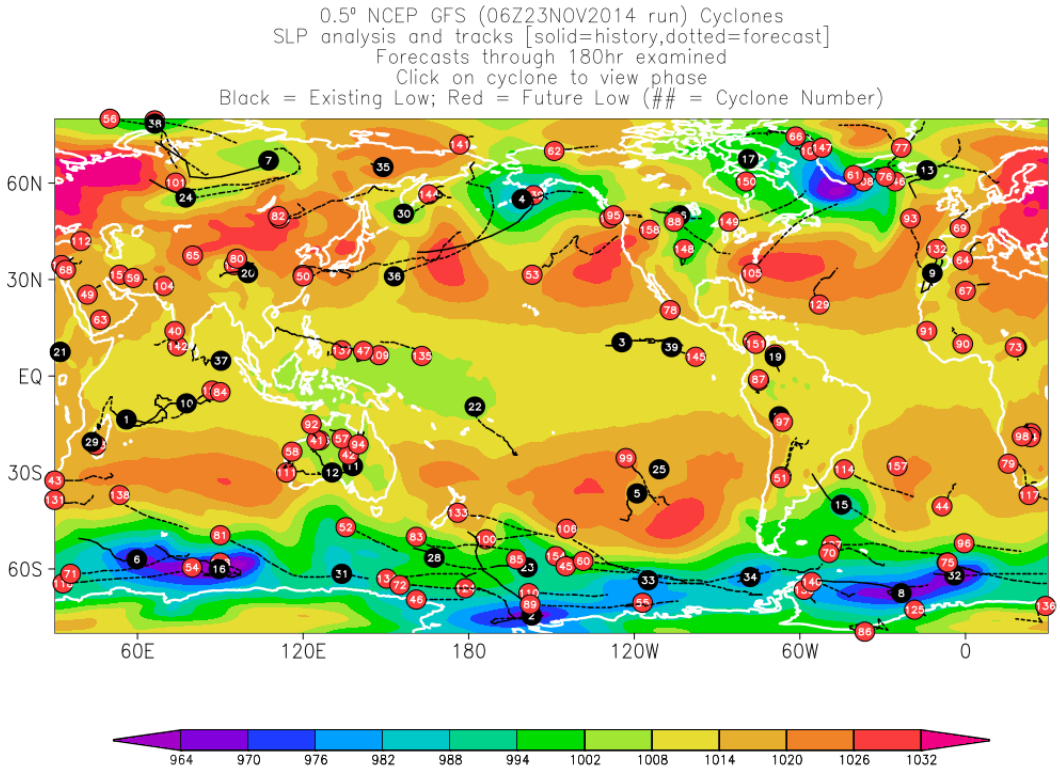

Figure 6.1.: Cyclone tracks obtained with the algorithm proposed by Hart, updated every 12 hours on the website `http://moe.met.fsu.edu/cyclonephase/`.

process to be executed only once and that requires a maximum of 10 seconds. Thus, the total computational burden required by the algorithm for a model run would result totally negligible, if compared to the model execution process (order of hours).

A

Test of Hart analysis

In this chapter an extensive analysis of two particular events is conducted, in order to test and evaluate the performance of the thermal phase detection algorithm proposed by Hart [48]. These examples demonstrates that the algorithm developed in Chapter 4 is able to deal with events of different scales, even with the approximations made (included the constant radius of exploration R_{ex}).

A.1. Hurricane Gonzalo Extra-Tropical transition

Gonzalo was a powerful Atlantic hurricane that had destructive impacts in the Lesser Antilles, British Overseas Territory of Bermuda and Great Britain by mid-October 2014. Forming from a tropical wave east of the Caribbean Sea on October 12, Gonzalo passed through the Leeward Islands and steadily strengthened. The storm tracked north-westward as it intensified into a Category 4 major hurricane on October 15 and peaked with maximum sustained winds of 230 km/h on the day after. Turning north-eastward, the cyclone gradually weakened before crossing directly over central Bermuda at Category 2 strength, around 00:30 UTC on October 18. Gonzalo accelerated toward the waters of the North Atlantic, passing close to south-eastern Newfoundland before becoming extra-tropical on October 19. The extra-tropical remnants of Gonzalo reached the United Kingdom on October 21 and then proceeded to batter Central Europe. The cold front associated with a weak surface low caused severe weather on Greece and intense snowfall on the Alps. This event assumes a particular meaning, since it has gone through the entire cycle from tropical depression to extra-tropical cyclone in less than 10 days. A BOLAM simulation has been performed using the same features described in Chapter 3 and the domain used in Chapter 5. Boundary conditions were derived from the GLOBO model simulation, that was initialized with GFS analysis of 19 October 2014 at 00 UTC and ran for 72 hours. This date was chosen in order to follow the track of the cyclone over the North-Atlantic and to include a few moments when the cyclone still had the tropical nature. Figure A.2 shows the MSLP forecasted by the BOLAM simulation in the first hours; at this time the cyclone was a Category 1 Hurricane with a central minimum (forecasted by BOLAM model) of about 972 hPa. The cyclone tracking algorithm described and used in Chapters 4 and 5 proved to correctly detect

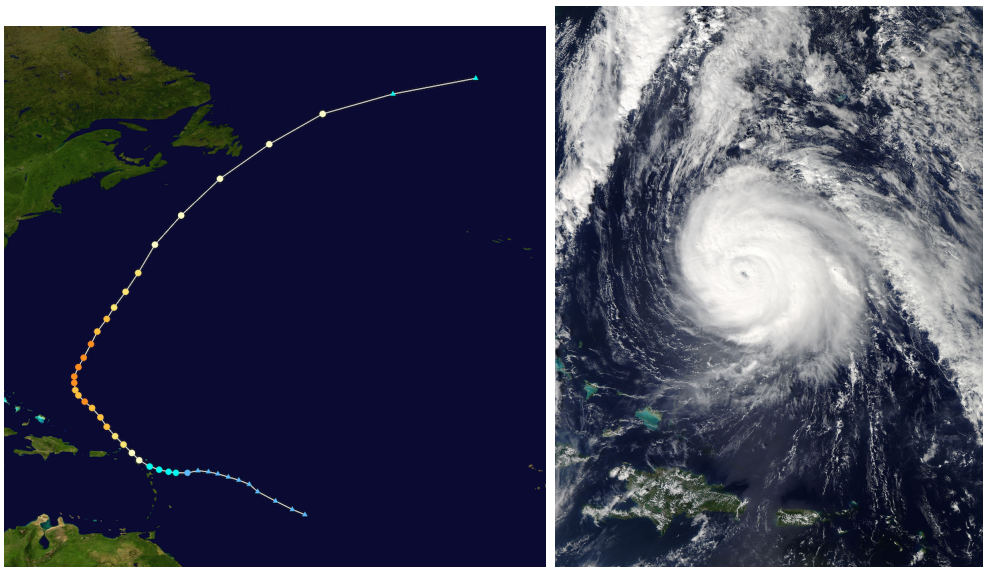

(a) Hurricane Gonzalo track

(b) Satellite image of Hurricane Gonzalo at intensity peak on Oct. 16 at 17:45 UTC

Figure A.1.: Track map and Satellite image of Hurricane Gonzalo. The points show the location of the storm at 6-hour intervals. The colour represents the storm's maximum sustained wind speeds as classified in the Saffir-Simpson Hurricane Scale, and the shape of the data points represent the nature of the storm (Tropical Cyclone/Tropical depression/Extra-tropical Cyclone) .

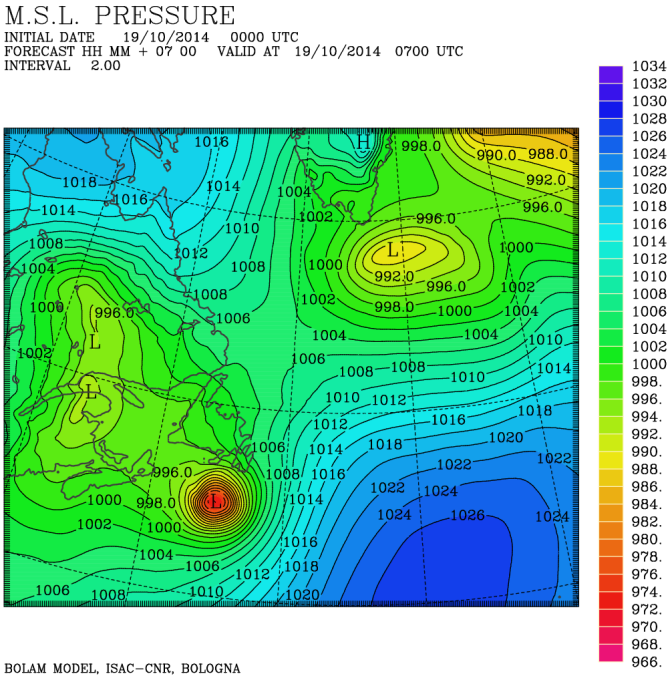

Figure A.2.: MSLP field forecasted by the BOLAM model on 19 October 2014 at 07 UTC.

and follow the cyclone over the North-Atlantic, until the final contact with Great Britain, forecasted for the 50$^{\text{th}}$ hour (21 October 02 UTC). The absolute pressure minimum of about

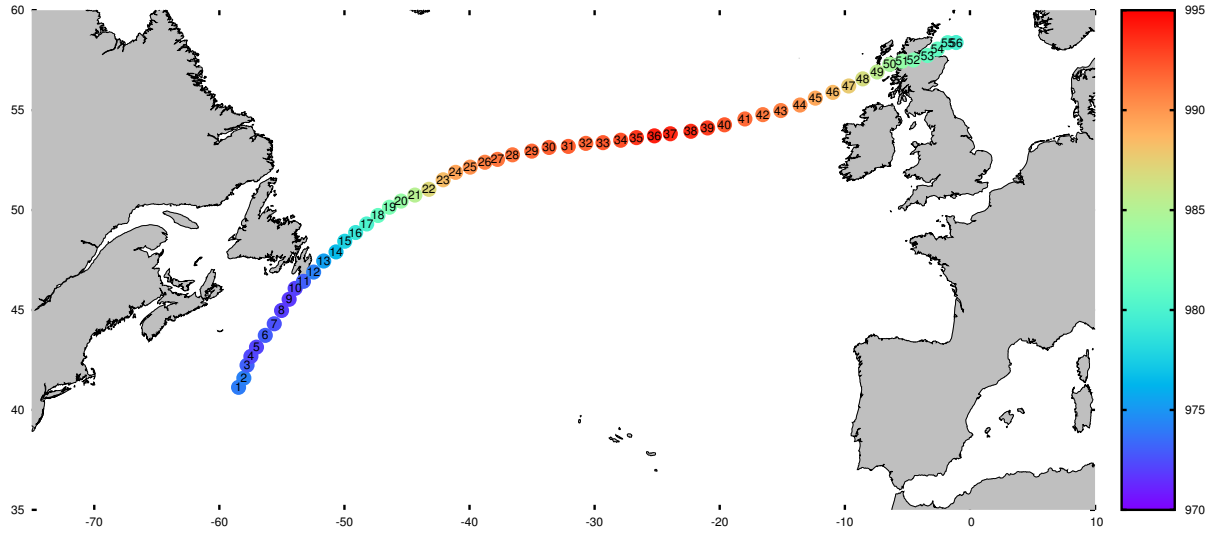

Figure A.3.: Cyclone path obtained with the BOLAM Model. The simulation starts on 19 October 2014 at 00 UTC = inst.1; positions are reported every hour.

971 hPa forecasted by the model on 19 October at 09 UTC sightly differs from the one indicated by the analysis (966 hPa), although the data available from reanalysis allow to identify a certain agreement between predicted and observed trajectory. In order to study the thermal phases of the cyclone, the parameters proposed by Hart [48] were computed. The radius of exploration R_{ex} was set to about 300 km for all the simulation time, after having tested a wide range of other possibilities. Figure A.4 (a) shows the transition to an asymmetric structure from the 2$^{\text{nd}}$ hour onwards: it should be remarked that the $B = 10$m value was never reached among the cases studied in Chapter 4. This can be explained by considering that hurricane Gonzalo was already weakening on 19 Oct, and that the loss of its tropical characteristics, including the symmetric structure, may have started before. The data contained in Figure A.4 reveal the presence of a deep warm core in the first 14 hours of simulation, showing great agreement with the official data from National Hurricane Center (NHC) that downgraded the Hurricane to an extra-tropical depression firstly on 19 October at 16 UTC. In the subsequent hours the system made a rapid transition to a deep-cold core structure, leading to a typical extra-tropical features.

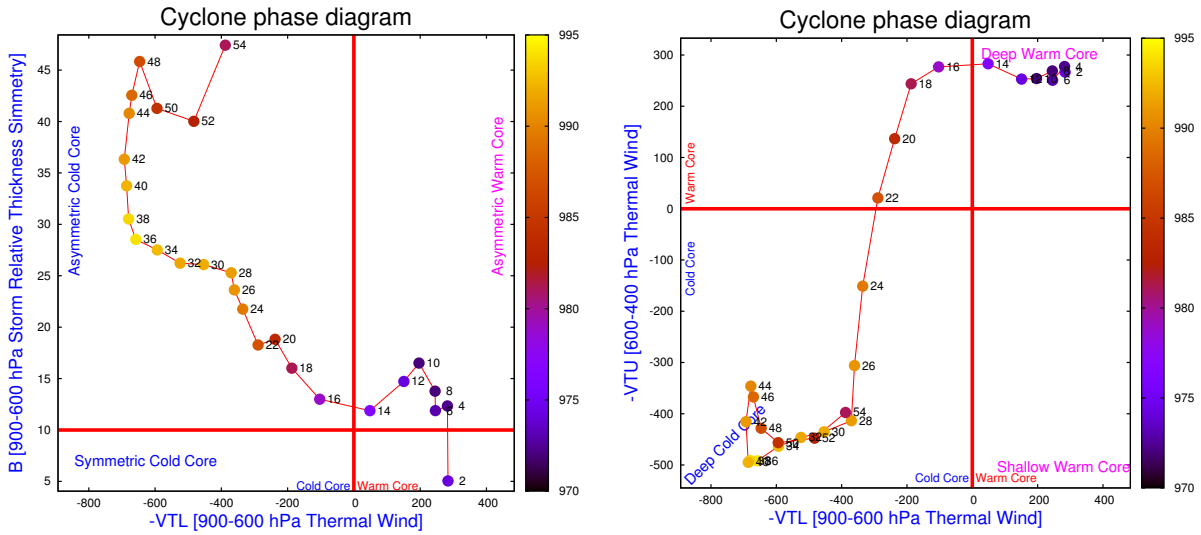

(a) $-V_t^{\mathrm{L}}$ versus B (b) $-V_t^{\mathrm{L}}$ versus $-V_t^{\mathrm{U}}$

Figure A.4.: Cyclone phase space diagrams for Hurricane Gonzalo.

A.2. ExtraTropical cyclone Magit

Magit was the name assigned by the Deutsche WetterDienst (DWD) to an Extra-Tropical cyclone that interested the north Atlantic between 13 and 19 October 2014. The genesis of this system has been not investigated in detail, but seems related to the interaction between an upper level cut-off and a low-level disturbance coming from North-America, as shown in Figure A.5. The cyclone deepened rapidly, from about 1000 hPa to a central minimum of 955 hPa on 14 October 2014 at 20 UTC. This rapid intensification was highlighted also by a well defined cloud pattern, shown in Figure A.6, where, curiously, an eye-like structure was present. This is probably due to the *explosive* cyclogenesis characterized by the rapid expansion of the occluded front and the subsequent seclusion of the warm air in the center. The synoptic maps produced by MetOffice on 15 October at 00 UTC shows the occluded front wrapped on itself (not shown). The satellite imagery reported in Figure A.7, both in the WV channel and in the visible band, showed the evidence of mesoscale vortices embedded in the higher-scale low. A BOLAM simulation has been carried out, using the same features and domain described in Chapters 3 and 5. The model was nested into a GLOBO simulation that was initialized using GFS analysis of 13 Oct. 2014 at 00 UTC and ran for 48 hours. This time span was chosen so as to cover the period of greater intensification of the cyclone, between 13 and 14 October. Figure A.8 shows that the entire system possessed a large-scale structure with a radius of approximately 20 degrees of latitude (about 2200 km) and 25 degrees of longitude (about 1700 km). The marked discontinuity in MSLP field highlights the position of the cold front, that become occluded from the 997 hPa isobar onwards: notice the even deeper discontinuity in the last isobars. A signal of mesoscale vortices was evident in the PV field at 350 hPa displayed in Figure A.9, where an initial filament of high PV

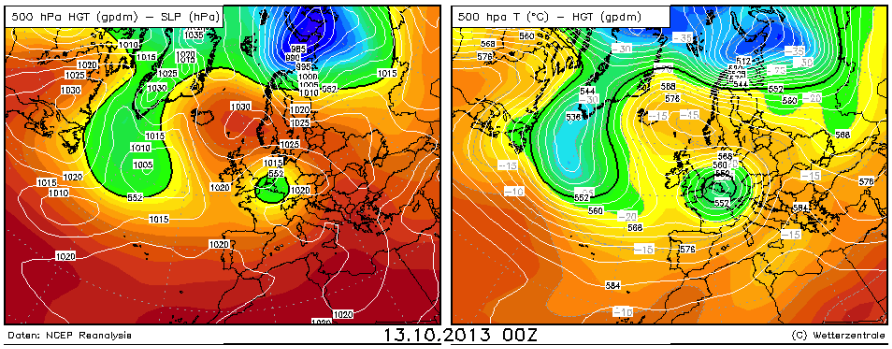

(a) 13 October 2014 00 UTC Analysis

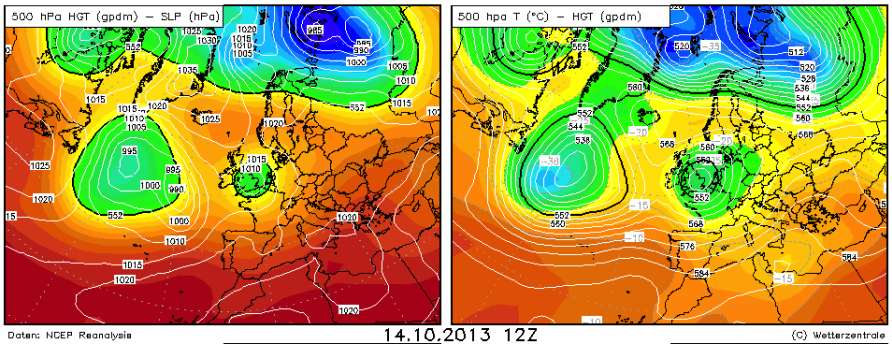

(b) 14 October 12 UTC Analysis

Figure A.5.: NCEP reanalysis plotted by Wetterzentrale. Left Panel: geopotential height at 500 hPa (decameters) and MSLP (hPa). Right panel: 500 hPa Temperature (°C) and geopotential height (decameters) .

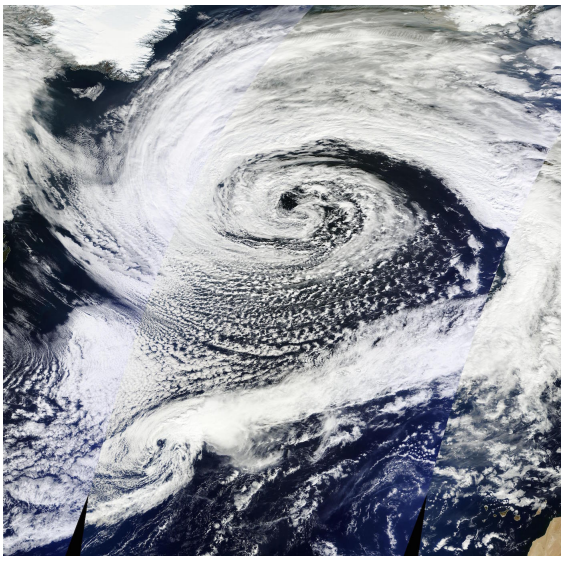

Figure A.6.: MODIS satellite imagery of the North Atlantic, showing the extra-tropical cyclone.

is fragmented in numerous secondary maxima. The cyclone tracking algorithm provided an

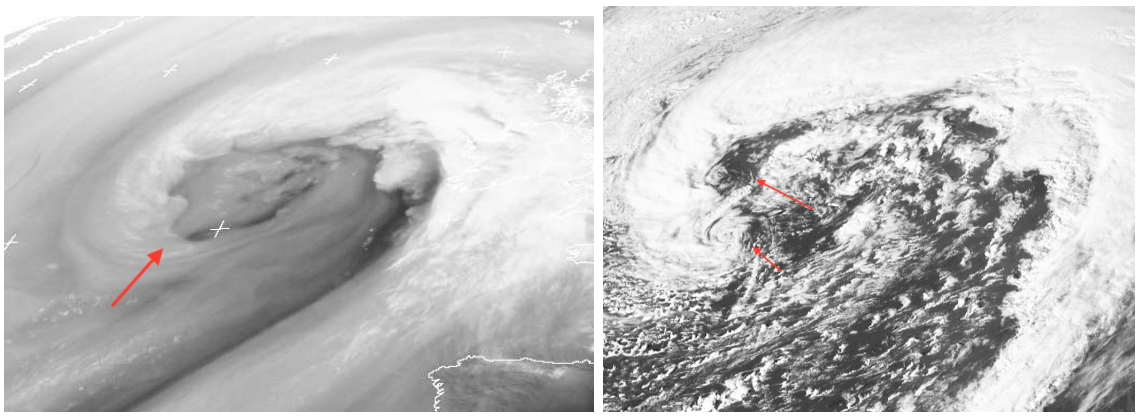

(a) Water Vapour Channel (b) Visible Channel

Figure A.7.: Satellite imagery of the mesoscale vortices embedded in the high-scale low pressure system over the North-Atlantic. Both images are acquired on 17 October 2014 at 15 UTC.

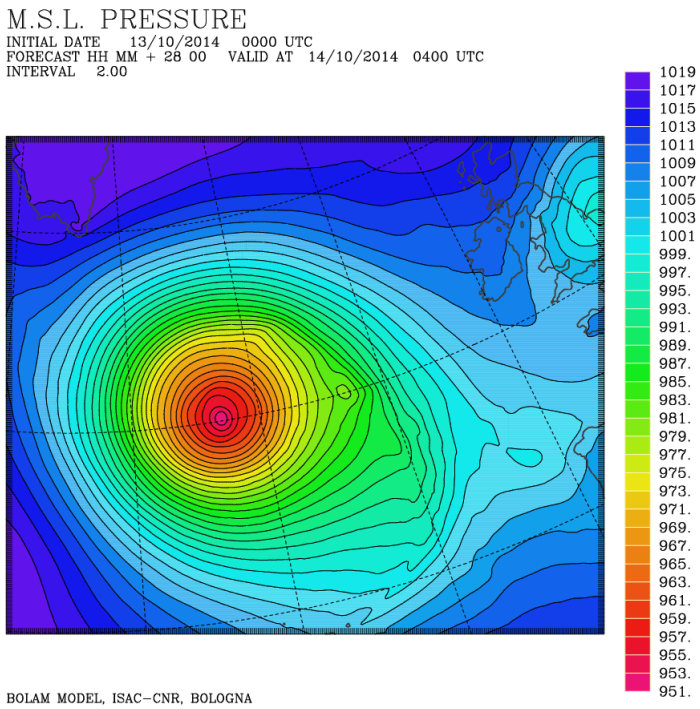

Figure A.8.: MSLP on 14 October 2014 at 4 UTC. At this time the cyclone was reaching a central minimum of about 955 hPa.

unambiguous path over the North-Atlantic, although the resulted image is not shown since the system does not moved much in the 48 hours of the simulation. Considering the size of the system estimated before, the radius of exploration R_{ex} has been set to 2000 km for the entire time period. The thermal asymmetry parameter B shown in Figure A.10 (a) assumes values higher than 10 for the entire simulation time, underlining the extra-tropical asymmetric nature of the cyclone. On the other hand, values of thermal wind highlights a deep-cold core

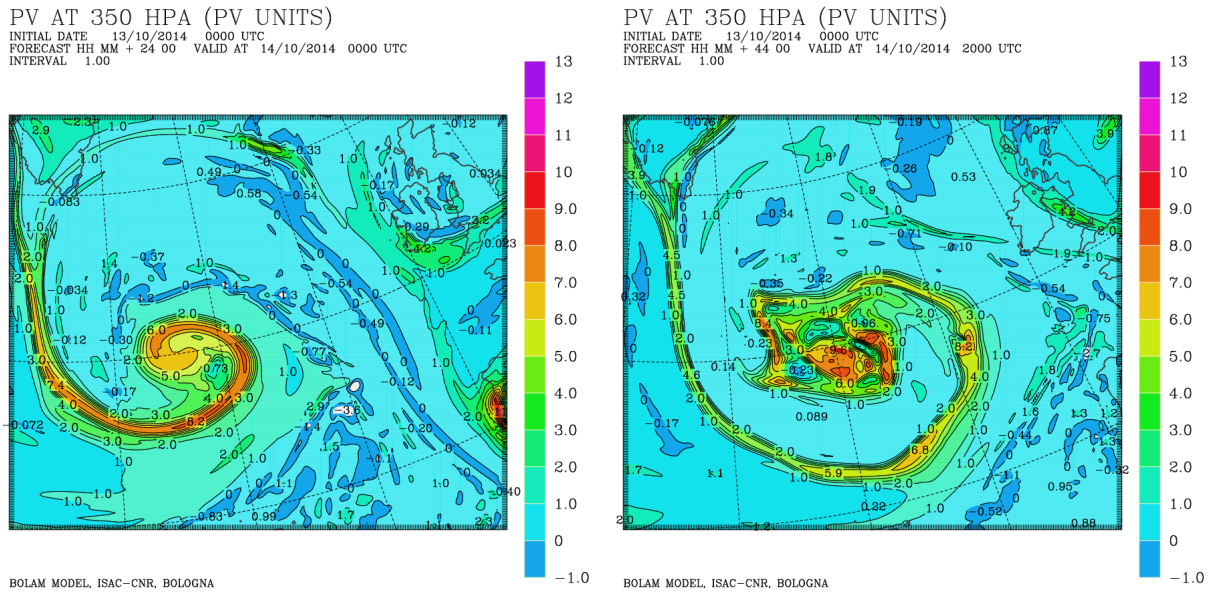

(a) 14 October 2014 00 UTC (b) 14 October 2014 20 UTC

Figure A.9.: Model output for PV on the isobaric level of 350 hPa. Notice the fragmentation of stratospheric intrusion around the center of the cyclone (see also Appenzeller et al. [3]).

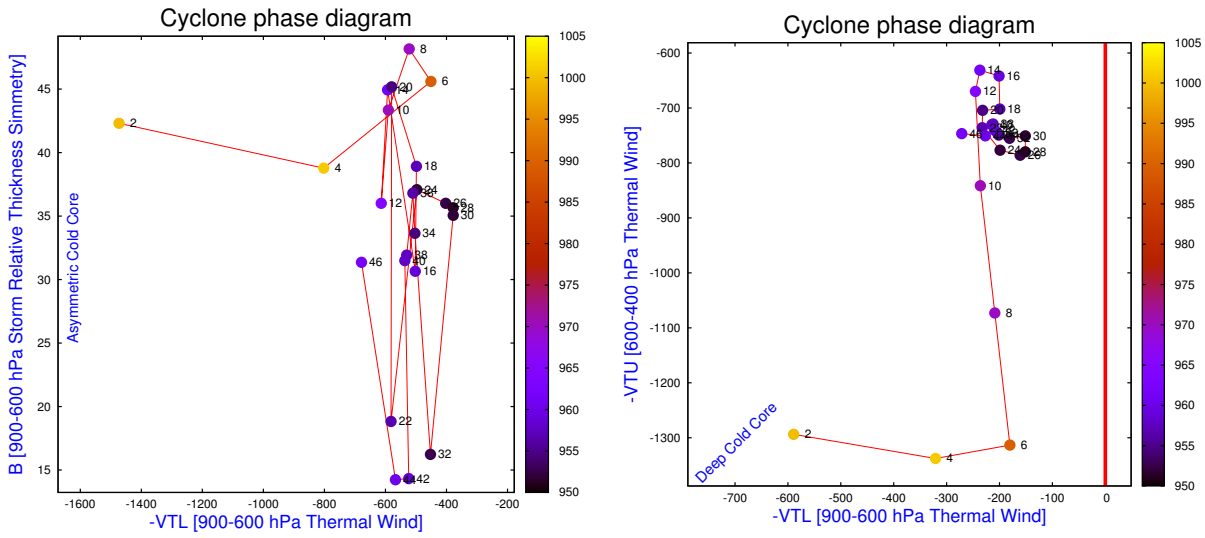

(a) $-V_t^{\mathrm{L}}$ versus B (b) $-V_t^{\mathrm{L}}$ versus $-V_t^{\mathrm{U}}$

Figure A.10.: Cyclone phase space diagrams for Extra-tropical cyclone Magit.

structure in both upper and lower troposphere. The oscillations of B parameter towards values close to 10, together with the low thermal wind in the low troposphere, may indicate the symmetric-like structure that was suggested by the analysis of Figure A.6.

B

On the cyclone radius estimation

In order to evaluate the size of a TC, the radius is often computed by mean of model output data or analysis. The NHC uses the radius of the outermost closed isobar by measuring the radii from the center of the storm to its outermost closed isobar in four quadrants, which is then averaged to obtain a scalar value. In this work the thermal phase analysis was performed using a fixed radius, as suggested by several authors and already explained in Chapter 4. In this section, after an estimation of cyclone size from satellite imagery, a method based on model output data has been developed.

B.1. Satellite-based size estimate

Since the analysis of raw data from satellite observations is beyond the purpose of this work, a qualitative analysis of satellite imagery has been performed by comparing known distances, e.g. the distance between Maiorca and Algeri, to the size of cloud bands associated with the cyclone. However, it must be noted that this method provides only a rough upper estimate of the cyclone size. Figure B.1 shows that the cloud cover associated to the low pressure system spans a wide diameter of about 500 km, where the spirally distributed cloud bands are noticeable. However the radius estimate of 250 km highly overestimates the low pressure dimension, as shown in the following section. As already observed in Chapter 4, the vortex signature reappears only on the morning of 20 January, since the interaction with Sardinia orography results in the formation of several pressure minima that compromise the identification of the original vortex in IR satellite imagery. The image acquired by the MODIS instrument on the late morning of 20 January, shown in Figure B.2, allows to make a more accurate estimate of the cyclone diameter of about 100-120 km. During the Adriatic phase the cyclone undergoes a new phase of intensification, where the tropical-like features are highlighted by the presence of an eye-shaped center, as shown in Figure B.3. At this time the cyclone reduced further up to 50 km of radius. In the last hours the cyclone reached radius of about 30 km, as shown in Figure B.4.

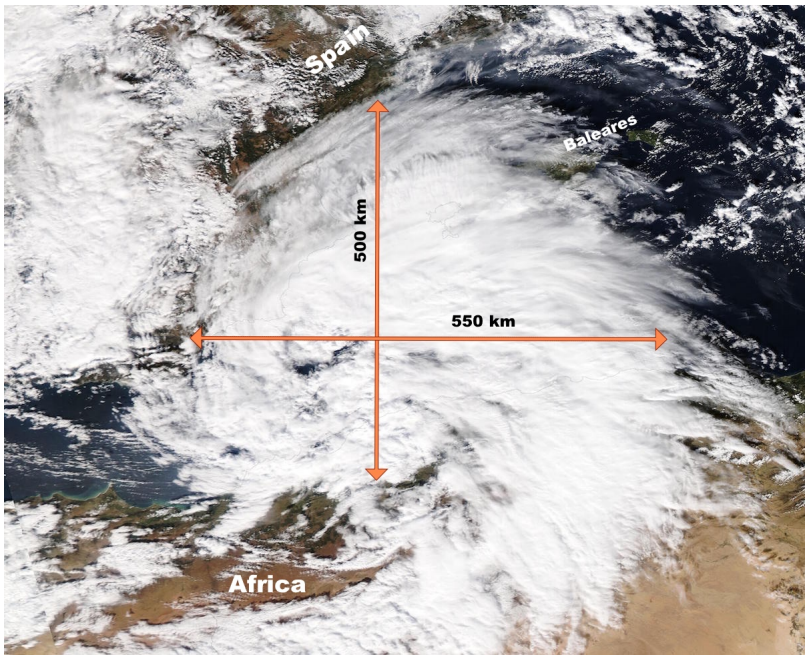

Figure B.1.: MODIS image of the cyclone on 19 January at 11 UTC.

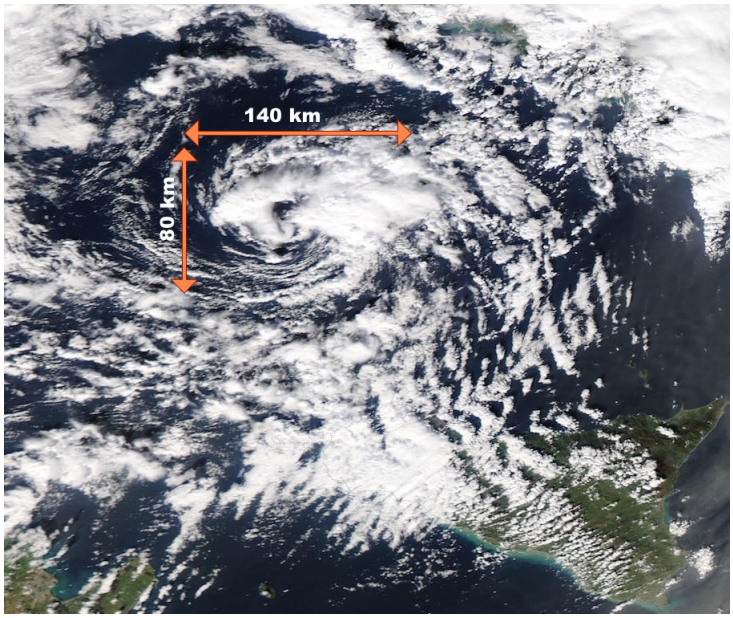

Figure B.2.: MODIS image of the cyclone on 20 January at 12 UTC.

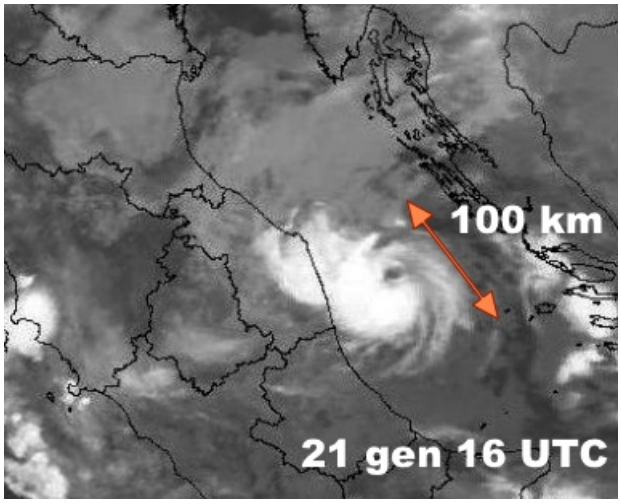

Figure B.3.: Satellite image of the cyclone on 21 January at 16 UTC .

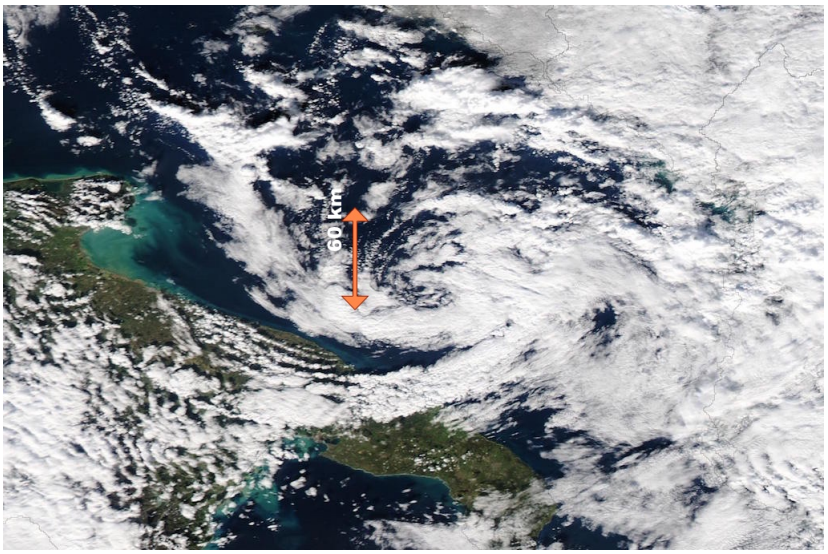

Figure B.4.: MODIS image of the cyclone on 22 January at 10 UTC .

B.2. BOLAM-based size estimate

In order to compute the cyclone radius from model data, an algorithm has been developed, by using the method suggested by Picornell [87]. First of all, a 9-point smoothing filter was applied to MSLP and to the 950, 900 and 850 hPa geopotential height values. Later on, a discrete Laplacian operator was applied to a data field chosen from the aforementioned one, on a box of 300×300 km^2 centred on the position of the MSLP minimum: the espression B.1 shows the formulation used for this operator (x is a generic variable).

$$\nabla^2 x(i,j) \propto x(i-1,j) + x(i+1,j) + x(i,j+1) + x(i,j-1) - 4 \cdot x(i,j) \tag{B.1}$$

Figure B.5 shows that this operator is able to identify the sharp pressure decrease around the cyclone. A tracking algorithm was then performed on the Laplacian maximum found in

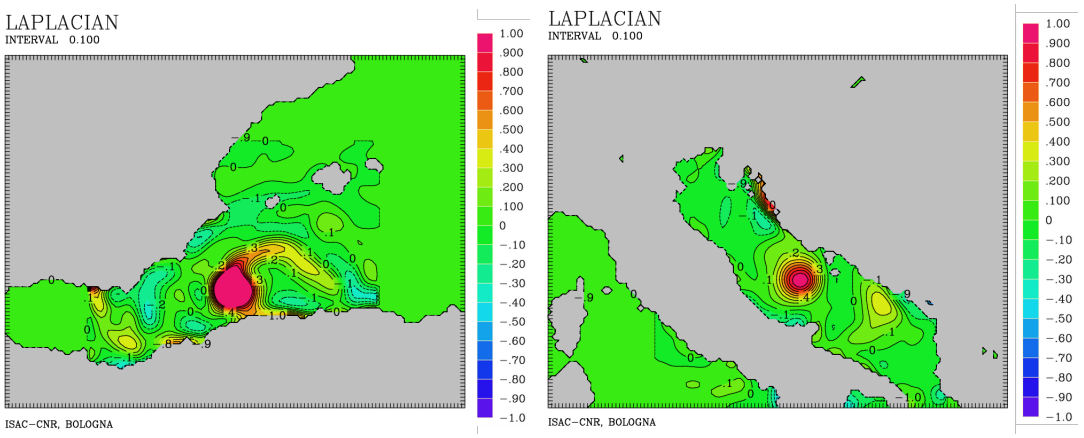

(a) 19 January 2014 15 UTC (b) 21 January 2014 23 UTC

Figure B.5.: Normalized discrete Laplacian computed in two different moments of the cyclone evolution.

a box of 200×200 km^2 surrounding the MSLP minimum center. The resulting coordinates of the Laplacian maximum were very similar, but not identical, to those found by tracking the pressure minimum. For each simulation hour, the algorithm finds the distance between the cyclone center (position of the pressure minimum) and the isoline of a chosen threshold, following four directions (Northward, Eastward, Southward and Westward), as shown in Figure B.6. In this way, it's possible to have an indication of the distance at which the pressure gradient becomes nearly constant, thus obtaining a cyclone radius estimate. This value was computed using 4 different data fields, namely MSLP and geopotential height at 950, 900 and 850 hPa; each time the threshold aforementioned was changed, based on the observations of maps similar to those presented in Figure B.5. Figure B.7 shows that the proposed method is able to correctly identify the shrink of the low-pressure system in the first hours, although the radii computed show a marked variability. This may be due to the cyclone structure, that was still forming and making a transition from extra-tropical to tropical structure (see Chapter 4). Aside from the observed trend, the values obtained does not show many similarities with the observed radius proposed in the previous section,

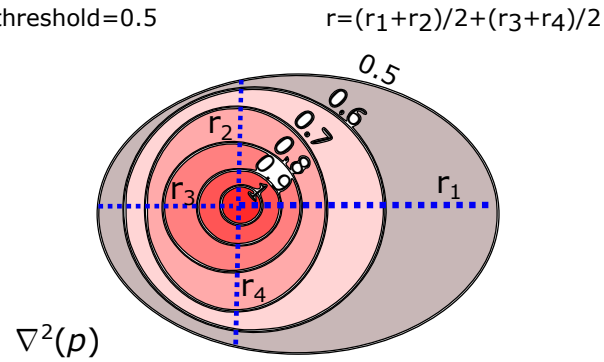

Figure B.6.: Graphical sketch of the algorithm explained in the text.

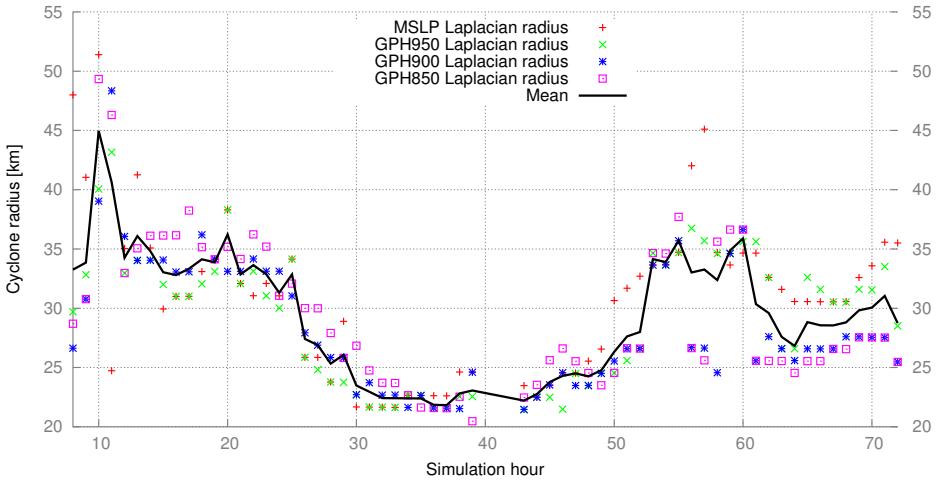

Figure B.7.: Radii computed using Laplacian operator to MSLP and geopotential height data from the B1 case (see text for details). Values related to the landfall phase has been omitted.

except for the Adriatic phase when the radius computed is of the order of 30 km. On the other hand, these results could already be imagined by comparing Figure B.5 (a) and Figure B.1 from which two very different values of radius may be derived. However, changing the threshold does not lead to very different results. The same algorithm has been applied also to the BOLAM simulation where MyOcean data were used. Figure B.8 shows that the radius computed in this case is very similar to that analysed before, except for a growth phase identified by the B3 simulation between hours 14 and 23. It may also be noted that the data presented in Figure B.8 are much more sparse and contain a greater variability. Among all the level tried for cyclone radius estimation, the MSLP shows the greater variability but seems to be the only quantity that correctly predicts the initial growth of the system over the Adriatic Sea with radius up to 50 km (see Figure B.3). These results prove that an estimation of cyclone radius from model data is very difficult and thus supports the initial assumption where R_{ex} was treated as a constant.

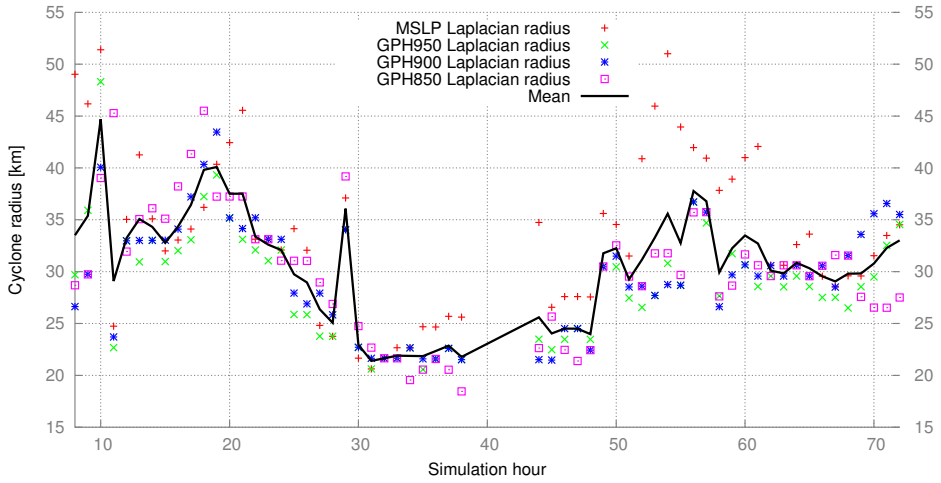

Figure B.8.: Radii computed using Laplacian operator to MSLP and geopotential height data from the B3 case (see text for details).

C

The Mediterranean Hurricane of November 2014

Shortly before the completion of the present thesis, an interesting Medicane case set up on the Central Mediterranean. An Atlantic trough, together with relatively warm waters, resulted in the formation of a powerful Mediterranean storm that interested Pantelleria, Lampedusa, Linosa, Malta and eventually the eastern coast of Sicily. The case was very interesting, since the BOLAM and MOLOCH operational models failed to forecast the cyclone path after the first 15 hours, although the intensity was predicted fairly well. Furthermore, the wind data collected from ship and weather stations on Malta revealed that this system was one of the strongest ever recorded in this part of the Mediterranean. In this chapter a brief presentation of the data collected and the simulation performed on this case are presented, as preliminary to further studies.

C.1. Observational analysis

The synoptic configuration prior to the cyclone formation illustrated in Figure C.1 identify a strong trough extending from North Sea up to the Lybian region. A few days earlier, the entrance of this trough in the Mediterranen area caused severe rainfall throughout North and Center Italy. Two days before the cyclone formation NWP models indicated the possibility of a cut-off near the Tunis coast, with the subsequent formation of a low-level MSLP minimum. The MOLOCH operational model forecast initialized on 6 November at 00 UTC already showed the chance of a deep minimum with several closed isobars for the day after. Given the strong pressure gradient, really intense winds (over 26 m/s) were predicted West of Sicily. However, at this time, the predicted cyclone seemed to be quite stationary. The next day, the same model forecast initialized on 7 November at 00 UTC recognized a very deep minimum (987 hPa) with a deep-warm core (up to 500 hPa) for the next 12 hours. At 9 UTC the satellite imagery reported in Figure C.2 captured for the first time a hardly noticeable swirl in cloud cover, an indication that cyclogenesis was already taking place at that moment. The weather station of Pantelleria island reported a pressure of 992 hPa at 08 UTC, while the system was still forming (not shown). The data retrieved from OSCAT satellite showed sustained winds of over 50 knots in the early morning (not shown). Between 9 and 12 UTC the low-pressure system rapidly deepened, as forecasted by BOLAM and

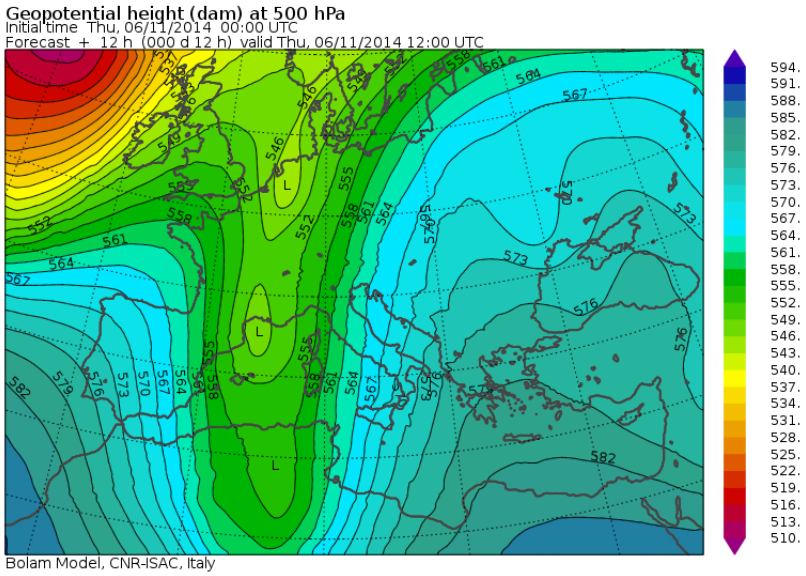

Figure C.1.: Geopotential height at 500 hPa forecasted for 6 november 2014 at 12 UTC.

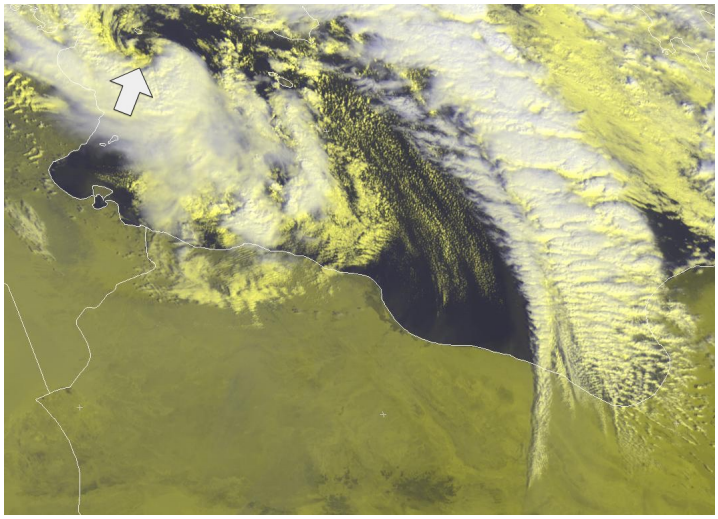

Figure C.2.: SEVIRI pancromatic-north satellite imagery for 7 November 2014 at 9 UTC.

MOLOCH operational models. The cloud structure clearly showed the presence of an *eye* in the center of the system, together with spirally distributed cloud bands. However, IR satellite data did not indicate presence of very intense convection near the eye-wall. Initially, this fact discouraged the hypothesis made on the tropical nature of the cyclone, although strong winds and clouds from satellite were typical of a TLC. At around 12.30 UTC the cyclone eye crossed Linosa island, where a weather station was collecting data every 5 minutes. Thanks to this high temporal resolution data the author was able to reconstruct the cyclone crossing in detail. Figure C.4 (a) underlines the sudden drop of pressure that occurred between 11 and 15 UTC, from approximately 1000 hPa to a minimum of 981.9 hPa. This low value is in good agreement with the one recorded shortly thereafter on the island of Malta, and represents a

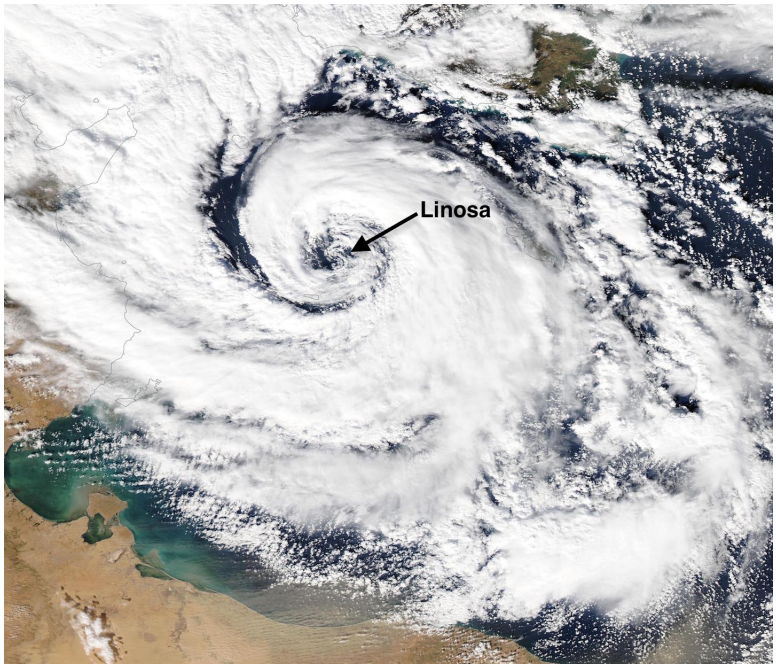

Figure C.3.: MODIS Satellite visible on 7 November 2014 at 12.15 UTC. The position of Linosa island is marked by a black arrow

good approximation of the pressure reached in the eye of the storm, since satellite imagery shows that the system crossed the island (see Figure C.3). If confirmed, this value is one of the lowest ever reached in a hurricane-like system over the Mediterranean (see Moscatello et al. [80]). A careful analysis of the two panels contained in Figure C.4 reveals some interesting features that are worth discussing. First of all, between 12 and 13 UTC the wind gusts dropped from about 90 km/h to very low values (10 km/h), as highlighted by the mean wind speed line draw in Figure C.4 (a). This is a strong indication of the calm that is often found in the eye of a TC. During the same period, the air temperature increased from 13°C to 18°C and fell again to about 16 °C at 14 UTC, when the cyclone had already crossed the island. This sudden rise of temperature is an indication of the presence of a low-level warm core in the eye of the cyclone. It may be also noticed that the cooling that preceded the cyclone arrival was caused by the cold front associated with the earlier phase of the cyclone, and also evident in Figure C.2 in the comma-shaped cloud structure. Furthermore, the eye crossing is outlined also by the change in UV radiation. The first arrival of thick cumulonimbus clouds marks a sudden drop to nearly 0 W/m^2, while the lowest pressure value are characterized by high values of UV radiation. The following decrease is due to sunset (15.59 UTC). The pressure drop was evident also in the weather station of Lampedusa island, where wind gusts reached 135.2 km/h at 12.06 UTC. Later on, the system began to show signs of moderate convection, as seen on the IR satellite imagery (not shown).
At 16.30 UTC the cyclone was approaching the island of Malta, where a weather radar was operating at the Malta international airport. Since the eye crossed the northern part of the island, a clear vortex echo was visible in the radar rain intensity estimate reported in Figure C.7 (a). A few photos from Malta island published on the web displayed an area free

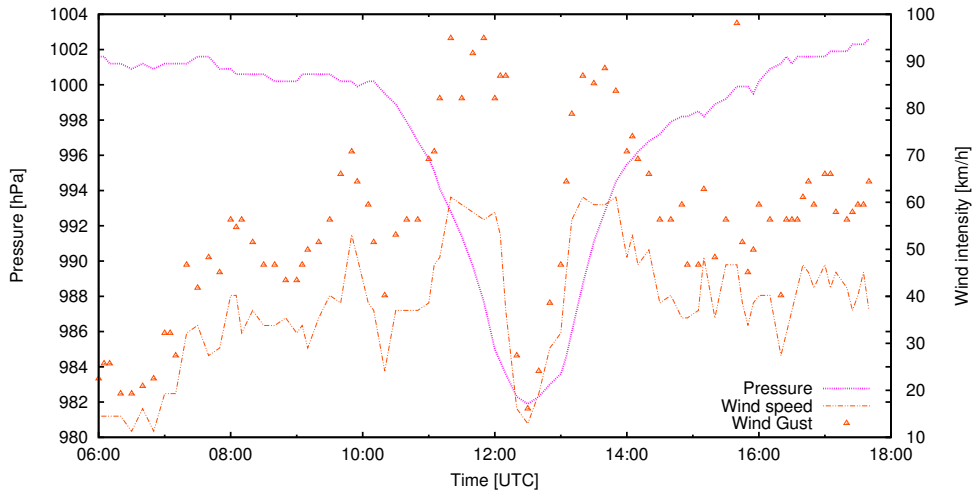

(a) Pressure (purple line), wind gust (orange triangles) and wind speed (mean)

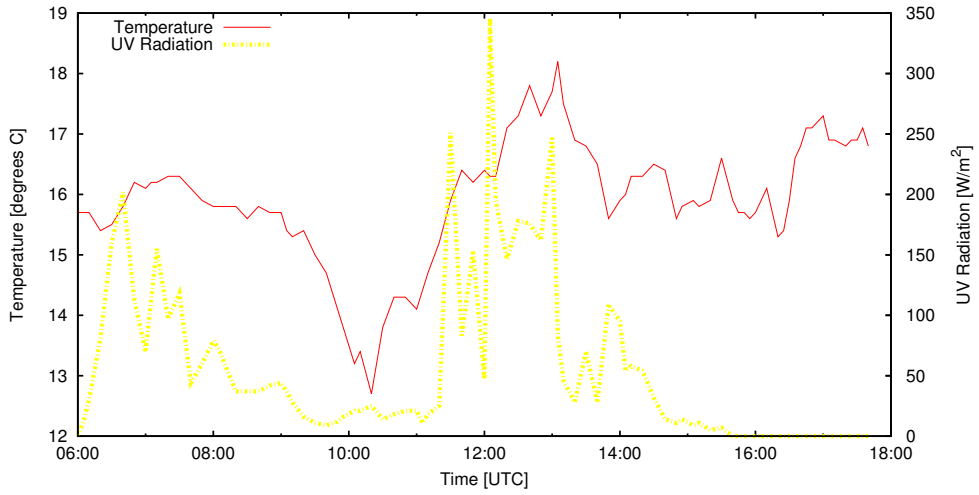

(b) Temperature (red line) and UV radiation (yellow line)

Figure C.4.: Detail of cyclone crossing Linosa island.

of clouds, surrounded by thick cumulonimbi clouds (not shown). The station of Bugibba, on the Northern side of the Malta island, recorded a minimum pressure of 978.6 hPa and a maximum wind gust of 153.7 km/h. The sudden drop of pressure due to the cyclone crossing was clearly visible also here, as shown in Figure C.6, together with the minimum of the wind in the eye. The nearby stations of Gharb and Malta airport reported a minimum pressure of respectively 988.7 hPa and 984.6 hPa with sustained winds and gusts up to 100 km/h. At this time, BOLAM and MOLOCH operational models emission led to believe that the cyclone would have moved eastward, towards Greece. However, the system made a left turn towards the Gulf of Catania, Sicily. Here the cyclone quickly rejuvenated and became quite stationary. As shown in Figure C.7, at 5 UTC the system was still bringing moderate intensity rainfall and strong winds. Several stations in the Gulf of Catania reported sustained winds with a peak of 82.1 km/h on Monte Tauro weather station at 00.48 UTC.

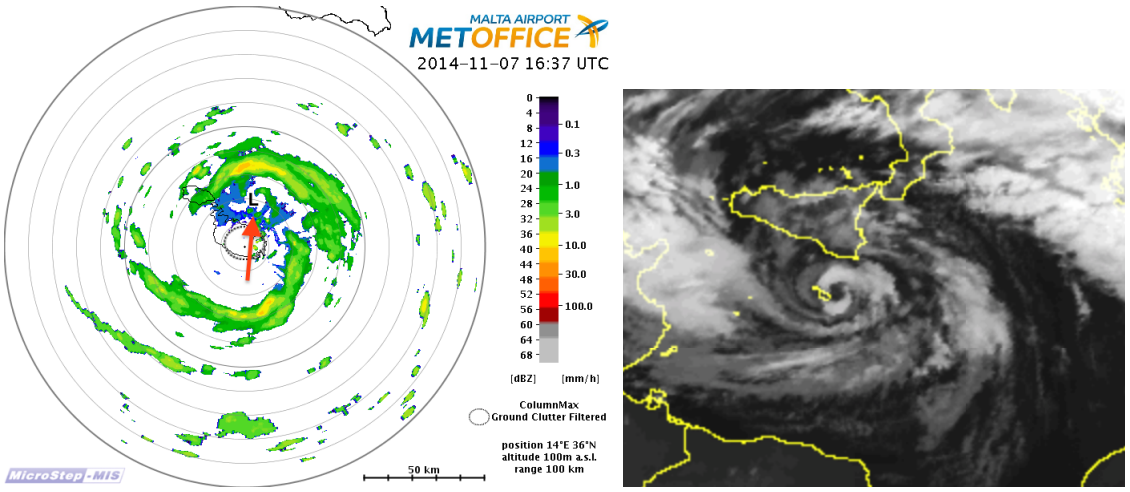

(a) Radar intensity estimate from Malta international airport at 16.37 UTC

(b) Satellite IR imagery at 17 UTC

Figure C.5.: Detail of cyclone crossing Malta island.

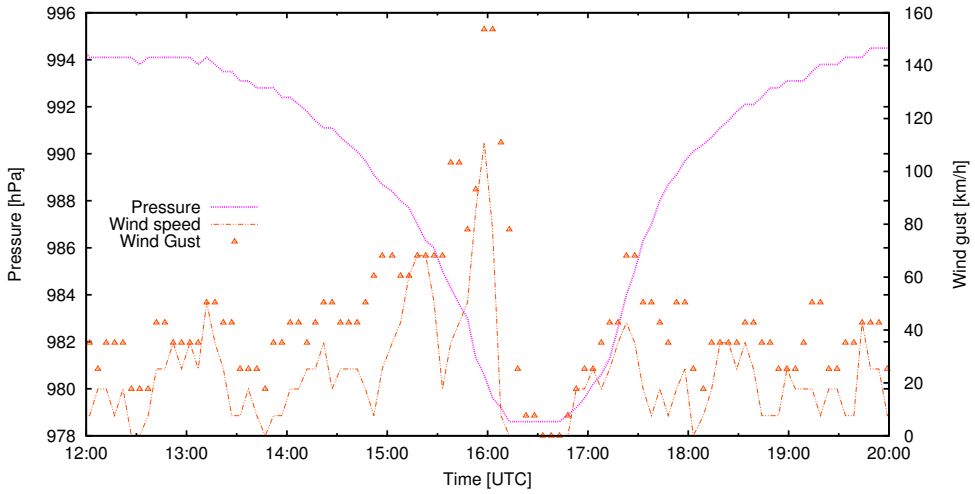

Figure C.6.: Pressure (purple line), wind gust (orange triangles) and wind speed (mean) recorded at Bugibba, Malta island.

At 9.30 UTC of 8 november the cyclone was finally leaving Sicily, and deviating eastward as expected before. Figure C.8 shows the cyclone trajectory reconstruction obtained by using satellite imagery and ground stations data.

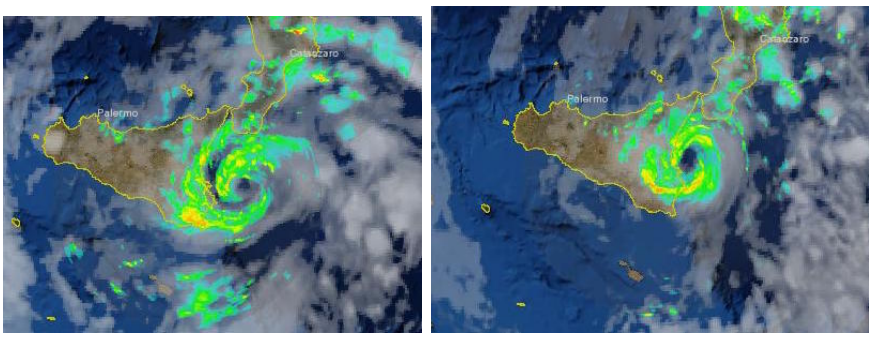

(a) 7 November at 23.30 UTC (b) 8 November at 4.40 UTC

Figure C.7.: Radar intensity estimate from the national Italian radar mosaic (Protezione Civile) of the landfall on Sicily.

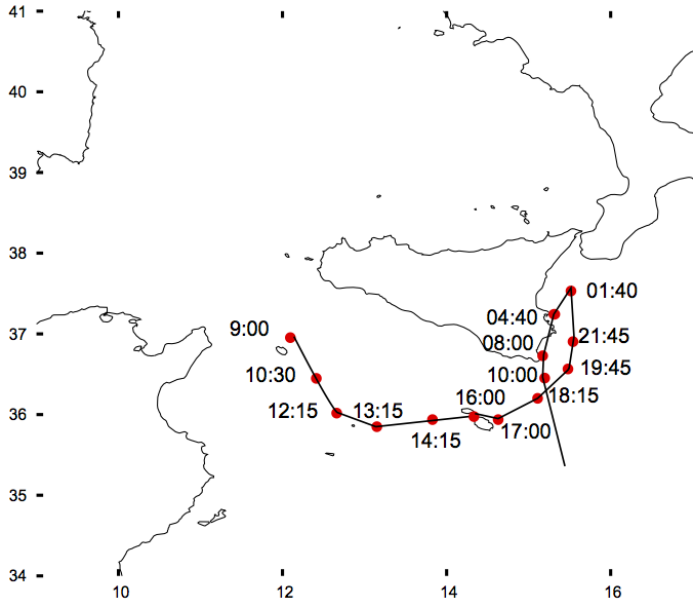

Figure C.8.: Cyclone trajectory reconstructed from satellite and weather stations data. Time starts from 7 November and hours are in UTC.

C.2. Case simulation

The event described was forecasted by the BOLAM and MOLOCH operational models only initialised by 7 November at 00 UTC; previous model runs failed to predict both minimum position and intensity. However, the forecast initialized on 7 November at 00 UTC predicted fairly well the initial rapid deepening of pressure (almost 25 hPa in 12 hours) but failed to predict the cyclone deviation towards Sicily, occurred on the evening of 7 November. For this reason the author was stimulated to test the knowledge gained from the study of the January case and to try to understand why simulations went wrong. In order to test the sensitivity to initial conditions, two simulations were performed based respectively on GFS and ECMWF analysis. In the first branch, a GLOBO 48-hours model simulation has been

used to nest a BOLAM 48-hours model simulation on a domain slightly shifted to the South with respect to the operational one, in order to better describe the area where the trough was placed. In the second branch, the BOLAM model was nested directly into the 6-hourly analysis provided by ECMWF. The 48-hours simulation obtained in both branches was then used to nest a MOLOCH model simulation of a smaller area near Sicily. In all cases, the cyclone has been tracked using the same algorithm developed in Chapter 4 and a thermal phase analysis was conducted. Figure C.9 shows that all models simulations have their pros

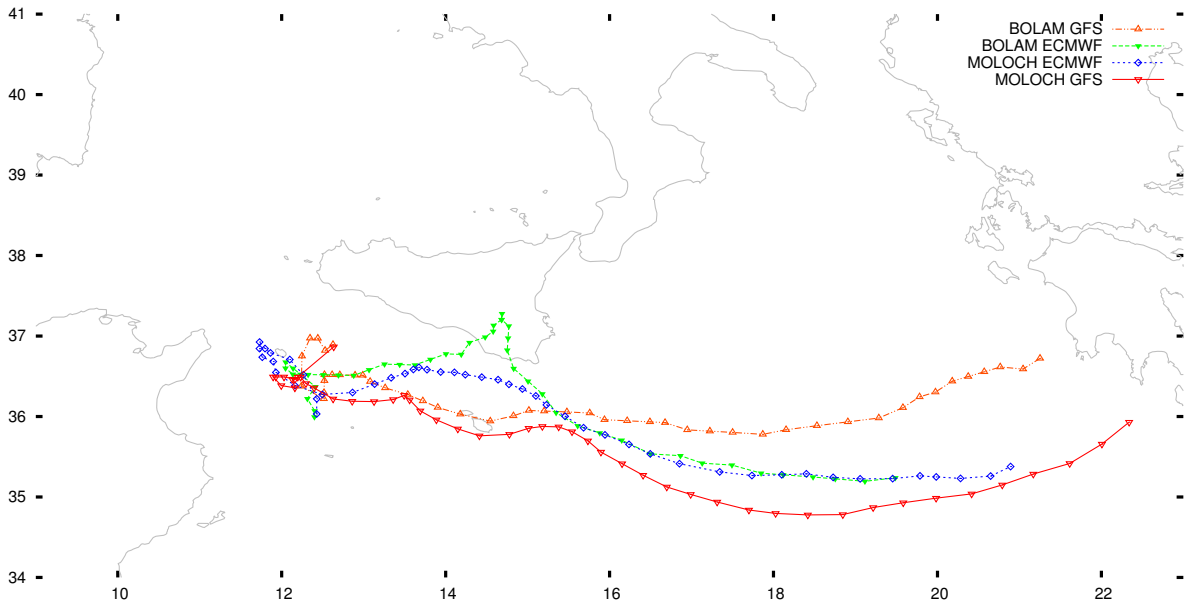

Figure C.9.: MSLP cyclone tracks in the 4 cases described in the text.

and cons. For instance:

- The BOLAM-GFS simulation is the only one that predicts the land-cross north of Malta Island, although several hours later, but deviates the cyclone to the east soon after.
- The BOLAM-ECMWF simulation seems to detect the change of the path towards Sicily, but the resulted trajectory is deviated to soon, thus missing the Malta landfall and making contact with the Southern part of Sicily.
- The MOLOCH-ECMWF simulation is also deviated to the North, but misses both landfall with Malta and Sicily.

It should be noted that all the cases do not predict neither the Linosa land-cross neither the eastern Sicily landfall. Although both GFS and ECMWF initialized simulations predict fairly well the rapid decrease of pressure, these two cases shows two different periods of intensification. Figure C.10 highlights these differences: while the cyclone forecasted in the BOLAM-ECMWF case reach its maximum in the morning of 7 November, the BOLAM-GFS tends to produce a stronger cyclone that persists also in the following days. While

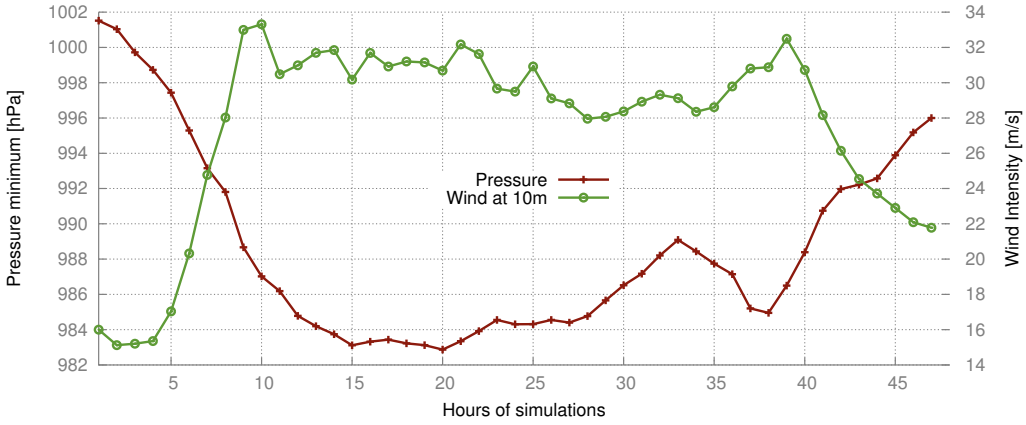

(a) BOLAM GFS

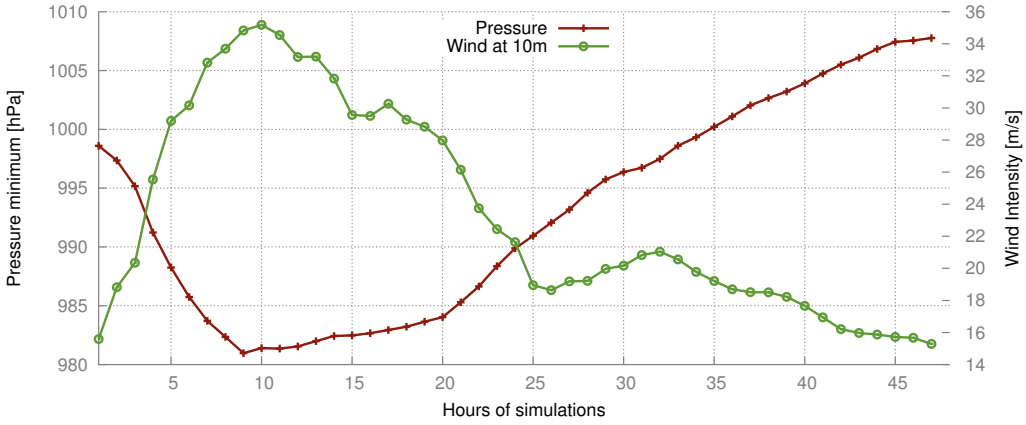

(b) BOLAM ECMWF

Figure C.10.: Comparison of pressure minimum and wind maximum intensity (found in a circle of radius R_{ex}) of the cyclone.

this may be due to the missed Sicily landfall in the BOLAM-GFS simulation, the winds predicted in the latter case are highly overestimated in the second day, when the cyclone had already weakened. Conversely, ECMWF-based simulation seems to better capture the rapid deepening of the system and the strong winds (up to 36 m/s) that characterize only the first phase of the cyclone lifetime.
The small-scale structure of the cyclone is clearly highlighted by the MOLOCH wind and pressure field showed in Figure C.11. Despite the very different results, all models agree on the tropical-like nature of the cyclone. The thermal analysis performed with the algorithm developed in Chapter 4 shows nearly zero values of the thermal asymmetry parameter B. Furthermore, the transition to a deep-warm core structure is identified in the ECMWF cases, from the 4^{th} hour onwards, and in the GFS cases, from the 8^{th} hour onwards. The phase diagrams reported in Figure C.12 highlights also a secondary transition to a shallow warm core, after the 34^{th} hour. Only in the BOLAM-GFS case, shown in Figure C.13, the cyclone starts from a deep-cold core structure and makes a transition to a shallow-warm

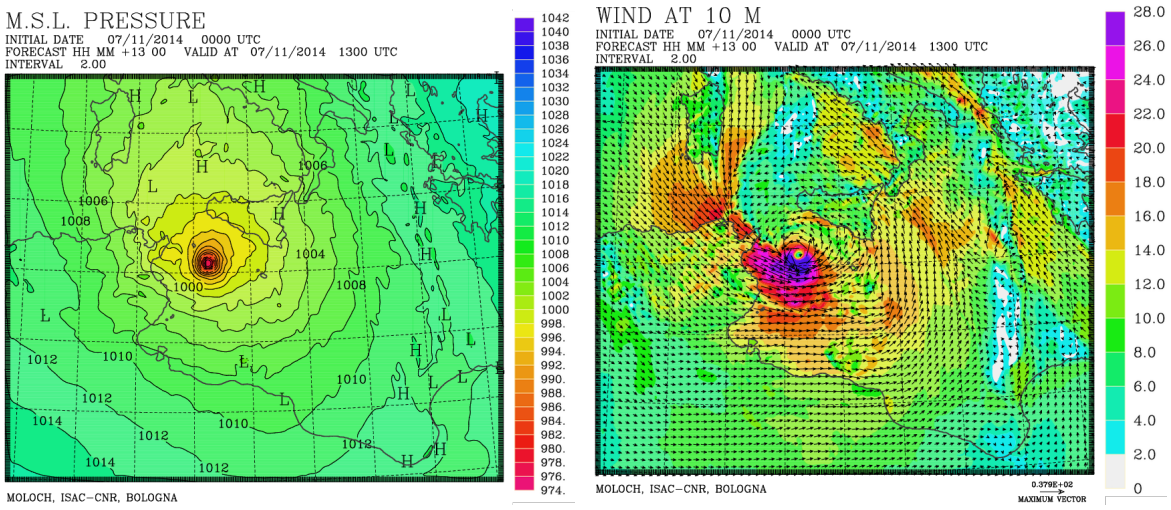

(a) MSLP on 7 November 2014 at 13 UTC

(b) Wind at 10 meters on 7 November 2014 at 13 UTC

Figure C.11.: MSLP and 10m wind predicted by the MOLOCH model, nested into the BOLAM model initialized with ECMWF.

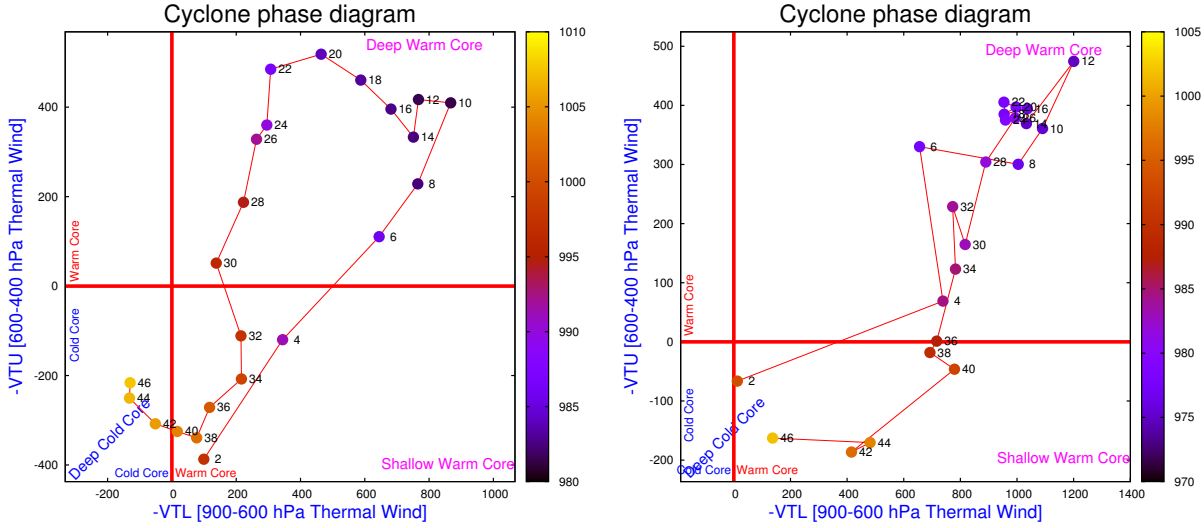

(a) BOLAM-ECMWF

(b) MOLOCH-ECMWF

Figure C.12.: Cyclone phase diagrams obtained in the simulations initialized with ECMWF. The parameters obtained are the same described in Chapter 4.

core and eventually deep-warm core structure. In this case, the loss of tropical-like features is predicted only from the 40th hour onwards. The 3-dimensional structure of the cyclone shows many similarities with the one commented in section 5.5. In particular, a formation of a PV-tower is observed hours before the sudden deepening of the pressure minimum in the

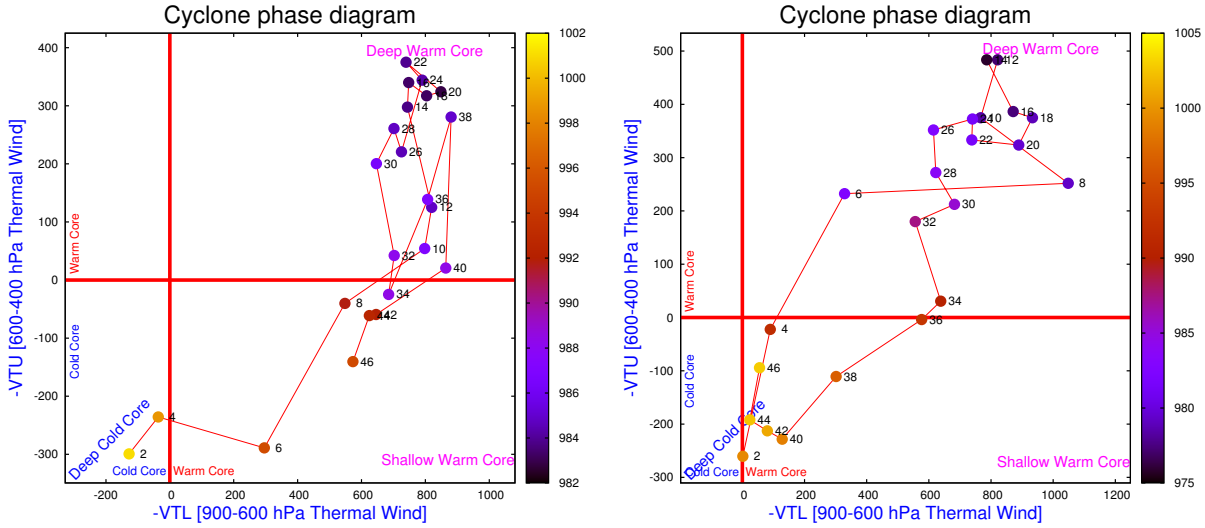

(a) BOLAM-GFS (b) MOLOCH-GFS

Figure C.13.: Cyclone phase diagrams obtained in the simulations initialized with GFS. The parameters obtained are the same described in Chapter 4.

Sicily Sea. In the following hours, the PV anomaly extends towards upper levels, eventually reaching the tropopause, as shown in Figure C.14.

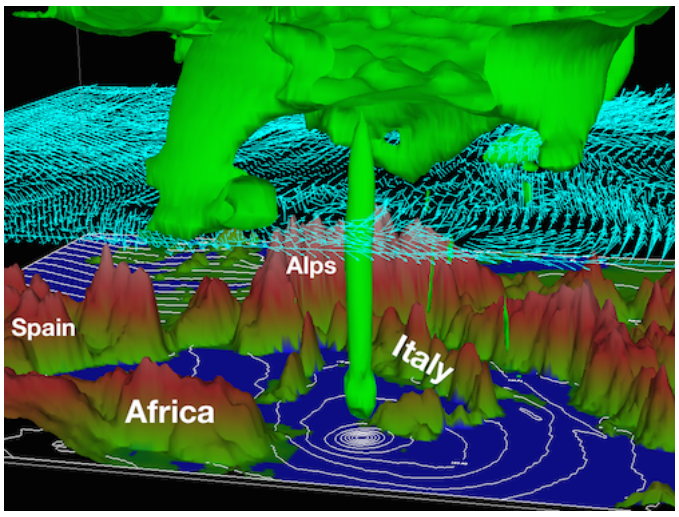

Figure C.14.: Vis5D graphical processing of the BOLAM model output on 7 November 2014 at 15 UTC. Green surface is the 1.8 PVU isosurface, while the white contours represent MSLP and blue vectors are the 500 hPa wind field.

D

List of symbols and of physical constants

D.1. Physical constants

gravity acceleration $g = 9.81\text{ms}^{-2}$

earth radius $a = 6.371 \cdot 10^6$ m

gas constant (dry air) $R_d = 287.05$ J/kg/K

gas constant (water vapour) $R_V = 461.51$ J/kg/K

specific heat at constant pressure (dry air) $c_p = 1004.6$ J/kg/K

specific heat at constant pressure (water vapour) $c_p^V = 1869.46$ J/kg/K

latent heat of evaporation (0° C) $L_v^W = 2.5008 \cdot 10^6$ J/kg

latent heat of fusion (0° C) $L_i^W = 0.3336 \cdot 10^6$ J/kg

reference pressure $p_0 = 10^5$ Pascal=Nm^{-2} =kg/ms^2

earth angular velocity $\Omega = 7.292 \cdot 10^{-5}\text{s}^{-1}$

water density $\rho_W = 10^3$ kg/m^3

water specific heat $c_W = 4186\text{J/kg/K}$

reference temperature T_0, usually triple point of water

reference pressure $p_0 = 1013.25$ hPa= 1 atm

troposphere scale height $H = \frac{R_d T_0}{g}$

D.2. Independent variables

horizontal spatial variables x, y

time variable t

longitude λ

latitude φ

height z

generalized vertical coordinate σ

D.3. Meteorological fields

zonal wind u

meridional wind v

vertical speed w

horizontal wind vector $\mathbf{V} = (u, v)$

generalized vertical speed $\dot{\sigma}$

temperature T

pressure p

total air density ρ

virtual temperature $T_v = \frac{T}{1-(1-\epsilon)e/p}$ where $\epsilon = R_d/R_V$ and $e = \rho_v R_v T$ is the partial pressure of water. This equation is approximated by $T_v = T(1 + 0.61 \cdot w)$ where w is the mixing ratio.

equivalent temperature $T_e \simeq T + \frac{L_v^W}{c_p} w$

potential temperature $\theta = T \left(\frac{p_0}{p}\right)^{R/c_p}$

virtual potential temperature $\theta_v \simeq \theta(1+0.61w-w_L)$ where w_L is the mixing ratio of liquid water in the air.

equivalent potential temperature $\theta_e = T_e \left(\frac{p_0}{p}\right)^{R_d/c_p}$

specific humidity q

vertical speed in pressure coordinates $\omega = \mathrm{d}p/\,\mathrm{d}t$

geopotential height $\Phi = gz$

surface pressure p_s

Geostrophic wind $\mathbf{V}_g = \frac{\hat{k}}{f} \times \nabla_p \Phi$

Thermal wind $\mathbf{V}_t$ implicitly defined by the equation $\frac{\partial \mathbf{V}_g}{\partial(\ln p)} = -\frac{R}{f}\hat{k} \times \nabla_p T$

D.4. Other symbols

hybrid vertical coordinate relaxing factor α

horizontal gradient $\nabla = (\partial_x, \partial_y)$

Coriolis parameter $f = 2\Omega \sin \varphi$

3D-pressure coordinate gradient $\nabla_p = (\partial_x, \partial_y, \partial_p)$

drag coefficient C_d

enthalpy exchange coefficient C_k

Bibliography

[1] Aebischer, U., and Schär, C. Low-level potential vorticity and cyclogenesis to the lee of the alps. *Journal of the atmospheric sciences 55*, 2 (1998), 186–207.

[2] Ahmadi-Givi, F., Nasr-Esfahany, M., and Mohebalhojeh, A. R. Interaction of North Atlantic baroclinic wave packets and the Mediterranean storm track. *Q.J.R. Meteorol. Soc. 140*, 680 (Apr. 2014), 754–765.

[3] Appenzeller, C., Davies, H., and Norton, W. Fragmentation of stratospheric intrusions. *Journal of Geophysical Research: Atmospheres (1984–2012) 101*, D1 (1996), 1435–1456.

[4] Arakawa, A., and Lamb, V. R. Computational design of the basic dynamical processes of the ucla general circulation model. *Methods in computational physics 17* (1977), 173–265.

[5] Argence, S., Lambert, D., Richard, E., Pierre Chaboureau, J., Philippe Arbogast, J., and Maynard, K. Improving the numerical prediction of a cyclone in the mediterranean by local potential vorticity modifications. *Quarterly Journal of the Royal Meteorological Society 135*, 641 (2009), 865–879.

[6] Argence, S., Lambert, D., Richard, E., Söhne, N., Chaboureau, J.-P., Crépin, F., and Arbogast, P. High resolution numerical study of the algiers 2001 flash flood: sensitivity to the upper-level potential vorticity anomaly. *Advances in Geosciences 7*, 7 (2006), 251–257.

[7] Avila, L. A., and Pasch, R. J. Atlantic tropical systems of 1993. *Monthly weather review 123*, 3 (1995), 887–896.

[8] Billett, S., and Toro, E. Aon waf-type schemes for multidimensional hyperbolic conservation laws. *Journal of Computational Physics 130*, 1 (1997), 1–24.

[9] Bister, M., and Emanuel, K. A. Dissipative heating and hurricane intensity. *Meteorology and Atmospheric Physics 65*, 3-4 (1998), 233–240.

[10] Blackadar, A. K. The vertical distribution of wind and turbulent exchange in a neutral atmosphere. *Journal of Geophysical Research 67*, 8 (1962), 3095–3102.

[11] Bougeault, P., and Lacarrere, P. Parameterization of orography-induced turbulence in a mesobeta–scale model. *Monthly Weather Review 117*, 8 (1989), 1872–1890.

[12] Brown, Z. G. Mesoscale precursors to the hurricane gaston flooding event as diagnosed from observations and numerical simulations.

[13] Browning, K. The dry intrusion perspective of extra-tropical cyclone development. *Meteorological Applications 4*, 04 (1997), 317–324.

[14] Buzzi, A. *Dynamic Meteorology Lectures*, 1 ed. Università di Bologna, 2013.

[15] Buzzi, A., Fantini, M., Malguzzi, P., and Nerozzi, F. Validation of a limited area model in cases of mediterranean cyclogenesis: surface fields and precipitation scores. *Meteorology and Atmospheric Physics 53*, 3-4 (1994), 137–153.

[16] Buzzi, A., and Foschini, L. Mesoscale meteorological features associated with heavy precipitation in the southern alpine region. *Meteorology and Atmospheric Physics 72*, 2-4 (2000), 131–146.

[17] Campa, J., and Wernli, H. A pv perspective on the vertical structure of mature midlatitude cyclones in the northern hemisphere. *Journal of the Atmospheric Sciences 69*, 2 (2012), 725–740.

[18] Campins, J., Genovés, A., Picornell, M., and Jansà, A. Climatology of mediterranean cyclones using the era-40 dataset. *International Journal of Climatology 31*, 11 (2011), 1596–1614.

[19] Campins, J., Jansà, A., and Genovés, A. Three-dimensional structure of western mediterranean cyclones. *International journal of climatology 26*, 3 (2006), 323–343.

[20] Cavicchia, L., von Storch, H., and Gualdi, S. A long-term climatology of medicanes. *Climate Dynamics* (2012), 1–13.

[21] Cavicchia, L., von Storch, H., and Gualdi, S. Mediterranean tropical-like cyclones in present and future climate. *Journal of Climate*, 2014 (2014).

[22] Chaboureau, J.-P., and Claud, C. Satellite-based climatology of mediterranean cloud systems and their association with large-scale circulation. *Journal of Geophysical Research: Atmospheres (1984–2012) 111*, D1 (2006).

[23] Chaboureau, J.-P., Pantillon, F., Lambert, D., Richard, E., and Claud, C. Tropical transition of a mediterranean storm by jet crossing. *Quarterly Journal of the Royal Meteorological Society 138*, 664 (2012), 596–611.

[24] Chagnon, J., Gray, S., and Methven, J. Diabatic processes modifying potential vorticity in a north atlantic cyclone. *Quarterly Journal of the Royal Meteorological Society 139*, 674 (2013), 1270–1282.

[25] Charney, J. G., and Eliassen, A. On the growth of the hurricane depression. *Journal of the Atmospheric Sciences 21*, 1 (1964), 68–75.

[26] Charnock, H. Wind stress on a water surface. *Quarterly Journal of the Royal Meteorological Society 81*, 350 (1955), 639–640.

[27] Cione, J. J., and Uhlhorn, E. W. Sea surface temperature variability in hurricanes: Implications with respect to intensity change. *Monthly Weather Review 131*, 8 (2003), 1783–1796.

[28] Collins, S. N., James, R. S., Ray, P., Chen, K., Lassman, A., and Brownlee, J. Grids in numerical weather and climate models.

[29] Craig, G. C., and Gray, S. L. Cisk or wishe as the mechanism for tropical cyclone intensification. *Journal of the atmospheric sciences 53*, 23 (1996), 3528–3540.

[30] Das, S. S., Sijikumar, S., and Uma, K. Further investigation on stratospheric air intrusion into the troposphere during the episode of tropical cyclone: Numerical simulation and mst radar observations. *Atmospheric Research 101*, 4 (2011), 928–937.

[31] Davolio, S., Miglietta, M., Moscatello, A., Pacifico, F., Buzzi, A., and Rotunno, R. Numerical forecast and analysis of a tropical-like cyclone in the ionian sea. *Natural Hazards and Earth System Science 9*, 2 (2009), 551–562.

[32] Dunn, G. E. Cyclogenesis in the tropical atlantic. *Bull. Amer. Meteor. Soc 21* (1940), 215–229.

[33] Emanuel, K. Genesis and maintenance of" mediterranean hurricanes". *Advances in Geosciences 2*, 2 (2005), 217–220.

[34] Emanuel, K. A. An air-sea interaction theory for tropical cyclones. part i: Steady-state maintenance. *Journal of the Atmospheric Sciences 43*, 6 (1986), 585–605.

[35] Emanuel, K. A. The dependence of hurricane intensity on climate. *Nature 326*, 6112 (1987), 483–485.

[36] Emanuel, K. A. The theory of hurricanes. *Annual Review of Fluid Mechanics 23*, 1 (1991), 179–196.

[37] Emanuel, K. A., and Nolan, D. Tropical cyclone activity and the global climate system. In *Preprints, 26th Conf. on Hurricanes and Tropical Meteorology, Miami, FL, Amer. Meteor. Soc. A* (2004), vol. 10.

[38] Ernst, J., and Matson, M. A mediterranean tropical storm? *Weather 38*, 11 (1983), 332–337.

[39] Evans, J. L., and Hart, R. E. Objective indicators of the life cycle evolution of extratropical transition for atlantic tropical cyclones. *Monthly weather review 131*, 5 (2003), 909–925.

[40] Fierli, F., Pinori, S., Dietrich, S., Medaglia, C., and Tripoli, G. Potential vorticity analysis of the storm event of the 9-10 november algerian flood. In *Proc. Fourth Plinius Conf. on Mediterranean Storms* (2003).

[41] Fita, L., Romero, R., Luque, A., Emanuel, K., and Ramis, C. Analysis of the environments of seven mediterranean tropical-like storms using an axisymmetric, nonhydrostatic, cloud resolving model. *Natural Hazards and Earth System Science 7*, 1 (2007), 41–56.

[42] Flaounas, E., Kotroni, V., Lagouvardos, K., and Flaounas, I. Cyclotrack (v1. 0)–tracking winter extratropical cyclones based on relative vorticity: sensitivity to data filtering and other relevant parameters. *Geoscientific Model Development 7*, 4 (2014), 1841–1853.

[43] Flaounas, E., Raveh-Rubin, S., Wernli, H., Drobinski, P., and Bastin, S. The dynamical structure of intense mediterranean cyclones. *Climate Dynamics* (2014), 1–17.

[44] Georgelin, M., Bougeault, P., Black, T., Brzovic, N., Buzzi, A., Calvo, J., Casse, V., Desgagné, M., El-Khatib, R., Geleyn, J.-F., et al. The second compare exercise: a model intercomparison using a case of a typical mesoscale orographic flow, the pyrex iop3. *Quarterly Journal of the Royal Meteorological Society 126*, 564 (2000), 991–1029.

[45] Georgiev, C. G. Quantitative relationship between meteosat wv data and positive potential vorticity anomalies: a case study over the mediterranean. *Meteorological Applications 6*, 02 (1999), 97–109.

[46] Gyakum, J. R., Carrera, M., Zhang, D.-L., Miller, S., Caveen, J., Benoit, R., Black, T., Buzzi, A., Chouinard, C., Fantini, M., et al. A regional model intercomparison using a case of explosive oceanic cyclogenesis. *Weather and forecasting 11*, 4 (1996), 521–543.

[47] Harrold, T., and Browning, K. The polar low as a baroclinic disturbance. *Quarterly Journal of the Royal Meteorological Society 95*, 406 (1969), 710–723.

[48] Hart, R. E. A cyclone phase space derived from thermal wind and thermal asymmetry. *Monthly Weather Review 131*, 4 (2003), 585–616.

[49] Hart, R. E., and Evans, J. Real-time use of cyclone phase diagrams to improve structural diagnosis and forecasting. In *26th Conference on Hurricanes and Tropical Meteorology* (2004).

[50] Hirschberg, P. A., and Fritsch, J. M. On understanding height tendency. *Monthly weather review 121*, 9 (1993), 2646–2661.

[51] Hoinka, K. P., Richard, E., Poberaj, G., Busen, R., Caccia, J.-l., Fix, A., and Mannstein, H. Analysis of a potential-vorticity streamer crossing the alps during map iop 15 on 6 november 1999. *Quarterly Journal of the Royal Meteorological Society 129*, 588 (2003), 609–632.

[52] Homar, V., Romero, R., Stensrud, D., Ramis, C., and Alonso, S. Numerical diagnosis of a small, quasi-tropical cyclone over the western mediterranean: Dynamical vs. boundary factors. *Quarterly Journal of the Royal Meteorological Society 129*, 590 (2003), 1469–1490.

[53] Hoskins, B. J., McIntyre, M., and Robertson, A. W. On the use and significance of isentropic potential vorticity maps. *Quarterly Journal of the Royal Meteorological Society 111*, 470 (1985), 877–946.

[54] Houze Jr, R. A. Clouds in tropical cyclones. *Monthly Weather Review 138*, 2 (2010), 293–344.

[55] ISAC. *BOLAM - Manuale Scientifico e d'uso*. National Research Council - Italy, 9 2011.

[56] Kain, J. S. The kain-fritsch convective parameterization: an update. *Journal of Applied Meteorology 43*, 1 (2004), 170–181.

[57] Kain, J. S., and Fritsch, J. M. A one-dimensional entraining/detraining plume model and its application in convective parameterization. *Journal of the Atmospheric Sciences 47*, 23 (1990), 2784–2802.

[58] Kieu, C. Q., Chen, H., and Zhang, D.-L. An examination of the pressure-wind relationship for intense tropical cyclones. *Weather and Forecasting 25*, 3 (2010), 895–907.

[59] Kumar, P. Analyses of ring of maximum wind, ring of maximum pressure gradient, inflow angle and rmw in tropical storm. In *29th Conference on Hurricanes and Tropical Meteorology* (2010).

[60] Kuo, H.-L. On formation and intensification of tropical cyclones through latent heat release by cumulus convection. *Journal of the Atmospheric Sciences 22*, 1 (1965), 40–63.

[61] Kuo, Y.-H., Guo, Y.-R., and Reed, R. J. Simulation of a mesoscale cyclone over the mediterranean sea.

[62] Lagouvardos, K., Kotroni, V., Jovic, S. N., Kallos, G., Tremback, C., et al. Observations and model simulations of a winter sub-synoptic vortex over the central mediterranean. *Meteorological Applications 6*, 04 (1999), 371–383.

[63] Landsea, C. W. A climatology of intense (or major) atlantic hurricanes. *Monthly Weather Review 121*, 6 (1993), 1703–1713.

[64] Langland, R. H., and Maue, R. N. Recent northern hemisphere mid-latitude medium-range deterministic forecast skill. *Tellus A 64* (2012).

[65] Lorenz, E. N. Energy and numerical weather prediction. *Tellus 12*, 4 (1960), 364–373.

[66] Malguzzi, P., Buzzi, A., and Drofa, O. The meteorological global model globo at the isac-cnr of italy assessment of 1.5 yr of experimental use for medium-range weather forecasts. *Weather and Forecasting 26*, 6 (2011), 1045–1055.

[67] Malguzzi, P., Grossi, G., Buzzi, A., Ranzi, R., and Buizza, R. The 1966 "century" flood in italy: A meteorological and hydrological revisitation. *Journal of Geophysical Research: Atmospheres (1984–2012) 111*, D24 (2006).

[68] Malguzzi, P., and Tartagione, N. An economical second-order advection scheme for numerical weather prediction. *Quarterly Journal of the Royal Meteorological Society 125*, 558 (1999), 2291–2303.

[69] Martius, O., and Schwierz, C. Dynamical aspects of the formation of a potential vorticity streamer over europe. In *Proc. Int. Conf. Alpine Meteorology and MAP-Meeting 2003* (2003), pp. 545–548.

[70] Martius, O., Schwierz, C., and Davies, H. Far-upstream precursors of heavy precipitation events on the alpine south-side. *Quarterly Journal of the Royal Meteorological Society 134*, 631 (2008), 417–428.

[71] Massacand, A. C., Wernli, H., and Davies, H. C. Heavy precipitation on the alpine southside: An upper-level precursor. *Geophysical Research Letters 25*, 9 (1998), 1435–1438.

[72] Miglietta, M., Davolio, S., Moscatello, A., Pacifico, F., Rotunno, R., et al. The role of surface fluxes in the development of a tropical-like cyclone in southern italy. *Advances in Science and Research 2* (2008), 35–39.

[73] Miglietta, M., Laviola, S., Malvaldi, A., Conte, D., Levizzani, V., and Price, C. Analysis of tropical-like cyclones over the mediterranean sea through a combined modeling and satellite approach. *Geophysical Research Letters 40*, 10 (2013), 2400–2405.

[74] Miglietta, M. M., Mastrangelo, D., and Conte, D. Influence of physics parameterization schemes on the simulation of a tropical-like cyclone in the mediterranean sea. *Atmospheric Research* (2014).

[75] Miglietta, M. M., Moscatello, A., Conte, D., Mannarini, G., Lacorata, G., and Rotunno, R. Numerical analysis of a mediterranean 'hurricane'over south-eastern italy: sensitivity experiments to sea surface temperature. *Atmospheric Research 101*, 1 (2011), 412–426.

[76] Mlawer, E. J., Taubman, S. J., Brown, P. D., Iacono, M. J., and Clough, S. A. Radiative transfer for inhomogeneous atmospheres: Rrtm, a validated correlated-k model for the longwave. *Journal of Geophysical Research: Atmospheres (1984–2012) 102*, D14 (1997), 16663–16682.

[77] Monin, A., and Obukhov, A. Basic laws of turbulent mixing in the surface layer of the atmosphere. *Contrib. Geophys. Inst. Acad. Sci. USSR 151* (1954), 163–187.

[78] Montgomery, M. T., and Farrell, B. F. Polar low dynamics. *Journal of the atmospheric sciences 49*, 24 (1992), 2484–2505.

[79] Morcrette, J.-J. Radiation and cloud radiative properties in the european centre for medium range weather forecasts forecasting system. *Journal of Geophysical Research: Atmospheres (1984–2012) 96*, D5 (1991), 9121–9132.

[80] Moscatello, A., Marcello Miglietta, M., and Rotunno, R. Observational analysis of a mediterranean 'hurricane'over south-eastern italy. *Weather 63*, 10 (2008), 306–311.

[81] Moscatello, A., Miglietta, M. M., and Rotunno, R. Numerical analysis of a mediterranean "hurricane" over southeastern italy. *Monthly Weather Review 136*, 11 (2008), 4373–4397.

[82] Nagata, M., Leslie, L., Kurihara, Y., Elsberry, R. L., Yamasaki, M., Kamahori, H., Abbey Jr, R., Bessho, K., Calvo, J., Chan, J. C., et al. meeting summary: Third compare workshop: A model intercomparison experiment of tropical cyclone intensity and track prediction. *Bulletin of the American Meteorological Society 82*, 9 (2001), 2007–2020.

[83] Ooyama, K. V. Conceptual evolution of the theory and modeling of the tropical cyclone. *J. Meteor. Soc. Japan 60*, 1 (1982), 369–380.

[84] Pantillon, F., Chaboureau, J. P., Lac, C., and Mascart, P. On the role of a Rossby wave train during the extratropical transition of hurricane Helene (2006). *Q.J.R. Meteorol. Soc. 139*, 671 (Jan. 2013), 370–386.

[85] Peng, M. S., Hendricks, E., Li, T., and Ge, X. Initialization of tropical cyclones in numerical prediction systems. In *29th Conference on Hurricanes and Tropical Meteorology* (2010).

[86] Petterssen, S. Weather analysis and forecasting.

[87] Picornell, M. A., Campins, J., and Jansà, A. Detection and thermal description of medicanes from numerical simulation. *Natural Hazards and Earth System Science 14*, 5 (2014), 1059–1070.

[88] Pytharoulis, I., Craig, G., and Ballard, S. The hurricane-like mediterranean cyclone of january 1995. *Meteorological Applications 7*, 03 (2000), 261–279.

[89] RAMIS, C., TOUS, M., HOMAR, V., ROMERO, R., and ALONSO, S. Medicanes: Quasi-tropical mesoscale cyclones in the mediterranean.

[90] Rasmussen, E. The polar low as an extratropical cisk disturbance. *Quarterly Journal of the Royal Meteorological Society 105*, 445 (1979), 531–549.

[91] Rasmussen, E. A case study of a polar low development over the barents sea. *Tellus A 37*, 5 (1985), 407–418.

[92] Rasmussen, E., and Zick, C. A subsynoptic vortex over the mediterranean with some resemblance to polar lows. *Tellus A 39*, 4 (1987), 408–425.

[93] Reale, O., and Atlas, R. Tropical cyclone-like vortices in the extratropics: observational evidence and synoptic analysis. *Weather and forecasting 16*, 1 (2001), 7–34.

[94] Reed, R., Kuo, Y.-H., Albright, M., Gao, K., Guo, Y.-R., and Huang, W. Analysis and modeling of a tropical-like cyclonein the mediterranean sea. *Meteorology and Atmospheric Physics 76*, 3-4 (2001), 183–202.

[95] Reed, R. J., Albright, M. D., Sammons, A. J., and Undén, P. The role of latent heat release in explosive cyclogenesis: Three examples based on ecmwf operational forecasts. *Weather and forecasting 3*, 3 (1988), 217–229.

[96] Riehl, H. *Waves in the easterlies and the polar front in the tropics.* University of Chicago Press, 1945.

[97] Ritter, B., and Geleyn, J.-F. A comprehensive radiation scheme for numerical weather prediction models with potential applications in climate simulations. *Monthly Weather Review 120*, 2 (1992), 303–325.

[98] Romero, R., and Emanuel, K. Space time probability density of mediterranean hurricane genesis in the light of an empirical tropical index. *V Asamblea Hispano-Portuguesa de Geodesia y Geofísica V Assembleia Luso-Espanhola de Geodesia e Geofísica: proceedings, Sevilla, Spain 30* (2006).

[99] Romero, R., and Emanuel, K. Medicane risk in a changing climate. *Journal of Geophysical Research: Atmospheres 118*, 12 (2013), 5992–6001.

[100] Romero, R., Martín, A., Homar, V., Alonso, S., Ramis, C., et al. Predictability of prototype flash flood events in the western mediterranean under uncertainties of the precursor upper-level disturbance. *Advances in Geosciences 7* (2006), 55–63.

[101] Rotunno, R., and Emanuel, K. A. An air-sea interaction theory for tropical cyclones. part ii: Evolutionary study using a nonhydrostatic axisymmetric numerical model. *Journal of the atmospheric sciences 44*, 3 (1987), 542–561.

[102] Santurette, P., and Georgiev, C. *Weather analysis and forecasting: applying satellite water vapor imagery and potential vorticity analysis*. Academic Press, 2005.

[103] Simpson, R. H., and Riehl, H. *The hurricane and its impact*. Louisiana State University Press Baton Rouge, LA, 1981.

[104] Sirvatka, P. *Tropical Meteorology Lecture Notes*. College of DuPage.

[105] Smith, R. K. On the theory of cisk. *Quarterly Journal of the Royal Meteorological Society 123*, 538 (1997), 407–418.

[106] Speranza, A., Buzzi, A., Trevisan, A., and Malguzzi, P. A theory of deep cyclogenesis in the lee of the alps. part i: Modifications of baroclinic instability by localized topography. *Journal of the atmospheric sciences 42*, 14 (1985), 1521–1535.

[107] Sutcliffe, R. A contribution to the problem of development. *Quarterly Journal of the Royal Meteorological Society 73*, 317-318 (1947), 370–383.

[108] Tous, M., and Romero, R. Medicanes: cataloguing criteria and exploration of meteorological environments, 2011.

[109] Tous, M., and Romero, R. Meteorological environments associated with medicane development. *International Journal of Climatology 33*, 1 (2013), 1–14.

[110] Tous, M., Romero, R., and Ramis, C. Surface heat fluxes influence on medicane trajectories and intensification. *Atmospheric Research 123* (2013), 400–411.

[111] Trenberth, K. E. On the interpretation of the diagnostic quasi-geostrophic omega equation. *Monthly Weather Review 106*, 1 (1978), 131–137.

[112] Trigo, I. F., Davies, T. D., and Bigg, G. R. Objective climatology of cyclones in the mediterranean region. *Journal of Climate 12*, 6 (1999), 1685–1696.

[113] Twitchett, A. F. *Predictability and dynamics of potential vorticity streamers and connections to high impact weather*. University of Leeds, 2012.

[114] Vich, M., Romero, R., and Brooks, H. Ensemble prediction of mediterranean high-impact events using potential vorticity perturbations. part i: Comparison against the multiphysics approach. *Atmospheric research 102*, 1 (2011), 227–241.

[115] Wang, Y. On the bogusing of tropical cyclones in numerical models: The influence of vertical structure. *Meteorology and Atmospheric Physics 65*, 3-4 (1998), 153–170.

[116] Weldon, R., and Holmes, S. Water vapor imagery: interpretation and applications to weather analysis and forecasting. Tech. rep., NOAA NESDIS 57, Washington D.C., 1991.

[117] Zampieri, M., Malguzzi, P., Buzzi, A., et al. Sensitivity of quantitative precipitation forecasts to boundary layer parameterization: a flash flood case study in the western mediterranean. *Natural Hazards and Earth System Science 5*, 4 (2005), 603–612.